Fabrication of Polyvinyl Alcohol Composites using Biomass-Derived Silicified Microcrystalline Cellulose and Zinc Oxide Nanoparticles

Thesis submitted to the
University of Calicut
in partial fulfillment of the requirements
for the degree of

Doctor of Philosophy
in
Chemistry

By

AJMAL THAYYULLATHIL

Under the Supervision of

Dr. SUBAIR NADUPARAMBATH
Professor of Chemistry



POST GRADUATE AND RESEARCH DEPARTMENT OF CHEMISTRY
GOVERNMENT COLLEGE MADAPPALLY, VADAKARA
FEBRUARY 2026

DEPARTMENT OF CHEMISTRY
GOVT. COLLEGE MADAPPALLY, VADAKARA

CERTIFICATE

This is to certify that the thesis entitled "**Fabrication of Polyvinyl Alcohol Composites using Biomass-Derived Silicified Microcrystalline Cellulose and Zinc Oxide Nanoparticles**" is an authentic record of research work carried out by **Mr. AJMAL THAYYULLATHIL** under my guidance and supervision, for the award of the degree of Doctor of Philosophy in Chemistry under the faculty of Sciences, University of Calicut, Kerala. The work embodied in this thesis is original and has not been presented/reported earlier for any degree or diploma of any University/Institute.

The thesis is revised as per the modifications and recommendations reported by the adjudicators. Soft copy attached is the same as that of the revised copy.

Madappally
24.07. 2026

Dr. SUBAIR NADUPARAMBATH
Professor
Department of Chemistry
Govt. College Madappally

DECLARATION

I, **AJMAL THAYYULLATHIL,** hereby declare that the work presented in the thesis entitled **"Fabrication of Polyvinyl Alcohol Composites using Biomass-Derived Silicified Microcrystalline Cellulose and Zinc Oxide Nanoparticles"** is based on the original work done by me under the guidance of **Dr. SUBAIR NADUPARAMBATH**, Professor, Department of Chemistry, Government College Madappally, Vadakara, Kerala and has not been included in any other thesis submitted previously for the award of any degree. The contents of the thesis have undergone plagiarism check using iThenticate software at C.H.M.K. Library, University of Calicut, and the similarity index found within the permissible limit. I also declare that the thesis is free from AI generated contents.

Madappally
24.07. 2026

AJMAL THAYYULLATHIL

Dr. SUBAIR NADUPARAMBATH
Professor
Department of Chemistry
Govt. College Madappally

UNIVERSITY OF CALICUT

CERTIFICATE ON PLAGIARISM CHECK

1.	Name of the Research Scholar	AJMAL THAYYULLATHIL	
2.	Title of thesis / dissertation	Fabrication of Polyvinyl Alcohol Composites using Biomass-Derived Silicified Microcrystalline Cellulose and Zinc Oxide Nanoparticles	
3.	Name of the Supervisor	Dr. Subair Naduparambath	
4.	Department/Institution	Department of Chemistry, Govt.College Madappally	
5.	Similar content (%) identified	Non Core	Core
		Introduction/ Theoretical overview/Review of literature/ Materials & Methods/ Methodology	Analysis/Result/Discussion / Summary/Conclusion/ Recommendations
		3	4
	Acceptable maximum limit (%)	10	10
6.	Software used	iThenticate	
7.	Date of verification	02.02.2026	

*Report of plagiarism check, specifying included/excluded items with % of similarity to be attached.

MOHAMMED KOYA LIBRARY
UNIV. CALICUT UNIVERSITY
UNIVERSITY OF CALICUT

SEEMA M.V.
Assistant Librarian
University of Calicut
Malappuram - 673 635

Verified by (with name , designation & signature) Seema

Name and signature of the Researcher

Name and signature of the Supervisor

Dr. SUBAIR NADUPARAMBA
Associate Professor
Department of Chemistry
Govt. College Madappally
PEN: 601438

The Doctoral Committee* has verified the report on plagiarism check with the contents of the thesis, as summarized above and appropriate measures have been taken to ensure originality of the Research accomplished herein.

Name & Signature of the HoD/HoI (Chairperson of the Doctoral Committee) Shima Fathimhasa Mohammad

*In case of languages like Malayalam, Tamil etc.,on which no software is available for plagiarism check, a manual check shall be made by the Doctoral Committee, for which an additional certificate has to be attached.

Principal
GOVERNMENT COLLEGE, MADAPPALLY
MADAPPALLY COLLEGE (P.O.)
PIN: 673 102

GOVT. COLLEGE MADAPPALLY
MADAPPALLY COLLEGE P.O -673102

ACKNOWLEDGEMENT

During the course of this research, many people supported and encouraged me, making this journey possible. Here, I would like to express my sincere gratitude to all those who contributed to the successful completion of this thesis. First and foremost, I am deeply thankful to my research supervisor Dr. Subair Naduparambath, Professor, Department of Chemistry, Government College Madappally, Vadakara, University of Calicut, for his valuable guidance, constant encouragement, and insightful suggestions throughout the course of this work.

I sincerely thank Mr. Shinu P.M, the Principal and all the former Principals of Government College Madappally, who served during my research period at Government College Madappally for their continuous encouragement and for providing the necessary departmental facilities to carry out and complete my research work.

I gratefully acknowledge Dr Preetha B, former Principal and Head of the Department of Chemistry, Government College Madappally, for her generous support in providing the necessary research facilities and other resources throughout my Ph.D. program, which played a crucial role in the successful execution of my research.

I sincerely thank all the faculty members of the Department of Chemistry for their guidance, constructive feedback, and steadfast assistance throughout my doctoral studies. Their expertise and commitment to academic excellence have profoundly shaped my research journey. The encouragement, thoughtful discussions, and valuable insights I received from them have not only strengthened the quality of my work but have also contributed greatly to my intellectual growth and confidence as a researcher. I am truly grateful to have been part of such a supportive academic community.

I would like to sincerely acknowledge all lab attenders of the department for their invaluable assistance, co-operation and support throughout the course of my research. Their timely help in laboratory management and day-to-day activities

greatly facilitated the smooth progress of my work. I am truly respectful for their dedication, patience and willingness to assist whenever needed.

I would like to express my sincere gratitude to research scholars Ms. Vydhehi E. K. and Ms. Anjana T. M. for their constant support and valuable assistance throughout my research work. Their help in conducting experiments, data analysis, manuscript preparation, and thesis writing was instrumental to the successful completion of this work.

I would also like to sincerely thank Dr. Swetha Sasidharan, Assistant Professor, SNDP Yogam College, Koyilandy, and Dr. Muhammad Ismail K. M. Associate Professor, NAM College Kallikkandy for their valuable help, guidance, and support during the course of my research work.

I deeply acknowledge the Head of the Institutions of CSIF-University of Calicut, STIC-Cochin University, CIF-NIT Calicut and SAIF-MG University for doing my analysis, which facilitated in completion of the research work on time.

I would like to express my deepest gratitude to my beloved father, Mr. Moosa, and my mother, Mrs. Jameela, for their unconditional love, constant encouragement, and lifelong support. I sincerely thank my wife, Mrs. Thasneema, for her patience, understanding, and unwavering support throughout this journey. I also extend my heartfelt thanks to my kids, Shanza Ajmal, Muhammad Haneen, and Fathima Mehar, whose love and motivation were a constant source of strength. I am equally grateful to all my family members for their prayers, encouragement, and moral support, which played a vital role in the successful completion of this work.

I would like to express my heartfelt gratitude to everyone who has offered their support, directly or indirectly, in the successful completion of my work.

Above all, I offer my humble thanks to God Almighty, the Most Merciful and Beneficent, for his blessings that have guided me in completing this research successfully.

Ajmal Thayyullathil

Dedicated to

My

Family

ABSTRACT

The environmental concerns associated with petroleum-based polymer have driven scientific and industrial interest towards the development of more sustainable and biodegradable polymers reinforced with renewable and eco-friendly resources. In this context, the present study systematically investigates the fabrication of Polyvinyl Alcohol (PVA) based composites reinforced with biomass-derived Microcrystalline Cellulose (MCC), silica, Silicified Microcrystalline Cellulose (SMCC) and Zinc Oxide (ZnO) nanoparticles. The aim of this study is the synergistic combination of an eco-friendly polymer matrix with organically and inorganically modified renewable fillers. The intention of this combination is to enhance structural, thermal, mechanical and barrier properties of PVA without compromising its degradability and renewability

Initially, both amorphous and crystalline silica were extracted from a highly invasive weed, Mission Grass (MG) through controlled thermal and chemical treatment. The effect of temperature and method of synthesis on the phase transition of silica was systematically studied. The MCC was independently extracted from another biomass, Screw Pine (SP) leaves through delignification, mercerization followed by acid hydrolysis. The morphological studies revealed that MCC have small and big sized lacunae with irregular shape and this void offers plenty of rooms for nanoparticles. In order to improve the properties such as poor dispersibility, low density and thermal stability, MCC was modified through silicification. The SMCC was synthesised by dispersing MCC in sodium silicate solution extracted from MG followed by controlled acid hydrolysis so as to induce precipitation within the voids and deposition of silica on the cellulose surface. This results a well-integrated organic-inorganic hybrid material where cellulose imparts structural reinforcement and deposited silica improves compatibility, thermal stability, surface reactivity and density. Further, ZnO nanoparticles were added to SMCC to introduce additional functionality to the hybrid filler system.

PVA composite films containing silica, MCC, SMCC and SMCC-ZnO were fabricated through solution casting method. The synthesised fillers and fabricated composite films were characterized by X-ray Diffraction (XRD), Fourier Transform

Infrared Spectroscopy (FT-IR), Thermogravimetric Analysis (TGA), Field Emission-Scanning Electron Microscopy (FE-SEM), Transmission Electron Microscopy (TEM) and Atomic Force Microscopy (AFM) to evaluate the structural, chemical, thermal and morphological properties. The analysis confirmed the successful extraction of both amorphous and crystalline silica from Mission Grass and also proved that the calcination temperature and method of synthesis have significant effect on the phase transition. The morphology studies proved that the MCC extracted from SP leaves contains a large number of lacunae so that in situ synthesis of nanosilica is possible within these voids. The analysis confirmed the effective silicification of MCC. The studies also revealed that SMCC-ZnO exhibit better dispersibility than MCC due to its hybrid organic and inorganic structure, which enhance interfacial compatibility and homogeneous distribution within the polymer matrix.

The studies revealed that the incorporation of SMCC and SMCC-ZnO to the PVA resulted a significant enhancement in mechanical strength, thermal stability and barrier properties compared to bare PVA and PVA/MCC composites. Additionally, the extent of swelling and water vapour transmission rate were considerably reduced, reflecting improved resistance to moisture diffusion. Moreover, SMCC and ZnO imparted additional functional properties to the PVA composites. The presence of ZnO nanoparticles enhanced the Ultraviolet (UV) absorption and exhibited notable antibacterial activity. An increase in contact angle was also observed in the case of PVA/SMCC-ZnO composites, which provides improved surface hydrophobicity.

Overall, the study demonstrates that the biomass-derived Silicified Microcrystalline Cellulose is an efficient and sustainable reinforcement for PVA based composites. The newly fabricated composites show strong potential for eco-friendly applications such as packaging, agricultural films and other biodegradable products and this study supports the advancement of green polymer composite technologies.

Keywords: Mission Grass, Sol Gel Silica, Silicified Microcrystalline Cellulose, SMCC-PVA Composites, Renewable Sources

സംഗ്രഹം

പെട്രോളിയാധിഷ്ഠിതമായ പോളിമറുകളുമായി ബന്ധപ്പെട്ട പാരിസ്ഥിതിക പ്രശ്നങ്ങൾ കാരണം പുനർനിർമ്മിക്കാവുന്നതും പാരിസ്ഥിതിക സൗഹൃദവുമായ വിഭവങ്ങൾ ഉപയോഗിച്ച് കൂടുതൽ ഉപകാരപ്രദവും ജൈവികമായി വിഘടിക്കുന്നതുമായ പോളിമറുകളുടെ നിർമാണത്തിലേക്ക് ശാസ്ത്ര-വ്യാവസായിക ലോകത്തിന്റെ ശ്രദ്ധ പതിഞ്ഞിട്ടുണ്ട്. ഈ പശ്ചാത്തലത്തിൽ ജൈവസ്രോതസ്സിൽ (BIOMASS) അധിഷ്ഠിതമായ മൈക്രോക്രിസ്റ്റലൈൻ സെല്ലുലോസ് (MCC), സിലിക്ക, സിലിസിഫൈഡ് മൈക്രോക്രിസ്റ്റലൈൻ സെല്ലുലോസ് (SMCC) എന്നിവ ഉപയോഗിച്ച് നിർമ്മിച്ച പോളിവിനൈൽ ആൽക്കഹോൾ (PVA) കോംപോസിറ്റുകളെ കുറിച്ചാണ് ഈ പഠനം. പുനരുപയോഗിക്കാവുന്ന ഓർഗാനിക്-ഇനോർഗാനിക് ഫില്ലറുകളും പരിസ്ഥിതി സൗഹൃദമായ പോളിമർ മട്രിക്സും സംയോജിപ്പിച്ച് കൂടുതൽ മെച്ചപ്പെട്ട പദാർത്ഥങ്ങൾ നിർമിക്കുക എന്നതാണ് ഈ പഠനത്തിന്റെ മുഖ്യ ലക്ഷ്യം. ഈ സംയോജനത്തിലൂടെ PVA യുടെ വിഘടന ക്ഷമതയും പുനർ നിർമ്മിക്കാനുള്ള കഴിവിനും കോട്ടം തട്ടാതെ അതിൻറെ ഘടനയും, താപസ്ഥിരതയും, യാന്ത്രിക ഗുണങ്ങളും മെച്ചപ്പെടുത്താനാണ് ഈ പഠനത്തിലൂടെ ശ്രമിക്കുന്നത്.

ദ്രുതഗതിയിൽ വളരുന്ന കളയായ മിഷൻ ഗ്രാസ്സിൽ (Mission Grass) നിന്നും നിയന്ത്രിതമായ താപ - രാസപ്രക്രിയകളിലൂടെ വഴി അമോർഫസ് രൂപത്തിലുള്ളതും ക്രിസ്റ്റലൈൻ രൂപത്തിലുള്ളതുമായ സിലിക്ക വേർതിരിച്ചെടുക്കലാണ് ഈ പഠനത്തിൻറെ ആദ്യഘട്ടം. സിലിക്കയുടെ ഘടനമാറ്റത്തിൽ താപനിലയുടെയും നിർമ്മാണ രീതിയുടെയും സ്വാധീനം ക്രമബന്ധമായി പഠിച്ചു. മറ്റൊരു ജൈവസ്രോതസ്സായ കൈതോലയിൽ (Screw Pine leaves) നിന്നും ഡീലിഗ്നിഫിക്കേഷൻ, മെർസെറൈസേഷൻ, ആസിഡ് ഹൈഡ്രോളിസിസ് എന്നീ പ്രക്രിയകളിലൂടെ മൈക്രോക്രിസ്റ്റലൈൻ സെല്ലുലോസ് (MCC) വേർതിരിച്ചെടുത്തു. MCC യുടെ മോർഫോളജിക്കൽ പഠനങ്ങൾ അവയുടെ ഉപരിതലത്തിൽ വിവിധ ആകൃതിയിലും വലിപ്പത്തിലുമുള്ള ധാരാളം സുഷിരങ്ങൾ (lacunae) ഉള്ളതായി വെളിവായി. ഈ സുഷിരങ്ങൾ നാനോകണങ്ങൾ ഉൾക്കൊള്ളാനുള്ള മതിയായ ഇടങ്ങൾ നൽകുന്നു. MCC യുടെ ന്യൂനതകളായ കുറഞ്ഞ ഡിസ്പെർസബിലിറ്റി, സാന്ദ്രത, താപസ്ഥിരത എന്നിവ മെച്ചപ്പെടുത്തുന്നതിന് വേണ്ടി അതിനെ സിലിസിഫിക്കേഷൻ നടത്തി. MCC യെ മിഷൻ ഗ്രാസ്സിൽ നിന്നും ലഭിച്ച സോഡിയം സിലിക്കേറ്റ് ദ്രാവകത്തിൽ ഡിസ്പെർസ് ചെയ്തതിനു ശേഷം നിയന്ത്രിതമായ ആസിഡ് ഹൈഡ്രോളിസിസ് നടത്തി. ഇതിന്റെ ഫലമായി MCC യുടെ ഉപരിതലത്തിലും സുഷിരങ്ങളിലും സിലിക്ക നിക്ഷേപിക്കപ്പെട്ട് ഓർഗാനിക്-ഇനോർഗാനിക് പദാർത്ഥങ്ങൾ സംയോജിക്കപ്പെട്ട് ഹൈബ്രിഡ് പദാർത്ഥമായ സിലിസിഫൈഡ് മൈക്രോക്രിസ്റ്റലൈൻ സെല്ലുലോസ് (SMCC) രൂപം കൊണ്ടു. ഇങ്ങനെ നിർമ്മിച്ച SMCCക്ക്, അതിലടങ്ങിയ സെല്ലുലോസ് ഘടനാപരമായ ശക്തി നൽകുമ്പോൾ മറ്റൊരു ഘടകമായ സിലിക്ക താപസ്ഥിരത, ഉപരിതല ക്രിയാശീലത, സാന്ദ്രത എന്നിവ മെച്ചപ്പെടുത്തുന്നു. കൂടാതെ SMCC യുടെ പ്രവർത്തനഗുണങ്ങൾ പരിപോഷിപ്പിക്കുന്നതിനായി സിങ്ക് ഓക്സയിഡ് (ZnO) നാനോകണങ്ങളും ചേർത്തു.

അടുത്ത ഘട്ടത്തിൽ സിലിക്ക, MCC, SMCC, SMCC-ZnO എന്നിവയടങ്ങിയ PVA കോംപോസിറ്റ് ഫിലിമുകൾ സൊല്യൂഷൻ കാസ്റ്റിംഗ് രീതിയിലൂടെ നിർമ്മിച്ചു. പുതുതായി നിർമ്മിച്ച ഫില്ലറുകളുടെയും കോംപോസിറ്റ് ഫിലിമുകളുടെയും രാസ, താപ, ഘടനാപരമായ

സവിശേഷതകൾ എക്സ് റേ ഡിഫ്റാക്ഷൻ (XRD), ഫൊറിയർ ട്രാൻസ്ഫോം-ഇൻഫ്രാ റെഡ് സ്പെക്ട്രോസ്കോപ്പി (FT-IR), തെർമോഗ്രാവിമെട്രിക് അനാലിസിസ് (TGA), ഫീൽഡ് എമിഷൻ - സ്കാനിംഗ് ഇലക്ട്രോൺ മൈക്രോസ്കോപ്പി (FE-SEM), ട്രാൻസ്മിഷൻ ഇലക്ട്രോൺ മൈക്രോസ്കോപ്പി (TEM), അറ്റോമിക് ഫോഴ്സ് മൈക്രോസ്കോപ്പി (AFM)എന്നീ സാങ്കേതിക വിദ്യകൾ ഉപയോഗിച്ച് വിശകലനം നടത്തി. ഈ വിശകലനത്തിൽ നിന്നും അമോർഫസ്, ക്രിസ്റ്റലൈൻ ഘടനയുള്ള സിലിക്ക മിഷൻ ഗ്രാസ്സിൽ നിന്നും വിജയകരമായി വേർതിരിച്ചെടുക്കാമെന്ന് സ്ഥിരീകരിക്കുകയും കാൽസിനേഷൻ താപനിലയും നിർമ്മാണ രീതിയും സിലിക്കയുടെ ഘടനയിൽ നിർണ്ണായക സ്വാധീനം ചെലുത്തുന്നു എന്ന് തെളിയിക്കുകയും ചെയ്തു. മോർഫോളജിക്കൽ പഠനങ്ങൾ, കൈതോലയിൽ നിന്നും വേർതിരിച്ച MCC യിൽ ധാരാളം സുഷിരങ്ങൾ ഉള്ളതായി വെളിവായി. ഇതിൽ നിന്നും ഇത്തരം ശൂന്യ അറകളിൽ സിലിക്കയുടെ ഇൻ സിറ്റു നിർമ്മാണം സാധ്യമാണെന്ന് തെളിഞ്ഞു. നടത്തിയ പരിശോധനകൾ MCC യെ ഫലപ്രദമായി സിലിസിഫിക്കേഷൻ നടത്താൻ കഴിഞ്ഞു എന്ന് തെളിയിച്ചു. കൂടാതെ, ഓർഗാനിക് -ഇനോർഗാനിക് ഹൈബ്രിഡ് ഘടനയുടെ ഫലമായി SMCC-ZnO ന് MCC യെക്കാൾ കൂടുതൽ ഡിസ്പെർസിബിലിറ്റി ഉള്ളതായി പഠനങ്ങൾ വെളിപ്പെടുത്തി. മാത്രമല്ല, ഇവയ്ക്ക പോളിമർ മെട്രിക്സ്നുള്ളിൽ മെച്ചപ്പെട്ട ഇന്റർഫേഷ്യൽ കോംപാറ്റിബിലിറ്റിയും യൂണിഫോം ഡിസ്പെർസിബിലിറ്റി യും കൈവരിക്കാൻ സാധിച്ചു.

SMCC, SMCC-ZnOഎന്നിവയുമായുള്ള സംയോജനത്തിലൂടെ PVA യുടെ മെക്കാനിക്കൽ സ്ട്രെങ്ത്, താപസ്ഥിരത, ബാരിയർ ഗുണങ്ങൾ തുടങ്ങിയവ ശുദ്ധമായ PVA, PVA/MCC എന്നിവയേക്കാൾ ഗണ്യമായി മെച്ചപ്പെടുന്നതായി പഠനങ്ങൾ തെളിയിച്ചു. കൂടാതെ സ്വെല്ലിങ് സ്വഭാവവും വാട്ടർ വേപ്പർ ട്രാൻസ്മിഷൻ റേറ്റും (WVTR) കുറയുന്നതായും SMCC, ZnO എന്നിവ PVA ക്ക് ചില സവിശേഷ ഗുണങ്ങൾ നൽകുന്നതായും കണ്ടെത്തി. അതായത് ZnO നാനോകണങ്ങളുടെ സാന്നിധ്യം, കോംപോസിറ്റുകൾക്ക് UV കിരണങ്ങൾ ആഗിരണം ചെയ്യാനുള്ള കഴിവ് വർധിപ്പിക്കുകയും ആന്റിബാക്ടീരിയൽ കഴിവ് പ്രകടിപ്പിക്കുന്നതായും കണ്ടെത്തി. അത് പോലെ PVA/SMCC-ZnO കോംപോസിറ്റുകൾക്ക് കൂടുതൽ കോൺടാക്ട് ഉള്ളതായും അതുവഴി ഉപരിതല ഹൈഡ്രോഫോബിസിറ്റി മെച്ചപ്പെട്ടതായും കണ്ടെത്തി.

മൊത്തത്തിൽ, ബയോമാസ് അധിഷ്ഠിത സിലിസിഫൈഡ് മൈക്രോക്രിസ്റ്റലൈൻ സെല്ലുലോസ് PVA കോംപോസിറ്റുകളെ കാര്യക്ഷമമായും സുസ്ഥിരമായും ശക്തിപ്പെടുത്താൻ കഴിയുന്ന ഒരു വസ്തുവാണെന്ന് ഈ പഠനം തെളിയിക്കുന്നു. പുതുതായി നിർമ്മിച്ച ഈ കോംപോസിറ്റുകൾ പാക്കേജിംഗ്, കൃഷി ഫിലിമുകൾ, മറ്റ് ജൈവമായി വിഘടിപ്പിക്കാവുന്ന ഉൽപ്പന്നങ്ങൾ എന്നിവ ഉൾപ്പെടെയുള്ള പരിസ്ഥിതി സൗഹൃദ പ്രയോഗങ്ങൾക്ക് വലിയ സാധ്യത കാണിക്കുന്നു. ഈ പഠനം ഗ്രീൻ പോളിമർ കോംപോസിറ്റ് സാങ്കേതിക വിദ്യകളുടെ പുരോഗതിക്ക് പിന്തുണ നൽകുന്നു.

സൂചകപദങ്ങൾ: മിഷൻ ഗ്രാസ്, സോൾ ജെൽ സിലിക്ക,
സിലിസിഫൈഡ്മൈക്രോക്രിസ്റ്റലൈൻസെല്ലുലോസ്,എസ്എംസിസി-പിവിഎ
കോമ്പോസിറ്റുകൾ, പുനരുപയോഗിക്കാവുന്ന ഉറവിടങ്ങൾ

CONTENTS

		Page No
Chapter 1		
Introduction		
1.1 Understanding Polymers		1
1.1.1	From Plastic to Progress: How do polymers influence our daily life	1
1.1.2	What are Polymers?	2
1.1.3	Classification of Polymers	3
1.1.4	Limitations of Synthetic Polymers	3
1.1.5	Biodegradable Polymers	4
	1.1.5.1 Classification of Biodegradable Polymers	5
	1.1.5.2 Applications of Biodegradable Polymers	5
	1.1.5.3 Limitations of Biodegradable Polymers	6
1.1.6	Polymer Composites	8
	1.1.6.1 Polymer matrix	9
	1.1.6.2 Reinforcement	11
1.1.7	Polyvinyl Alcohol (PVA)	13
1.2 Microcrystalline Cellulose (MCC)		14
1.3 Nanosilica		16
1.4 Silicified Microcrystalline Cellulose (SMCC)		18
1.5 Zinc Oxide Nanoparticles		20
1.6 Scope and Overall Objectives of the Study		21
References		24
Chapter 2		
A Comprehensive Review of Polyvinyl Alcohol Composites Reinforced with Silica, MCC, Silicified MCC and ZnO Nanoparticles		
2.1 Introduction		33
2.2 Recent Advances in Nanosilica and Biosilica		34
2.3 A Review of Silica-Polymer Composites		36
2.4 Microcrystalline Cellulose: A Review of Recent Studies		39
2.5 Recent Modifications of Microcrystalline Cellulose		41
2.6 Microcrystalline Cellulose-Polymer composites: A Review		44

2.7 Recent studies on Microcrystalline Cellulose-Polyvinyl Alcohol Composites 46
2.8 Studies on Silicified Microcrystalline Cellulose 48
2.9 Silicified Microcrystalline Cellulose-Polymer Composites: A Review 49
2.10 Role of Zinc Oxide as a Multifunctional Filler in PVA Composites 50
References 52
Chapter 3
Analytical Methodologies and Techniques
3.1 Introduction 63
3.2 Structural and Phase Characterisation 63
3.2.1 X-ray Diffraction Analysis (XRD) 63
3.3 Chemical and Functional Group Analysis 65
3.3.1 Fourier Transform-Infrared (FT-IR) Spectroscopy 65
3.3.2 Attenuated Total Reflectance-FTIR (ATR-FTIR) 65
3.4 Thermal Characterisation 66
3.4.1Thermogravimetric Analysis (TGA) 66
3.5 Morphological and Surface Characterisation 67
3.5.1 Scanning Electron Microscopy (SEM) 68
3.5.2 Atomic Force Microscopy (AFM) 68
3.5.3 High Resolution-Transmission Electron Microscopy (HR-TEM) 69
3.6 Determination of True Density (TD), Bulk Density (BD) and Porosity 69
3.7 Optical Characterisation (UV-Visible Spectroscopy) 71
3.8 Surface Wettability Test (Contact Angle Measurement) 71
3.9 Water Absorption (Swelling) Test 71
3.10 Water Vapour Transmission Rate (WVTR) Analysis 72
3.11 Biodegradability Test (Soil Burial Degradation) 73
3.12 Anti-Bacterial Test 73
3.13 Mechanical Properties Analysis 74
References 75
Chapter 4
A Comparative Study on Amorphous and Crystalline Nanosilica Extracted from Mission Grass (*Pennisetum polystachion*)
4.1 Introduction 77

4.1.1 Background on Silica Nanoparticles 77
4.1.2 Nanosilica from Biomasses 77
4.1.3 Mission Grass (Pennisetum Polystachion) 78
4.1.4 Aim and Objectives of the Study in the Present Chapter 79
4.2 Materials 80
4.3 Methods 80
4.3.1 Synthesis of Amorphous Silica 80
4.3.2 Synthesis of Crystalline Silica 81
4.4 Results and Discussion 82
4.4.1 Fourier Transform-Infrared (FT-IR) Spectroscopy Analysis 82
4.4.2 X-ray Diffraction Analysis 84
4.4.3 Thermal Analysis 87
4.4.4 Field Emission-Scanning Electron Microscopy (FE-SEM) and Energy Dispersive X-ray Spectroscopy (EDS) 89
References 92

Chapter 5

Valorization of Screw Pine (*Pandanus tectorius)* leaves: Isolation and Characterisation of Microcrystalline Cellulose

5.1 Introduction 97
5.1.1 Understanding Cellulose Derivatives 97
5.1.2 Aim and Objectives of the study in the Present Chapter 99
5.2 Materials 100
5.3 Methods 100
5.3.1 Extraction of Holocellulose through Delignification 100
5.3.2 Isolation of α-Cellulose from Holocellulose 101
5.3.3 Isolation of Microcrystalline Cellulose 101
5.4 Results and Discussion 102
5.4.1 Chemical Composition 102
5.4.2 Fourier Transform-Infrared Spectroscopy Analysis 103
5.4.3 X-ray Diffraction Analysis 104
5.4.4 Thermogravimetric Analysis 106
5.4.5 Morphological Analysis 108
5.4.5.1 Field Emission -Scanning Electron Microscopy Analysis 108
5.4.5.2 Atomic Force Microscopy Analysis 109
5.4.5.3 High Resolution- Transmission Electron Microscopy Analysis 110

References 112

Chapter 6

Biomass-Derived Silicified Microcrystalline Cellulose (SMCC): A Novel Method Based on Screw Pine leaves and Mission Grass

6.1 Introduction 117
6.1.1 Overview and Importance of Microcrystalline Cellulose 117
6.1.2 Limitations and Challenges of MCC 117
6.1.3 Recent Advancements in the Modifications of MCC 118
6.1.4 Silicified MCC (SMCC): A Promising Solution to Enhance MCC Performance 119
6.1.5 Aim and Objectives of the Study in the Present Chapter 119
6.2 Materials 120
6.3 Methods 120
6.3.1 Preparation of Silicified Microcrystalline Cellulose 120
6.3.1.1 Isolation of Microcrystalline Cellulose 120
6.3.1.2 Preparation of Sodium Silicate 121
6.3.1.3 Synthesis of Silicified Microcrystalline Cellulose 121
6.4 Results and Discussion 122
6.4.1 True Density, Bulk Density and Porosity measurements 122
6.4.2 Fourier Transform-Infrared (FT-IR) Spectroscopy Analysis 124
6.4.3 X-ray Diffraction Analysis 126
6.4.3.1 Rietveld Refinement of MCC 127
6.4.3.2 Rietveld Refinement of SMCC10 128
6.4.3.3 Rietveld Refinement of SMCC20 130
6 .4.4 Thermogravimetric Analysis 133
6.4. 5 Morphological Analysis 134
References 138

Chapter 7

Comparative Study of Polyvinyl Alcohol Composites Reinforced with MCC, Silica and Silicified MCC

7.1 Introduction 143
7.1.1 Background on Polyvinyl Alcohol 143
7.1.2 Use of Fillers to Improve PVA film 144
7.1.3 Use of Microcrystalline Cellulose as Filler in PVA film 145
7.1.4 Nanosilica as Filler in PVA Composites 146
7.1.5 Silicified MCC-A Hybrid Filler in PVA Composites 147

7.1.6 Aim and Objectives of the Study in the Present Chapter 147
7.2 Materials 149
7.3 Methods 149
7.3.1 Preparation of Bare PVA film 149
7.3.2 Fabrication of PVA/MCC Composite film 149
7.3.3 Fabrication of PVA/Silica and PVA/SMCC Composite film 149
7.3.4 Fabrication of PVA Composite films with Higher Composition 150
7.4 Results and Discussion 151
7.4.1 Fourier Transform-Infrared Spectroscopy Analysis 151
7.4.2 X-ray Diffraction Analysis 152
7.4.3 Thermogravimetric Analysis 158
7.4.4 Morphological Analysis 160
7.4.5 Mechanical Properties 162
References 166

Chapter 8

Application Studies and Functional Evaluation of Biodegradable PVA Composite films Reinforced with MCC, SMCC and ZnO

8.1 Introduction 171
8.1.1 Relevance and Application of Biodegradable PVA-Based Composite 171
8.1.2 Role of MCC, Silica, Silicified MCC and ZnO as Functional Fillers as PVA-Based films 173
8.1.3 Aim and Objectives of the Study in the Present Chapter 175
8.2 Materials 176
8.3 Methods 176
8.3.1 Fabrication of PVA/SMCC-ZnO Composite film 176
8.4 Results and Discussion 177
8.4.1 Water Absorption (Swelling) Analysis 177
8.4.2 Water Vapour Transmission Rate (WVTR) Analysis 178
8.4.3 Antibacterial Performance of PVA Composites 179
8.4.4 Evaluation of Soil Burial Degradability of PVA Composites 181
8.4.4.1 Weight Loss Analysis 181
8.4.4.2 Field Emission-Scanning Electron Microscopy Analysis 182
8.4.5 Fourier Transform-Infrared Spectroscopy Analysis 184
8.4.6 X-ray Diffraction Analysis 186

8.4.7 Optical Absorption Behaviour of Films in UV-Visible Region 189
8.4.8 Contact Angle/Surface Wettability Study of PVA Composites 191
8.4.9 Tensile Behaviour of PVA Composites 193
References 196
Chapter 9
Summary and Future Scope of the Work 203

LIST OF TABLES

Table No.	*Title*	*Page No.*
1.1	Comparative Properties of HPVA and CPVA	13
4.1	Crystallinity Indices of 600ALS, 600SGS,850ALS and 850 SGS	86
5.1	Percentage Composition of Oven Dried Sample of Screw Pine leaves	102
6.1	Phase Composition of MCC, SMCC10 and SMCC20 Obtained from Rietveld Refinement	132
7.1	Crystallinity Indices of PVA, PVA/MCC, PVA/Silica, PVA/SMCC10 and PVA/SMCC20	158
7.2	Qualitative Comparison of Mechanical Properties of Different Films Based on the Stress-Strain Curve	163
8.1	Antibacterial Activity of PVA Composite Films Against *E. coli* and *S. aureus*	179
8.2	Percentage Weight Loss of PVA-Based films After Soil-Burial Test	181
8.3	Crystallinity Indices of PVA, PVA/MCC, PVA/SMCC and PVA/SMCC-ZnO	189

LIST OF FIGURES

Figure No.	*Title*	*Page No.*
4.1	FT-IR Spectra of(a) 600ALS (b) 850ALS (c) 600SGS (d) 850 SGS	82
4.2	X-ray Diffraction Patterns of(a) 600MGA (b) 850MGA (c) 600 ALS (d)850ALS (e) 600SGS and (f) 850SGS	84
4.3	Thermogravimetry of (a) 600SGS and 850SGS (b) DTG of 600 SGS and 850SGS (c) DTA of 600SGS and 850SGS	87
4.4	FE-SEM and EDS of (a) 600ALS (b) 600SGS and (c) 850SGS	89
5.1	FT-IR spectra of (a) Holocellulose (b) Alpha cellulose (c) MCC	103
5.2	X-ray Diffraction Patterns of (a) Holocellulose (b) Alpha cellulose and (c) MCC	104
5.3	Thermogravimetric curves of (a) Holocellulose (b) Alpha cellulose and (c) (MCC)	106
5.4	FE-SEM Images of a) Oven Dried Sample (ODS) b) Holocellulose (HC) c) α-cellulose (AC) and d) MCC	108
5.5	AFM Images of MCC a) 2D (3μm) b) 3D (3μm)	109
5.6	HR-TEM Image of MCC	110
6.1	(a)True Density(g/ml) (b)Bulk Density(g/ml) and (c)Porosity (%) of MCC, SMCC10, SMCC20 and Silica	123
6.2	FT-IR spectra of (a)MCC (b)Amorphous silica (c)SMCC10 and (d)SMCC20	124
6.3	X-ray Diffraction Pattern of (a)MCC (b)SMCC10 (c)SMCC20 and (d) Silica	126
6.4	Rietveld Refined XRD of MCC with Refinement Statistics	127
6.5	Full Pattern XRD of MCC showing Phase Composition.	128
6.6	Rietveld Refined XRD of SMCC10 with Refinement Statistics	129
6.7	Full Pattern XRD of SMCC10 showing Phase Composition.	130
6.8	Rietveld Refined XRD of SMCC20 with Refinement Statistics	131
6.9	Full Pattern XRD of SMCC20 showing Phase Composition.	131
6.10	(a) TG and (b) DTG of MCC, SMCC10, SMCC20 and Silica	133
6.11	FE-SEM Images of (a) MCC (b) Nanosilica and (c) SMCC 20	135
7.1	FT-IR Spectra of PVA, PVA/MCC, PVA/Silica and PVA/SMCC	151

7.2	XRD of (a) PVA, (b) PVA/MCC, (c) PVA/Silica, (d)PVA/SMCC10 and (e) PVA/SMCC20	152
7.3	Rietveld fit, Refinement Statistics and Deconvoluted XRD of PVA	153
7.4	Rietveld fit, Refinement Statistics and Deconvoluted XRD of PVA/MCC	154
7.5	Rietveld fit, Refinement Statistics and Deconvoluted XRD of PVA/Silica	155
7.6	Rietveld fit, Refinement Statistics and Deconvoluted XRD of PVA/SMCC10	156
7.7	Rietveld fit, Refinement Statistics and Deconvoluted XRD of PVA/SMCC20	157
7.8	TG of PVA, PVA/MCC, PVA/SMCC20, and PVA/Silica	158
7.9	FE-SEM Images of (a) PVA (b) PVA/MCC (c) PVA/Silica and (d) PVA/SMCC20	160
7.10	Photographs of PVA Composite films	161
7.11	Tensile Strength and Stress- Strain Curves of PVA, PVA/MCC, PVA/Silica, PVA/SMCC10 and PVA/SMCC20	162
7.12	Tensile Strength and Stress- Strain Curves of PVA/SMCC20 films containing (2%), (4%), (6%) and (8%) SMCC20	163
8.1	Comparative Swelling Behaviour of PVA, PVA/MCC, PVA/SMCC and PVA/SMCC-ZnO over time	177
8.2	a) Water Vapour Transmission through PVA, PVA/MCC, PVA/SMCC and PVA/SMCC-ZnO as a function of time b) Water Vapour Transmission Rate	178
8.3	Antibacterial Activity against (A) *Escherichia coli* (B) *Staphylococcus aureus* PVAP= PVA, M_1=PVA/MCC, M_2=PVA/SMCC and PVAPC=PVA/SMCC-ZnO	180
8.4	FE-SEM Images of PVA, PVA/MCC, PVA/SMCC and PVA/SMCC-ZnO before (1(a)- 4(a)) and after (1(b)-4(b)) Soil Burial	183
8.5	FT-IR Spectra of PVA, PVA/MCC, PVA/SMCC and PVA/SMCC-ZnO	184
8.6	XRD Spectra of (a) PVA, (b) PVA/MCC, (c) PVA/SMCC and (d) PVA/SMCC-ZnO	186
8.7	Reitveld Refined and Deconvoluted XRD of PVA/SMCC-ZnO	188
8.8	a) UV-Visible Spectra of (a) PVA, PVA/MCC, PVA/SMCC and PVA/SMCC-ZnO b) UV-Visible Spectra of PVA/SMCC-ZnO Different Composition	189
8.9	Contact Angle Images of (a) PVA (b) PVA/MCC (c) PVA/SMCC and (d) PVA/SMCC-ZnO	191

8.10	Comparison of Contact Angles for PVA, PVA/MCC, PVA/SMCC and PVA/SMCC-ZnO	192
8.11	a) Stress-Strain Curves b) Tensile Strength, Elongation at Break and Young's Modulus of PVA Composites	193

LIST OF SCHEMES

Scheme No.	*Title*	*Page No.*
4.1	Schematic Representation of Synthesis of Amorphous and Crystalline Nanosilica from Mission Grass.	81
5.1	Schematic Representation of Extraction of MCC from Screw Pine leaves	102
6.1	Schematic Representation of Formation of Silicified Microcrystalline Cellulose	122
7.1	Schematic Representation of Synthesis of PVA/MCC, PVA/SiO_2 and PVA/SMCC	150

Preface

The present thesis entitled “Fabrication of Polyvinyl Alcohol Composites using Biomass-Derived Silicified Microcrystalline Cellulose and Zinc Oxide Nanoparticles” deals with the development of biodegradable polymer composites reinforced with biomass derived fillers. In response to the environmental concern associated with non-biodegradable polymers, increasing attention has been directed towards the utilization of renewable and sustainable resources for the design of advanced polymer composite materials. In this context, the present work investigates the use of biomass-derived functional fillers with Polyvinyl Alcohol based composite system.

The thesis is divided into eight chapters. Chapter 1 presents a general introduction to biodegradable polymers, Polyvinyl Alcohol and the role of natural and inorganic fillers in polymer composites. Chapter 2 provides a critical survey of literature related to biomass-derived silica, Microcrystalline Cellulose, Zinc Oxide nanoparticles and their PVA based composites. Chapter 3 describes the principles of analytical techniques employed for the systematic study of newly synthesised fillers and polymer composites. Chapter 4 deals with the extraction and characterization of amorphous and crystalline silica from Mission Grass. The extraction and characterization of Microcrystalline Cellulose from lignocellulosic biomass is described in chapter 5. Chapter 6 focuses on the synthesis and characterization of Silicified Microcrystalline Cellulose through the controlled deposition of biomass-derived silica on to a cellulose framework. Chapter 7 discusses the fabrication and characterization of PVA composite films reinforced with MCC, SMCC and silica with emphasis on their structural, thermal and mechanical properties. Chapter 8 examines PVA/SMCC-ZnO composite film with respect to application-oriented properties including UV absorption, surface wettability, antibacterial activity and moisture barrier performance. The work presented in this thesis aims to contribute the development of sustainable polymer composite materials through the effective utilization of biomass-derived reinforcements.

Chapter 1
Introduction

1.1 Understanding Polymers

1.1.1 From Plastic to Progress: How do polymers influence our daily lives?

The 'intimacy' of men with polymer has begun with the evolution of life itself, since the polymers like proteins, RNA and DNA played a crucial role in the origin and evolution of life. Polymers provide us food in the form of carbohydrates, proteins, lipids, etc. Nylon, poly esters, etc., are used for making wide range of clothing materials [1]. Polymers are widely used in electronic industries for developing flexible electronic displays, solar panels, batteries, capacitors, insulations, etc. [2]. Transportation became easier and faster with the use of rubber, light weight polymers such as polycarbonates [3]. Polyethylene (PE), Polypropylene (PP), Polyethylene Terephthalate (PET), etc., are used for making packaging materials, bottles, bags, food containers, etc. Medicine and health care became safer and cheaper with the use of polymer-based syringes, catheters, prosthetics, etc. [4]. Drug delivery became more efficient with the use of polymer encapsulated drugs. Biodegradable polymers like Polylactic Acid (PLA) and Polyglycolic Acid (PGA) promotes easy healing of wound and they get absorbed by the body [5]. Building materials became safer, cheaper and more durable due to the intervention of polymers in the construction field [6].

Polymeric membranes are widely used to remove contaminants and to purify water [7]. Classical household materials like cushions, mattresses, furniture, etc., are replaced by polymers like Polyurethanes. Nowadays, superior quality polymer-based sponges, cleaning wipes, trash bags, etc. are available in the market [8]. Textured smoothness of shampoos and conditioners improved with the use of polymers [9]. Polymers are used as emulsifier, moisturiser, and gelling agent in creams and lotions. Polymers like hydrogels are used as scaffold for tissue engineering and tissue regeneration [10]. Polymer based test strip microfluid devices are developed to test

and monitor the diseases [11]. As a whole, polymer is a versatile material whose impact is big in all aspects of life. They conquered almost all fields including pharmaceuticals, health care, electronics, transportation, construction, food packaging, etc. Owing to their high mechanical strength, flexibility, cost effectiveness, etc., polymers play a leading role in the field of material science.

1.1.2 What are Polymers?

Polymers are giant complex molecules with high molecular weight, made up of large number of monomers. Monomers are chemically bonded to form long chain or network of polymers. Diversity in property is the main advantage of polymers. Depending upon the nature of monomer and structure of polymers they may be flexible or rigid [12]. Polymers with high molecular weight often have better mechanical properties. Linear polymers have high density and close packed structure. Branched chain polymers have low density, lower mechanical strength but higher flexibility. On the other hand, cross linked polymers have high rigidity, thermal stability and show high chemical stability. Some polymers are soluble in certain solvents whereas others do not. The solubility depends on the chemical structure, molecular weight and phase interaction between the polymer and solvent molecule. The presence of polar functional groups such as -OH, -COOH, -CO-, etc., in polymers will favour the solubility in polar solvents like water and alcohol. Thus, Polyvinyl Alcohol (PVA), Polyethylene Glycol (PEG), Polyvinyl Pyrrolidone (PVP), etc., are soluble in water. Some polymers such as PE, PVA, etc., are electrical insulators whereas polymers like Polyaniline and Polythiophene shows conductivity hence they are used in electronic devices [13]. Thermoplastic polymers such as PE, PVC, etc., can be melted and re-moulded without changing its chemical nature. However, the thermosetting plastics undergo chemical changes when heated and cannot be re-moulded. Epoxy resins, phenolic resins, etc., are examples of thermosetting plastics. The polymers like PVA are known to be hydrophilic polymers since, they can absorb water and swell on exposure to moisture. Whereas, the hydrophobic polymers such as PE, PP, etc., do not absorb water and repel moisture. Polymer like Polymethyl Methacrylate (PMMA) is transparent and their colour can

be modified by adding dyes or pigments. Some polymers like PVC undergoes degradation on exposure to UV light, however, the polymers like PP are resistant to degradation. Polymers show variation in crystallinity. They may be crystalline, amorphous or semi-crystalline. Biodegradable polymers like PLA, PVA, etc., are environmentally friendly; on the other hand, majority of polymers are non-biodegradable and they raise environmental concerns. Thus, polymers are versatile materials with wide range of properties and selection of polymers depends on our needs.

1.1.3 Classification of Polymers

Polymers are classified based on their source, structure, thermal behaviour, composition, biodegradability, etc. Based on origin, polymers may be natural (eg: -Rubber), semi-synthetic (eg:-Rayon) or synthetic (eg:-Polyethylene). Structurally, there are linear (eg:-Polyethylene), branched (eg:-LDPE) and cross-linked (eg:-Bakelite) polymers. Polymers are formed by addition (eg:-Polyethylene) and condensation (eg:-Nylon) polymerisation methods. Based on thermal behaviour polymers are classified into thermoplastics (eg:-PVC) and thermosetting plastics (eg:-Bakelite). Based on compositions polymers are homopolymers (eg:-PVC) or copolymers (eg:-Buna S). Polymers can also be classified based on their mechanical behaviour. They may be rigid polymers (eg:-Polystyrene) or flexible (eg:-Polyethylene). Some of the polymers are biodegradable (eg:-PVA) some others are non-biodegradable (eg:-Polyethylene). Based on surface characteristics, polymers are classified into hydrophilic (eg:-PVA), hydrophobic (eg:-PVC) or super hydrophobic (eg:-PTFE).

1.1.4 Limitations of Synthetic Polymers

Synthetic polymers such as Polyethylene, Polypropylene and Polystyrene are widely used because of their durability, excellent mechanical properties, chemical resistance and cost-effectiveness. However, most synthetic polymers pose significant environmental challenges. Since, they are primarily derived from non-renewable fossil resources, they are resistant to natural degradation, leading to persistent environmental pollution, plastic waste accumulation and greenhouse gas emissions.

Improper disposal and inadequate waste management have resulted in accumulation of large quantities of plastic debris in aquatic and terrestrial environments. Marine ecosystems are severely affected by plastic pollution through entanglement, ingestion and disruption of food web. Environmental weathering transforms plastic waste in to micro plastic and nano plastic which pose potential risks to ecosystem and human health. These environmental concerns have accelerated research into biodegradable and bio-based polymeric materials that can reduce long-term ecological impact while maintaining desirable functional properties.

1.1.5 Biodegradable Polymers

Polymers due to its wide applications, have become an essential part of our daily life. Most of the polymers that we use in daily life are non-degradable and have huge impact on the environment. Therefore, studies must be focused on the development of environmentally friendly biodegradable polymers. Biodegradable polymers are materials that can be used for a limited time and then degrade to simple, non-toxic substances by the action of heat, water or other natural environmental factors. Traditional plastics take hundreds of years for degradation, whereas biodegradable polymers degrade within a short period, and the products are natural substances like H_2O, CO_2 and biomasses. Thus, we can save our earth, rivers, lakes and oceans from the pollution of plastics.

Most of the biodegradable polymers are derived from renewable sources such as plants (starch, cellulose), agricultural wastes or from animals like sea shells. They are superior to conventional plastics in use since it reduces fossil fuel dependency. Moreover, the amount of greenhouse gases produced during the production of biodegradable polymers are less compared to the conventional plastics which are derived from petroleum products.

The biodegradability of polymers depends on different factors. If the polymer has hydrolysable linkages, they undergo degradation easily. Amorphous polymer undergoes more degradation than crystalline polymer. Degradability is low for the polymer having high melting point [14]. Biodegradability of polymer decreases with increase in molecular weight [15].

1.1.5.1 Classification of Biodegradable Polymers.

Based on their origin, chemical structure, biodegradation mechanism, physical state, applications, etc., biopolymers are classified into different categories.

Based on origin

1. Natural biodegradable polymers

- Polysaccharides (eg: starch, cellulose, chitosan)
- Polypeptides (Eg: gelatine, collagen, casein and wheat gluten)
- Natural Rubber

2. Synthetic biodegradable polymers

- Aliphatic Polyesters (PLA, PGA, Poly Caprolactone)
- Polyhydroxy Alkanoates, Polyurethanes, Polyvinyl Alcohol

1.1.5.2 Applications of Biodegradable Polymers.

The use of biodegradable polymer is rapidly growing due to their environmental benefits and ability to decompose naturally within a short time. Some of the important applications of biodegradable polymers are given below.

1- Packaging

The polymers like PLA and PHA are widely used to make eco-friendly food packaging containers, films and wrappers [16]. Nowadays, one-time-use materials like disposable cups, plates, cutlery straws are manufactured using biodegradable polymers.

2-Medical and pharmaceuticals

Since biodegradable polymers are biocompatible with human body, they are widely used in drug delivery system and implantable devices [17]. They degrade in the body and releases drugs in controlled manner.

3-Agriculture

Agricultural mulch films are made up of PHA and PLA and they decompose after use [18]. Controlled release of fertilizers is possible by biodegradable polymer coating. Biodegradable pots are used for germination of seeds, which allows the easy transplantation to the soil.

4-Textiles

Polymers like PHA and PLA are used for making biodegradable fabrics [19]. Starch based polymers and cellulose derivatives are used in clothing and upholstery.

5-Food industry.

Protein based and starch-based biodegradable polymers are used as edible coating over the fruits and vegetables, so that their shelf life can be extended [20].

6- Cosmetics and Personal care.

Biodegradable polymers are used in formulations like creams, lotions and sprays [21] .

7-Enviornmental remediations.

PVA can be used to remove contaminants in water treatment process [22]. Some other polymers are also used to absorb or degrade oil and other pollutants in water bodies [23]

1.1.5.3 Limitations of Biodegradable Polymers

Though biodegradable polymers have numerous environmental benefits, it has several limitations also.

- Compared to conventional petroleum-based polymers, biodegradable polymers require more expensive raw materials and processing cost is also high [24].
- The mechanical properties such as tensile strength, flexibility, etc., of most of the biodegradable polymers are low compared to conventional polymers.

Moreover, some of them are brittle, making them unsuitable for many applications [25].

- Some biodegradable polymers require special environmental conditions such as heat, moisture or microbes for degradation. In external environment they degrade slowly or not at all. In some other cases, polymers may not degrade completely, and the residue will become an environmental problem. Some fillers added to improve the properties of such polymers will also slow down the degradation process [26].

- The polymers like PLA are very sensitive to harsh environmental conditions such as heat, humidity or UV light. Therefore, they are unsuitable for outdoor applications [27].

- If the raw material used for production of biodegradable polymer is corn or sugarcane, there will be significant emission of greenhouse gases.

- Some biodegradable polymers like PHA requires specialized industrial waste management facilities for proper degradation. But this may not be available at all circumstances [28].

- If the degradation take place in unfavourable conditions, there will be possibility of production of harmful byproducts.

- Currently there is no standardized testing for biodegradable polymers.

- Though people buy biodegradable polymers, most of them are not aware of proper disposal methods [29].

- Performance of biodegradable polymers are not impressive compared to traditional polymers. They are less heat resistant, more brittle, susceptible to chemical attack, etc.

These limitations suggest that while biodegradable polymers are addressing the plastic pollution, they are not a perfect solution. So, research should be intensified

in the area to develop more powerful, cost-effective and easily biodegradable polymers

1.1.6 Polymer Composites

The limitations of biodegradable polymers can be mitigated by converting them into composites. Polymer composites are materials formed by combining the polymer with reinforcing agent such as fibres or particulates. It consists of fillers embedded in matrix. The properties of the polymers such as strength, stiffness, durability and thermal stability will be enhanced during the composite formation. Composites are usually heterogeneous and anisotropic. Polymer composites have several advantages over pure polymers in the following aspects.

- By adding fillers, mechanical properties like tensile strength, flexural strength and stiffness can be enhanced [30].
- Polymer composites show better resistance to wear and tear, and they can resist UV radiation, chemical and harsh environmental conditions.
- Polymer composites are lighter and stronger than some metals, thus they can be used in aerospace and automotive sectors.
- By changing the type and amount of filler, the material with desired properties can be developed.
- Filler can improve thermal and electrical properties of polymers [31].
- Composites show better dimensional stability and they are less likely to wrap, shrink or deform when exposed to environmental changes like temperature, fluctuations or moisture [32].
- Some composites have excellent vibration damping properties [33]. Thus, they are used in automotive parts.
- Polymer composites made of bio-based polymers are more sustainable compared to traditional materials like metals [34].

- Polymer composites exhibit lower creep compared to pure polymer, since they resist long-term load conditions [35].

- In the aesthetic aspects, polymer composites are better than metals. The product with intricate geometries, and variety of finish options are extensively used in consumer products, automobiles and architectural applications [36].

As mentioned earlier, polymer composites usually contain polymer matrix and reinforcement, the influence of these components on performance of composites are discussed below.

1.1.6.1 Polymer matrix

It is the continuous phase that holds composites together. The function of matrix is to distribute the constraints and loads, protect the reinforcement, gives chemical resistance and desired shape to the final product. It may be thermoplastics like Polypropylene, Polyethylene, Polyoxyethylene, Polyether Ketones, Polyether Imide, etc. The commonly used thermosetting matrices are Epoxy resins, Phenolic resins, Urea Formaldehyde resins, Melamine Formaldehyde resins, Polyurethanes, silica resins, Polyamides, etc. Elastomers can also act as matrix. Examples are Rubber, Synthetic Rubber such as Styrene Butadiene, Polybutadiene Rubber, Nitrile Butadiene Rubber, Silicone Rubber, etc.

Favourable characteristics of matrix.

- It should have sufficient strength to complement the reinforcements. It should be capable for preventing cracking and should have adequate elasticity to hold the reinforcement together.

- Matrix should be compatible with the corresponding reinforcement and there should be strong interfacial bond.

- Usually, composites are produced by the thermal process. Therefore, all the matrix should have enough thermal stability and their thermal expansion coefficient should match with the reinforcement.

- Matrix should be resistant to chemicals and environmental factors like moisture, UV light, etc.
- Matrix should have medium viscosity.
- Finally, the cost is an important parameter in selecting the matrix.

Selection of the proper matrix is very important so as to get specific properties for required applications. In the current study, we focus on the use of biodegradable matrix. Biodegradable matrix is used to get sustainable and eco-friendly products. They break down within a specific time to give nontoxic product. They are derived from renewable resources and they can be easily processed to give various shapes.

Commonly used biodegradable polymers are: -

1-Natural polymers

- Polysaccharides eg: starch [37], cellulose [38]
- Protein eg: - gelatine [39], casein [40].
- Others eg: - chitosan [41], alginate [42].

2-Synthetic polymers

- Polylactic Acid (PLA) derived from sugarcane or cone [43].
- Polyhydroxy Alkanoates (PHAs) produced by bacteria [44].

3-Petroleum based polymer.

- Poly Caprolactone (PCL) [45]
- Polybutylene Adipate-co- Terephthalate (PBAT) [46]
- Polyhydroxy Butyrate -co-Valerate (PHBV) [47].

4-Blend of natural and synthetic polymers

- Starch – PLA blend [48],
- Cellulose-PCL-PLA blend [49].

1.1.6.2 Reinforcement

These are the constituents in the polymer composites, which enhances the mechanical strength, thermal stability and other physical properties. It may be filamentary in nature (organic or inorganic) or particles. The main types of reinforcements are: -

Fibre reinforcements: -

i) Glass fibres [50]

- Widely used in thermosetting plastic composites
- Good strength-to-weight ratio
- Low cost

ii) Carbon fibres [51]

- Used in thermosetting composites
- Provide high tensile strength, thermal stability and superior rigidity
- Provide thermal conductivity
- More expensive than glass fibres
- Used to make aerospace, automobiles and sporting goods.

iii) Aramid fibres [52]

- Also known as Aromatic Polyamide fibres
- Best example: KELVAR synthesised by poly condensation of Terephthaloyl Chloride with para-Phenylene Diamine
- Used in applications like ballistic protection, safety gears and automotive components.

iv) Natural fibres

- Derived from renewable sources
- Used to make biodegradable light weight composites
- It is less expensive compared to others
- Does not produce toxic fumes during processing or disposal

- Plant based fibres (eg: -hemp [53], flax [54], jute [55])
- Animal based fibres (eg: -wool [56])

Particulate reinforcement: -

i) Inorganic fillers

- Most common type of particular fillers and its source is minerals
- Cost effective and enhance electrical, mechanical and thermal properties
- Examples:
  Silica: fumed silica or precipitated silica. Enhance thermal stability and electrical insulation [57] $CaCO_3$: Improve stiffness, dimensional stability and impact resistance [58].

  Talc: Silicate mineral that provides flow properties [59].

  Clay: Natural clay (bentonite and kaolin) and modified clay (organoclay) are used [60]

ii) Organic fillers

- Derived from natural or synthetic organic sources
- Examples:
  Wood fillers: Ground wood particles, they reduce the weight of polymer composites [61]
- Cellulose: Derived from plants. It is widely used in polymercomposites [62]

iii) Metal fillers

- Examples: Al_2O_3: Improve hardness, wear resistance, thermal conductivity [63]
  Copper and Bronze powder: enhance electrical and thermal conductivity [64]

iv) Nanomaterials

- Nano clays, carbon nanotubes, graphene and other nanomaterials [65]
- They improve the mechanical, thermal and electrical properties.

1.1.7 Polyvinyl Alcohol (PVA)

Polyvinyl alcohol is a biodegradable, water soluble, synthetic polymer produced by the hydrolysis of Polyvinyl Acetate (PVAc). PVAc is prepared by the polymerization of Vinyl Acetate monomer (CH_2=CH-$OCOCH_3$). During hydrolysis, acetate groups are converted to -OH groups. The degree of hydrolysis and molecular weight of polymer can be controlled during the process, thus PVA with different molecular weights, water solubility and mechanical properties can be synthesised [66]. Fully hydrolysed PVA contains more -OH group and they are highly soluble in water, whereas, partially hydrolysed PVA is less soluble in water. The PVA having high molecular weight is resistant to dissolution in water and requires more time and energy for dissolution. The PVA having low molecular weight dissolves very easily in water, since small polymer chain can move freely in water and viscosity of solution will not increase much during dissolution. Temperature also has significant effect on the solubility of PVA. Based on this, PVA is classified into Hot water soluble PVA (HPVA) and Cold water soluble (CPVA). The comparative properties of HPVA and CPVA are given in **Table 1.1**

Table 1.1 Comparative Properties of HPVA and CPVA

HPVA	CPVA
• Dissolves in hot water (Above 80°C) • Polymer chains are longer and are less hydrolysed • It has higher molecular weight • Forms more viscous solution • Less susceptible to biodegradation • More expensive and harder for processing since it requires high temperature • Used for making hot water-based adhesive, packing films and in textiles industries	• Dissolves in cold water (below 30^0) • Polymer chains are shorter and are more hydrolysed • Usually, it has low molecular weight • Forms less viscous solution • Undergo degradation very easily • Easier for processing and production cost is low • Used for making water soluble films for pharmaceutical capsules and laundry bag

Applications of Polyvinyl Alcohol

Polyvinyl Alcohol is widely used for different applications due its water solubility, film-forming ability and biocompatibility. Since it is water soluble, it is used for making single use packaging such as laundry pods or detergent pods [67]. It is used as sizing agent to increase the strength of fabrics [68]. It is used in adhesives such as school glue and wood glue [69]. It has application in medical field also. It is used as eye drops, wound dressing, and drug delivery system [70]. Since PVA acts as flocculant, it is used for water treatment [71]

Though it has a lot of advantages and applications, it has some limitations also

1- PVA films are not strong as other synthetic polymers.
2- Compared to other polymers, it is more expensive.
3- It is water sensitive and absorbs moisture, so film formed by PVA may break down or dissolve [72]

These disadvantages can be addressed by converting them into composites, so that tensile strength, thermal stability, water resistance, etc., can be enhanced.

1.2 Microcrystalline Cellulose (MCC)

MCC is a purified form of cellulose generally derived from wood pulp, cotton or other plant-based resources [73]. Here glucose units are connected by β-1,4-glycosidic bonds. Cellulose consists of long and linear chain of glucose units. It has crystalline and amorphous regions. On chemical treatment, amorphous region will be removed, leaving behind crystalline region. MCC is a white, odourless and tasteless powder. It is insoluble in water but absorbs the water, swells and forms gel at high concentration. Depending upon the method of synthesis, MCC with varying particle sizes are obtained. Even though MCC appears as fine powder, its particles have irregular shape due to its natural structure. Their bulk density is low compared to other fillers, so it has wide applications in forming lightweight materials. MCC is chemically inert but it reacts with strong acids and bases. MCC remains stable in the broad range of pH. It is a good binder and holds the ingredients together. MCC is less

compressible and thermal stability is good, therefore it can withstand up to 250 ^{0}C temperature during manufacturing.

MCC retains water even at high temperature, therefore it is used in food products where moisture retention is important. MCC is indigestible by humans, so it passes through the digestive tract without being absorbed. Hence it is considered as a good dietary fibre, alleviate constipation problem and good for gut health [74]. MCC is a biodegradable material, therefore it is a good choice for making sustainable packaging and biodegradable product. MCC has high surface area, therefore it is used as efficient binder, filler or absorbent. MCC can interact electrostatically with positively charged ions, therefore it can act as ion exchangers [75]. During chemical treatment, lignin and hemicellulose is removed, hence it is considered as highly pure. The surface of MCC contains large number of -OH groups, therefore it can undergo chemical reactions and can be modified very easily. Carboxymethyl Cellulose [76], Hydroxypropyl Cellulose [77], Ethyl Cellulose, etc. are modified forms of MCC.

Applications of MCC

MCC is widely used in pharmaceuticals, foods, polymers and personal care industries due to its biodegradability, non-toxicity, high surface area and excellent binding properties**.** MCC is used as binder, diluent and disintegrant in the formulation of tablets and capsules [78]**.** It is used as stabilizers, emulsifiers and thickening agents in food products like ice creams, salads, bakery foods and cosmetics [79]**.** MCC is used as mild exfoliant in skin care products and when it is added to paper, the resistance to wear and tear of the paper will be improved [80]**.** MCC is an important reinforcement in biodegradable plastics [81]. Since MCC has the capacity to water retention, it is used as soil conditioner and promote plant growth [82]**.** Its abrasive properties, make it advantageous in scrubber and other cleaning products**.** MCC is added to wound care products, since it has the ability to absorb moisture [83]. MCC added to paints and coatings to improve the smoothness and easiness of their application [84]. Absorption power of MCC makes it useful in absorbing oils or other hydrophobic substances.

While MCC is a highly valuable filler due to its excellent binding, compressibility and stability characteristics, it has some practical limitations also. MCC is hydrophilic but most of the polymers are hydrophobic and this will lead to poor interfacial adhesion between MCC and polymer matrix when they are used as filler in polymer composites [85]. Moreover, MCC tends to agglomerate due to hydrogen bonding and this will result in the formation of heterogeneous composite. It absorbs moisture from the environment and this will lead to dimensional instability, microcracking and interface weakening. Up to a certain limit of loading, MCC improves mechanical properties, beyond this point MCC reduces tensile strength and impact resistance, since excessive filler creates discontinuous phase [86]. MCC has lower degradation temperature compared to other polymers, therefore there is possibility of damage in cellulose structure if conditions are not carefully controlled during processing.

1.3 Nanosilica

Silica (SiO_2) is one of the most abundant inorganic compounds found on earth. It exists in both crystalline forms such as quartz, tridymite, etc., and amorphous forms such as silica gel, colloidal silica, etc. The crystalline silica exhibits well defined lattice arrangements, whereas amorphous silica shows irregular packing of atoms without long-range order. Therefore, physical and chemical properties of crystalline and amorphous silica are different. If the size of silica particles is within the range of 1-100 nm, they are referred to as nanosilica. The properties of nanosilica are remarkably different from bulk silica due to the quantum size effect and high surface-to- volume ratios. The amorphous silica is preferred over crystalline silica in the field of material science due to its greater processing flexibility and lower heath risk [87]. At nanoscale, amorphous silica contains abundant silanol groups on its surface, which can be easily modified by physical and chemical treatment.

Silica is abundantly found in geological sources such as quartz, sand clays and soil minerals. However, silica can be produced from some plants and animals and is referred to as bio silica. The agricultural wastes, such as rice husks and sugarcane bagasse, are rich sources of silica and can be extracted from them through chemical

and thermal treatments. This valorisation helps to reduce waste and enables cost-effective and eco-friendly production of nanosilica with desirable characteristics.

Applications of Nanosilica

Nanosilica is widely used in different fields due to its versatile physical and chemical characteristics. Some of the applications are given below

- Nanosilica is used as filler in polymers to improve the mechanical properties such as hardness, tensile strength, wear resistance and stiffness. Nanosilica enhances the stress transfer ability when it is immersed in polymers [88].
- Mesoporous silica with controlled pore size supports catalysis and enhance the selectivity and reaction efficiency [89].
- Functionalised nanosilica is used for controlled targeted drug delivery. Its large surface area and predefined pore structure improve the drug loading and release profile [90].
- When nanosilica is added to coatings and paints the properties such as abrasion resistance and scratch resistance will be improved. It acts as a protective layer and improves the durability [91].
- Nanosilica is added to cement, concrete and mortar to improve compressive strength, durability and density [92].
- Functionalised nanosilica is used for adsorbing pollutants, purifying contaminated water, soil treatment, etc. [93].
- Silica based materials are used in skin care, hair care and other cosmetic products [94].

While nanosilica provides high surface area, enhanced mechanical reinforcements and tuneable surface energy, it has some practical challenges also. Nanosilica is prone to agglomeration when dispersed in solvents or matrices.

Therefore, homogeneous dispersion in polymers and other host matrix is challenging. To improve the compatibility with polymers some modification has to be performed.

1.4 Silicified Microcrystalline Cellulose (SMCC)

The properties of microcrystalline cellulose can be improved by silicification. It gives the structural benefits of MCC and functional properties of silica [95]. SMCC is widely used in pharmaceuticals and food applications [96]. SMCC has better properties than MCC and are given below-

- SMCC has better flowability than MCC. Silica particles reduce the friction between MCC particles and improve the flowability of powder [97]. Thus, powder flows more easily during processing, provides uniform mixing and better batch-to-batch consistency. As a filler in polymer composites, better flowability of SMCC will help in the better dispersion of fillers in the matrix and reduce the chance of clamping or agglomeration. Thus, the consistency of the properties throughout the material can be ensured.

- Compressibility of SMCC is higher than that of MCC, which is advantageous as a filler in polymer composites [98]. Better compressibility allows SMCC particles to pack more efficiently within the matrix. Thus, mechanical properties like tensile strength or stiffness will be improved. Moreover, the gap between the fillers will be reduced, and it will also improve the structural integrity and provide better performance. This property also helps to get smooth finished product and possibility of shrinkage during cooling can be minimized.

- Thermal stability of SMCC is higher than that of MCC. Thus, the polymer composites consisting SMCC filler will degrade at higher temperature. This property is beneficial in the applications such as automotives or electronic devices. Moreover, the coefficient of thermal expansion will be low and this will give dimensional stability under various conditions.

- SMCC has the ability to control moisture, which will reduce swelling, degradation and changes in medicinal properties at humid environment.
- SMCC will improve the dielectric properties of the composites. Thus, SMCC polymer composites will be useful for making insulation materials like cables, connectors, etc.
- SMCC is derived from cellulose, which is a renewable source and biodegradable. Thus, SMCC polymer composites will be more sustainable and environmentally friendly.
- Bulk density and true density of SMCC will be higher than that of MCC [99].

Applications of SMCC

- Since SMCC is biodegradable, it is used for making eco-friendly packaging materials.
- SMCC can be used as a filler in textile industry. It improves the mechanical strength and durability of fibres. It will also improve the smoothness of the fabrics.
- Since SMCC has excellent flowability, it can be used for making cosmetics and personal care products.
- SMCC is widely used as binders and fillers in tablet manufacturing. Its excellent compressibility, flow properties and moisture control ability would improve the consistency and stability of tablets.
- SMCC based composites can be used for making food packaging materials.
- It can be used for adsorbing both hydrophilic and hydrophobic materials, since it has MCC and silica.

1.5 Zinc Oxide Nanoparticles

Zinc Oxide (ZnO) is a white, odourless powder, insoluble in water but soluble in acids and bases. It has a hexagonal wurtzite crystal structure, which gives mechanical stability and structural rigidity. It acts as a semiconductor with wide band gap. Therefore, ZnO exhibits strong absorption in the UV region and shows transparency in the visible region. Additionally, ZnO shows luminescence, which is exploited in optoelectronic applications. ZnO is chemically inert and thermally stable, it reacts with acid to form salt and form zincate when it reacts with base. Zinc oxide can be produced in a variety of nanostructured forms such as nanoparticles, nanorods and nanowires. Zinc Oxide nanoparticles have dimensions less than 100nm, with high surface-to-volume ratio. This will increase the chemical reactivity and interfacial interaction with polymers.

Applications of Zinc Oxide Nanoparticles

- Due to the inherent ability to absorb and block UV radiation, ZnO particles are widely used in sunscreens and personal care products [100].
- ZnO particles show strong antimicrobial activity against a wide range of bacteria and fungi. Therefore, it is used in food packaging and preservations [101].
- ZnO nanoparticles have high photocatalytic activity, therefore it is used in wastewater treatment since they can degrade organic pollutants and dyes[102].
- Fabrics coated with ZnO provide UV protection, antibacterial properties and deodorizing effect [103].
- The semi-conductivity and surface properties of ZnO makes it useful in gas sensors, biosensors, UV photodetectors, etc. [104].
- Polymer composites incorporated with ZnO nanoparticles enhance thermal stability, UV shielding, antimicrobial behaviour and barrier performance [105].

1.6 Scope and Overall Objectives of the study

Mission Grass (*Pennisetum polystachion*) is an aggressive, invasive weed, widely grown in tropical and subtropical regions of the world. It may be used as cattle feed and prevent soil erosion, but its rapid growth outcompetes the native plants and causes negative impact on ecology. Moreover, it is a big threat to agriculture and spread wild fire quickly. But it is a good source of biosilica. Silica is stored in the cell wall in the form of phytoliths. By changing the calcination temperature, both crystalline and amorphous silica can be extracted. Once silica is extracted, it can be used for the production of silica gel, construction of materials, agricultural products, cosmetics, etc. Valorisation of silica can control the invasive species like MG, and it can be used as a renewable source of biosilica.

Microcrystalline cellulose is a purified, partially depolymerized form of cellulose produced by removing the amorphous region from the cellulose. Different sources are used for the extraction of MCC. In the current study, we used locally available Screw Pine leaves (*Pandanus tectorius*) as the source of MCC, which is completely biodegradable and renewable. Screw Pine is a morphologically variable species distributed in Pacific Islands, South Asia, and Northern Australia. In India, it is widely grown in the Western Ghats, the Himalayas and Andaman Nicobar Islands. In this study, we focus on the determination of the composition of Screw Pine leaves. MCC have some disadvantages such as low bulk density, poor solubility in aqueous and other polar solvents and low compressibility. Moreover, the interaction between MCC and polymer matrix is weak, and it will affect the overall performance of polymer composites. Due to its fibrous and crystalline structure, it is difficult to disperse MCC evenly in polar matrix. MCC degrades at high temperature and it limits its use at high temperature. The crystalline nature of MCC sometimes makes the polymer brittle and prone to degradation under UV light. This limitation can be addressed by the modification of MCC. Here, silicification of MCC is carried out through a novel method. The MCC extracted from Screw Pine leaves is dispersed in sodium silicate solution obtained from Mission Grass. This on acid hydrolysis silicified MCC is obtained.

Polyvinyl Alcohol is a synthetic polymer, made by the polymerisation of vinyl acetate followed by hydrolysis. It is a water soluble, non-toxic, biodegradable polymer with a lot of synthetic and industrial applications. But it has low mechanical strength, thermal stability, water sensitivity, poor UV stability, low chemical resistance, etc. This limitation can be overcome by converting it into composites. In the current study, PVA composites are prepared by adding MCC, silica and SMCC as fillers. Since MCC is not fully compatible with PVA due to weak interfacial interaction between them, silicified MCC is a better choice. Moreover, if pure silica is added to PVA, there will be agglomeration, possibility of cracking and swelling. In this study, blend of hot water-soluble and cold water-soluble PVA is used as a matrix and their properties were compared. In order to get better applications, PVA/SMCC-ZnO composite films are also prepared and studied.

The overall objectives of the research are: -

- Extraction of amorphous and crystalline nano silica from Mission Grass through appropriate techniques.
- Characterisation of the extracted silica using FTIR, TG, XRD, FESEM, etc.
- Isolation of holocellulose, α-cellulose and MCC from Screw Pine leaves, followed by quantitative determination of their percentage composition.
- Structural, thermal and morphological characterisation of isolated cellulose fractions using FTIR, TG, XRD and FE-SEM and compare their properties.
- To synthesise Silicified Micro Crystalline Cellulose using MCC isolated from Screw Pine leaves and sodium silicate solution extracted from Mission Grass.
- Determination of bulk density, true density, and porosity of silica, MCC and SMCC by the solvent displacement method.
- To perform FTIR, XRD, TG and FE-SEM analysis of silica, MCC and SMCC and to comparatively evaluate their properties.

- Fabrication of PVA/MCC, PVA/Silica and PVA/SMCC films, followed by comparative evaluation with bare PVA film.
- Structural, thermal, morphological and mechanical characterisation of all prepared films using XRD, FTIR, TG, FE-SEM and UTM, along with systematic comparison.
- Preparation of PVA/SMCC20 films with different compositions, followed by detailed comparison of mechanical properties.
- Fabrication of PVA/SMCC-ZnO composite films and evaluation of their optical properties, hydrophobicity, mechanical properties, Water Vapour Transmission Rate, etc., with comparative assessment against other developed films

References

[1] Deopura BL, Padaki N V. Synthetic Textile Fibres: Polyamide, Polyester and Aramid Fibres. Textiles and Fashion: Materials, Design and Technology, Elsevier Inc.; 2015, p. 97–114. https://doi.org/10.1016/B978-1-84569-931-4.00005-2.

[2] Dhanasekar S, Stella TJ, Thenmozhi A, Bharathi ND, Thiyagarajan K, Singh P, et al. Thiyagarajan K, Singh P, et al. Study of Polymer Matrix Composites for Electronics Applications. J Nanomater 2022;2022. https://doi.org/10.1155/2022/8605099.

[3] Koniuszewska AG, Kaczmar JW. Application of polymer based composite materials in transportation. Prog Rubber Plast Recycl Technol 2016;32(1):1–24. https://doi.org/10.1177/147776061603200101.

[4] Kiminami H, Krueger AB, Abe Y, Yoshino K, Carpenter JF. Impact of Sterilization Method on Protein Aggregation and Particle Formation in Polymer-Based Syringes. J Pharm Sci 2017;106:1001–7. https://doi.org/10.1016/j.xphs.2016.12.007.

[5] Daristotle JL, Lau LW, Erdi M, Hunter J, Djoum A, Srinivasan P, et al. Sprayable and biodegradable, intrinsically adhesive wound dressing with antimicrobial properties. Bioeng Transl Med 2020;5. https://doi.org/10.1002/btm2.10149.

[6] Shen J, Liang J, Lin X, Lin H, Yu J, Yang Z. Recent progress in polymer-based building materials.Int J Polym Sci 2020;2020. https://doi.org/10.1155/2020/8838160.

[7] Bassyouni M, Abdel-Aziz MH, Zoromba MS, Abdel-Hamid SMS, Drioli E. A review of polymeric nanocomposite membranes for water purification. J. Ind. Eng. Chem. 2019;73:19–46. https://doi.org/10.1016/j.jiec.2019.01.045.

[8] Pecquet A, McAvoy D, Pittinger C, Stanton K. Polymers Used in US Household Cleaning Products: Assessment of Data Availability for Ecological Risk Assessment. Integr Environ Assess Manag 2019;15:621–32. https://doi.org/10.1002/ieam.4150.

[9] Alves TFR, Morsink M, Batain F, Chaud M V., Almeida T, Fernandes DA, et al. Applications of natural, semi-synthetic, and synthetic polymers in cosmetic formulations. Cosmetics 2020;7. https://doi.org/10.3390/COSMETICS7040075.

[10] Yu C, Yao F, Li J. Rational design of injectable conducting polymer-based hydrogels for tissue engineering. Acta Biomater 2022;139:4–21. https://doi.org/10.1016/j.actbio.2021.04.027.

[11] Fang CC, Chou CC, Yang YQ, Wei-Kai T, Wang YT, Chan YH. Multiplexed Detection of Tumor Markers with Multicolor Polymer Dot-Based Immunochromatography Test Strip.Anal Chem. 2018 Feb 6;90(3):2134-2140. https://doi.org/10.1021/acs.analchem.7b04411.

[12] Tsvetkov, V. N. The structure of the monomer unit and the flexibility of rigid chain polymer molecules. Review. Polymer Science U.S.S.R. 1977, *19*(10), 2485–2508. https://doi.org/10.1016/0032-3950(77)90329-X

[13] Sumdani MG, Islam MR, Yahaya ANA, Safie SI. Recent advancements in synthesis, properties, and applications of conductive polymers for electrochemical energy storage devices: A review. Polym Eng Sci 2022;62:269–303. https://doi.org/10.1002/pen.25859.

[14] Lotto NT, Calil MR, Guedes CGF, Rosa DS. The effect of temperature on the biodegradation test. Mater Sci Eng C. 2004;24(5):659–662. https://doi.org/10.1016/j.msec.2004.08.009.

[15] Chandra R, Rustgi R. Biodegradable polymers. Prog Polym Sci. 1998;23(7):1273–1335. https://doi.org/10.1016/S0079-6700(97)00039-7.

[16] Mirpoor SF, Patanè GT, Corrado I, Giosafatto CVL, Ginestra G, Nostro A, et al. Functionalization of Polyhydroxyalkanoates (PHA)-Based Bioplastic with Phloretin for Active Food Packaging: Characterization of Its Mechanical, Antioxidant, and Antimicrobial Activities. Int J Mol Sci 2023;24. https://doi.org/10.3390/ijms241411628.

[17] Doppalapudi S, Jain A, Khan W, Domb AJ. Biodegradable polymers-an overview. Polym Adv Technol 2014;25:427–35. https://doi.org/10.1002/pat.3305.

[18] Othman NAF, Selambakkannu S, Seko N. Biodegradable dual-layer Polyhydroxyalkanoate (pha)/Polycaprolactone (pcl) mulch film for agriculture: Preparation and characterization. Energy Nexus 2022;8. https://doi.org/10.1016/j.nexus.2022.100137.

[19] Mehta S. Biodegradable textile polymers: a review of current scenario and future opportunities. Environ. Technol. Rev. 2023;12:441–57. https://doi.org/10.1080/21622515.2023.2227391.

[20] Galgano F. Biodegradable packaging and edible coating for fresh-cut fruits and vegetables. Ital J Food Sci. 2015;27(1):1–20. https://doi.org/10.14674/1120-1770/ijfs.v70.

[21] Picken CAR, Buensoz O, Price PD, Fidge C, Points L, Shaver MP. Sustainable formulation polymers for home, beauty and personal care: challenges and opportunities. Chem Sci 2023; 14:12926–40. https://doi.org/10.1039/d3sc04488b.

[22] Das L, Das P, Bhowal A, Bhattachariee C. Synthesis of hybrid hydrogel nano-polymer composite using Graphene oxide, Chitosan and PVA and its application in waste water treatment. Environ Technol Innov 2020;18. https://doi.org/10.1016/j.eti.2020.100664.

[23] Xue Z, Sun Z, Cao Y, Chen Y, Tao L, Li K, et al. Superoleophilic and superhydrophobic biodegradable material with porous structures for oil absorption and oil-water separation. RSC Adv 2013; 3:23432–7. https://doi.org/10.1039/c3ra41902a.

[24] Luckachan GE, Pillai CKS. Biodegradable Polymers- A Review on Recent Trends and Emerging Perspectives. J Polym Environ 2011; 19:637–76. https://doi.org/10.1007/s10924-011-0317-1.

[25] Doppalapudi S, Jain A, Khan W, Domb AJ. Biodegradable polymers-an overview. Polym Adv Technol 2014;25:427–35. https://doi.org/10.1002/pat.3305.

[26] Maurya AK, de Souza FM, Dawsey T, Gupta RK. Biodegradable polymers and composites: Recent development and challenges. Polym Compos 2024;45:2896–918. https://doi.org/10.1002/pc.28023.

[27] Rasal RM, Janorkar AV, Hirt DE. Poly(lactic acid) modifications. Prog Polym Sci. 2010;35(3):338–356. https://doi.org/10.1016/j.progpolymsci.2009.12.003.

[28] Kalia VC, Singh Patel SK, Shanmugam R, Lee JK. Polyhydroxyalkanoates: Trends and advances toward biotechnological applications. Bioresour Technol 2021;326. https://doi.org/10.1016/j.biortech.2021.124737.

[29] Kim LS, Seo Y. Possibilities and limitations of biodegradable plastics. Biosci eng: int j 2024;11:01–10. https://doi.org/10.5121/bioej.2024.11301.

[30] Hsissou R, Seghiri R, Benzekri Z, Hilali M, Rafik M, Elharfi A. Polymer composite materials: A comprehensive review. Compos Struct 2021;262. https://doi.org/10.1016/j.compstruct.2021.113640.

[31] Kashfipour MA, Mehra N, Zhu J. A review on the role of interface in mechanical, thermal, and electrical properties of polymer composites. Adv Compos Hybrid Mater 2018;1:415–39. https://doi.org/10.1007/s42114-018-0022-9.

[32] Zhang Y, Zhang SY, Yang DQ, Wan H. Dimensional stability of wood-polymer composites. J Appl Polym Sci 2006;102:5085–94. https://doi.org/10.1002/app.23581.

[33] Geethamma, V.G., Asaletha, R., Kalarikkal, N. et al. Vibration and sound damping in polymers. Reson 19, 821–833 (2014). https://doi.org/10.1007/s12045-014-0091-1

[34] Subadra SP, Griskevicius P. Sustainability of polymer composites and its critical role in revolutionising wind power for green future. Sustain Technol Green Econ 2021;1(1):1–7. https://doi.org/10.21595/stge.2021.21974.

[35] Eftekhari M, Fatemi A. Tensile, creep and fatigue behaviours of short fibre reinforced polymer composites at elevated temperatures: A literature survey. Fatigue Fract Eng Mater Struct 2015;38:1395–418. https://doi.org/10.1111/ffe.12363.

[36] Alla RK, Sanka GSSJ L, Saridena USNG, Ramaraju AV, Raju MAKV, Mantena SR. Fiber-Reinforced composites in dentistry: enhancing structural integrity and aesthetic appeal. Int J Dent Mater. 2023;5(3):78–85. https://doi.org/10.37983/IJDM.2023.5303.

[37] Ismail NA, Mohd Tahir S, Yahya N, Abdul Wahid MF, Khairuddin NE, Hashim I, Rosli N, Abdullah MA. Synthesis and characterization of biodegradable starch-based bioplastics. Mater Sci Forum. 2016;846:673–678. https://doi.org/10.4028/www.scientific.net/MSF.846.673.

[38] Guzman-Puyol S, Hierrezuelo J, Benítez JJ, Tedeschi G, Porras-Vázquez JM, Heredia A, et al. Transparent, UV-blocking, and high barrier cellulose-based bioplastics with naringin as active food packaging materials. Int J Biol Macromol 2022;209:1985–94. https://doi.org/10.1016/j.ijbiomac.2022.04.177.

[39] Matonis SJ, Zhuang B, Bishop AF, Naik DA, Temel Z, Bettinger CJ. Edible Origami Actuators Using Gelatin-Based Bioplastics. ACS Appl Polym Mater 2023;5:6288–95. https://doi.org/10.1021/acsapm.3c00919.

[40] Qazanfarzadeh Z, Kumaravel V. Hydrophobisation approaches of protein-based bioplastics. Trends Food Sci Technol 2023;138:27–43. https://doi.org/10.1016/j.tifs.2023.06.002.

[41] Schnabl KB, Mandemaker LDB, Nierop KGJ, Deen OVB, Eefting DD, Vollmer I, et al. Green Additives in Chitosan-Based Bioplastic Films: Physical, Mechanical, and Chemical Properties. ChemSusChem 2023;16. https://doi.org/10.1002/cssc.202300585.

[42] Dalal SR, El-Naggar NEA, El Naeem GA. Biosynthesis of sustainable biodegradable bioplastics using alginate extracted from Padina pavonica, optimization and characterization. Algal Res 2023;76. https://doi.org/10.1016/j.algal.2023.103325.

[43] Rueda-Duran CA, Ortiz-Sanchez M, Cardona-Alzate CA. Detailed economic assessment of polylactic acid production by using glucose platform: sugarcane bagasse, coffee cut stems, and plantain peels as possible raw materials. Biomass Convers Biorefin 2022;12:4419–34. https://doi.org/10.1007/s13399-022-02501-5.

[44] Desouky SE, Shiekh HHE-, Elabd MA, Shehab AM. Screening, Optimization and Extraction of Polyhydroxyalkanoates (PHAs) from Bacillus thuringienesis. J. Adv. Biol. Biotechnol 2014;1(1):40-54. https://10.9734/JABB/2014/12286.

[45] Ali Akbari Ghavimi S, Ebrahimzadeh MH, Solati-Hashjin M, Abu Osman NA. Polycaprolactone/starch composite: Fabrication, structure, properties, and applications. J Biomed Mater Res A 2015;103:2482–98. https://doi.org/10.1002/jbm.a.35371.

[46] Ferreira F V., Cividanes LS, Gouveia RF, Lona LMF. An overview on properties and applications of poly(butylene adipate-co-terephthalate)–PBAT based composites. Polym Eng Sci 2019;59:E7–15. https://doi.org/10.1002/pen.24770.

[47] Mazur K, Kuciel S. Mechanical and hydrothermal aging behaviour of polyhydroxybutyrate-co-valerate (PHBV) composites reinforced by natural fibres. Molecules 2019;24. https://doi.org/10.3390/molecules24193538.

[48] Martinez Villadiego K, Arias Tapia MJ, Useche J, Escobar Macías D. Thermoplastic Starch (TPS)/Polylactic Acid (PLA) Blending Methodologies: A Review. J Polym Environ 2022;30:75–91. https://doi.org/10.1007/s10924-021-02207-1.

[49] Tuancharoensri N, Ross G, Mahasaranon S, Topham P, Ross S. Ternary blend nanofibers of PLA/PCL/CAB for skin tissue scaffolds: Influence of blend ratio and PCL molecular mass on miscibility, morphology, crystallinity and thermal properties. Polymer Int. 2017;66(8):1008–1018. https://doi.org/10.1002/pi.5393.

[50] Sathishkumar TP, Satheeshkumar S, Naveen J. Glass fiber-reinforced polymer composites — a review. J Reinf Plast Compos. 2014;33(13):1258–1275. https://doi.org/10.1177/0731684414530790.

[51] Lionetto F. Carbon fiber reinforced polymers. Materials 2021;14. https://doi.org/10.3390/ma14195545.

[52] Zhang B, Wang W, Tian M, Ning N, Zhang L. Preparation of aramid nanofiber and its application in polymer reinforcement: A review. Eur Polym J 2020;139. https://doi.org/10.1016/j.eurpolymj.2020.109996.

[53] Tanasă F, Zănoagă M, Teacă CA, Nechifor M, Shahzad A. Modified hemp fibers intended for fiber-reinforced polymer composites used in structural applications—A review. I. Methods of modification. Polym Compos 2020;41:5–31. https://doi.org/10.1002/pc.25354.

[54] More AP. Flax fiber–based polymer composites: a review. Adv Compos Hybrid Mater 2022;5. https://doi.org/10.1007/s42114-021-00246-9.

[55] Chandekar H, Chaudhari V, Waigaonkar S. A review of jute fiber reinforced polymer composites. Mater. Today Proc., vol. 26, Elsevier Ltd; 2020, p. 2079–82. https://doi.org/10.1016/j.matpr.2020.02.449.

[56] Bharath KN, Pasha M, Nizamuddin BA. Characterization of natural fiber (sheep wool)-reinforced polymer-matrix composites at different operating conditions. J Ind Textiles. 2016;45(5):730–751. https://doi.org/10.1177/1528083714540698

[57] Alameri I, Oltulu M. Mechanical properties of polymer composites reinforced by silica-based materials of various sizes. Appl Nanosci (Switzerland) 2020;10:4087–102. https://doi.org/10.1007/s13204-020-01516-6.

[58] Rajamuneeswaran S, Vairamuthu J, Nagarajan S, Stalin B, Jayabal S. A comparative study on mechanical properties of coir fiber reinforced polymer composites filled with calcium carbonate particles. Mater. Today Proc., vol. 33, Elsevier Ltd; 2020, p. 4790–2. https://doi.org/10.1016/j.matpr.2020.08.366.

[59] Lee C, Pang MM, Koay SC, Choo HL, Tshai KY. Talc filled polylactic-acid biobased polymer composites: tensile, thermal and morphological properties. SN Appl Sci 2020;2. https://doi.org/10.1007/s42452-020-2172-y.

[60] Rane AV, Kanny K, Abitha VK, Patil SS, Thomas S. Clay-polymer composites: design of clay polymer nanocomposite by mixing. In: Jlassi K, Chehimi MM, Thomas S, editors. Clay-Polymer Nanocomposites. Amsterdam: Elsevier Inc.; 2017. 113–144

[61] Teuber L, Osburg VS, Toporowski W, Militz H, Krause A. Wood polymer composites and their contribution to cascading utilisation. J Clean Prod 2016;110:9–15. https://doi.org/10.1016/j.jclepro.2015.04.009.

[62] Venkatarajan S, Athijayamani A. An overview on natural cellulose fiber reinforced polymer composites. Mater. Today Proc., 37, Elsevier Ltd; 2020, 3620–4. https://doi.org/10.1016/j.matpr.2020.09.773.

[63] Mallakpour S, Khadem E. Recent development in the synthesis of polymer nanocomposites based on nano-alumina. Prog Polym Sci 2014;51:74–93. https://doi.org/10.1016/j.progpolymsci.2015.07.004.

[64] Eichner E, Heinrich S, Schneider GA. Influence of particle shape and size on mechanical properties in copper-polymer composites. Powder Technol 2018;339:39–45. https://doi.org/10.1016/j.powtec.2018.07.100.

[65] Solangi NH, Karri RR, Mubarak NM, Mazari SA, et al. Mechanism of polymer composite-based nanomaterial for biomedical applications. Adv Ind Eng Polym Res. 2024;7:1–19. https://doi.org/10.1016/j.aiepr.2023.09.002.

[66] Hdidar M, Chouikhi S, Fattoum A, Arous M. Effect of hydrolysis degree and mass molecular weight on the structure and properties of PVA films. Ionics (Kiel) 2017;23:3125–35. https://doi.org/10.1007/s11581-017-2103-0.

[67] Ma J. Alternative water soluble polymeric films to poly(vinyl alcohol) for single unit dose products [dissertation]. Tarragona, Spain: Universitat Rovira i Virgili; 2020.

[68] Zhou, Wenlong & Yang, Charles & Lickfield, Gary. Mechanical strength of durable press finished cotton fabric Part V: Poly(vinyl alcohol) as an additive to improve fabric abrasion resistance. J Appl Polym Sci 2004;91:3940-3946. https://doi.org/10.1002/app.13606

[69] Jaffe HL, Rosenblum FM. Poly(vinyl alcohol) for adhesives. In: Skeist I, editor. Handbook of Adhesives. Boston, MA: Springer; 1990. p. 401–407. https://doi.org/10.1007/978-1-4613-0671-9_22.

[70] Rivera-Hernández G, Antunes-Ricardo M, Martínez-Morales P, Sánchez ML. Polyvinyl alcohol based-drug delivery systems for cancer treatment. Int J Pharm 2021;600. https://doi.org/10.1016/j.ijpharm.2021.120478.

[71] Nasim T, Bandyopadhyay A. Introducing different poly (vinyl alcohol)s as new flocculant for kaolinated waste water. Sep Purif Technol 2012;88:87–94. https://doi.org/10.1016/j.seppur.2011.12.016.

[72] Jain N, Singh VK, Chauhan S. A review on mechanical and water absorption properties of polyvinyl alcohol based composites/films. J Mech Behav Mater 2017;26:213–22. https://doi.org/10.1515/jmbm-2017-0027.

[73] Trache D, Hussin MH, Hui Chuin CT, Sabar S, Fazita MRN, Taiwo OFA, et al. Microcrystalline cellulose: Isolation, characterization and bio-composites application—A review. Int J Biol Macromol 2016;93:789–804. https://doi.org/10.1016/j.ijbiomac.2016.09.056.

[74] Nsor-Atindana J, Chen M, Goff HD, Zhong F, Sharif HR, Li Y. Functionality and nutritional aspects of microcrystalline cellulose in food. Carbohydr Polym 2017;172:159–74. https://doi.org/10.1016/j.carbpol.2017.04.021.

[75] Järvenpää J. Suitability of microcrystalline cellulose as an ion exchanger [master's thesis]. Helsinki, Finland: University of Helsinki; 2019. http://hdl.handle.net/10138/308240

[76] Fouad H, Jawaid M, Karim Z, Meraj A, Abu-Jdayil B, Nasef MM, et al. Preparation and characterization of carboxymethyl microcrystalline cellulose from pineapple leaf fibre. Sci Rep 2024;14:23286. https://doi.org/10.1038/s41598-024-73860-4.

[77] Bilbao-Sáinz C, Avena-Bustillos RJ, Wood DF, Williams TG, Mchugh TH. Composite edible films based on hydroxypropyl methylcellulose reinforced with microcrystalline cellulose nanoparticles. J Agric Food Chem 2010;58:3753–60. https://doi.org/10.1021/jf9033128.

[78] Thoorens G, Krier F, Leclercq B, Carlin B, Evrard B. Microcrystalline cellulose, a direct compression binder in a quality by design environment - A review. Int J Pharm 2014;473:64–72. https://doi.org/10.1016/j.ijpharm.2014.06.055.

[79] Schvartz T, Shoseyov O. Defibrillated microcrystalline cellulose as an efficient emulsion stabilizer – Study of food-grade Pickering emulsions resistant to extreme conditions. LWT 2022;155. https://doi.org/10.1016/j.lwt.2021.113006.

[80] Ismail FS, Mohamed Asa'ari AZ, Mohd Yussof NA, Chin Hao L, Mohammad Padzil FN, Hua LS, et al. Physical and Mechanical Properties of Paper Made from Beaten Empty Fruit Bunch Fiber Incorporated with Microcrystalline Cellulose. J. Nat. Fibers. 2020:1–13. https://doi.org/10.1080/15440478.2020.1779896.

[81] Nor Amira Izzati A, John WC, Nurul Fazita MR, Najieha N, Azniwati AA, Abdul Khalil HPS. Effect of empty fruit bunches microcrystalline cellulose (MCC) on the thermal, mechanical and morphological properties of biodegradable poly (lactic acid) (PLA) and polybutylene adipate terephthalate (PBAT) composites. Mater Res Express 2020;7. https://doi.org/10.1088/2053-1591/ab6889.

[82] Arun L, Sujatha ER, Baldovino JA, Nuñez de la Rosa YE. Microcrystalline Cellulose—A Green Alternative to Conventional Soil Stabilizers. Polymers (Basel) 2024;16. https://doi.org/10.3390/polym16142043.

[83] Liu S, Zhao Y, Wei H, Nie L, Ding P, Sun H, Guo Y, Chen T, Okoro OV, Shavandi A, Fan L. Injectable hydrogels based on silk fibroin peptide grafted hydroxypropyl chitosan and oxidized microcrystalline cellulose for scarless wound healing. Colloids Surf A Physicochem Eng Asp. 2022;647:129062. https://doi.org/10.1016/j.colsurfa.2022.129062.

[84] Sulaiman L, Hazrin ZHZ, Zakir NIM, Halim NA, Rusdi RAA, Khair ASA, Tajuddin HA. The effect of microcrystalline cellulose (MCC) on coating paint film's surface performance as non-stick coating. Pigment Resin Technol. 2020;49(5):341–345. https://doi.org/10.1108/PRT-07-2019-0060.

[85] Gaidukovs S, Platnieks O, Gaidukova G, Starkova O, Barkane A, Beluns S, et al. Understanding the Impact of Microcrystalline Cellulose Modification on Durability and Biodegradation of Highly Loaded Biocomposites for Woody Like Materials Applications. J Polym Environ 2022;30:1435–50. https://doi.org/10.1007/s10924-021-02291-3.

[86] Kiziltas A, Gardner DJ, Han Y, Yang HS. Mechanical Properties of Microcrystalline Cellulose (MCC) Filled Engineering Thermoplastic Composites. J Polym Environ 2014;22:365–72. https://doi.org/10.1007/s10924-014-0676-5.

[87] Merget R, Bauer T, Küpper H, Philippou S, Bauer H, Breitstadt R, et al. Health hazards due to the inhalation of amorphous silica. Arch Toxicol 2002;75:625–34. https://doi.org/10.1007/s002040100266.

[88] Alameri I, Oltulu M. Mechanical properties of polymer composites reinforced by silica-based materials of various sizes. Applied Nanoscience (Switzerland) 2020;10:4087–102. https://doi.org/10.1007/s13204-020-01516-6.

[89] Velty A, Corma A. Advanced zeolite and ordered mesoporous silica-based catalysts for the conversion of CO_2 to chemicals and fuels. Chem Soc Rev 2023;52:1773–946. https://doi.org/10.1039/d2cs00456a.

[90] Mirzaei M, Zarch MB, Darroudi M, Sayyadi K, Keshavarz ST, Sayyadi J, et al. Silica mesoporous structures: Effective nanocarriers in drug delivery and nanocatalysts. Applied Sciences (Switzerland) 2020;10:1–36. https://doi.org/10.3390/app10217533.

[91] Malaki M, Hashemzadeh Y, Fadaei Tehrani A. Abrasion resistance of acrylic polyurethane coatings reinforced by nano-silica. Prog Org Coat 2018;125:507–15. https://doi.org/10.1016/j.porgcoat.2018.07.034.

[92] Barbhuiya GH, Moiz MA, Hasan SD, Zaheer MM. Effects of the nanosilica addition on cement concrete: A review. Mater. Today Proc., vol. 32, Elsevier Ltd; 2020, 560–6. https://doi.org/10.1016/j.matpr.2020.02.143.

[93] Kobylinska NG, Kessler VG, Seisenbaeva GA, Dudarko OA. In situ Functionalized Mesoporous Silicas for Sustainable Remediation Strategies in Removal of Inorganic Pollutants from Contaminated Environmental Water. ACS Omega 2022;7:23576–90. https://doi.org/10.1021/acsomega.2c02151.

[94] Latini V, Feliczak-Guzik A, Wawrzyńczak A. Application Possibilities of Sustainable Nanostructured Silica-Based Materials in Cosmetics. Cosmetics 2025;12. https://doi.org/10.3390/cosmetics12040134.

[95] Aljaberi A, Chatterji A, Shah NH, Sandhu HK. Functional performance of silicified microcrystalline cellulose versus microcrystalline cellulose: a case study SMCC versus MCC. Drug Dev Ind Pharm 2009;35:1066–71. https://doi.org/10.1080/03639040902774131.

[96] Guo M, Augsburger LL. Potential application of silicified microcrystalline cellulose in direct-fill formulations for automatic capsule-filling machines. Pharm Dev Technol 2003;8:47–59. https://doi.org/10.1081/PDT-120017523.

[97] Luukkonen P, Schaefer T, Hellén L, Juppo AM, Yliruusi J. Rheological characterization of microcrystalline cellulose and silicified microcrystalline cellulose wet masses using a mixer torque rheometer. Int J Pharm. 1999; 188(2): 181-92. https://doi.org/10.1016/s0378-5173(99)00219-7. PMID: 10518674.

[98] Alfa J, Odeniyi MA, Jaiyeoba KT. Direct compression properties of microcrystalline cellulose and its silicified product. East Cent Afr J Pharm Sci. *2006*;7(3):56–59. https://doi.org/10.4314/ecajps.v7i3.9714.

[99] Van Veen B, Bolhuis GK, Wu YS, Zuurman K, Frijlink HW. Compaction mechanism and tablet strength of unlubricated and lubricated (silicified) microcrystalline cellulose Eur J Pharm. Biopharm 2005;59:133–8. https://doi.org/10.1016/j.ejpb.2004.05.009.

[100] Cavalcanti IMGA, Valeriano CCS, Marçal AC, de Lima Ferreira Novais A, do Nascimento Souza D. Optical and structural properties of sunscreens evaluated by physical techniques with emphasis on zinc oxide: A critical review. Appl Radiat Isot. 2025 ;226:112217. https://doi.org/10.1016/j.apradiso.2025.112217.

[101] Espitia PJP, Soares N de FF, Coimbra JS dos R, de Andrade NJ, Cruz RS, Medeiros EAA. Zinc Oxide Nanoparticles: Synthesis, Antimicrobial Activity and Food Packaging Applications. Food Bioproc Tech 2012;5:1447–64. https://doi.org/10.1007/s11947-012-0797-6.

[102] Alberti S, Basciu I, Vocciante M, Ferretti M. Experimental and physico-chemical comparison of zno nanoparticles' activity for photocatalytic applications in wastewater treatment. Catalysts 2021;11. https://doi.org/10.3390/catal11060678.

[103] Mousa MA, Khairy M. Synthesis of nano-zinc oxide with different morphologies and its application on fabrics for UV protection and microbe-resistant defense clothing. *Text Res J.* 2020;90(21-22):2492–2503. https://doi.org/10.1177/0040517520920952.

[104] Krishna MS, Singh S, Batool M, Fahmy HM, Seku K, Shalan AE, et al. A review on 2D-ZnO nanostructure based biosensors: from materials to devices. Mater Adv 2022;4:320–54. https://doi.org/10.1039/d2ma00878e.

[105] Shankar S, Wang LF, Rhim JW. Incorporation of zinc oxide nanoparticles improved the mechanical, water vapor barrier, UV-light barrier, and antibacterial properties of PLA-based nanocomposite films. Mater Sci Eng C. 2018;93:289–298. https://doi.org/10.1016/j.msec.2018.08.002.

Chapter 2

A Comprehensive Review of Polyvinyl Alcohol Composites Reinforced with Silica, MCC, Silicified MCC and ZnO Nanoparticles

2.1 Introduction

Traditionally, polymers are derived from non-renewable fossil fuel resources. But from the production to disposal, polymers significantly harm the environment through plastic pollution, elevated greenhouse gas emission and global warming. Therefore, the research on the development of sustainable and high-performance polymer composites has gained significant importance in recent years. Sustainable polymer composites usually comprise of biodegradable matrices like Polylactic Acid (PLA), Polyhydroxy Alkanoates (PHA) or other biopolymers and natural fillers like cellulose and silica derived from plants and animals. Natural fillers are often biodegradable and environmentally friendly. So, the composites made from them break down more easily and hence reduces long term waste and pollution. The use of bioderived fillers support circular economy goal by converting agricultural waste into value-added materials. Additionally, the composites made from these natural fillers exhibit improved mechanical and functional properties.

This review discusses the recent research on the extraction of silica and cellulose from the biomasses. It also covers how these materials are modified and added to the polymer matrices and the effect of these fillers on the properties of polymer composites. Here, the special focus is on silica nanoparticles, Microcrystalline Cellulose, Silicified MCC and ZnO. Polyvinyl Alcohol (PVA) is a widely studied biodegradable polymer due to its excellent film forming ability and flexibility. It is used for making composites because it can easily form strong intermolecular interactions and hydrogen bonds with hydrophilic fillers. Numerous studies have been reported regarding the reinforcement of PVA with natural fillers. This review focuses on the recent works on PVA, especially on the studies that explore how composites are fabricated and the effect of fillers on properties such as

mechanical strength, thermal behaviour, barrier performance and functional characteristics.

2.2 Recent Advances in Nanosilica and Biosilica

Silicon dioxide (SiO_2) with particle size (1 to 100 nm) is known as nanosilica. Large surface area, small size, high surface reactivity and high porosity made it a favourable candidate in the field of material science. Nanosilica has high mechanical strength and can withstand high temperature without decomposition. It is widely used as a catalyst [1], filler in polymer composites to improve the performance of coatings and paints [2] and in the production of electronic components and semiconductor devices [3]. Synthesis of nanosilica can be achieved through different methods such as sol-gel process (from the precursors like Tetra Ethyl Ortho Silane) [4], precipitation method (from sodium silicate) [5], hydrothermal process (from silica gel), [6], etc.

Stöber et al. in 1968 pioneered the synthesis of spherical silica particles (0.05-2μm) through the ammonia catalysed hydrolysis of alkyl silicate followed by condensation of silicic acid in alcoholic solution [7]. Bogush et al. in 1988 extended the Stöber process by correlating reaction conditions with silica particle size [8]. Matsoukas and Gulari in 1988 elucidated the growth kinetics of monodisperse silica particles formed by ammonia catalyzed TEOS hydrolysis [9]. Arriagada and Osseo-Asare in 1992 synthesized silica nanoparticles using a reverse microemulsion method with controlled particle formation and stability [10].

Nanosilica can also be extracted from renewable sources such as rice husk [11],bamboos [12], shellfish, lichens, diatomaceous earths, etc. The nanosilica extracted from plants and animals are referred to as biosilica, which have numerous advantages over synthetic nano silica. Biosilica is a natural material obtained from renewable sources and offers greener alternatives for various applications. There is concern about the potential toxicity and long-term effects on the living organisms by synthetic nanosilica [13]. Whereas, biosilica exhibits high biocompatibility, lower toxicity and hence more suitable for biomedical and pharmaceutical applications.

Moreover, the cost of production of biosilica is lower than that of synthetic nanosilica. Numerous studies have been reported related to the synthesis of biosilica.

Wang et al. in 2002 demonstrated that ordered biosilica structures can be synthesised under ambient conditions using plant cell wall as natural templates and TEOS as the silica precursor [14]. Perry and Keeling in 2003 demonstrated that protein containing biosilica extracts from Equisetum telmateia regulate silica formation kinetics, produces small and more ordered silica structures [15]. Shadiya et al. in 2021, isolated and characterised nanosilica from the flowers of Pampas Grass. Metal ions are removed and silica is extracted in mild acid solution of 0.1 N HCl. BET analysis reveals that surface area of silica is 126 m^2/g [16]. An eco-friendly method of synthesis of amorphous nanosilica from rice husk was reported by Pradeepkumar et al. in 2023. Less toxic Na_2CO_3 is used for the conversion of silicic acid to sodium silicate. Carbon dioxide is not produced in this process. The recovered nanosilica has amorphous nature with an average particle size of 35 nm [17]. Bekkam and Thiyagarajan in 2024 derived nanosilica from rice husk to mitigate drought stress in hybrid maize by boosting antioxidant defence system. They synthesised nanosilica with 99% purity and sprayed it on maize grown under both irrigated and drought conditions. They found that nanosilica improved the stress tolerance, growth and photosynthetic parameters. However, an overdose of silica leads to retarded growth and decreased antioxidant property [18] .

Nanosilica was also synthesised from rice straw. Singh et al. in 2022, synthesised biogenic nanosilica from rice straw and studied its application in photocatalytic degradation of cationic dye. Both amorphous and crystalline silica were prepared by tuning the calcination temperature. Photocatalytic degradation studies show that, 66.26% methylene blue degraded in the first 10 minutes. The degradation follows first order kinetics with half-life of 6.79 min [19]. Morsy et al. in 2014 synthesised nanosilica and $SiO_2/CaCO_3$ composite from semi-burned rice straw ash. Its application as a filler in paper was studied and found that optical properties (brightness, whiteness, opacity) were improved, but mechanical strength was slightly reduced [20]. Paddy straw can also be used for the synthesis of nanosilica. Jyani et al.

in 2024 extracted silica particles from green solvent pretreated paddy straw. Paddy straw was treated with ethyl lactate followed by 0.55 N NaOH and 1.5 N HCl for the leaching process. The synthesised silica appeared as agglomerated with size in the range of 50-200 nm and is in amorphous form [21]. Falk et al. in 2019 synthesised nanosilica from sugar cane bagasse through sol-gel method. Result showed that amorphous SiO_2 particles with average size of 10 nm were obtained by controlling the variables such as pH, temperature and SiO_2/ H_2O molar ratio. Nanosilica with 96% purity was obtained during the process [22]. Akhayere and Kavas in 2020 synthesised nanosilica and nanozeolite from barley grass for the removal of gasoline from aqueous solution. Nanoparticles were seen to have a zeta potential of -28.2 and sorption efficiency is better than other adsorbents. Uptake efficiency of 95% was recorded and adsorption follows second order kinetics [23].

2.3 A Review of Silica-Polymer Composites

The silica-polymer composites were prepared by dispersing silica in the form of fine particles, nanoparticles or fibres in a polymer matrix. Silica is an important filler because of its unique properties such as better mechanical properties, improved thermal stability and electrical properties. Due to the presence of enormous -OH groups on the surface it can be easily modified both physically and chemically [24]. Important chemical modification is by silane coupling agents like 3-aminopropyl triethoxy silane (APTES) [25], 3-glycidoxy propyl trimethoxy silane (GPTMS) [26]etc. The hydrophilic form of silica can be converted to hydrophobic using chemicals such as octadecyl trichlorosilane [27]. Polar groups like amino [28], thiol [29] or carboxyl group [30] can also be introduced to the silica very easily. The choice of the polymer includes epoxy resins [31], Polyurethanes [32], Polyvinyl Alcohol [33], Polyamides [34], PMMA [35], Polycarbonate [36], Polylactic Acid [37] ,etc. Numerous studies have been reported regarding silica-polymer composites.

Steinbach et al. in 2022 synthesised porous silica-polymer nanocomposites. Polymer was tetraethylenepentaamine functionalised Poly(glycidylmethacrylate) co-ethyleneglycol dimethacrylate. The effect of water, TEOS and ammonia were studied

[38] . Yang et al. in 2022 synthesised PVA/nanosilica composite through in situ impregnation of poplar wood via ultrasound and vacuum impregnation method. The results showed that PVA/Silica sol had no negative effect during impregnation and compressive strength of modified wood improved significantly [39]. Transparent film of Polyvinyl Alcohol/ Polyethylene Glycol film loaded with different contents were prepared by Mousa et al. in 2021. Optical properties were studied within the region of 200-700 nm. The parameters such as band tail width, extinction coefficient, refractive index and optical dielectric constants were calculated as a function of nanosilica content. The result showed that optical properties were affected by SiO_2 content [40]. Takeno et al. in 2021 investigated the effect of silica and clay nanoparticles on the tensile properties of PVA hydrogel containing borax. They found that tensile strength of the hydrogel increased with increasing concentration, possibly due to the interaction between PVA-clay, PVA – Borax and PVA-Silica. Both the extensibility and modulus were largely improved. Synchrotron small angle X-ray scattering analysis showed that addition of silica and clay increases the homogeneity [41].

Optical and thermo-optical properties of PVA and PVA/Silica nanocomposite films were studied by Doudou et. al. in 2021 through prism coupler technique. Studies showed that refractive index of PVA films increases with increasing molecular weight of PVA but decreases with amount of SiO_2 in PVA. Addition of silica in the PVA effect thermo-optic coefficient of the film. The whole studies showed that the composite is a suitable material in optical devices and optical temperature sensors due to its tuneable refractive indices [42]. Sabr et al. in 2020 studied the properties of PVA filled with nanosilica for food packaging applications. Thin films were prepared by adding different weights of silica. Studies showed that on increasing nanosilica content to 7%, the tensile strength increases from 62 MPa to 143 MPa and crystallinity increases from 0.97 to 1.159. FTIR result showed the physical interaction between nano silica and PVA [43]. Hidayati and Munasir in 2021 studied the electrical and thermal properties of PVA/ nanosilica composite. They found that PVA can be used as a substitute for polyolefin for making super capacitors. Addition of silica improved thermal stability and electrical properties. Resistance and conductance of PVA/TEOS

membrane is 5.65×10^{6} ohm and 1.044×10^{-7} S/m whereas that of PVA/SiO_2 is 6.31×10^{6} ohm and 1.012×10^{-7} S/m respectively [44].

Hashim and Hamad in 2020 prepared low cost, light weight PVA/Silica nanocomposite with excellent UV shielding properties. The result showed that absorbance, absorption coefficient, refractive index, real and imaginary parts of dielectric constants and optical conductivity enhanced with increasing silica concentration. Therefore, it can be used for making solar cells, diodes and transistors [45]. da Silva et al. in 2020 extracted silica from rice husk and fabricated PVA/silica hybrid membrane which have desalination performance by pervaporation. The citric acid leaching was applied for the extraction of silica and was incorporated into PVA with different compositions viz, 0%, 10% and 20%. The flux of hybrid membrane reached the maximum value of 1.23 $kgm^{-2}h^{-1}$ at 60 °C for 10% silica loading with 3.5 wt.% NaCl [46]. Soliman et al. in 2020 fabricated PVA nanocomposite film through dispersing SiO_2 nanoparticle and their structural, thermal and optical properties were measured. Analysis showed that the composite is more stable than PVA and optical analysis showed the red shift with increase of SiO_2 particles and there is decrease in band gap. The direct band gap increased by 0.6V and indirect band gap by 0.35 V when the concentration of SiO_2 was up to 10 wt.%. The refractive index of polymer increases from 1.492 to 1.76 nm in the visible region [47]. Kariminejad et al. in 2021 studied the effect of two ratios of PVA/Chitosan (3:1 and 1:1) and nanosilica on the structural and physicochemical properties of PVA/Chitosan/Silica. Analysis showed that the addition of silica decreases the water vapour permeability of the film. Tensile strength increases to 35.86 MPa. But light emission value did not differ greatly [48].

Even though a number of methods and numerous varieties of silica-polymer composites were prepared and reported, it faces some challenges also. Agglomeration of silica leads to non-uniform dispersion and processing difficulties. Though silica increases mechanical strength like stiffness and hardness, there are the possibilities of brittleness and poor flexibility. Wide difference in thermal expansion coefficient between polymer and silica also causes delamination, wrapping or cracking under temperature fluctuation.

2.4 Microcrystalline Cellulose: A Review of Recent Studies

Cellulose is a complex polysaccharide and is the most abundant natural, organic polymer with production of 50 billion tons per year [49].It is a linear polymer which consists of 500 to 15000 β l,4- D anhydro glucopyranosyl units connected by glycosidic linkage [50]. The length of the chain depends on the source of material and method of processing. Microcrystalline Cellulose is a purified, partially depolymerised form of cellulose which contain fewer number of glucose units than cellulose. Dispersibility in water, flowability and compressibility of MCC is higher than that of native cellulose. MCC is prepared by acid hydrolysis of cellulose, during this lignin and other amorphous region will be removed. Therefore, MCC is purer than crude cellulose and is used in wide applications. In 1955 O.A Battista and P.A Smith discovered MCC and commercialised under the brand named Avicel® [51]. In 1964, FMC corporation introduced Avicel® PH, as an ingredient for direct compression tableting. MCC is usually obtained from wood, but it is extracted from a lot of non-woody lignocellulosic materials also. Numerous studies have been reported with respect to the extraction and application of MCC

Hanani et al. in 2017, extracted MCC from rice husk and also studied the effect of various acids viz, HNO_3, H_2SO_4 and HCl on the yield and properties of MCC. It was found that higher yield is produced when HNO_3 is used, and it has great potential to replace HCl and H_2SO_4 [52]. Rice straw is also a good source of MCC. Guo-Zhi Fan et al. 2017 introduced an effective microwave-assisted method for isolation of MCC from rice straw. This method requires milder condition including shorter time and lower temperature compared to traditional method [53]. Instead of mineral acid, other organic acid can be also used for leaching purposes. Weng et al. in 2022, used p-Toluene sulphonic acid to remove hemicellulose and lignin from corncob, to achieve green synthesis. They found that compared to commercial MCC, aspirin tablet made with this MCC exhibits better sustained release performance [54]. Homyuen et al. in 2023 isolated MCC from sugarcane bagasse and its impregnation with Sappan wood extract gives an antioxidant dietary fibre for bread preparation. Hydrolysis of sugarcane bagasse at 85 °C for 90 minutes gives MCC with highest crystallinity index

and suitable size [55]. Debnath et al. in 2023, modified the traditional synthesis method of MCC. They synthesised MCC from tea waste, using alkaline hydrogen peroxide instead of conventional acid hydrolysis. Through microwave heating, delignification could be done in 2 minutes and bleaching is done in 30 seconds, while the conventional method required more than 1 h of heating. Synthesised MCC is almost free from hemicellulose and lignin. They could prepare highly crystalline and thermally stable MCC [56]. Porous MCC is prepared from agave bagasse by sequential alkaline H_2O_2 at low concentration of reagents. Hernandez et al. in 2023 studied that concentration of H_2O_2 and reaction time do not affect the crystallinity of the material. Microporous nature of the product will be useful as a good adsorbent [57].

Waste cloth is a nonconventional resource of MCC. Singhal et al. in 2023 adopted chemical recycling of waste cloth into cellulose. Up to 80.4% of MCC was recovered during optimum reaction conditions. The product has appreciable water holding capacity and is thermally stable up to 350 ˚C. The whiteness index of the FE-SEM image of MCC estimated by MATLAB was 81.27 [58]. Liang et al. in 2023 prepared MCC from Jute. They adopted microwave assisted acid hydrolysis, followed by the use of N-methyl morpholine-N-oxide and water as a solvent to obtain homogeneous casting liquid. During membrane formation crystal structure changed from cellulose I to cellulose II, but no significant change in the chemical structure. The tensile strength of membrane is 13.49 MPa with 68.12% elongating at break [59] . Olive stone, a waste produced from olive industry is a good source of MCC. Hasnain et al. in 2023, isolated MCC from olive stone by acid hydrolysis using HCl and H_2SO_4. They found that thermal stability of MCC prepared using HCl is higher than that of MCC prepared by sulphuric acid hydrolysis. The properties of MCC produced from olive stone is in good agreement with commercially available Avicel PH101 [60]. Gopal PM et al. in 2023, extracted MCC from Millettia Pinnata leaf through a series of chemical treatment. The isolated MCC has a band gap of 4.21 eV, crystallinity index of 87.3% and dislocation density is 0.0019. It is stable up to 530 ˚C [61]. Sunesh et al. in 2023 isolated MCC from Valoniopsis Pachynema Green Macro algae. The

crystallinity index of MCC is 71.9% and crystallinity size is 69.81nm. Thermal studies show that the onset temperature is 290 °C and activation energy of cellulose is 55.93 kJ/mol [62].

2.5 Recent Modifications of Microcrystalline Cellulose

Though MCC is used in various applications, it has some limitations also. MCC is insoluble in water, which limits its use in certain applications, where solubility is important. The bulk density of MCC is very low, therefore it can't be used to make high-density material [63]. Unmodified MCC exhibits poor flowability and does not provide enough mechanical strength for the products. Moreover, depending up on the nature of source and method of production, MCC with different grades and quality can be synthesised. Low thermal stability of MCC also limits its application in the field which requires high processing temperature. MCC is susceptible to microbial contamination and is an issue to be addressed during manufacturing and storage. These limitations can be surpassed by adopting several strategies and modification depending up on the requirement. Several studies were reported with regards to modification of MCC.

Amino functionalisation of MCC were carried out by Do et al. in 2022. Here, MCC is converted into tosyl MCC by tosylation in eco-friendly medium. Tosyl group is later substituted by three different types of amino groups viz, 3-aminopropyltrimethyl silane, ethylene diamine, and tri ethylene tetramine. Biological studies revealed that amino cellulose exhibited high antimicrobial activity [64]. Li et al. in 2023 modified MCC with N-(2-aminoethyl)-3-aminopropyl methyl dimethoxy silane for the adsorption of formaldehyde. The mechanism of adsorption is due to protonated $-NH_3^+$ group in the composite with formaldehyde to form a Schiff base. Moreover, modification increases the average pore size to 14.56 nm, which enhances the adsorption capacity [65]. Kenawy et al. in 2023, synthesised quarternized graft co-polymer of MCC. MCC is grafted with acrylonitrile, this is aminated and finally it is quaterinized with methyl iodide. The product is found to have good antioxidant properties. Anti-inflammatory properties were investigated and result showed that the polymer aminated with tris (2-amino ethyl) amine have significant anti-inflammatory

effects. The polymer also exhibited moderate effect against cancerous cell line HEPG 2 [66]. The adsorption capacity of MCC can also be enhanced by modification. Mello et al. in 2023, grafted (3-trimethoxy silyl propyl) diethylene triamine on MCC for the adsorption of dyes. Based on Bayesian information criterion, pseudo-first-order model is best to describe the kinetic behaviour for Reactive Red 35 and Reactive Red 19 dyes [67].

Jabli et al. in 2023 functionalized MCC with polyethylene imine solution and hydrazine sulphate salt using an impregnation method. Analysis revealed that, cellulose-polyethylene imine (5%) and cellulose hydrazine (1:1) displayed the highest adsorption capacities for calmagite (anionic dye). Adsorption complied with pseudo-second-order kinetics and Langmuir adsorption isotherm [68]. Yuan et al. in 2022 modified MCC with bio-based phytic acid and condensed tannins. The product is an excellent flame retardant and cationic dye adsorbent. Adsorption follows pseudo-second-order-kinetics and Langmuir-Nernst dual isotherm model [69]. Shahbazi et al. in 2022, modified MCC by the Tea polyphenols and cationic ε- poly lysine. Polylysine offers surface activity with antimicrobial effect. But MCC/ ε -PL lacks enough emulsifying ability. To overcome this, polyphenol was initially introduced to MCC by the free radical grafting method to decrease the charge density on MCC [70]. Bulk density, flow property and crystallinity of MCC were modified by Tasnim et al. in 2022. The prepared MCC is treated with different concentrations of NaOH at room temperature or at $^{-}$20 ^{o}C followed by precipitation with HCl or ethanol. Bulk density of MCC increased from 0.253 to 0.594 and flow property get improved and were evaluated by Hausner index, Carr's index and angle of repose [71].

Decreasing the degree of polymerization enhances the properties like solubility, processibility, mechanical property, etc. Thielman et al. in 2022, depolymerised MCC to form short fibres with an average degree of polymerisation between 29 and 70. They conducted the process with intensive ball mill treatment followed by mild acid hydrolysis. The MCC fibre with desired degree of

polymerisation could be obtained by tuning the processing parameters [72]. Said et al. in 2023, phosphorylated MCC using phosphoric acid in presence of urea. It was used as an adsorbent for methylene blue dye from aqueous solution. Adsorption follows pseudo-second-order kinetics and retention capacity depends on the phosphate content and the surface charge of the adsorbent. Study revealed that, presence of phosphate group improved the adsorption capacity of MCC [73]. MCC is a good filler in fabrication of epoxy composites, but its hydrophilic nature and strong H- bonding power reduces its compatibility with epoxy resin. Thus, Sei et al. in 2022 epoxidized the MCC using epichlorohydrin and NaOH in presence of phase transfer catalyst tetramethyl ammonium bromide. They found that the dispersibility of epoxidized MCC was significantly improved. Moreover, the modulus and toughness of the composites increased [74]. MCC is a promising filler in polymer, but stronger intermolecular H-bonding between MCC deteriorates the mechanical properties of composite. To overcome this, Jang et al. in 2022 modified MCC with hydroxy propyl group. They found that hydroxy propyl group interrupt the filler-filler intermolecular H-bonding and reduces the crystallinity and density [75]. Neves et al. modified MCC with 3-amino propyl trimethoxy silane with different composition. The process did not alter the shape of MCC, but crystallite size is reduced to half and there was hike in number of hydrophilic groups [76]. MCC was modified with Ferulic acid, methacrylolyl chloride and oleoyl chloride by Chartrand et al. in 2016. Grafting was confirmed by X-ray photoelectron spectroscopy and observed significant increase in hydrophobicity from contact angle measurement. Modification improved the dispersion in LDPE and enhanced the mechanical strength of the composites [77]. Madrid and Abad in 2015, modified MCC through gamma radiation induced grafted polymerisation of glycidyl methacrylate. The effect of monomer concentration, type of solvent and dose of adsorption were analysed. XRD studies revealed that crystalline region of MCC is not affected during the grafting. TGA analysis showed that, grafted MCC have higher thermal stability than MCC [78].

Bezerra et al. in 2017 modified MCC with ethylene diamine in the absence of solvent and studied the adsorption of amitriptyline drug from aqueous solution. The effectiveness of modification was confirmed by Density Functional Theory (DFT) at level B3LYP/6-31G(d). Analysis showed that different factors such as pH, time, concentration and temperature have significant effect on extent of adsorption [79]. Chen et al. in 2019 used MCC modified with stearic acid to prepare cassava starch composite films. Modification enhanced the mechanical and thermal properties of the film. 0.5% modification had higher enhancement in the properties and hydrophobicity increased by 65% with 2% modification [80].

2.6 Microcrystalline Cellulose-Polymer composites: A Review

Pure polymer often has some limitations such as poor strength, stiffness, thermal stability and other mechanical or functional properties. These limitations can be overwhelmed by reinforcing them with materials like fibres, particles etc. Converting the base polymer to polymer composites improve the strength, stiffness, durability, corrosion resistance, fatigue resistance, thermal stability and sometimes electrical conductivity. This improvement makes the polymer as a widely accepted candidate in the field of aerospace, automotive, construction, sports and electrical industries. Fillers are the materials added to the polymer matrix to improve certain properties or reduce the cost of production. It may be inorganic or organic and biodegradable or non-biodegradable. Biodegradable fillers enhance the properties while ensuring that the composites are environmentally friendly. Micro crystalline cellulose (MCC) is a widely used filler in polymer composites due to its biodegradability, renewability and the ability to enhance the mechanical and thermal properties. Numerous studies have been reported in the area of MCC-polymer composites.

Gorgun et al. in 2024 developed green composite of Polylactic Acid and MCC through solution casting technique. They used maleic acid and maleic anhydride as the coupling agent. Incorporation of maleic anhydride-maleic acid led to increase in the tensile strength and tensile modulus. It is thermally stable and the improvement in

properties is due to efficient dispersion of MCC, chemical interaction and esterification between MCC and coupling agent [81]. When MCC is incorporated to recycled high density polyethylene, there is significant improvement in the performance of the composites. Raharjo et al. in 2023 developed composite of recycled HDPE/cantala fibre/MCC via twin screw extruder followed by hot press. Adding 4% weight of MCC increased the tensile strength by 50.7% and crystallinity of composites increased by 6.7% [82]. Hen et al. in 2023 grafted 2,2-Bis (hydroxy methyl)-propionic acid on the MCC and transferred to branched structure through poly condensation. This modification enhanced the dispersion between poly (3-hydroxy butyrate-co-3-hydroxy valerate) and bio-based engineering polyester elastomer. Studies revealed that tensile strength and elongation at break of PHBV/BEPE composites were improved by 559.7% and 221.8% respectively [83]. Benaouda et al. in 2022 developed polyaniline/ microcrystalline cellulose composites. It is synthesised by in situ-polymerization of aniline using ammonium per sulphate as oxidizing agent. The analysis shows that the composites have more compact, homogeneous morphology and better thermal stability. Moreover, it can be used for catalytic degradation of toxic anionic dye, methyl orange in presence of U.V light [84].

Polymethyl Methacrylate (PMMA) based composites are recently used in dental applications. Sosiati et al. 2023 reinforced PMMA with MCC and sisal fibre. Studies revealed that adding MCC to PMMA decreases flexural and impact strength but hardness increased. Addition of MCC increases the water absorption and lowest value is obtained for the composites added with 1 volume % of MCC [85]. The properties of Polypropylene can also be improved by adding MCC. Ratnakumar et al. in 2020 reinforced Polypropylene by adding 0-5% of MCC. Tensile strength, hardness and impact strength of the composites increased by 5%, 8% and 51% respectively for 5% MCC composites. It was also confirmed that MCC is comprised of higher percentage of cellulose I-β structure and the polymer matrix is isotactic [86]. Fish gelatine is used in medicinal field due to its low pathogen infection risk. But poor mechanical strength limits its application. Pan et al. in 2020 reinforced fish gelatine

with MCC using a biological cross-linking agent genipin under ultrasonic treatment. They found that the tensile strength and modulus of elasticity of the new composites increased, whereas elongation at break and swelling ratio decreased. Thermogravimetry analysis indicates that the thermal stability of composites improved [87]. Rasheed et al. in 2021 developed a biodegradable polymer blend of Polylactic Acid and Polybutylene Succinate and added MCC to form composites. Thermal stability got improved by 1% due to their uniform dispersion in the polymer matrix. Addition of MCC increased the tensile strength but decreased the brittleness [88]. Botta et al. in 2021 fabricated bio compostable composite consisting of Polybutylene adipate-co-terephthalate as polymer matrix and MCC derived from almond as filler. The composite showed a drastic reduction in the elongation at break [89].

2.7 Recent studies on Microcrystalline Cellulose- Polyvinyl Alcohol Composites

MCC-PVA composite is an important candidate in the field of material science, due to their sustainable and eco-friendly application. PVA is a synthetic polymer, soluble in water, biodegradable and have excellent film forming ability. It is commonly used in medical, agricultural and packing applications. MCC is mixed with PVA through the methods like blending, casting or electrospinning. Addition of MCC to the PVA increases the tensile strength, flexibility and thermal stability. Since both MCC and PVA are biodegradable, the composite will certainly be biodegradable. Numerous research has been reported in association with MCC-PVA composites.

Seera et al. in 2020 synthesised MCC/PVA co-polymerized, cross-linked hydrogel through physical and chemical methods. Physical cross linking was done by freeze thawing whereas ethylene glycol di glycidyl ether is used for chemical cross-linking. The hydrogel was used as a carrier for the drug, 5-Fluorouracil and invitro release was carried out in phosphate saline buffer [90]. MCC/PVA composite shows antibacterial property also. Kong et al. in 2019 prepared oxidised micro crystalline cellulose. Then 3-(2-amino ethyl)-5,5 dimethyl hydantoin (N-halamine) was grafted on oxidised MCC. This was chlorinated and was added to PVA and film was made by

solution casting. Antibacterial studies were conducted against *S.aureus* and *E. coli* and result showed that all bacteria became inactive within 1 h [91]. Uto et al. in 2024 fabricated humidity responsive shape memory polymer composites containing PVA and MCC. It would be useful for maintaining hair curls in humid environments. The films were prepared by blending method. They showed that increasing the MCC content increases the mechanical properties and the maximum curl-shape recovery was achieved for 20-25% MCC filling [92]. Naduparambath et al. in 2017 isolated MCC from sago seed shell and incorporated to PVA in different percentages by intense sonication followed by solution casting. Analysis showed that thermal stability of PVA enhanced during the addition of MCC and DSC analysis revealed the variation in glass transition temperature. UTM analysis showed the improvement of mechanical strength also [93].

Gadhave et al. in 2020 studied the effect of boric acid on thermo-mechanical properties of MCC/PVA blend and its applicability as wood adhesive. DSC studies showed the shift in glass transition temperature with increasing concentration of boric acid. Tensile shear strength became twice of the original value during the addition of 0.2wt% of boric acid [94]. Hussin et al. in 2018 extracted MCC from Organosolv oil palm frond pulp via by acid hydrolysis. This is incorporated with PVA-$LiClO_4$ through solution casting to produce biodegradable polymer composite. The film was analysed using electrochemical impedance spectroscopy and cyclic voltammetry and found that maximum conductivity is observed for MCC-PVA-20% $LiClO_4$ composite [95] . Maiti et al. in 2011 studied structural changes of starch/PVA bio composite reinforced with MCC, due to biodegradation in simulated aerobic compost environment. They prepared the film by casting method using glycerol as plasticizer. Biodegradation study was conducted by putting the film in the compost pit. The melting point of PVA shifted from, 204 to 223 °C with a significant increase in melting enthalpy [96]. The properties of Microcrystalline Cellulose/ PVA composites stabilised by Polyvinyl Acetate emulsion were studied by Ghadhave et al. in 2023. Adhesive was prepared by mixing MCC at different concentrations. Addition of MCC improved the elastic stiffness and bond quality. Water resistance and mechanical

properties were also increased [97]. Santos et al. in 2017, synthesised and studied the properties of bio-based Polylactic Acid/Poly lactic acid-co-glycolic acid reinforced with MCC and organophilic silica. The material was prepared by solution casting using chloroform as solvent. Studies revealed that MCC acts as a nucleating agent for the crystallisation of the polymer matrix. Increase in the MCC content increased the crystallinity of film [98]. An improvement of the mechanical performance was observed with MCC addition, especially when silica was added together with cellulose. Bio-based poly (butylene-succinate)/MCC/ nano fibrillated cellulose-based sustainable polymer composites are prepared by Platnieks et al. in 2020. Young's modulus and storage modulus at 20 °C have increased about two-fold. Thermal degradation temperature increased by 60 °C and the polymer disintegrated under the condition in a period of 75 days [99].

2.8 Studies on Silicified Microcrystalline Cellulose

SMCC is a modified form of Microcrystalline Cellulose formed by impregnating MCC with silica. It is commonly used in pharmaceuticals and food industry. Addition of silica to the MCC improves the flow properties, prevent clumping or sticking, improve compressibility, etc. SMCC can act as filler or bulking agent in tablet formation. Only a few studies have been reported associated with the synthesis of SMCC.

Recently MCC was isolated from Musa balbisiana and silicified with 2% silicon dioxide. Analysis revealed reduced crystallinity but enhanced thermal stability and flowability. Pharmaceutical evaluation proved that silicification reduced plastic deformation but enhanced compactivity, tabletibility and overall manufacturability [100]. Tomar et al. in 2017 developed a co-processed excipient of silicon dioxide and MCC, which was used for direct compression of paracetamol tablets [101]. The potential application of SMCC in direct-fill formulations for automatic capsule-filling machines was studied by Guo et al. in 2003. They found that SMCC exhibited faster drug dissolution than starch or lactose-based fillers and SMCC is an effective recipient for hard shell capsule applications [102]. The physicochemical properties of MCC and

SMCC were compared by Tobyn et al. using FT-IR, solid state NMR, XRD, pycnometer and electron microscopy to identify any chemical or physical changes during silicification. The results showed no distinguishable chemical or structural differences [103]. Edge et al. in 1999 studied the location of silica in SMCC using Scanning Electron Microscope (SEM) and Electron Probe micro analysis. The result suggested that silica is primarily located on the surface and portions of them are in the internal region of MCC [104].

Kachrimani et al. in 2003 studied the effect of particle size and moisture content on the tensile strength and disintegration time of standard MCC and SMCC. Studies showed that SMCC have slightly higher tensile strength but remarkably higher disintegration time in the pH range of 0.7-0.9. Silicification affects the moisture uptake of cellulose particles, packing behaviour and plastic yielding [105]. From their studies in 2006, it was found that the moisture sorption-desorption properties of SMCC is significantly different from MCC, particularly at higher humidity [106]. Surface coating of MCC with silica nanoparticles through dry coating significantly enhanced the flowability, while retaining its inherent tabletabilty [107]. Buckton et al. in 2000 used near IR spectroscopy to quantify the silica content and analysed the difference between SMCC and physical mixture of MCC and silica. The spectroscopic studies revealed that the peak at 2194 nm is due to colloidal silica content in co-processed SMCC.

2.9 Silicified Microcrystalline Cellulose -Polymer Composites: A Review

Although MCC and silica have individually been widely studied fillers in polymer composites, the studies related to SMCC- Polymer composites are extremely limited. However, Kiziltaz et al. in 2010 studied the effect of various cellulose based fillers on the mechanical, thermal and rheological properties of polystyrene composites. They found that SMCC shows better mechanical properties than untreated MCC [108]. Iskakov et al. in 2025 fabricated ecofriendly polypropylene composites incorporated with cellulose and silica, which exhibited stable pseudoplastic rheological behaviour suitable for injection moulding. When cellulose

was replaced with MCC, the homogeneity and mechanical performance was further improved [109]. Sun et al. in 2016 prepared MCC-nanosilica hybrid material and studied their applications in tyre tread compounds. When it was used to partially replace silica in silica/SSBR there was enhancement of physico-mechanical and dynamic properties, including higher wet-skid resistance and lower rolling resistance [110]. The partial replacement of silica in natural rubber composites was also achieved by using nanocellulose modified with 3-aminopropyl triethoxysilane. The resulting NR/MNCC/Silica system exhibited improved vulcanization behaviour, mechanical strength and dynamic performance [111]. Du et al. in 2020, prepared heterostructures of MCC-silica nanoparticles by adsorption phase reaction technology. It acted as effective reinforcing filler in tyre tread compounds. Compared to MCC, this heterostructure significantly improved tensile strength, enhanced abrasion resistance and reduced rolling resistance [112].

2.10 Role of Zinc Oxide as a Multifunctional Filler in PVA Composites

Zinc Oxide (ZnO) nanoparticles have been widely used as a functional filler in PVA composites due to its multifunctional properties. ZnO have inherent antibacterial activity and UV shielding properties. When ZnO is incorporated to PVA, there will be improvement in thermal stability and reduced water vapour permeability. Owing to strong interfacial interaction with hydroxyl group of PVA, ZnO contributes to mechanical reinforcement at optimized filler loading. These advantages highlight the potential of ZnO as functional additives in PVA/SMCC composites.

Recently, Song et al. fabricated an active biocomposite packaging material based on ZnO/Polyphenols/Cellulose/PVA via hydrothermal and casting method. The composite exhibited uniform dispersion, enhanced water barrier, UV shielding and antibacterial properties due to synergistic interactions [113]. Ismardi et al. in 2025 incorporated nanocellulose into PVA/ZnO nanocomposites to exploit their high surface area and abundant hydroxyl groups. It was found that the resulting composites exhibited enhanced optical, mechanical, electrical and electrochemical properties [114]. Abutalib in 2019 synthesised ZnO nanorods by chemical vapour deposition and

was incorporated in PVA/carboxy methyl cellulose nanocomposites prepared by casting. The electrical and dielectric studies revealed that it is suitable for electrochemical device applications [115].

Jayachandiran et al. in 2019 extracted cellulose microfibres from Barassus flabellifer, incorporated with ZnO and added to PVA matrix, via ultrasonic assisted solution process. The composite exhibited strong ZnO-cellulose intercalation and notable changes in thermal, optical, mechanical and electrical properties [116]. Driven by transition towards a circular economy, Giannakas et al. in 2022 developed a hybrid food packaging film via incorporation of ZnO rod into chitosan/PVA composite. The structural, barrier, mechanical and antibacterial properties were studied and the results demonstrated their potential as a sustainable active packaging material [117].

From the literature review, it is clear that PVA based composites reinforced with cellulose, silica, modified silica and Zinc Oxide have been widely studied due to their biodegradability, mechanical reinforcement, barrier performances and functional properties such as antimicrobial activity and UV shielding. The studies demonstrate the importance of filler modification and uniform dispersion in achieving superior performances. However, incorporation of Silicified Microcrystalline Cellulose and Zinc Oxide as hybrid functional filler with PVA matrix remains unexplored. Consequently, the present study seeks to fill this gap by developing SMCC from renewable sources and incorporating into PVA to achieve enhanced functional properties.

References

[1] Chong CC, Cheng YW, Bahari MB, Teh LP, Abidin SZ, Setiabudi HD. Development of nanosilica-based catalyst for syngas production via CO2 reforming of CH4: A review. Int J Hydrogen Energy 2021;46:24687–708. https://doi.org/10.1016/j.ijhydene.2020.01.086.

[2] Dileep P, Jacob S, Narayanankutty SK. Functionalized nanosilica as an antimicrobial additive for waterborne paints. Prog Org Coat 2020;142. https://doi.org/10.1016/j.porgcoat.2020.105574.

[3] Radu ER, Panaitescu DM, Andrei L, Ciuprina F, Nicolae CA, Gabor AR, et al. Properties of polysiloxane/nanosilica nanodielectrics for wearable electronic devices. Nanomaterials 2022;12. https://doi.org/10.3390/nano12010095.

[4] Chruściel, J., Ślusarski, L.: Synthesis of nanosilica by the sol-gel method and its activity toward polymers. Mater. Sci 2003: 21(4), 461–469

[5] Jal PK, Sudarshan M, Saha A, Patel S, Mishra BK. Synthesis and characterization of nanosilica prepared by precipitation method. Colloids Surf A Physicochem Eng Asp 2004;240:173–8. https://doi.org/10.1016/j.colsurfa.2004.03.021.

[6] Qisti N, Indrasti NS, Suprihatin. Optimization of process condition of nanosilica production by hydrothermal method. IOP Conf. Ser. Mater. Sci. Eng., vol. 162, 34Institute of Physics Publishing; 2016. https://doi.org/10.1088/1757-899X/162/1/012036.

[7] Stöber W, Fink A, Bohn E. Controlled growth of monodisperse silica spheres in the micron size range. J Colloid Interface Sci 1968;26:62–69. https://doi.org/10.1016/0021-9797(68)90272-5

[8] Bogush GH, Tracy MA, Zukoski CF. Preparation of monodisperse silica particles: Control of size and mass fraction. J Non-Cryst Solids 1988;104:95–106. https://doi.org/10.1016/0022-3093(88)90187-1

[9] Matsoukas T, Gulari E. Dynamics of growth of silica particles from ammonia-catalyzed hydrolysis of tetra-ethyl-orthosilicate. J Colloid Interface Sci 1988;124(1):252–261. https://doi.org/10.1016/0021-9797(88)90346-3

[10] Arriagada FJ, Osseo-Asare K. Phase and dispersion stability effects in the synthesis of silica nanoparticles in a non-ionic reverse microemulsion. Colloids Surf 1992;69:105–115. https://doi.org/10.1016/0166-6622(92)80221-Mss

[11] Carmona VB, Oliveira RM, Silva WTL, Mattoso LHC, Marconcini JM. Nanosilica from rice husk: Extraction and characterization. Ind Crops Prod 2013;43:291–6. https://doi.org/10.1016/j.indcrop.2012.06.050.

[12] Makhlouf ASH, Ali GAM, editors. Waste Recycling Technologies for Nanomaterials Manufacturing. Cham, Switzerland: Springer Nature; 2021. https://doi.org/10.1007/978-3-030-68031-2.

[13] Sharma N, Jha S. Amorphous nanosilica induced toxicity, inflammation and innate immune responses: A critical review. Toxicology 2020;441. https://doi.org/10.1016/j.tox.2020.152519.

[14] Wang L, Wang YH, Li M, Fan MS. Synthesis of ordered biosilica materials. Chin J Chem 2002;20(1):107–110. https://doi.org/10.1002/cjoc.20020200121

[15] Perry CC, Keeling-Tucker T. Model studies of colloidal silica precipitation using biosilica extracts from Equisetum telmateia. Colloid Polym Sci 2003;281(7):652–664. https://doi.org/10.1007/s00396-002-0816-7

[16] Shadiya MA, Dominic CM, Nandakumar N, Joseph R, George KE. Isolation and characterization of fibrillar nanosilica of floral origin: Cortaderia selloana flowers as the silica source. Silicon 2022 Jun;14(8):4139-47. https://doi.org/10.1007/s12633-021-01185-2/Published.

[17] Pradeepkumar S, Yassin MM, Marimuthu S, Kalarani MK, Thiyageshwari S, Gurumeenakshi G. Eco-friendly Synthesis and Characterization of Amorphous Nanosilica from Rice Husk. Agricultural Science Digest 2023;43:790–5. https://doi.org/10.18805/ag.D-5792.

[18] Bekkam R, Thiyagarajan C. Foliar application of rice husk derived nanosilica for mitigating drought stress in hybrid maize by boosting antioxidant defense system. J. Hazard. Mater. Adv. 2024;16. https://doi.org/10.1016/j.hazadv.2024.100482.

[19] Singh G, Dizaji HB, Puttuswamy H, Sharma S. Biogenic Nanosilica Synthesis Employing Agro-Waste Rice Straw and Its Application Study in Photocatalytic Degradation of Cationic Dye. Sustainability (Switzerland) 2022;14. https://doi.org/10.3390/su14010539.

[20] Morsy FA, El-Sheikh SM, Barhoum A. Nano-silica and $SiO_2/CaCO_3$ nanocomposite prepared from semi-burned rice straw ash as modified papermaking fillers. Arab. J. Chem. 2019;12:1186–96. https://doi.org/10.1016/j.arabjc.2014.11.032.

[21] Jyani M, Palanisamy K, Phutela UG. Characterization and extraction of silica particles from green solvent pretreated paddy straw. Bull Mater Sci 2024 Jul 16;47(3):154. https://doi.org/10.1007/s12034-024-03266-5S.

[22] Falk G, Shinhe GP, Teixeira LB, Moraes EG, de Oliveira APN. Synthesis of silica nanoparticles from sugarcane bagasse ash and nano-silicon via magnesiothermic reactions. Ceram Int 2019;45:21618–24. https://doi.org/10.1016/j.ceramint.2019.07.157.

[23] Akhayere E, Kavaz D. Nano-silica and nano-zeolite synthesized from barley grass straw for effective removal of gasoline from aqueous solution: a comparative study. Chem Eng Commun 2021;208:1419–35. https://doi.org/10.1080/00986445.2020.1786373.

[24] Rahman IA, Padavettan V. Synthesis of Silica nanoparticles by Sol-Gel: Size-dependent properties, surface modification, and applications in silica-polymer nanocompositesa review. J Nanomater 2012;2012. https://doi.org/10.1155/2012/132424.

[25] Wang Y, Sun Y, Wang J, Yang Y, Li Y, Yuan Y, et al. Charge-Reversal APTES-Modified Mesoporous Silica Nanoparticles with High Drug Loading and Release Controllability. ACS Appl Mater Interfaces 2016;8:17166–75. https://doi.org/10.1021/acsami.6b05370.

[26] Mousavi M, Fini E. Silanization Mechanism of Silica Nanoparticles in Bitumen Using 3-Aminopropyl Triethoxysilane (APTES) and 3-Glycidyloxypropyl Trimethoxysilane (GPTMS). ACS Sustain Chem Eng 2020;8:3231–40. https://doi.org/10.1021/acssuschemeng.9b06741.

[27] Flinn DH, Guzonas DA, Yoon RH. Characterization of silica surfaces hydrophobized by octadecyltrichlorosilane. Colloids Surf. A: Physicochem. Eng. Asp.1994 Aug 16;87(3):163-76. https://doi.org/10.1016/0927-7757(94)80065-0

[28] Karim AH, Jalil AA, Triwahyono S, Sidik SM, Kamarudin NHN, Jusoh R, et al. Amino modified mesostructured silica nanoparticles for efficient adsorption of methylene blue. J Colloid Interface Sci 2012;386:307–14. https://doi.org/10.1016/j.jcis.2012.07.043.

[29] Gaslain FOM, Delacote C, Walcarius A, Lebeau B. One-step preparation of thiol-modified mesoporous silica spheres with various functionalization levels and different pore structures. J Solgel Sci Technol 2009;49:112–24. https://doi.org/10.1007/s10971-008-1845-6.

[30] Cash BM, Wang L, Benicewicz BC. The preparation and characterization of carboxylic acid-coated silica nanoparticles. J Polym Sci A Polym Chem 2012;50:2533–40. https://doi.org/10.1002/pola.26029.

[31] Palraj S, Selvaraj M, Maruthan K, Rajagopal G. Corrosion and wear resistance behavior of nano-silica epoxy composite coatings. Prog Org Coat 2015;81:132–9. https://doi.org/10.1016/j.porgcoat.2015.01.005.

[32] Gajdošová V, Špírková M, Aguilar Costumbre Y, Krejčíková S, Strachota B, Šlouf M, et al. Morphology, Micromechanical, and Macromechanical Properties of Novel Waterborne Poly(urethane-urea)/Silica Nanocomposites. Materials 2023;16. https://doi.org/10.3390/ma16051767.

[33] Xiong Z, Chen N, Wang Q. Preparation and properties of melamine formaldehyde resin modified by functionalized nano-SiO_2 and polyvinyl alcohol. Polym. polym. compos. 2021;29:96–106. https://doi.org/10.1177/0967391120903548.

[34] Kausar A. Polyamide/nanosilica nanocomposite: a chronicle of design and high-tech progressions. Mater. Res. Innov. 2022;26:52–63. https://doi.org/10.1080/14328917.2021.1873479.

[35] Lin CK, Xie JW, Tsai PJ, Wang HY, Lu ZW, Lin TY, et al. The Effects of Different Blending Methods on the Thermal, Mechanical, and Optical Properties of

PMMA/SiO_2 Composites. J. Compos. Sci.2024;8. https://doi.org/10.3390/jcs8090369.

[36] Kodali D, Umerah CO, Idrees MO, Jeelani S, Rangari VK. Fabrication and characterization of polycarbonate-silica filaments for 3D printing applications. J Compos Mater 2021;55:4575–84. https://doi.org/10.1177/00219983211044748.

[37] Montes-Zavala I, Pérez-González MJ, Castrejón-González EO, Santamaría-Razo DA, Almendárez-Camarillo A, Pérez E, et al. Thermal and mechanical properties of poly(lactic acid) filled with modified silicon dioxide: importance of the surface area. Polym. Bull. 2022;79:1409–35. https://doi.org/10.1007/s00289-021-03571-7.

[38] Steinbach JC, Fait F, Mayer HA, Kandelbauer A. Monodisperse Porous Silica/Polymer Nanocomposite Microspheres with Tunable Silica Loading, Morphology and Porosity. Int J Mol Sci 2022;23. https://doi.org/10.3390/ijms232314977.

[39] Yang H, Wang D, Han Y, Tian P, Gao C, Yang X, et al. Preparation and properties of modified poplar impregnated with PVA-nano silica sol composite dispersion system. J. Wood Chem. Technol. 2022;42:211–21. https://doi.org/10.1080/02773813.2022.2064875.

[40] Mousa E, Hafez Y, Nasr GM. Optical Study on PVA/PEG Blend Doped with Nano-Silica. J Electron Mater 2021;50:2594–604. https://doi.org/10.1007/s11664-021-08785-z.

[41] Takeno H, Aoki Y, Kimura K. Effects of silica and clay nanoparticles on the mechanical properties of poly (vinyl alcohol) nanocomposite hydrogels. Colloids Surf. A: Physicochem. Eng. Asp.2021 Dec 5;630:127592. https://doi.org/10.1016/j.colsurfa.2021.127592

[42] Ben Doudou B, Jaouadi H, Dridi C. Prism coupling technique investigation of optical and thermo-optical properties of polyvinyl alcohol and polyvinyl alcohol/silica nanocomposite films. Opt Commun 2021;492. https://doi.org/10.1016/j.optcom.2021.126984.

[43] Sabr OH, Hussein AA, Obaid MN. Improving Mechanical and Morphological Characteristics PVA/SiO_2 Nanocomposites for Food Packing Applications . IOP Conf Ser Mater Sci Eng 2021;1094:012146. https://doi.org/10.1088/1757-899x/1094/1/012146.

[44] Hidayati N, Munasir. Study of electrical and thermal properties of PVA-nanosilica as a candidate for supercapacitor separators. J. Phys. Conf. Ser., vol. 2110, Institute of Physics; 2021. https://doi.org/10.1088/1742-6596/2110/1/012012.

[45] Hashim A, Hamad ZS. Lower cost and higher UV-Absorption of polyvinyl alcohol/ silica nanocomposites for potential applications. Egypt J Chem 2020;63:461–70. https://doi.org/10.21608/ejchem.2019.7264.1593.

[46] Reino Olegário da Silva DA, Bosmuler Zuge LC, de Paula Scheer A. Preparation and characterization of a novel green silica/PVA membrane for water desalination by pervaporation. Sep Purif Technol 2020;247. https://doi.org/10.1016/j.seppur.2020.116852.

[47] Soliman TS, Vshivkov SA, Elkalashy SI. Structural, thermal, and linear optical properties of SiO_2 nanoparticles dispersed in polyvinyl alcohol nanocomposite films. Polym Compos 2020;41:3340–50. https://doi.org/10.1002/pc.25623.

[48] Kariminejad M, Zibaei R, Kolahdouz-Nasiri A, Mohammadi R, Mortazavian AM, Sohrabvandi S, et al. Chitosan/polyvinyl alcohol/SiO_2 nanocomposite films: Physicochemical and structural characterization. Biointerface Res Appl Chem 2022;12:3725–34. https://doi.org/10.33263/BRIAC123.37253734.

[49] Chaerunisaa AY, Sriwidodo S, Abdassah M. Microcrystalline cellulose as pharmaceutical excipient. Pharmaceutical formulation design-recent practices. 2019 Jul 19:1-21. https://doi.org/10.5772/intechopen.88092.

[50] Kumar Gupta P, Sai Raghunath S, Venkatesh Prasanna D, Venkat P, Shree V, Chithananthan C, et al. An Update on Overview of Cellulose, Its Structure and Applications. Cellulose, IntechOpen; 2019. https://doi.org/10.5772/intechopen.84727.

[51] Nguyen T. Evaluation of AaltoCellTM as a filler for tablets compressed from high-shear wet granulated formulations. Technology. 2023 May.

[52] Nur Hanani AS, Zuliahani A, Nawawi WI, Razif N, Rozyanty AR. The Effect of Various Acids on Properties of Microcrystalline Cellulose (MCC) Extracted from Rice Husk (RH). IOP Conf. Ser. Mater. Sci. Eng., vol. 204, Institute of Physics Publishing; 2017. https://doi.org/10.1088/1757-899X/204/1/012025.

[53] Fan GZ, Wang YX, Song G Sen, Yan JT, Li JF. Preparation of microcrystalline cellulose from rice straw under microwave irradiation. J Appl Polym Sci 2017;134. https://doi.org/10.1002/app.44901.

[54] Wang J, Zhang R, Quan C, Shao X, Hu N, Yao X, et al. Green preparation of porous corncob microcrystalline cellulose, and its properties and applications. Cellulose 2022;29:7125–38. https://doi.org/10.1007/s10570-022-04724-1.

[55] Homyuen A, Vanitjinda G, Yingkamhaeng N, Sukyai P. Microcrystalline Cellulose Isolation and Impregnation with Sappan Wood Extracts as Antioxidant Dietary Fiber for Bread Preparation. ACS Omega 2023;8:31100–11. https://doi.org/10.1021/acsomega.3c03043.

[56] Debnath B, Duarah P, Purkait MK. Microwave-assisted quick synthesis of microcrystalline cellulose from black tea waste (Camellia sinensis) and characterization. Int J Biol Macromol 2023;244. https://doi.org/10.1016/j.ijbiomac.2023.125354.

[57] Gómora-Hernández JC, Tecante A, del Carmen Carreño-de-León M, Flores-Álamo N, Ventura-Cruz S. Preparation of porous microcrystalline cellulose from mezcal industry agave bagasse by low reagent loading sequential chemical treatment. Cellulose 2023;30:2067–84. https://doi.org/10.1007/s10570-022-05022-6.

[58] Singhal S, Agarwal S, Kumar A, Kumar V, Prajapati SK, Kumar T, et al. Waste Clothes to Microcrystalline Cellulose: An Experimental Investigation. J Polym Environ 2023;31:358–72. https://doi.org/10.1007/s10924-022-02609-9.

[59] Liang Z, Li X, Li M, Hong Y. Study on the Preparation and Properties of Jute Microcrystalline Cellulose Membrane. Molecules 2023;28. https://doi.org/10.3390/molecules28041783.

[60] Hasanin, M.S., Kassem, N. & Hassan, M.L. Preparation and characterization of microcrystalline cellulose from olive stones. Biomass Conv. Bioref 2023. 13, 5015–5022 (2023). https://doi.org/10.1007/s13399-021-01423-

[61] Gopal PM, Suganya Priyadharshini G, Suyambulingam I, Divakaran D, Kavimani V, Sanjay MR, et al. Exfoliation and physicochemical characterization of novel biomass-based microcrystalline cellulose derived from Millettia pinnata leaf. Biomass Convers Biorefin 2024;14:20189–99. https://doi.org/10.1007/s13399-023-04059-2.

[62] Sunesh NP, Suyambulingam I, Divakaran D, Siengchin S. Isolation of Microcrystalline Cellulose from Valoniopsis pachynema Green Macroalgae: Physicochemical, Thermal, Morphological, and Mechanical Characterization for Biofilm Applications. Waste Biomass Valorization 2024;15:1247–66. https://doi.org/10.1007/s12649-023-02228-y.

[63] Tasnim S, Tipu MFK, Rana MS, Rahim MA, Haque M, Amran MS, et al. Modification of Bulk Density, Flow Property and Crystallinity of Microcrystalline Cellulose Prepared from Waste Cotton. Materials 2023;16. https://doi.org/10.3390/ma16165664.

[64] Do MH, Van Thi Khuat K, Huynh PT, Nguyen LNT, Do BH, Pham PD, et al. Synthesis, characterization, and antibacterial activity of amino-functionalized microcrystalline cellulose derivatives from cotton fibers. Biomass Convers Biorefin 2023;13:10595–603. https://doi.org/10.1007/s13399-022-02391-7.

[65] Li Y, Liu Z, Chi C, Yuan B, Zhang Y, Jiang G, et al. Preparation of Microcrystalline Cellulose/N-(2-aminoethyl)-3- Aminopropyl Methyl Dimethoxysilane Composite Aerogel and Adsorption Properties for Formaldehyde. Polymers (Basel) 2023;15. https://doi.org/10.3390/polym15153155.

[66] Kenawy ER, Khattab SA, Tenhu H, Azaam MM. Ammonium salts of microcrystalline cellulose-g-poly (acrylonitrile): toxicity, antioxidant and anti-inflammatory properties. Cellulose 2023;30:11665–80. https://doi.org/10.1007/s10570-023-05582-1.

[67] Mello BL, Thue PS, da Silva PV, Machado FM, Naushad M, Sellaoui L, et al. Grafting 3-trimethoxysilylpropyl)diethylenetriamine on microcrystalline cellulose for the adsorption of dyes: Experimental and modeling studies. React Funct Polym 2024;196. https://doi.org/10.1016/j.reactfunctpolym.2024.105836.

[68] Jabli M, Sebeia N, El-Ghoul Y, Soury R, Al-Ghamdi YO, Saleh TA. Chemical modification of microcrystalline cellulose with polyethyleneimine and hydrazine: Characterization and evaluation of its adsorption power toward anionic dyes. Int J Biol Macromol 2023;229:210–23. https://doi.org/10.1016/j.ijbiomac.2022.12.309.

[69] Yuan H Bin, Tang RC, Yu CB. Microcrystalline cellulose modified by phytic acid and condensed tannins exhibits excellent flame retardant and cationic dye adsorption properties. Ind Crops Prod 2022;184. https://doi.org/10.1016/j.indcrop.2022.115035.

[70] Shahbazi M, Jäger H, Ettelaie R. Dual-Grafting of Microcrystalline Cellulose by Tea Polyphenols and Cationic ε-Polylysine to Tailor a Structured Antimicrobial Soy-Based Emulsion for 3D Printing. ACS Appl Mater Interfaces 2022;14:21392–405. https://doi.org/10.1021/acsami.1c19430.

[71] Tasnim S, Tipu MFK, Rana MS, Rahim MA, Haque M, Amran MS, et al. Modification of Bulk Density, Flow Property and Crystallinity of Microcrystalline Cellulose Prepared from Waste Cotton. Materials 2023;16. https://doi.org/10.3390/ma16165664.

[72] Thielemans K, De Bondt Y, Van den Bosch S, Bautil A, Roye C, Deneyer A, et al. Decreasing the degree of polymerization of microcrystalline cellulose by mechanical impact and acid hydrolysis. Carbohydr Polym 2022;294. https://doi.org/10.1016/j.carbpol.2022.119764.

[73] Said HA, Ait Bourhim I, Ouarga A, Iraola-Arregui I, Lahcini M, Barroug A, et al. Sustainable phosphorylated microcrystalline cellulose toward enhanced removal performance of methylene blue. Int J Biol Macromol 2023;225:1107–18. https://doi.org/10.1016/j.ijbiomac.2022.11.172.

[74] Su C, Guo J, Cheng J, Zhang J, Gao F. Heterogeneous Epoxidation of Microcrystalline Cellulose and the Toughening Effect toward Epoxy Resin. Ind Eng Chem Res 2023;62:2671–86. https://doi.org/10.1021/acs.iecr.2c03919.

[75] Jhang S, Cho W, Lee SK, Yu AR, Lee JG, Jung K, et al. Functional group effect of chemically modified microcrystalline methyl cellulose on thermoplastic polyurethane composites. Cellulose 2023;30:6917–31. https://doi.org/10.1007/s10570-023-05335-0.

[76] Motta Neves R, Ornaghi HL, Duchemin B, Zattera AJ, Campos Amico S. Grafting amount and structural characteristics of microcrystalline cellulose functionalized with different aminosilane contents. Cellulose 2022;29:3209–24. https://doi.org/10.1007/s10570-022-04484-y.

[77] Chartrand A, Lavoie JM, Huneault MA. Surface modification of microcrystalline cellulose (MCC) and its application in LDPE-based composites. J Appl Polym Sci 2017;134. https://doi.org/10.1002/app.44348.

[78] Madrid JF, Abad L V. Modification of microcrystalline cellulose by gamma radiation-induced grafting. Radiat. Phys. Chem. 2015;115:143–7. https://doi.org/10.1016/j.radphyschem.2015.06.025.

[79] Bezerra RDS, Leal RC, Da Silva MS, Morais AIS, Marques THC, Osajima JA, et al. Direct modification of microcrystalline cellulose with ethylenediamine for use as adsorbent for removal amitriptyline drug from environment. Molecules 2017;22. https://doi.org/10.3390/molecules22112039.

[80] Chen Q, Shi Y, Chen G, Cai M. Enhanced mechanical and hydrophobic properties of composite cassava starch films with stearic acid modified MCC (microcrystalline cellulose)/NCC (nanocellulose) as strength agent. Int J Biol Macromol 2020;142:846–54. https://doi.org/10.1016/j.ijbiomac.2019.10.024.

[81] Gorgun E, Ali A, Islam MS. Biocomposites of Poly(Lactic Acid) and Microcrystalline Cellulose: Influence of the Coupling Agent on Thermomechanical and Absorption Characteristics. ACS Omega 2024;9:11523–33. https://doi.org/10.1021/acsomega.3c08448.

[82] Raharjo WW, Salam R, Ariawan D. The Effect of Microcrystalline Cellulose on the Physical, Thermal, and Mechanical Properties of Composites Based on Cantala Fiber and Recycled High-Density Polyethylene. J. Nat. Fibers 2023;20. https://doi.org/10.1080/15440478.2023.2204454.

[83] Han X, Han Y, Jin Y, Wang Z, Tian H, Huang J, Guo M, Men S, Lei H, Kumar R, Hu J. Microcrystalline cellulose grafted hyperbranched polyester with roll comb structure for synergistic toughening and strengthening of microbial PHBV/bio-based polyester elastomer composites. Int J Biol Macromol. 2023 Jul 1;242(Pt 1):124608. https://doi.org/10.1016/j.ijbiomac.2023

[84] Benaouda SN, Chaker H, Abidallah F, Bachir C, Tawheed H, Weidler PG, et al. Heterogeneous photocatalytic degradation of anionic dye on polyaniline/microcrystalline cellulose composite. J. Porous Mater. 2023;30:327–41. https://doi.org/10.1007/s10934-022-01342-x.

[85] Sosiati H, Rizky AM, Latief ALM, Adi RK, Hamdan S. The mechanical and physical properties of microcrystalline cellulose (MCC)/sisal/PMMA hybrid composites for dental applications. Mater Res Express 2023;10. https://doi.org/10.1088/2053-1591/acbb57.

[86] Ratnakumar A, Rathnayake WSM, Karunanayake L, Samarasekara AMPB, Amarasinghe DAS. Microcrystalline Cellulose as Reinforcing Agents for Polypropylene Composites. Trop. Agric. Res. 2020;31:106. https://doi.org/10.4038/tar.v31i3.8401.

[87] Pan L, Li P, Tao Y. Preparation and properties of microcrystalline cellulose/fish gelatin composite film. Materials 2020;13:1–15. https://doi.org/10.3390/ma13194370.

[88] Rasheed M, Jawaid M, Parveez B, Bhat AH, Alamery S. Morphology, structural, thermal, and tensile properties of bamboo microcrystalline cellulose/poly(Lactic acid)/poly(butylene succinate) composites. Polymers (Basel) 2021; 13:1–15. https://doi.org/10.3390/polym13030465.

[89] Botta L, Titone V, Mistretta MC, La Mantia FP, Modica A, Bruno M, et al. PBAT based composites reinforced with microcrystalline cellulose obtained from softwood almond shells. Polymers (Basel) 2021;13. https://doi.org/10.3390/polym13162643.

[90] Seera SDK, Kundu D, Banerjee T. Physical and chemical crosslinked microcrystalline cellulose-polyvinyl alcohol hydrogel: freeze–thaw mediated synthesis, characterization and in vitro delivery of 5-fluorouracil. Cellulose 2020; 27:6521–35. https://doi.org/10.1007/s10570-020-03249-9.

[91] Kong X, Zhang S, Wang Y, Liu Y, Li R, Ren X, et al. Antibacterial polyvinyl alcohol films incorporated with N-halamine grafted oxidized microcrystalline cellulose. Compos Commun 2019; 15:25–29. https://doi.org/10.1016/j.coco.2019.06.005.

[92] Uto K, Liu Y, Mu M, Yamamoto R, Azechi C, Tenjimbayashi M, et al. Humidity-Responsive Polyvinyl Alcohol/Microcrystalline Cellulose Composites with Shape Memory Features for Hair-Styling Applications. Adv Mater Interfaces 2024;11. https://doi.org/10.1002/admi.202300274.

[93] Naduparambath S, Sreejith MP, Jinitha T V., Shaniba V, Aparna KB, Purushothaman E. Development of green composites of poly (vinyl alcohol) reinforced with microcrystalline cellulose derived from sago seed shells. Polym Compos 2018;39:3033–39. https://doi.org/10.1002/pc.24307.

[94] Gadhave R V., Vineeth SK, Mahanwar PA, Gadekar PT. Effect of addition of boric acid on thermo-mechanical properties of microcrystalline cellulose/polyvinyl alcohol blend and applicability as wood adhesive. J Adhes Sci Technol 2021;35:1072–86. https://doi.org/10.1080/01694243.2020.1832775.

[95] Hussin MH, Husin NA, Bello I, Othman N, Bakar MA, Mohamad Haafiz MK. Isolation of microcrystalline cellulose (MCC) from oil palm frond as potential natural filler for PVA-LiClO4 polymer electrolyte. Int J Electrochem Sci 2018;13:3356–71. https://doi.org/10.20964/2018.04.06.

[96] Maiti S, Ray D, Mitra D, Sengupta S, Kar T. Structural changes of starch/polyvinyl alcohol biocomposite films reinforced with microcrystalline cellulose due to biodegradation in simulated aerobic compost environment. J Appl Polym Sci 2011;122:2503–11. https://doi.org/10.1002/app.34377.

[97] Gadhave R V., Vineeth SK. Synthesis of Microcrystalline Cellulose—Polyvinyl Alcohol Stabilized Polyvinyl Acetate Emulsion. Green Sustain. Chem.2023;13:23–33. https://doi.org/10.4236/gsc.2023.131003.

[98] dos Santos FA, Valle Iulianelli GC, Bruno Tavares MI. Development and properties evaluation of bio-based PLA/PLGA blend films reinforced with microcrystalline cellulose and organophilic silica. Polym Eng Sci 2017;57:464–72. https://doi.org/10.1002/pen.24447.

[99] Platnieks O, Gaidukovs S, Barkane A, Sereda A, Gaidukova G, Grase L, et al. Bio-based poly(butylene succinate)/microcrystalline cellulose/nanofibrillated cellulose-based sustainable polymer composites: Thermo-mechanical and biodegradation studies. Polymers (Basel) 2020;12:1–20. https://doi.org/10.3390/polym12071472.

[100] Kalita P, Roy PK, Das N, Pachuau L. Silicified microcrystalline cellulose from renewable banana pseudostem: Physicochemical and functional analysis. Int J Biol Macromol 2024;283. https://doi.org/10.1016/j.ijbiomac.2024.137620.

[101] Tomar M, Sinha A R, Singh A K Process and Development of Co-Processed Excipient Silicified Microcrystalline Cellulose andManufacture Paracetamol Tablet by Direct Compression Int. J. Pharm. Sci. Rev. Res., 42(1), January - February 2017; 32, 191-196.

[102] Guo M, Augsburger LL. Potential application of silicified microcrystalline cellulose in direct-fill formulations for automatic capsule-filling machines. Pharm Dev Technol 2003;8:47–59. https://doi.org/10.1081/PDT-120017523.

[103] Tobyn, Mike & McCarthy, Gerard & Staniforth, John & Edge, Stephen. Physicochemical comparison between microcrystalline cellulose and silicified microcrystalline cellulose. Int. J. Pharm 1998; 169. 183–194. https://doi.org/10.1016/S0378-5173(98)00127-6.

[104] Edge S Potter U Steele D Tobyn M Chen A Staniforth J. The Location of Silicon Dioxide in Silicified Microcrystalline Cellulose. Pharm. Pharmacol. Commun. 1999, 5, 371–376, https://doi.org/10.1211/146080899128734983.

[105] Kachrimanis K, Nikolakakis I, Malamataris S. Tensile strength and disintegration of tableted silicified microcrystalline cellulose: influences of interparticle bonding. J Pharm Sci. 2003 Jul;92(7):1489-501. https://doi.org/10.1002/jps.10403

[106] Kachrimanis K, Noisternig MF, Griesser UJ, Malamataris S. Dynamic moisture sorption and desorption of standard and silicified microcrystalline cellulose. Eur. J. Pharm. Biopharm. 2006;64:307–15. https://doi.org/10.1016/j.ejpb.2006.05.019.

[107] Zhou Q, Shi L, Chattoraj S, Sun CC. Preparation and characterization of surface-engineered coarse microcrystalline cellulose through dry coating with silica nanoparticles. J Pharm Sci 2012;101:4258–66. https://doi.org/10.1002/jps.23301.

[108] Kiziltas, Alper & Han, Yousoo & Gardner, Douglas & Nader, Jacques. The Effect of Filler Type on the Mechanical, Thermal and Rheological Properties of Cellulose-filled Thermoplastic Composites . Proceedings of the International Convention of Society of Wood Science and Technology and United Nations Economic Commission for Europe – Timber Committee October 11-14, 2010, Geneva.

[109] Iskakov RM, Bukanova AS, Kalauova AS, Kairliyeva FB, Nauashev AN, Shambilova GK, et al. Eco-Friendly Polypropylene Composites Reinforced with Cellulose Fibers and Silica Nanoparticles. Polymers (Basel) 2025;17. https://doi.org/10.3390/polym17101290.

[110] Sun J, Liu X, Liang Y, Wang L, Liu Y. The preparation of microcrystalline cellulose–nanoSiO_2 hybrid materials and their application in tire tread compounds. J Appl Polym Sci 2017;134:11. https://doi.org/10.1002/app.44796.

[111] Xu SH, Gu J, Luo YF, Jia DM. Effects of partial replacement of silica with surface modified nanocrystalline cellulose on properties of natural rubber nanocomposites. Express Polym Lett 2012;6:14–25. https://doi.org/10.3144/expresspolymlett.2012.3.

[112] Du, Yu & Wu, Yueqiao & Ma, Xiaofan & Hu, Yunhao & Bi, Honghua & Sun, Jutao. Effects Of Heterogeneity Of Microcrystalline Cellulose With Nano-SiO_2 On Its Application In Tire Tread Compounds. Cellul. Chem. Technol 2020. 54. 371-380. 10.35812/CelluloseChemTechnol.2020.54.38.

[113] Song D, Ma LW, Pang B, An R, Nie JH, Guo YR, et al. An Active Bio-Based Food Packaging Material of ZnO@Plant Polyphenols/Cellulose/Polyvinyl Alcohol: DESIGN, Characterization and Application. Int J Mol Sci 2023;24. https://doi.org/10.3390/ijms24021577.

[114] Ismardi A, Mayundri SAF, Suhendi A, Fathona IW, Fauzan MZ. Effect of incorporating cellulose nanocrystals into ZnO/PVA nanocomposite for the production of electrochemical sensor to detect cadmium in water. Results Chem 2025;17. https://doi.org/10.1016/j.rechem.2025.102626.

[115] Abutalib MM. Effect of zinc oxide nanorods on the structural, thermal, dielectric and electrical properties of polyvinyl alcohol/carboxymethyle cellulose composites. Physica B Condens Matter 2019;557:108–16. https://doi.org/10.1016/j.physb.2019.01.018.

[116] Jayachandiran J, Vajravijayan S, Nandhagopal N, Gunasekaran K, Nedumaran D. Fabrication and characterization of ZnO incorporated cellulose microfiber film: structural, morphological and functional investigations. J. Mater. Sci.: Mater. Electron. 2019;30:6037–49. https://doi.org/10.1007/s10854-019-00904-1.

[117] Giannakas AE, Salmas CE, Moschovas D, Baikousi M, Kollia E, Tsigkou V, et al. Nanocomposite Film Development Based on Chitosan/Polyvinyl Alcohol Using ZnO@montmorillonite and ZnO@Halloysite Hybrid Nanostructures for Active Food Packaging Applications. Nanomaterials 2022;12. https://doi.org/10.3390/nano12111843.

Chapter 3

Analytical Methodologies and Techniques

3.1 Introduction

Analytical methods and characterisation techniques play a crucial role in elucidation of structure, composition, morphology and functional properties of materials. In the field of materials research, especially for the development of functional and biodegradable composites, the relationship between structure and properties is essential for improving performance and application selection. The present work focuses on the synthesis of silica, Microcrystalline Cellulose (MCC), and Silicified Microcrystalline Cellulose (SMCC), and the fabrication of Polyvinyl Alcohol (PVA) based composite films. A set of analytical techniques was employed for the systematic study of these materials. This chapter describes the principles and methodology of different analytical techniques used throughout the study. The phase analysis was carried out using XRD, the functional groups were detected by FTIR and the surface morphology was examined using FE-SEM. Advanced microscopic techniques such as the Atomic Force Microscope (AFM) and Transmission Electron Microscopy (TEM) were also employed for investigation. Additionally, bulk and true density measurement by the solvent displacement method was also performed. In the final stage, application-oriented tests were conducted to assess the performance of PVA composite films.

3.2 Structural and Phase Characterisation

The crystallinity structure, phase composition, and degree of order in materials were determined using the structural and phase characterisation techniques such as X-ray Diffraction (XRD).

3.2.1 X-ray Diffraction Analysis (XRD)

It is a widely used analytical technique which gives information about the arrangement of atoms within the material, phase composition, crystallinity, chemical

composition and other properties of organic and inorganic materials. It is widely used in the field of material science, chemistry, geology, mineralogy, metallurgy, pharmaceutical biotechnology, electronics, nuclear science, etc. When X-rays strike a material, they are diffracted due to the regular arrangement of atoms [1]. Crystalline material has an ordered arrangement of atoms or ions which forms a plane, and there are definite interplanar distances. When X-rays having the wave length in the order of interplanar distance strike the sample, there will be scattering. The scattered X-rays interfere with each other and at a particular condition they interfere constructively to give a distinct diffraction pattern.

The condition for constructive interference is given by Bragg's law,

$$n\lambda = 2d \sin \theta$$

According to Bragg's law, constructive interference occurs only if the path difference between X-rays reflected from adjacent planes is an integral multiple of the wavelength. XRD pattern consists of a series of peaks; the position (angle) and intensity of these peaks provide the information about the crystal structure of the material. If the diffraction peaks are compared with known references in databases like the International Centre of Diffraction Data (ICCD), the unknown compound can be identified. The crystallinity of the sample can be determined by analysing the sharpness and symmetry of diffraction peaks. A typical XRD instrument consists of an X-ray tube having a copper (Cu) anode, which produce X-ray with a characteristic wavelength. The sample is placed on a rotating platform called a goniometer, which controls the angle at which the X-ray strikes and detects the diffraction angle. A detector measures the intensity of the diffracted angle as a function of the scattered angle(2θ). XRD studies of all the samples were conducted using X pert Powder Diffractometer.

In this study, XRD analysis was conducted to distinguish the amorphous and crystalline nature of extracted silica, to assess the crystallinity changes in MCC and SMCC and to analyse the structural modification in PVA composite films when the fillers are incorporated

3.3 Chemical and Functional Group Analysis

It refers to the identification and study of the functional groups and molecular interactions present in the material. The techniques, such as Fourier Transform-Infrared spectroscopy (FTIR) and Attenuated Total Reflectance-FTIR (ATR-FTIR), are used to detect the functional groups, and changes in peak positions or intensity indicate chemical interactions or bonding between the materials

3.3.1 Fourier Transform-Infrared (FT-IR) Spectroscopy

It is a powerful and widely used spectroscopic technique which gives precise insight into the structure and composition of the molecules. It is based on the principle that when IR radiation is passed through a specific molecule, different chemical bonds in the molecule absorb characteristic frequencies, corresponding to the vibrational frequency of the bond. These absorption frequencies are recorded as an absorption spectrum, and are unique for a particular molecule. The fundamental vibrational and vibrational- rotational frequencies of a molecule lie in the region of 400-4000 cm^{-1}. A typical FT-IR instrument includes an infrared light source, interferometer, detector, and computer software.

Fourier transform is a mathematical method to convert the raw data into a readable format. Here, the time-domain signals collected by the interferometer are converted to frequency domain spectrum. The FT-IR spectrum represents the absorbance of the sample versus wave number. Each peak in the spectrum corresponds to a specific type of vibration of a chemical bond in the molecule. The intensity of the peak measures the interaction of the light with a particular bond. The stronger the bond or the higher the concentration, the higher will be intensity. The peak shape and width give information about the extent of intermolecular interaction, such as H-bonding [2]. In the current study, the powder form of the sample, such as MCC, silica and MCC were analysed using Agilent Technologies Carry 660 instruments in the wave number range of 400-4000 cm^{-1} using KBr pellets.

3.3.2 Attenuated Total Reflectance-FTIR (ATR-FTIR)

It is a sampling technique in conjunction with IR spectroscopy. This method allows the analysis of solid, liquid or film directly without sample preparation. Here,

a beam of radiation passing through a crystal undergoes total internal reflection, producing an evanescent wave orthogonal to the sample. When the evanescent wave interacts with the sample, part of the IR light will be absorbed by the sample at different frequencies corresponding to the bond and the remaining light is reflected to the ATR crystal. The detector measures the intensity of the reflected light, and a change in intensity is analysed to produce an IR spectrum [3]. This technique is used to study surface layers of the sample. Thus, polymers, composites, coatings, corrosion or oxidation on metals can be analysed by ATR-FIIR. In the present study, PVA composites films were analysed using a Perkin Elmer Spectrum-II instrument.

In the present study, FT-IR spectroscopy was used to confirm the presence of characteristic groups in silica, MCC and Silicified MCC. ATR-FTIR was used to study the features of PVA composite films, such as hydrogen bonding and interaction between PVA and fillers. The shift in position of the peaks and changes in intensity of bands give the molecular-level interaction, which influences the performance of composites.

3.4 Thermal Characterisation

Thermal characterisation means how the material responds to changes in temperature. Generally, it is used to study the thermal stability, decomposition behaviour and phase transition of the material. This analysis is very important as it gives the information about the long-term performance of the material at various temperatures. Here, thermal analysis of all the samples was carried out by Thermogravimetry.

3.4.1 Thermogravimetric Analysis (TGA)

Thermogravimetry is the study of the behaviour of a material as a function of temperature. Here, the sample is placed in a furnace, and the changes in mass are monitored by a sensitive balance. Thermograms are obtained by plotting mass loss against temperature [4]. This curve is used for identifying the thermal behaviour like decomposition, phase transition, oxidation or dehydration, etc. The material is heated or cooled at a controlled rate, often from room temperature to thousand and above

degree Celsius. Heating is conducted in a controlled atmosphere. A typical thermogram includes initial weight loss due to evaporation of moisture or volatile components, decomposition temperature due to the breakdown of polymers or organic material and a residual mass after decomposition

Derivative Thermogravimetry (DTG) is the first derivative of TGA, which gives the rate of mass loss at each temperature point by calculating the slope at each point. The DTG curve consists of a number of peaks which tell about temperature at which the sample undergoes the most significant mass loss. A sharp peak indicates the rapid weight loss, whereas a broad peak indicates a gradual or complex degradation process. DTG is very useful for characterisation of polymer composites, since they undergo multiple stages of degradation. Moreover, it is very useful if multiple thermal events such as evaporation, decomposition or oxidation take place within a short range of temperature.

Differential Thermal Analysis (DTA) is a technique that measures the difference between a sample and a reference material when they are subjected to the same heating or cooling conditions. The DTA curve is obtained by plotting this temperature difference as a function of temperature or time. The negative peak in the DTA curve is due to an exothermic reaction like crystallisation or oxidation. Endothermic reaction such as melting, sublimation produces positive peak. In some cases, the area under the peak may be used to estimate the heat involved in the reaction. But a more accurate result is obtained from the Differential Scanning Calorimeter (DSC). In this study, Perkin-Elmer's STA 8000 instrument is used for thermal studies, and the heating rate is 10^0 C/minute in an inert atmosphere of N_2.

3.5 Morphological and Surface Characterisation

Morphological analysis focuses on examining the surface features, particle size and shape of the material. The analysis gives insight into surface roughness, porosity and dispersion of components. The techniques such as FE-SEM, AFM and TEM are commonly used to visualise morphology and structure-property relationships.

3.5.1 Scanning Electron Microscopy (SEM)

SEM is a powerful tool to study micro- and nano-scale features of a material. It is the most versatile tool for imaging and analysing the surface of chemical and biological specimens. It gives high-resolution and 3D images of the sample surface. The instrument consists of an electron gun which produce high-energy electron beam. The electron beam hit the surface of the sample, producing secondary electrons, back-scattered electrons and X-rays. In conventional SEM, the detector captures emitted electrons and create high resolution image of the sample structure [5]. SEM can achieve a resolution up to 1-10 nm and magnification up to 1 million times or more. Based on the type of electron gun, there are conventional SEM and Field Emission SEM (FE-SEM). Conventional SEM uses tungsten filaments as the electron source. It offers resolution of 1-5 nm, whereas FE-SEM uses field emission gun, which provide much finer electron beam and offer resolution less than 1nm [6]. FE-SEM is often coupled with EDS, which analyses the elemental composition of the sample. High energy electron beams knock the inner electron from the atoms of the sample. Now the electrons from the high energy level falls to fill the vacancy. Due to this, energy is released in the form of X-rays, and its wavelength is unique for a particular element [7].

3.5.2 Atomic Force Microscopy (AFM)

It is a scanning probe microscope used to study the surface properties of micro and nano-materials. Here, a sharp, flexible tip known as a probe is scanned over the surface. The tip is mounted on a cantilever, as it moves over the surface, it detects the interactive force between the tip and the atoms of the surface. The interaction may be attractive or repulsive, and based on this, topographical map is made by AFM. A scanning probe is made up of silicon or silicon nitride with a sharp end that is often less than 10 nm in radius. When the probe approaches the surface, there will be deflection in the cantilever due to van der Waals force, electrostatic force and other mechanical forces. A laser beam is used to analyse the deflection of the cantilever. The reflected laser beam from the cantilever strikes a photodetector, and the movement of the spot is recorded. This data is used to determine the height of the

surface at each point and 3D map is formed [8]. In this study AFM image of MCC was taken using WI Tec GmbH, Alpha 3000RA instrument in non-contact mode. A dilute aqueous suspension of MCC was deposited on a glass plate as a layer and was dried at room temperature.

3.5.3 High Resolution-Transmission Electron Microscopy (HR-TEM)

In this microscopy technique, a high-energy beam of electrons is transmitted through the sample to form an image. The image is formed due to the interaction of electrons with the sample as it passes through the specimen. The image is then magnified and focuses to the device, such as a fluorescent screen or photographic film. Since electrons have a much shorter wavelength than visible light, TEM can achieve much higher resolution and magnification than an optical microscope. Generally, the thickness of the specimen should be less than 100 nm. High Resolution-TEM (HR-TEM) allows resolution down to the individual atom. It reveals the internal details like crystal structure, defects and cellular components. TEM analysis is widely used in material science, biology and nanotechnology for analysing nanofibrils, cellular structure, nanoparticles, etc.

Typically, TEM has an electron source (electron gun) that produces a focused beam of electrons accelerated by a high voltage system and a column of electromagnetic lenses and apertures that control and focus the electron beam on the sample and magnify the transmitted electrons to form an image. The specimen is held on a precise specimen holder that allows positioning and tilting. All these elements, together with computer control, make high resolution images at the nanoscale. In this study, HR-TEM images of MCC were recorded using JEOL/JEM2100.

3.6 Determination of True Density (T.D), Bulk Density (B.D) and Porosity(P)

True density is a measure of the density of a material excluding voids, pores or air gaps. The value T.D is helpful in assessing the purity and composition of the material. Consistency in true density is very important in maintaining the quality and reliability of the product. T.D plays a fundamental role in deciding the mechanical,

physical and chemical behaviour of a substance. The material having high true density have higher thermal conductivity.

Bulk density is the mass of the material per unit volume including void space of the material. The filler with high bulk density enhances overall strength, thermal conductivity and stability of the composites. Porosity is the ratio of the volume of voids to the total volume of the powder. The particles having small size having high surface area can pack tightly, thus resulting in lower porosity. Moreover, the particles with irregular shapes also increase the porosity. Moisture content also increases the porosity, and the method of production of powder also influences the porosity.

True Density, Bulk Density and Porosity of MCC, Silica and SMCC were determined in the following method [9]

True density (T.D) is the density of the powder excluding pores and voids

$$T.D = \text{Weight of Powder/True Volume of Powder} \quad \textbf{(3.1)}$$

T. D is determined by the solvent displacement method.

Let, W_1 be the weight of an empty pycnometer with a stopper.
Fill it with water and again weighed (W_2).
Remove the water and transfer the sample (approximately 1 g) to the pycnometer and weighed(W_3).
Fill the same bottle with water and again weighed (W_4).

Now, Weight of Powder(X) $= W_3-W_1$

(Weight of Pycnometer + Water present with Powder), ie $W_5 = W_4-X$

Weight of water displaced by powder= W_2-W_5

Assuming the density of water is 1, then

Weight of water displaced by powder= Volume of water≅ True volume of powder

Bulk Density (B.D) is the density of the powder, including all pores and voids within the sample

B. D= Weight of Powder/ Bulk volume of Powder

(3.2)

The known weight of the sample is transferred to a measuring cylinder, and the bulk volume of the powder is determined.

Porosity (P) is the measurement of empty space in the powder

$$\text{Porosity (\%)} = \frac{Void\ Volume \times 100}{Bulk\ Volume} \quad \textbf{(3.3)}$$

Void Volume= Bulk Volume- True Volume

3.7 Optical Characterisation (UV-Visible Spectroscopy)

It is the study of how materials interact with light in U.V and visible region of the electromagnetic spectrum. It is used to evaluate the properties like light absorption, transparency, and UV blocking behaviour, which are important for applications like packaging, coating and optoelectronic materials. In this study, the transparency of PVA composite films was measured using a Systronics 117 spectrophotometer.

3.8 Surface Wettability Test (Contact Angle Measurement)

Contact angle measurement is an effective and widely used technique for analysing the surface wettability and hydrophobicity of solid materials. It is based on measuring the angle formed at the boundary where water droplets come in contact with the solid surface. A lower contact angle indicates high wettability and greater affinity with water, while a high contact angle reflects lower wettability and hydrophobicity. In the current study, contact angle measurements were performed on PVA composite to evaluate the effect of fillers on surface wettability. These results were correlated with the water absorption behaviour and water vapour transmission rate of the polymer film.

3.9 Water Absorption (Swelling) Test

This study was carried out to assess the moisture uptake behaviour of PVA composite films. Water absorption is the quantity of water withdrawn by a particular

sample at specific conditions. The polymer films, each with dimensions 2 cm ×2 cm, were dried in an air oven at a temperature of 60 °C for 2 h. They were cooled, weighed and immersed in 100 ml deionised water. Every 30 minutes, the films were removed, blotted carefully to remove surface water and weighed. This process continued till an equilibrium is achieved.

Now,

$$\textbf{Percentage of water absorption (Swelling)} = \frac{W_t - W_0 \times 100}{W_0} \qquad \textbf{(3.4)}$$

W_0 = Weight of the dry film before immersion

W_t = Weight of the film at 30 minutes after blotting the surface.

3.10 Water Vapour Transmission Rate (WVTR) Analysis

Water vapour Transmission Rate is the measure of the rate of water vapour permeation through the polymer films. This parameter is crucial for evaluating barrier properties, especially for packaging applications. In this study WVTR of the polymer films was determined gravimetrically according to ASTM E96, dry cup procedure. Polymer films with uniform thickness were cut into dimensions slightly higher than the mouth of the cup. The cups were filled with anhydrous $CaCl_2$ to create low humidity. The polymer films were sealed over the mouth of the cup, ensuring to prevent the leakage of vapour through the sides. The entire assembly was weighed using an analytical balance, and the initial weight is noted. This is placed in a desiccator containing water. The cup assemblies were taken out in every 6 h and weighed to determine the mass change over time, until an equilibrium is achieved. Mass versus time was plotted, and WVTR was calculated from the slope of the linear portion

$$WVTR = \frac{\Delta m}{A \times t} \qquad \textbf{(3.5)}$$

Δm is the mass gain in grams over a steady state interval, 'A' is the exposed area of the film (m^2) and 't' is the time interval in hours.

3.11 Biodegradability Test (Soil Burial Degradation)

The biodegradability of polymer films was assessed to evaluate the eco-friendly behaviour of polymer films. The biodegradability of the fabricated films was evaluated by the soil burial method. The bare PVA, PVA/MCC, PVA/SMCC and PVA/SMCC-ZnO film samples, each with dimensions 2 cm× 2 cm, were initially weighed after drying. All the samples were then buried at a depth of 10 cm in locally available soil for 30 days under ambient environmental conditions. To sustain microbial activity, water was sprinkled once ~~in~~ a week. After 30 days, the films were carefully taken, gently cleaned to remove adhered soil and dried to get a constant weight. The percentage weight loss, which is a direct indicator of the extent of biodegradability, was calculated using the equation

$$\textbf{Percentage of Soil Burial Degradation} = \frac{W_i - W_f \times 100}{W_i} \qquad (3.6)$$

Where W_i is the initial dry weight of the specimen, W_f is the weight of film after 30 days.

All the films were characterised with a Field Emission-Electron Microscope (FE-SEM) before the soil burial. After the burial period, the FE-SEM images of all films were also captured to assess the morphological changes, such as surface erosion, microcracks, etc.

3.12 Anti-Bacterial Test

The anti-bacterial test is performed to assess the ability of the polymer film to inhibit or prevent the growth of microorganisms. This assessment is important for determining the suitability of polymers for applications such as food packaging, biomedical applications, wound dressing, etc. In polymer composite films, antibacterial test helps to understand the influence of fillers on antibacterial activity. The antibacterial activity was evaluated by preparing a 0.5 McFarland suspension of *Escherichia coli* (ATCC 25922) and *Staphylococcus aureus* (ATCC 25923), seeding

them onto plates containing 20 mL of Muller-Hinton Agar (33.8 g/L) and placing sterile 10 mm filter-paper discs with test samples (and a streptomycin control, 10 mg/L) onto the surface. After incubation at 37 °C for 24 h, zones of inhibition around the discs were measured in mm to quantify antibacterial efficacy (NCCLS, 1993).

3.13 Mechanical Properties Analysis

Mechanical properties describe how a polymer behaves under mechanical stress and strain. These properties determine the performance, durability and application of the polymer. The important mechanical properties are Tensile Strength (T.S), Young's modulus, Elongation at break, hardness, stiffness, viscoelasticity, etc. T.S is the maximum stress that a polymer can withstand while it is stretched [10]. It is measured in megapascal (MPa) or $N/mm^{2.}$ It gives the ability of the material to resist rupture. Young's modulus is the measure of the stiffness of a polymer. It tells how much a polymer will deform under a given stress. It gives the material resistance to elastic deformation. Elongation at break is the percentage of strain that a polymer can undergo before it breaks. It gives the idea of the flexibility and ductility of the polymer. Yield strength is the stress at which a polymer begins to deform plastically. Impact resistance is the ability of a polymer to absorb energy when subjected to a sudden force.

The mechanical properties of the polymer depend on molecular weight, crystallinity, polymer structure, processing conditions, presence of additives. The mechanical properties can be significantly enhanced by adding fillers like glass, fibres, silica, MCC, etc. The mechanical properties of the films were studied using a universal testing machine model no. SHIMADZU AE-X plus 10 kN.

References

[1] Epp J. X-Ray Diffraction (XRD) Techniques for Materials Characterization. Materials Characterization Using Nondestructive Evaluation (NDE) Methods, Elsevier Inc.; 2016, p. 81–124. https://doi.org/10.1016/B978-0-08-100040-3.00004-3.

[2] Coates J. Interpretation of infrared spectra, a practical approach. Encyclopedia of analytical chemistry. 2000 Sep 15;12:10815-37

[3] Berthomieu C, Hienerwadel R. Fourier transform infrared (FTIR) spectroscopy. Photosynth Res 2009;101:157–70. https://doi.org/10.1007/s11120-009-9439-x.

[4] Wiedemann HG, Bayer G. Trends and applications of thermogravimetry. In: Inorganic and Physical Chemistry. Topics in Current Chemistry, vol 77. Berlin, Heidelberg: Springer; 1978. p. 67–140. doi:10.1007/BFb0048038.

[5] Zhou W, Apkarian R, Wang ZL, Joy D. (2006). Fundamentals of Scanning Electron Microscopy (SEM). In: Zhou, W., Wang, Z.L. (eds) Scanning Microscopy for Nanotechnology. Springer, New York, NY. https://doi.org/10.1007/978-0-387-39620-0_1

[6] Lewczuk B, Szyryńska N. Field-emission scanning electron microscope as a tool for large-area and large-volume ultrastructural studies. Animals 2021;11. https://doi.org/10.3390/ani11123390.

[7] Abd Mutalib M, Rahman MA, Othman MHD, Ismail AF, Jaafar J. Scanning Electron Microscopy (SEM) and Energy-Dispersive X-Ray (EDX) Spectroscopy. Membrane Characterization, Elsevier Inc.; 2017,161–79. https://doi.org/10.1016/B978-0-444-63776-5.00009-7.

[8] Johnson D, Hilal N, Bowen WR. Basic Principles of Atomic Force Microscopy. Atomic Force Microscopy in Process Engineering: An Introduction to AFM for Improved Processes and Products, Elsevier; 2009,1–30. https://doi.org/10.1016/B978-1-85617-517-3.00001-8.

[9] Dane, Jacob & Topp, Clarke & Flint, Alan & Flint, Lorraine. 2002. 2.2 Particle Density. https://doi.org/10.2136/sssabookser5.4.c10

[10] McPhee C, Reed J, Zubizarreta I. Geomechanics Tests. Developments in Petroleum Science, 64, Elsevier; 2015,671–779. https://doi.org/10.1016/B978-0-444-63533-4.ssss00012-3.

Chapter 4

A Comparative Study on Amorphous and Crystalline Nanosilica Extracted from Mission Grass (*Pennisetum polystachion*)

4.1 Introduction

4.1.1 Background on Silica Nanoparticles

Silica nanoparticles are tiny particles, typically with 1-100 nm diameter in size, is one of the most accepted nanoparticles in research field because of its chemical inertness, thermal stability and generally non-toxic and biocompatible nature. They have high surface area, porosity and abundant -OH groups on the surface which can be easily modified with the functional groups such as -NH_2, -COOH, etc. Silica nanoparticles are robust, tunable and versatile materials with wide application spanning advanced catalysis [1], drug delivery [2], biomedical applications [3], polymer composites [4], concrete fillers [5], anticorrosion agents [6] etc. Silica exists in two major structural forms-crystalline and amorphous, with distinct properties and applications. The crystalline silica has long range ordered lattice and it exists in polymorphic forms such as quartz, tridymite, cristobalite, coesite etc. In contrast, amorphous silica lacks ordered structure and it exist as silica gel, colloidal silica, silica fumes precipitated silica etc. Both crystalline and amorphous nanoparticles have wide applications. The crystalline nanosilica is used in photovoltaic cell [7], ceramics [8], humidity sensors [9] etc. But crystalline nanosilica poses significant health risk, since its respirable dust can cause silicosis, and lung cancer, whereas amorphous silica is generally considered as less hazardous. Amorphous silica is extensively used in micro encapsulation [10], stabilizing agents in therapeutics [11], coatings, catalysis, desiccants, reinforcement fillers, etc. Nanosilica can be prepared by methods like vapour phase reduction, sol gel method, thermal reduction, acid leaching, etc.

4.1.2 Nanosilica from Biomasses

Conventionally, nanosilica is synthesised from metal alkoxides such as Tetra Ethyl Ortho Silane (TEOS), Tetra Methyl Ortho Silane (TMOS), inorganic silicates (Na_2SiO_3), silicon halides ($SiCl_4$), etc. [12]. But these have significant drawbacks due to their toxicity, high cost, processing constraints and environmental impact. To address these limitations researchers have developed several effective strategies. In

recent years, agricultural products, agricultural wastes, and various biomasses have emerged as the most promising raw material for extracting biosilica. Plants, especially those under the class of grass family take up silica during their growth and when they are burned, organic components will decompose, and the remaining ash contains silica as the major products [13]. The most widely explored raw material for the extraction of biosilica is rice husk due to its high silica content, abundancy and renewability. One of the recent studies demonstrated an industrial method for the extraction of biogenic silica from the rice husk by one pot alkali hydrothermal treatment and ball milling [14]. In 2025, Jeong et al. compared the mechanical properties of silicon rubber by adding the biosilica extracted from the rice husk and conventional silica [15]. In the same year Santos et al. derived silica from rice husk by sol-gel method and its surface is hydrophobized using stearic acid or hydrogenated castor oil [16]. Recently, Islam et al. studied the effect of temperature and time on purity, morphology, and phase transition of silica from rice husk [17]. Numerous studies were conducted on biosilica extracted from other sources also. Sing et al. synthesised biogenic nanosilica from rice straw and studied its photocatalytic degradation on cationic dyes [18]. Firdaus et al. extracted natural silica from lemon grass by acid leaching followed by thermal combustion at 600 °C [19]. Shim et al. extracted and characterized amorphous silica from corn cob ash at variable pH conditions [20]. Nanosilica was also extracted from sugarcane bagasse [21], banana stem [22], elephant grass, [23], etc.

4.1.3 Mission Grass (Pennisetum polystachion)

Mission Grass (MG), is a robust perennial, tussock forming grass, reaching up to 3 m tall, widely distributed in India, tropical Africa, Australia, etc. The MG is highly invasive, since it spreads quickly via wind-blown seeds, over-run road sides, fallow lands and protected areas. This aggressive spread pushes out native species, disturb crops and alter entire ecosystem. Thus, it is considered as a dangerous weed in most countries. Not only a big threat to the agricultural crops but also it facilitates frequent fire at the field and forest. It produces huge amount of dry fuel which is higher than native grass. This continuous layer of flammable material makes fire much

hotter and faster. The management of this weed became a big challenge. Due to heavy monsoon, which covers half of the year, the expansion of MG in Kerala (One of the states in India) is very rapid and it creates ecological problems. There are currently no documented applications for MG beyond its role as fodder. While a few studies examined ethanol production from MG [24] and it is generally assumed that it is a rich source of biosilica, yet no research has specifically investigated these aspects.

4.1.4 Aim and Objectives of the Study in the Present Chapter

The aim of the study is to evaluate and compare the structural, morphological and physicochemical properties of amorphous and crystalline silica extracted from MG through acid leaching and sol-gel process. The silica synthesis was carried out by adjusting the temperature and employing different methodologies. The silica extracted from MG was characterized using the techniques such as X-ray Diffraction (XRD), Fourier Transform- Infrared (FT-IR) spectroscopy, Field Emission-Scanning Electron Microscopy (FE-SEM), and Thermogravimetry (TGA). The objective of the study includes.

- Calculating the Crystallinity Index of amorphous and crystalline silica extracted through acid leaching and sol-gel method.
- Analyzing the hygroscopic behaviour and difference in water retention properties of amorphous and crystalline silica via TGA.
- Determining the morphology, extent of agglomeration, purity level and particle size of different samples using FE-SEM and EDS.
- Finally, explore the potential pathways for the valorization of MG through the production of silica.

4.2 Materials

The Mission Grass (MG) were collected from road sides of Kerala, India. The chemicals used are hydrochloric acid (HCl), sodium hydroxide (NaOH), silver nitrate ($AgNO_3$), Whatman No 1 filter paper, all procured from Sigma Aldrich. All the chemicals were of analytical grade and were used without further purification.

4.3 Methods

4.3.1 Synthesis of Amorphous Silica

a) Washing and Drying

The MG collected from road sides is cut into small pieces, washed with water to remove dust and mud and then sun-dried for 24 h. The dried, materials were ground well, and 20 g portion of this dried, powdered MG is heated in a muffle furnace at 600 °C for 8 h, yielding 1.4 g mission grass ash (MGA), corresponding to 7% ash yield.

b) Formation of 600 °C Acid Leached Silica (600ALS)

One gram of MGA was digested with 40 ml of 2N HCl for 5 h using a magnetic stirrer kept at 200 ° C. It was then heated in a Bunsen burner for 45 minutes. HCl is added at regular intervals to compensate for the loss due to evaporation. This was then kept in a water bath, allowed to stand overnight and filtered through Whatman No 1 filter paper. The residue was then washed with hot water till the washings were free from chloride ions. The residue was then dried in an air oven at 150 °C and the process yielded 0.6 g (4.2% of original MG mass) 600ALS. The dried residue was characterized by XRD, FT-IR, FE-SEM and EDS for structural and composition analysis.

c) Synthesis of 600 °C Sol Gel Silica (600SGS)

One gram of 600ALS was digested with 25 ml of 3M NaOH, (since percentage yield of pure silica is higher with 3M NaOH) in a magnetic stirrer at 80 °C for 5 h [25]. The mixture was allowed to settle overnight and filtered through Whatman No 1 filter paper. To the filtrate, which is presumed to be sodium silicate (Na_2SiO_3), 2N

HCl is added dropwise with constant stirring, till a white gelatinous precipitate was formed [26]. It was allowed to settle for 12 h for complete gelation and then filtered. The precipitate was washed several times with hot water and then with cold water to ensure the removal of all soluble impurities. The resulting gel was dried in an air oven at 150 °C for 3 h yielding approximately 0.4 g of 600SGS (1.68% of MG). This dried sample was subjected to further physicochemical characterization.

4.3.2 Synthesis of Crystalline Silica

The same procedure was followed for the synthesis of 850 °C Acid Leached Silica (850ALS) and 850 °C Sol Gel Silica (850SGS) with the exception that the washed, dried and powdered MG is heated in a muffle furnace at 850 °C for 8 h. This process yielded 1.1g MGA, representing 5.5% ash yield. Subsequent synthesis produced 0.59 g of 850ALS is 0.59 g (3.25% of MG) and 0.23 g of 850SGS (1.25% of MG). All the samples were characterized and their properties were compared. A schematic overview of all steps and images of silica is provided in **Scheme 4.1.**



Scheme 4.1. Schematic Representation of Synthesis of Amorphous and Crystalline Nanosilica from Mission Grass.

4.4 Results and Discussion

4.4.1 Fourier Transform-Infrared (FT-IR) Spectroscopy

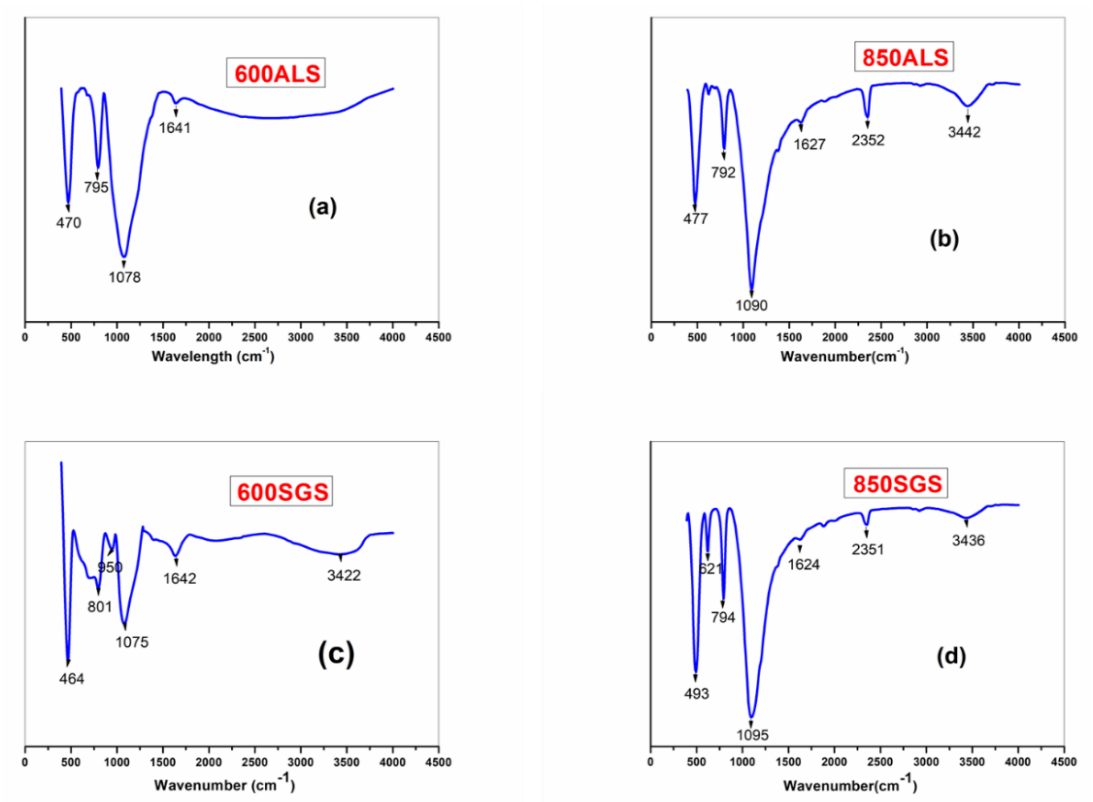

Figure 4.1 FT-IR Spectra of (a) 600ALS (b) 850ALS (c) 600 SGS (d) 850SGS

The presence of silica in the different samples was confirmed by FT-IR spectroscopy, which was taken in transmittance mode. **Figure 4.1 (a-d)** shows the FT-IR spectra of 600ALS, 850ALS, 600SGS and 850SGS respectively. All the samples exhibit prominent and characteristic peaks in the fingerprint region. The FT-IR spectra are consistent with those typically observed for silica derived from tetraethyl orthosilicate (TEOS) precursor [27] . The main chemical groups present in silica are silanol (Si-OH) and siloxane (Si-O-Si) [28]. The absence of peak between 2800 cm^{-1} and 3000 cm^{-1} shows that all samples are free from organic components [29].In **Figure 4.1(a)** the most intense peak at 1078 cm^{-1} is attributed to the asymmetric stretching of Si-O-Si bond and the less intense band at 795 cm^{-1} corresponds to symmetric stretching of Si-O-Si bond of 600ALS [30]. The medium intense peak at 470 cm^{-1} arises from rocking vibration of Si-O-Si bond [31]. The peak at 1641 cm^{-1} is attributed to O-H bending motion of silanol group or adsorbed water molecule [32].

A broad peak around 3500 cm^{-1} is attributed to the hydrogen bonded O-H group of silanol or physisorbed H_2O molecule [33].

Figure 4.1(b) presents the FT-IR spectrum of 850ALS which is similar to that of 600ALS, but has a more pronounced IR band with narrow line width. This indicates the more crystalline nature which was corroborated by XRD analysis. The prominent peak at 1090 cm^{-1} is due to asymmetric stretching and other characteristic peaks at 792 cm^{-1} and 477 cm^{-1} are attributed to symmetric stretching and rocking vibration of Si-O-Si bond. The peak at 1627 cm^{-1} which is attributed to O-H bending motion diminishes and the peak at 3442 cm^{-1} becomes very narrow compared to that of 600ALS. This is because calcination at higher temperature leads to more dehydration of silanol and desorption of water molecules from the compound. The distinct peak which is found at 2350 cm^{-1}in both 850ALS and 850SGS is tentatively attributed to the stretching vibration of Si-C bond. This is likely due to the conversion of silicon containing organic components in the grass precursor into Si-C bonds during high temperature calcination [34]. **Figure 4.1(c)** displays the FT-IR spectrum of sol gel silica (600SGS) which was extracted from MGA heated at 600 °C and subsequent acid leaching. The spectrum is entirely different from the other three samples. The broad and rounded peaks are typical of amorphous solids. The prominent peaks appear at 1056 cm^{-1}, 803 cm^{-1} and 465 cm^{-1} which are characteristic of silica [35]. The intensity of the peak at 1641 cm^{-1}, which is due to the O-H bending, is higher than that in other spectra and this confirms the highly hydrophilic silanol rich surface [36]. A distinct small peak at 951 cm^{-1}, which is absent in other spectra, is attributed to Si-H bending [37]. There is no peak at 2350 cm^{-1} which rules out the existence of Si-C bond and indicates that the compound is pure. This was further confirmed by XRD and FE-SEM/EDS analysis. The broad band due to O-H stretching becomes much more diffused and irregular. This is because in 600SGS, O-H group is extensively H-bonded due to silanol group and adsorbed water molecules [38].

Figure 4.1(d) shows the spectrum of 850SGS where all peaks appear exceptionally sharp and narrow, reflecting its crystalline nature, which was further confirmed by XRD studies. The characteristic silica vibrational peaks are present at 493 cm^{-1}, 794 cm^{-1}, and 1095 cm^{-1}. Moreover, the peaks at 1624 cm^{-1} and 3436 cm^{-1} attributed to the bending and stretching vibration of O-H groups which prevails even

though the sample was calcinated at higher temperature. This is due to the presence of physically adsorbed water molecules from the surrounding environment [39]. This peak appears to be narrower due to dehydration of silanol groups and rupturing of H-bonds.

4.4.2 X-ray Diffraction Analysis

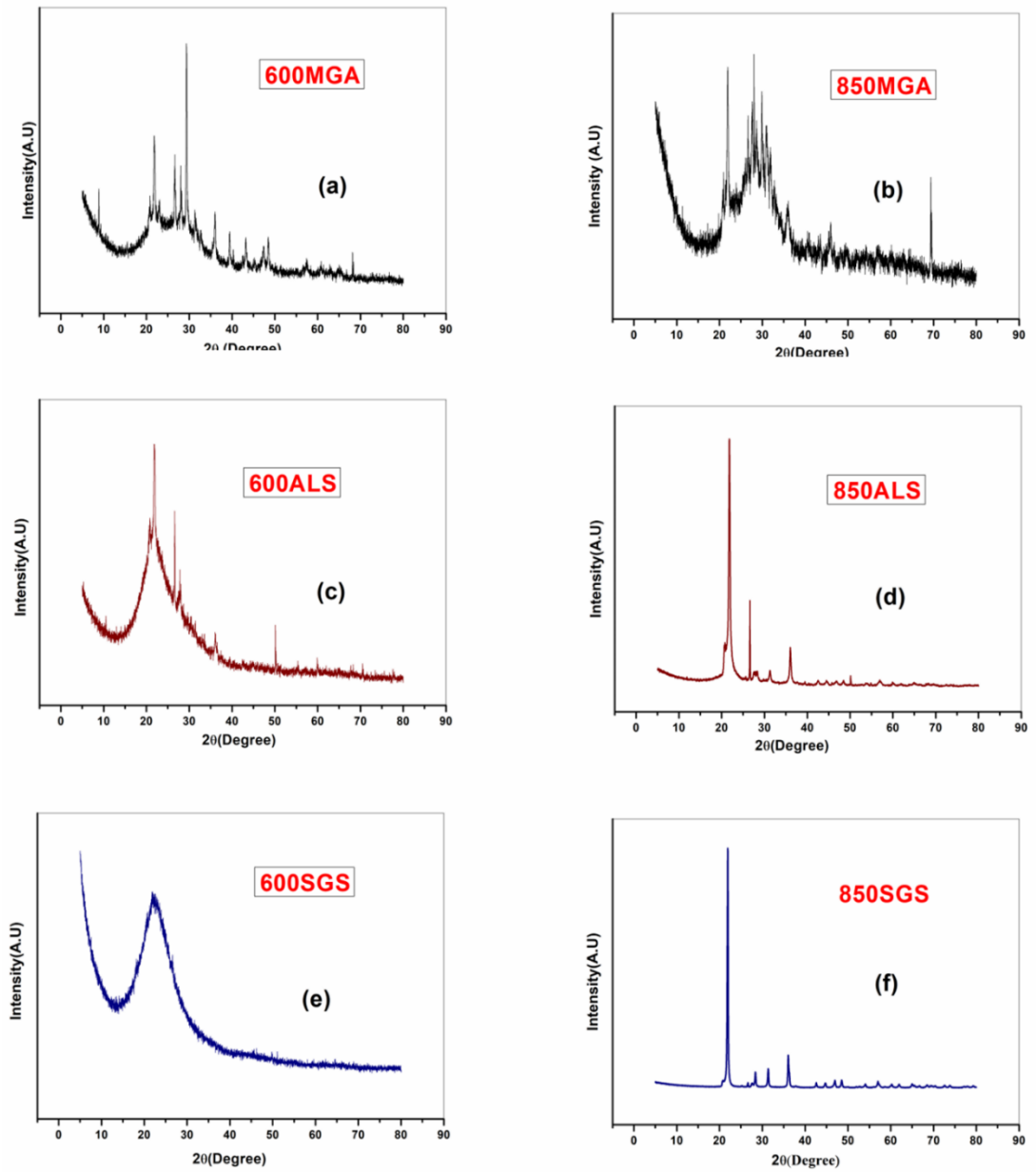

Figure 4.2. X-ray Diffraction Patterns of (a) 600MGA (b) 850MGA (c) 600ALS (d) 850ALS (e) 600SGS and (f) 850SGS

Figure **4. 2(a-f)** shows the X-ray diffractograms of various silica samples, highlighting how different preparation methods and calcination temperature affect their structural characteristics. **Figure 4.2 (a)** and **4.2 (b)** displays the X-ray diffraction (XRD) patterns of mesoporous Mission Grass Ash (MGA) obtained by heating the dried grass at 600 °C and 850 °C respectively. During calcination at high temperature, almost all organic contents will be removed but this will lead to crystallization of some ash. Both the spectra reveal characteristic diffraction peaks corresponding to crystalline silica polymorphs such as cristobalite, tridymite and quartz. The crystalline parts of the ash exist in the form of cristobalite, tridymite and quartz. Specifically, the peaks at 2θ= 21.9°,28.2°, 31.5° and 36.1° are indicative of cristobalite [40], whereas the signals at 2θ= 20.8°,26.6°,49.3° and 60° correspond to quartz [41]. The peaks at 23.3°, 27.8°, 30° and 36.1° are attributed to tridymite [42]. Notably, **Figure 4.2 (b)** shows a greater number of peaks in the range of 2θ=20°-35°, indicating the increased crystallinity at the elevated calcination temperature of 850 °C.

Figure 4.2 (c) and **4.2 (d)** shows the diffractogram of 600ALS and 850ALS respectively. Both are distinct in their appearance. In **Figure 4.2 (c)**, there is a broad hump with a few sharp peaks, characteristic of mostly amorphous silica with minor crystalline impurities. In **Figure 4.2 (d)**, only sharp peaks are present, which is clear evidence of crystalline nature resulting from high temperature treatment followed by acid leaching [35]. The prominent broad peak around 2θ≈21.9° is the characteristic of amorphous silica, which is consistent with findings in silica extracted from rice husk [43, 44]. The sharp peaks at 2θ= 26.6°, 49.9° and 60° are evidence for the existence of trace quantities of crystalline form of quartz [41]. Heating at 850 °C and subsequent acid leaching converts the silica content in the MG into crystalline form [45]. The observed sharp peak at 2θ= 21.8° signifies the formation of crystalline silica, while the additional minor peaks is the characteristic of crystalline form and the minor peaks at 26.7°, 31.3° and 36° is attributed to the presence of other forms like cristobalite and tridymite, which was previously observed in the XRD of MGA.

Figure 4.2 (e) and **4.2 (f)** illustrate the XRD of amorphous and crystalline forms of silica obtained by sol-gel method. **Figure 4.2 (e)** clearly indicates the amorphous nature of 600SGS. There is a broad hump from 15°-30° with a centered peak at 21.9° which confirms the formation of silica which is purely in amorphous form. The absence of any additional peaks indicates the purity of the product and the absence of other minerals in the sample, which aligns well with earlier FT-IR findings for 600SGS.

In contrast, **Figure 4.2 (f)** shows that 850SGS is purely in crystalline nature, indicating cristobalite structure and is comparable with the silica obtained from sodium silicate [39]. The major peaks at 2θ= 21.9° and minor peaks at 28.5°, 31.5° and 36.3° is the clear evidence for the cristobalite structure for 850SGS [40]. The diffractogram is almost similar to 850ALS, but here the major peaks are more pronounced. The shoulder at major peak was diminished and some other peaks vanished, which suggests that 850SGS is purer than 850ALS. These XRD results demonstrate that it is possible to isolate both amorphous and crystalline silica from MG either by acid leaching or sol gel method with high purity. While the sol gel method is costlier and time consuming, one can choose any method based on the desired purity. The crystallinity index of different products was calculated by peak area method and is given in the **Table 4.1**

Table 4.1. Crystallinity Indices of 600ALS, 600SGS, 850ALS and 850SGS

Sample	Crystallinity Index
600ALS	51.4%
600SGS	43.0%
850ALS	59.0%
850SGS	82.0%

As shown in **Table 4.1** 600SGS is highly amorphous and exist in agglomerated form which will be later confirmed from FE-SEM imaging. This has significant application in the realm of material science. Thus, MG is considered as a good source of amorphous silica and crystalline silica as well.

4.4.3 Thermal Analysis

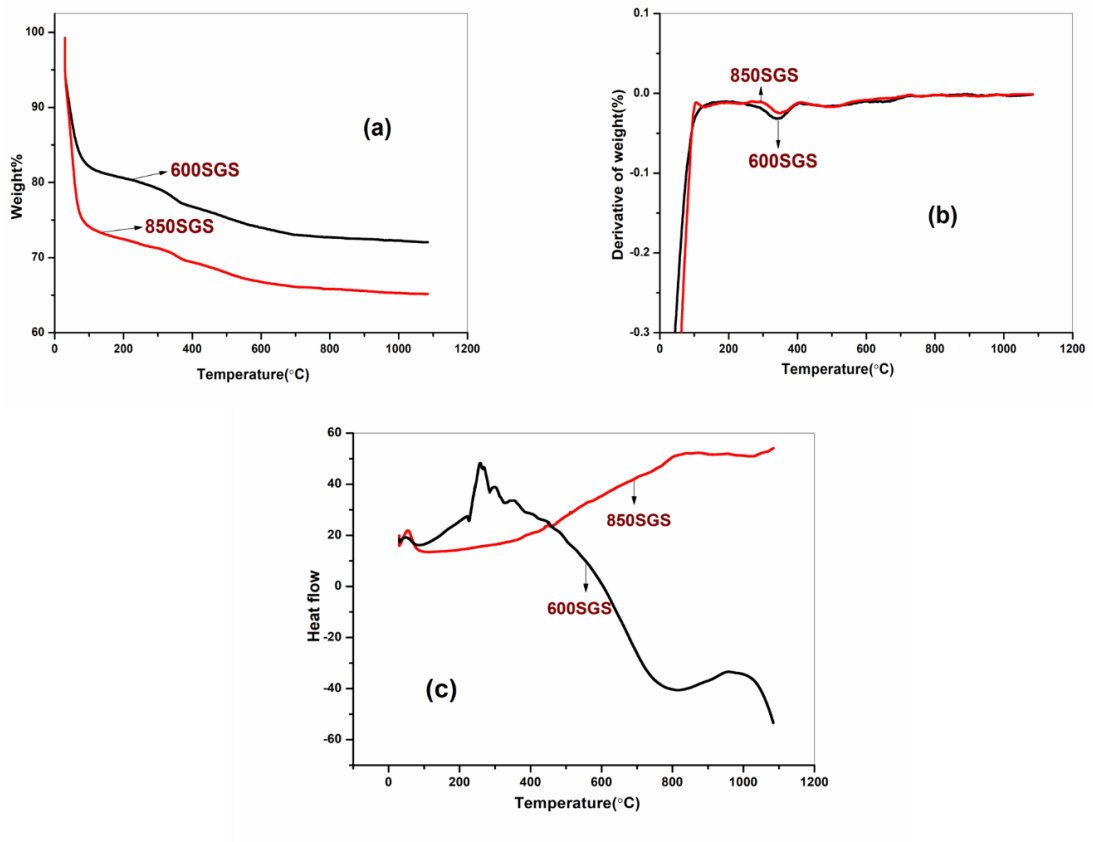

Figure 4.3 (a) Thermogravimetry of 600SGS and 850SGS (b) DTG of 600SGS and 850SGS (c) DTA of 600SGS and 850SGS

A detailed thermal analysis of 600SGS and 850SGS was conducted from room temperature to 1100 °C. **Figure 4.3 (a)** and **4.3 (b)** present the thermogravimetric and corresponding differential thermogravimetric curves of 600SGS and 850SGS respectively. Both samples exhibit the rapid initial weight loss. This is due to the removal of physiosorbed water i.e., moisture [46]. In the temperature range 30-90 °C the weight loss is 16% for 600SGS and 24% for 850SGS. This indicates that crystalline silica has higher hygroscopicity compared to amorphous silica, making crystalline silica a strong candidate for moisture adsorption applications. The removal of physically bonded water is possible if heated up to 120 °C and if the sample contains micropores it will be retained even at higher temperature.

The second stage of weight loss occurs between 90 °C and 330 °C. At this stage, weight loss is 4.2% and 3.4% for 650SGS and 850SGS respectively. This

reduction is attributed to the removal of internal water and dehydration of silanol group [47]. Upon heating, hydrogen bonded hydroxyl groups in silica are rapidly removed between 200 °C and 400 °C whereas isolated hydroxyl groups will be removed only at higher temperature [48]. The weight loss percentage shows that the amorphous silica has more internal water due to its more porous nature. A minor dip at 370 °C in both samples is due to the decomposition of any residual carbonaceous matter. In the third stage, both the curve has a steady slope up to 700 °C. Beyond this point the slope diminishes and becomes parallel to X-axis indicating that both the silica samples are thermally stable at higher temperature.

The concentration of hydroxyl groups present in the sample was also calculated. It is obtained by measuring the difference in weight percentage of the sample at which all physisorbed water molecules are removed and at the end point of the analysis [48] .

It is given by equation 4.1

$$\boldsymbol{nO-H(SiO_2)=\frac{2\{W(T_0)-W(T_{final})\}\times 10}{MH_2O}} \quad \textbf{(4.1)}$$

where ***n* O-H** is the number of moles of O-H group, ***W(T₀)*** and ***W (T$_{final}$)*** are the weight percentages at 90 °C and 1100 °C (current study) respectively and ***M H₂O*** is the molecular weight of water.

The number of O-H groups calculated from the thermogram is 12.6 mmol/gram and 10 mmol/gram for amorphous silica and crystalline silica respectively. Hence amorphous silica is more susceptible to chemical modification.

Figure 4.3 (b) presents the DTG curves of 600SGS and 850SGS, which appear nearly identical. The initial weight loss is very high up to 100 °C due to the removal of moisture content, since silica is inherently hygroscopic. There is no observable weight loss from 125 °C to 250 °C (300 °C for 850SGS), then there is a sharp dip in the curve which is attributed to decomposition of any of the organic matter. Following this, both curves level off and run nearly parallel to X- axis [49]. This suggests that a steady weight loss occurs in both cases due to removal of water

from silanol group [50]. The heat changes during thermogravimetric analysis of 600SGS and 850SGS from room temperature to 1100 °C is recorded as DTA curve (**Figure 4.3 (c)**). The graph shows that in the case of 600SGS up to 260 °C the process is endothermic due to desorption of water molecule. Then the process is exothermic, which is due to the condensation of Si-OH groups with the release of water molecules. But in the case of 850SGS, the process is endothermic up to 800 °C, which shows that there is a limited number of Si-OH group in the sample and the weight loss is prominently due to the desorption of water molecules [51].

4.4.4 Field Emission-Scanning Electron Microscopy (FE-SEM) and Energy Dispersive X-ray Spectroscopy (EDS)

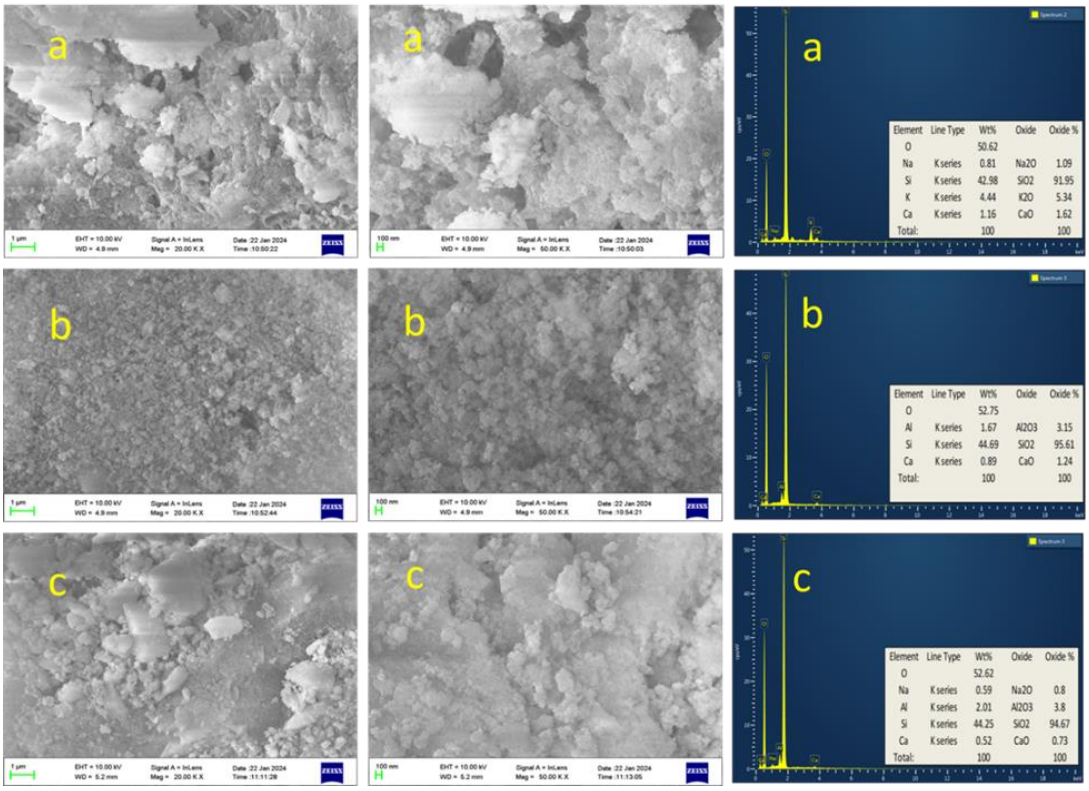

Figure.4.4 FE-SEM and EDS of (a) 600ALS (b) 600SGS and (c) 850SGS

The morphology and chemical composition of the samples were studied using FE-SEM and EDS. **Figure 4.4 (a-c)** shows the low as well as the high-resolution images and EDS data of 600ALS, 600SGS and 850 SGS respectively. The images show that the morphology of the synthesised silica depends on the methodology and

annealing temperature [52]. The irregular structures seen in all images are due to the formation of oxygenated siliceous compounds during annealing [53]. The FESEM image of 600ALS (**Figure 4.4 (a)**) reveals that silica sample exhibits a highly irregular, porous and heterogeneously aggregated morphology. There are large plate-like fragments and it appears as densely packed which is attributed to partial fusion during calcination. Numerous open pores and cavities are visible and these voids create continuous porous network which are the characteristic of plant derived silica. The entire surface exhibits prominent micro-roughness with numerous ridges and granular domains which will enhance surface area. The porous nature of the silica particles emerged due to the acid leaching and calcination of the organic matter during the synthesis. The EDS confirms a high silica content (91.95%) with trace Na, K, and Ca oxides.

The FE-SEM micrographs of the 600SGS sample (**Figure 4.4 (b)**) reveal a homogeneous distribution of nanoparticles without large voids or plate-like structures. It appears as closely packed nanoclusters giving the sample a cotton-wool appearance. The shapes of particles are spherical or sub spherical with sizes in the range of 20-50 nm. Many particles have merged into secondary agglomerates. The uniform nano aggregation and spherical particles are the features of silica formed via localized nucleation growth as seen in sol-gel process. Since 600SGS possess a very high surface area and interconnected nanoscale porosity, their power of adsorption, catalysis and interaction with other materials will be enhanced. Their uniform nano aggregation will provide advantages in applications like composites, drug delivery and functional coatings. The EDS data shows that 600SGS comprises about 95.61% of silica which is consistent with the studies reported for the extraction of silica from rice husk. A 3.5% of Al_2O_3 is found in 600 SGS which is attributed to the conversion of Al ion into sodium aluminate. Sodium aluminate is soluble in water and subsequently precipitates as Al $(OH)_3$ during sol-gel formation. The FE-SEM micrographs of 850SGS shows densely compacted silica structure comprising of both large crystalline plate-like particles and small partially fused nanograins. The surface appears less porous, which indicates significant sintering and grain growth during

high temperature calcination. Overall, the images shows that temperature have significant effect on the size of the particles [54].

Conclusion

This study establishes that Mission Grass (MG) is an underreported source of biosilica. Both amorphous and crystalline silica nanoparticles were extracted from MG through two established methods viz, acid leaching and sol-gel method. The effect of annealing temperature and the method of synthesis on the morphology and phase transition were also studied. This approach enabled the controlled synthesis of both amorphous and crystalline silica by adjusting the thermal treatment. Annealing at 600 °C favors the nanoscale amorphous particle with minimum agglomeration, while 850 °C annealing yielded larger, more crystalline and more hygroscopic particles. The key findings include high purity silica was obtained in the 600 °C sol-gel sample (600SGS), which achieved 95.6% SiO_2 content. The XRD studies reveals the phase transition with crystallinity index (43%) for 600SGS verses high crystallinity index (82%) for 850SGS. Thermal analysis established that 850SGS exhibit greater hygroscopicity compared to 600SGS. The study established that both high purity amorphous and crystalline nanosilica can be obtained from MG, but acid leaching method offers a simpler and cost-effective route compared to sol-gel process.

Overall, this work introduces novel sustainable and economical pathways for the synthesis of high purity silica nanoparticles from MG. The study urges that MG is not simply a weed, it is a rich source of biosilica and further studies should be conducted to make it value added product.

References

[1] Agrwal A, Kumar V, Kasana V. Preparation and application of highly efficient and reusable TBAPIL@Si(CH2)3@nano-silica-based nano-catalyst for preparation of benzoxanthene derivatives. J. Iran. Chem. 2021;18:2583–95. https://doi.org/10.1007/s13738-021-02211-1.

[2] Rangaraj S, Venkatachalam R. A lucrative chemical processing of bamboo leaf biomass to synthesize biocompatible amorphous silica nanoparticles of biomedical importance. Appl. Nanosci. (Switzerland) 2017;7:145–53. https://doi.org/10.1007/s13204-017-0557-z.

[3] Bakhsheshi-Rad HR, Hamzah E, Kasiri-Asgarani M, Saud SN, Yaghoubidoust F, Akbari E. Structure, corrosion behavior, and antibacterial properties of nano-silica/graphene oxide coating on biodegradable magnesium alloy for biomedical applications. Vacuum 2016;131:106–10. https://doi.org/10.1016/j.vacuum.2016.05.021.

[4] Vijayan M, Selladurai V, Balaganesan G, Suganya Priyadharshini G. Comprehensive characterization of AA 2024T3 fiber metal laminate with nanosilica-reinforced epoxy based polymeric composite panel for lightweight applications. Polym Compos 2022;43:8274–96. https://doi.org/10.1002/pc.26998.

[5] Etli S, Yılmaz T, Hansu O. Effect of White-Portland cement containing micro and nano silica on the mechanical and freeze-thaw properties of self compacting mortars. Eng. Sci. Technol. Int. J. 2024;50. https://doi.org/10.1016/j.jestch.2023.101614.

[6] Sun X, Xie J, Zhang J, Sang M, Li Y, Lyu P, et al. Hydrophobic Al_2O_3/SiO_2/PDMS Composite Coatings for Anti-corrosion Application of 304 Stainless-Steel. J Inorg Organomet Polym Mater 2022;32:4237–49. https://doi.org/10.1007/s10904-022-02423-9.

[7] Sarkar P, Moyez SA, Dey A, Roy S, Das SKK. Experimental investigation of photocatalytic and photovoltaic activity of titania/rice husk crystalline nano-silica hybrid composite. Sol. Energy Mater. Sol. Cells 2017;172:93–98. https://doi.org/10.1016/j.solmat.2017.07.021.

[8] Hossain SKS, Mathur L, Roy PK. Rice husk/rice husk ash as an alternative source of silica in ceramics: A review. J. Asian Ceram. Soc. 2018;6:299–313. https://doi.org/10.1080/21870764.2018.1539210.

[9] Lv R, Peng J, Chen S, Hu Y, Wang M, Lin J, et al. A highly linear humidity sensor based on quartz crystal microbalance coated with urea formaldehyde resin/nano silica composite films. Sens Actuators B Chem 2017;250:721–25. https://doi.org/https://doi.org/10.1016/j.snb.2017.03.074.

[10] Green LJ, Bhatia ND, Toledano O, Erlich M, Spizuoco A, Goodyear BC, et al. Silica-based microencapsulation used in topical dermatologic applications. Arch Dermatol Res 2023;315:2787–93. https://doi.org/10.1007/s00403-023-02725-z.

[11] Gao Y, Zhang Y, Hong Y, Wu F, Shen L, Wang Y, et al. Multifunctional Role of Silica in Pharmaceutical Formulations. AAPS PharmSciTech 2022;23. https://doi.org/10.1208/s12249-022-02237-5.

[12] Bazzi L, Hesemann P, Laassiri S, Hankari S El, Bazzi L, Hesemann P, et al. Alternative approaches for the synthesis of nano silica particles and their hybrid composites: synthesis, properties, and applications. Int. J. Environ. Sci. Technol. 2023;20:11575-614 https://doi.org/10.1007/s13762-023-04845-5.

[13] Deshmukh P, Bhatt J, Peshwe D, Pathak S. Determination of silica activity index and XRD, SEM and EDS studies of amorphous SiO_2 extracted from rice Husk Ash. Trans. Indian Inst. Met. 2012;65:63–70. https://doi.org/10.1007/s12666-011-0071-z.

[14] Park JY, Gu YM, Chun J, Sang BI, Lee JH. Pilot-scale continuous biogenic silica extraction from rice husk by one-pot alkali hydrothermal treatment and ball milling. Chem. biol. technol. agric. 2023;10:102 https://doi.org/10.1186/s40538-023-00479-4.

[15] Jeong HW, Park KT, Oh SM, Shim SE, Qian Y. Sustainable Reinforcement of Silicone Rubber: Comparative Analysis of Biosilica from Rice Husk and Conventional Silica. Polymers (Basel) 2025;17:406. https://doi.org/10.3390/polym17030406.

[16] Cotrim M, Ayres E, De LCG, Santos S, Cotrim MA, Almeida MLB. Eco-Friendly Coatings Obtained by Silica from Rice Husk Waste and Hydrophobization with Bio-Based Materials. Am. J. Mater. Sci.;2024:45–53. https://doi.org/10.5923/j.materials.20241403.01.

[17] Islam MdT, Hossen MdF, Kudrat-E-Zahan Md, Asraf MdA, Zakaria CM, Hayatullah, et al. Effect of temperature and time on purity, morphology and phase transformations of silica from rice husk. Chem. Inorg. Mater. 2025;5:100092. https://doi.org/10.1016/j.cinorg.2025.100092.

[18] Singh G, Dizaji HB, Puttuswamy H, Sharma S. Biogenic Nanosilica Synthesis Employing Agro-Waste Rice Straw and Its Application Study in Photocatalytic Degradation of Cationic Dye. Sustainability (Switzerland) 2022;14:539. https://doi.org/10.3390/su14010539.

[19] Firdaus MY, Osman H, Metselaar HSC, Rozyanty AR. A simple method for the production of pure crystalline silica from lemon grass. BioResources. 2016;11(1):1270–1279.

[20] Shim J, Oh BT, Velmurugan P. Extraction and physical characterization of amorphous silica made from corn cob ash at variable pH conditions via sol gel processing. J Ind Eng Chem. 2015;30:249–253. https://doi.org/10.1016/j.jiec.2015.05.029.

[21] Saed B, Ziaee M, Kiasat AR, Jafari nasab M. Preparation of nanosilica from sugarcane bagasse ash for enhanced insecticidal activity of diatomaceous earth against two stored-products insect pests. Toxin Rev 2022;41:516–22. https://doi.org/10.1080/15569543.2021.1903038.

[22] Yusaidi NJ, Abdullah SA, Zarib NA. X-ray diffractometer (XRD) and scanning electron microscopy (SEM) of silica extracted from banana stems via acid leaching treatment. IOP Conf. Ser. Mater. Sci. Eng., vol. 834, Institute of Physics Publishing; 2020. https://doi.org/10.1088/1757-899X/834/1/012053.

[23] Akpotu SO, Moodley B. Effect of synthesis conditions on the morphology of mesoporous silica from elephant grass and its application in the adsorption of cationic and anionic dyes. J Environ Chem Eng 2018;6:5341–50. https://doi.org/10.1016/j.jece.2018.08.027.

[24] Prasertwasu S, Khumsupan D, Komolwanich T, Chaisuwan T, Luengnaruemitchai A, Wongkasemjit S. Efficient process for ethanol production from Thai Mission grass (Pennisetum polystachion). Bioresour Technol 2014;163:152–59. https://doi.org/10.1016/j.biortech.2014.04.043.

[25] Thuadaij N, Nuntiya A. Synthesis and characterization of nanosilica from rice husk ash prepared by precipitation method. J. Nat. Sci. Special Issue on Nanotechnology. 2008;7(1):59-65.

[26] Vijayaraj S, Vijayarajan K. Mechanical wear and hydrophobicity behaviour of Digitaria ischaemum fibre-reinforced finger millet husk biosilica toughened epoxy composites. Biomass Convers Biorefin 2023. https://doi.org/10.1007/s13399-023-04638-3.

[27] Haque FZ, Nandanwar R, Singh P, Dharavath K, Syed FF. Effect of Different Acids and Solvents on Optical Properties of SiO_2 Nanoparticles Prepared by the Sol-Gel Process. Silicon 2018;10:413–19. https://doi.org/10.1007/s12633-016-9464-2.

[28] Rafiee E, Shahebrahimi S, Feyzi M, Shaterzadeh M. Optimization of synthesis and characterization of nanosilica produced from rice husk (a common waste material). Int Nano Lett 2012;2. https://doi.org/10.1186/2228-5326-2-29.

[29] Shadiya MA, Dominic CM, Nandakumar N, Joseph R, George KE. Isolation and characterization of fibrillar nanosilica of floral origin: Cortaderia selloana flowers as the silica source. Silicon. 2022 Jun;14(8):4139-47. https://doi.org/10.1007/s12633-021-01185-2/Published.

[30] Athinarayanan J, Periasamy VS, Alhazmi M, Alatiah KA, Alshatwi AA. Synthesis of biogenic silica nanoparticles from rice husks for biomedical applications. Ceram Int 2015;41:275–81. https://doi.org/10.1016/j.ceramint.2014.08.069.

[31] Yadav VK, Fulekar MH. Green synthesis and characterization of amorphous silica nanoparticles from fly ash. Mater Today Proc. 2019 Jan 1;18:4351-9.Y https://doi.org/10.1016/j.matpr.2019.07.

[32] Guo Y, Wang YQ, Wang ZM, Shen CJ. Study on the preparation and characterization of high-dispersibility nanosilica. Sci. eng. compos. mater. 2016;23:401–6. https://doi.org/10.1515/secm-2014-0010.

[33] Rafiee E, Shahebrahimi S. Nano silica with high surface area from rice husk as a support for 12-tungstophosphoric acid: An efficient nano catalyst in some organic reactions. Chin. J. Catal. 2012;33:1326–33. https://doi.org/10.1016/S1872-2067(11)60420-8.

[34] Krishnarao RV, Godkhindi MM. Distribution of silica in rice husks and its effect on the formation of silicon carbide. Ceram Int 1992 Jan 1;18(4):243-9. https://doi.org/10.1016/0272-8842(92)90102-J

[35] Banoth S, Babu VS, Raghavendra G, Rakesh K, Ojha S. Sustainable thermochemical extraction of amorphous silica from biowaste. Silicon. 2022 Jul;14(10):5289-96.https://doi.org/10.1007/s12633-021-01293-z/Published.

[36] Sutha S, Sakthipandi K, Rajendran V, Palanivelu R, Rani CU, Jayakumar T, et al. Structural studies of nano silica employing on-line ultrasonic studies. Phase Transi 2012;85:565–76. https://doi.org/10.1080/01411594.2011.648933.

[37] Battisha IK, El Beyally A, El Mongy SA, Nahrawi AM. Development of the FTIR properties of nano-structure silica gel doped with different rare earth elements, prepared by sol-gel route. J Solgel Sci Technol 2007;41:129–37. https://doi.org/10.1007/s10971-006-0520-z.

[38] Peerzada JG, Chidambaram R. A statistical approach for biogenic synthesis of nano-silica from different agro-wastes. Silicon. 2021 Jul;13(7):2089-101.https://doi.org/10.1007/s12633-020-00629-5/Published.

[39] Joni IM, Nulhakim L, Vanitha M, Panatarani C. Characteristics of crystalline silica (SiO_2) particles prepared by simple solution method using sodium silicate (Na_2SiO_3) precursor. J. Phys. Conf. Ser., vol. 1080, Institute of Physics Publishing; 2018. https://doi.org/10.1088/1742-6596/1080/1/012006.

[40] Kordatos K, Gavela S, Ntziouni A, Pistiolas KN, Kyritsi A, Kasselouri-Rigopoulou V. Synthesis of highly siliceous ZSM-5 zeolite using silica from rice husk ash. Micropor Mesopor Mat 2008;115:189–96. https://doi.org/10.1016/j.micromeso.2007.12.032.

[41] Chisholm J. Comparison of quartz standards for X-ray diffraction analysis: HSE A9950 (Sikron F600) and NIST SRM 1878. Ann. Occup. Hyg. 2005;49:351–8. https://doi.org/10.1093/annhyg/meh095.

[42] Prasetyoko D, Ramli Z, Endud S, Hamdan H, Sulikowski B. Conversion of rice husk ash to zeolite beta. Waste Management 2006;26:1173–79. https://doi.org/10.1016/j.wasman.2005.09.009.

[43] Ma X, Zhou B, Gao W, Qu Y, Wang L, Wang Z, et al. A recyclable method for production of pure silica from rice hull ash. Powder Technol 2012;217:497–501.https://doi.org/10.1016/j.powtec.2011.11.009.

[44] Ali HH, Hussein KA, Mihsen HH. Antimicrobial Applications of Nanosilica Derived from Rice Grain Husks. Silicon 2023;15:5735–45. https://doi.org/10.1007/s12633-023-02467-7.

[45] Bheel N, Memon FA, Meghwar SL. Study of fresh and hardened properties of concrete using cement with modified blend of millet husk ash as secondary cementitious material. Silicon. 2021;13(12):4641–4652. https://doi.org/10.1007/s12633-020-00794-7.

[46] Ali HH, Mihsen HH, Hussain KA. Synthesis, Characterization and Antimicrobial Studies of Modified Silica Materials Derived from Rice Husks. Bionanoscience 2023;13:1163–76. https://doi.org/10.1007/s12668-023-01144-8.

[47] Sarangi M, Bhattacharyya S, Behera RC. Effect of temperature on morphology and phase transformations of nano-crystalline silica obtained from rice husk. Phase Transit 2009;82:377–86. https://doi.org/10.1080/01411590902978502.

[48] Huang M, Cao J, Meng X, Liu Y, Ke W, Wang J, et al. Preparation of SiO_2 nanowires from rice husks by hydrothermal method and the RNA purification performance. Chem Phys Lett 2016;662:42–46. https://doi.org/10.1016/j.cplett.2016.09.012.

[49] Ek S, Root A, Peussa M, Niinistö L. Determination of the hydroxyl group content in silica by thermogravimetry and a comparison with 1H MAS NMR results. Thermochim Acta 2001;379:201–12. https://doi.org/10.1016/S0040-6031(01)00618-9.

[50] Yu LY, Huang ZX, Shi MX. Synthesis and characterization of silica by sol-gel method. Adv. Mat. Res., vol. 1030–1032, Trans Tech Publications Ltd; 2014, p. 189–92. https://doi.org/10.4028/www.scientific.net/AMR.1030-1032.189.

[51] Kurbanov M, Tulaganov S, Nuraliev U, Andriyko L, Goncharuk O, Guzenko N, et al. Comparative Characteristics of the Structure and Physicochemical Properties of Silica Synthesized by Pyrogenic and Fluoride Methods. Silicon 2023;15:1221–33. https://doi.org/10.1007/s12633-022-02087-7.

[52] Karumanchi M, Nerella R, Mikkili I. An integrated approach on extraction methodologies of nanosilica from cultivated agricultural wastes and microstructural characteristics – A review. Mater Today Proc 2022;62:2883–91. https://doi.org/10.1016/j.matpr.2022.02.476.

[53] Rodríguez-Díaz JM, García JOP, Sánchez LRB, da Silva MGC, da Silva VL, Arteaga-Pérez LE. Comprehensive Characterization of Sugarcane Bagasse Ash for Its Use as an Adsorbent. Bioenergy Res 2015;8:1885–95. https://doi.org/10.1007/s12155-015-9646-6.

[54] Morales-Paredes CA, Rodríguez-Linzán I, Saquete MD, Luque R, Osman SM, Boluda-Botella N, et al. Silica-derived materials from agro-industrial waste biomass: Characterization and comparative studies. Environ Res 2023;231. https://doi.org/10.1016/j.envres.2023.116002

Chapter 5

Valorization of Screw Pine (*Pandanus tectorius*) leaves: Isolation and Characterisation of Microcrystalline Cellulose (MCC)

5.1 Introduction

5.1.1 Understanding Cellulose Derivatives

Cellulose is a versatile and abundant long chain biopolymer composed of β-1,4-linked D-glucopyranose units [1]. The average degree of polymerisation of cellulose ranges from 1,000 to 15,000 glucose units and it depends on the nature of sources [2]. Cellulose microfibrils are embedded in a matrix of other polysaccharides such as hemicellulose and lignin forming a composite material [3]. It helps the plant to maintain their shape, resist turgor pressure and stand upright. Cellulose plays a crucial role in the field of material science due to its abundance, renewability, biodegradability, and versatile physical and chemical properties. It exists in various forms, each with distinct characteristics and applications.

Holocellulose represents all the carbohydrate components in the cell wall, excluding lignin and extractives [4]. It is the total carbohydrate portion of plants, mainly consisting of cellulose and hemicellulose. Cellulose is a linear polymer of glucose units, while hemicellulose is heterogeneous group of branched polysaccharides (e.g. Xylan, Mannans) that associate with the cellulose fibres in the plant cell wall and imparts flexibility [5]. The lignin present in the native cellulose can be removed by various methods, including sodium chlorite bleaching [6], sodium hypochlorite treatment [7], the Kraft process [8], using organic solvent [9], fungal treatment [10], steam explosion [11] and others. The holocellulose content in the wood can serve as an indicator of quality for both industrial and scientific applications. The holocellulose on hydrolysis forms glucose and other sugars, which can be fermented to produce bioethanol-an alternative to fossil fuel [12]. When combined with other polymers like starch or chitosan, holocellulose is used for making biodegradable films

and composites [13]. Hydrolysis of holocellulose also produces valuable chemicals like furfural [14], levulinic acid [15] and xylitol [16] and these can be used as resins, solvents and food additives. Derivatives of holocellulose are also employed for making porous structures for water purification [17], heavy metal adsorption and gas filtration [18]. The percentage yield of holocellulose is given by equation 5.1

$$\textbf{\% Yield of holocellulose} = \frac{\boldsymbol{Weight\ of\ holocellulose\ extracted} \times \mathbf{100}}{\boldsymbol{Weight\ of\ Oven\ Dry\ Sample}} \quad \textbf{(5.1)}$$

Alpha cellulose is the most refined and stable form of cellulose. Holocellulose comprises both crystalline and amorphous form of cellulose along with amorphous hemicellulose. However, α-cellulose, which is obtained by the removal of hemicellulose, exhibits high crystallinity, high molecular weight and exceptional stability, making it more durable than holocellulose. The α-cellulose is typically extracted from holocellulose through alkaline treatment using 17.5% sodium hydroxide (NaOH) solution [19]. During alkali treatment, hemicellulose, along with beta and gamma cellulose fractions dissolves, leaving alpha cellulose as the residue. The percentage yield is given by equation 5.2

$$\textbf{\% Yield of alpha cellulose} = \frac{\boldsymbol{Weight\ of\ alpha\ cellulose\ extracted} \times \mathbf{100}}{\boldsymbol{Weight\ of\ Oven\ Dry\ Sample}} \quad \textbf{(5.2)}$$

The high purity and stability of α- cellulose makes it an ideal candidate for the production of high-quality paper and textiles [20]. Due to the presence of longer polymer chain and more crystallinity, alpha cellulose is well suited for making more rigid composite materials and bioplastics [21]. Alpha cellulose exhibits superior chemical resistance compared to holocellulose, making it ideal for making archival papers, filter papers and other materials, intended for long term use [22]. The holocellulose is reactive due to the presence of hemicellulose and hence it is undesirable in certain applications. On the other hand, α-cellulose offers enhanced control over other reactions during the processing, which is crucial in material science. Moreover, α-cellulose has better thermal stability, making it suitable for high temperature applications such as thermoplastics or insulation materials.

Microcrystalline Cellulose (MCC) is a partially depolymerised form of cellulose produced by partial hydrolysis of α-cellulose using mineral acid, typically HCl. This process selectively degrades amorphous region of cellulose, resulting in shorter and crystalline fragments. Crystallinity, bulk density and tapped density of MCC is higher than that of α-cellulose. The percentage yield of MCC from α-cellulose is given by equation 5.3

$$\textbf{\% Yield of MCC} = \frac{\boldsymbol{Weight\ of\ MCC} \times \mathbf{100}}{\boldsymbol{Weight\ of\ Alpha\ Cellulose}} \quad \textbf{(5.3)}$$

The yield depends on various factors such as source, method of extraction and processing conditions [23]. MCC offers several advantages over α-cellulose particularly in industrial applications such as pharmaceuticals, cosmetics and food processing. MCC have more purity and crystallinity compared to α-cellulose. The fine and crystalline structure of MCC provides excellent flow properties and compressibility, making it ideal for tablet formation [24]. MCC is a valuable additive in polymer composites, because it enhances mechanical, thermal and barrier properties of polymers. Since, it is derived from renewable sources, MCC is an important candidate for the development of sustainable material suitable for various applications. The fine crystalline structure of MCC provides a large surface area for the interaction with polymer matrix, leading to enhanced dispersion and bonding. Moreover, the hydroxyl group present in the MCC facilitate the H- bonding with the polymer chain. MCC is an economically viable filler and can reduce the cost of the composites. MCC is typically synthesised from the raw materials such as wood pulp [25] and purified cotton linters [26] due to their high cellulose content and purity. However alternative resources such as grasses [27], rice husk [28], soyabean hull [29], algae [30], etc. can also be utilised for the synthesis of MCC.

5.1.2 Aim and Objectives of the Study in the Present Chapter

As a part of our effort to develop sustainable, biodegradable MCC from underutilised biomass, we focused on Screw Pine (*Pandanus tectorius*) leaves, a naturally abundant and locally available plant material. *Pandanus tectorius* (Screw

Pine), a morphologically diverse species of the Pandanus family, is widely distributed across South Asia and Pacific Island. In India, it is found in Western Ghats, Himalayan region and Andaman Nicobar Islands. Traditionally, its leaves are used for making mats, baskets, hats and other goods, since it is a good source of natural fibre. Though a few studies regarding the extraction of nanocellulose from Screw Pine (SP) leaves and its application in polymer composites have been reported [31], detailed composition analysis, especially of Indian varieties remain limited. Therefore, the present chapter focuses on extraction of holocellulose, α-cellulose, and MCC from SP leaves via bleaching and acid hydrolysis. The compositions of isolated components are determined and their physical, chemical and morphological features were studied by advanced techniques.

5.2. Materials

The raw material, Screw Pine leaves (*Pandanus tectorius*) were collected locally. The reagents including ethanol, toluene, sodium chlorite ($NaClO_2$), acetic acid (CH_3COOH), sodium hydroxide (NaOH), hydrochloric acid (HCl), pH paper and Whatman No 1 Filter paper were procured from Merck India. All the chemicals and solvents were of analytical grade and used without further purification.

5.3 Methods

Thoroughly washed SP leaves were sun dried for 2-3 days, then cut into small pieces and finely powdered. The powder was subsequently sieved through a mesh and again dried in a hot air oven at 100-105 °C for 3-4 h until a constant weight was obtained. One gram of Oven Dried Sample (ODS) was subjected to Soxhlet extraction using 150 ml of ethylene-toluene mixture (2:1) for 5 h. The obtained residue was dried in a hot air oven at 105 °C for 3-4 h till a constant weight was achieved. The difference in weight of ODS and the extracted residue gives the weight of extractives.

5.3.1 Extraction of Holocellulose through Delignification

One gram of the residue obtained in the above step was treated with 20 ml of 0.7 % sodium chlorite ($NaClO_2$) solution in a water bath shaker kept at 80 °C for 5 h.

The acetic acid was added drop by drop so as to maintain the pH of the solution at 5. The mixture was filtered, washed with water till the washings become neutral and the residue was dried in an air oven at 100 °C for 4 h. During the process the lignin will be removed and holocellulose will be obtained. The percentage of lignin was determined by subtracting the weight of holocellulose from ODS (after removing extractives).

5.3.2 Isolation of α-cellulose from holocellulose

The α-cellulose was isolated from the holocellulose through the procedure outlined by Ohwoavworhua et al. with slight modification [32]. One gram of holocellulose was treated with 15 ml of 17 % sodium hydroxide (NaOH) solution. This addition was performed in three increments of 5 ml each in 45 mins. The mixture was allowed to stand for 1 h and distilled water was added to dilute the concentration of NaOH to 8.5%. The solution was filtered, washed with water and finally with 10% acetic acid. The residue obtained, termed α-cellulose was again washed with distilled water till the washings became neutral. The α-cellulose was dried at 105 °C for 4 h to achieve constant weight. During the process hemicellulose will be removed and the difference in weight between holocellulose and α-cellulose gives the weight of hemicellulose.

5.3.3 Isolation of Micro Crystalline Cellulose

One gram of α-cellulose was hydrolysed with 17 ml of 2.5N HCl at boiling temperature for 15 minutes. The hot solution was poured into 50 ml cold water with vigorous stirring. It was continuously stirred well for 15 minutes and kept overnight. The MCC obtained after filtration was washed with distilled water till the washing becomes neutral and dried in a hot air oven at 60 ˚C for 30 minutes. The overall process of extraction and the image of cellulose derivatives are schematically represented in **Scheme 5.1.**

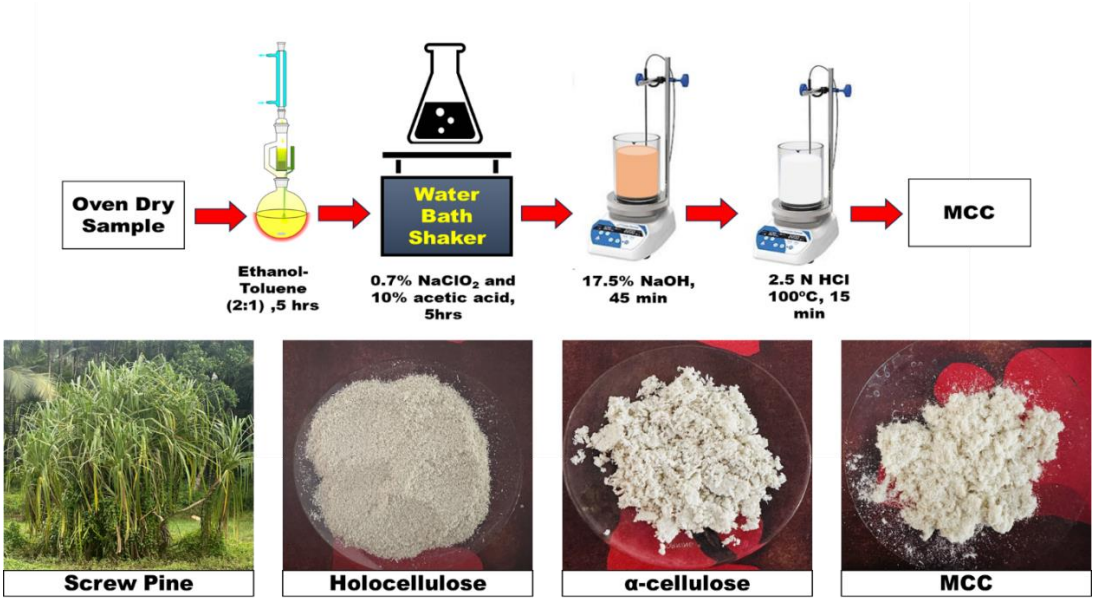

Scheme 5.1- Schematic Representation of Extraction of MCC from Screw Pine leaves

5.4 Results and Discussion

5.4.1 Chemical Composition

The composition of different components in the ODS of SP leaves were determined as per equation (1), (2) and (3) and is given in **Table 5.1**. The result showed that the series of chemical treatment effectively enrich and isolate the crystalline cellulose and the final MCC yield align with previously reported sources. The analysis shows that the fixed amount of α-cellulose on acid hydrolysis yields 66% of MCC, which is 24% of initial weight of ODS.

Table 5.1 Percentage Composition of Oven Dried Samples of Screw Pine leaves

Components	Weight%
Extractives	12.0±1
Lignin	19.5±1
Holocellulose	68.5±1
α-cellulose	37.5±1
Hemicellulose	31.0±1
MCC	66.0±1

5.4.2 Fourier Transform-Infrared Spectroscopy Analysis

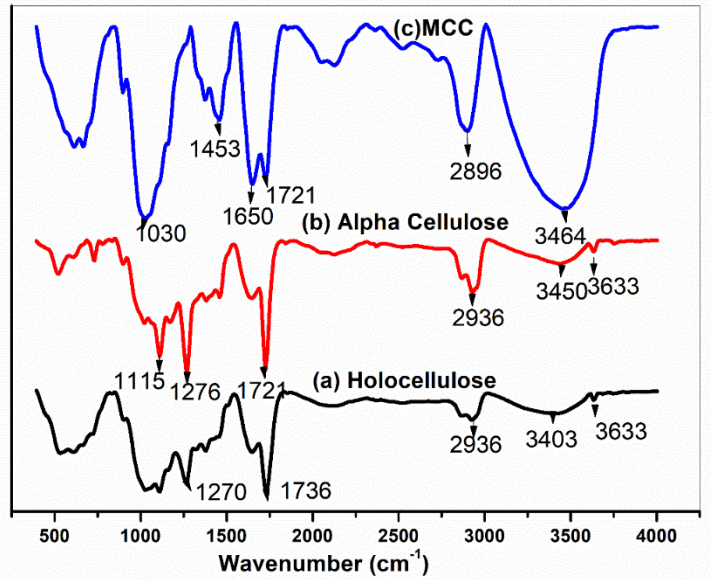

Figure 5.1 FT-IR spectra of (a)Holocellulose (b)Alpha cellulose and (c)MCC

FT-IR analysis was carried out to study the structural features of holocellulose, α-cellulose, and MCC extracted from SP leaves. **Figure 5.1 (a)** represent the FT-IR spectrum of holocellulose. Holocellulose is the polysaccharide fraction of the biomass obtained after the removal of lignin and extractives from the crude sample. A small peak at 3633 cm^{-1} corresponds to the O-H stretching vibration of water molecule which is loosely bounded to holocellulose [33]. The broad band observed between 3200-3500 cm^{-1} is attributed to extensive H-bonded O-H groups of cellulose and hemicellulose [34]. The medium intensity band at 2936 cm^{-1} is due to C-H stretching vibration of methyl and methylene group present in cellulose and hemicellulose, while the medium peak at 1450 cm^{-1} is due to CH_2 wagging vibration [35]. The carbonyl stretching vibration seen at 1736 cm^{-1} is due to acetyl group of hemicellulose and ester group in the sample [36]. The peak at 1270 cm^{-1} is due to C-H bending vibration, which may be attributed to trace lignin content.

FT-IR spectra of α-cellulose which was obtained by removing hemicellulose through alkali treatment is given in **Figure 5.1 (b).** The small peak at 3633 cm^{-1}, due to the presence of water molecule is seen in the case of α-cellulose also. The broad

band at 3450 cm^{-1} is attributed to inter and intramolecular H- bonded O-H group. The medium intensity peak at 2936 cm^{-1} is due to C-H stretching of methyl and methylene group, which is a typical feature of polysaccharides [37]. The presence of peak at 1276 cm^{-1}, particularly even after alkali treatment is an indicative of lignin content in the sample. The medium peak at 1115 cm^{-1} is due to C-O stretching vibration of glycosidic linkage [38]. The FT-IR of holocellulose and α-cellulose exhibit notable similarities with minor differences in wave number and intensity. The FT-IR spectrum of MCC (**Figure 5.1 (c)**) is very distinct, reflecting the change in crystallinity during the conversion from α- cellulose. The characteristic peak at 3464 cm^{-1}, which is due to O-H stretching vibration is more intense and have higher wave number than α- cellulose, indicating stronger H-bonding and increased crystallinity. The peak at 2896 cm^{-1} which is attributed to C-H stretching of methyl and methylene group appears more intense. The frequency at1453 cm^{-1}often known as "crystallinity band" appeared more intense [39]. The frequency at 1650 cm^{-1} is attributed to bending vibration of adsorbed water molecules [40]. The prominent peak at 1030 cm^{-1} is attributed to C-O-C stretching vibration within the pyranose ring skeleton [41]. Thus, FT-IR spectra show more purity and crystallinity for MCC than α-cellulose and holocellulose.

5.4.3 X-ray Diffraction Analysis

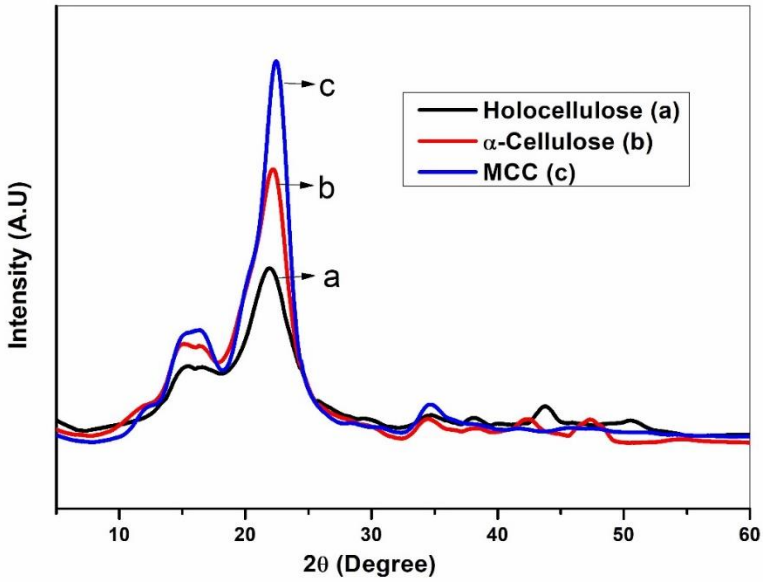

Figure 5.2 X-ray Diffraction Patterns of (a) Holocellulose (b) α-cellulose and (c) MCC

The diffraction patterns of all samples were recorded using Cu-K_α radiation source. The Crystallinity Index (CrI) was then determined using the peak height method developed by Segal et al. (1959), i.e., equation 5.4,

$$\textbf{Cr I (\%)} = \frac{I_{002} - I_{am}}{I_{002}} \qquad \textbf{(5.4)}$$

Where I_{002} is the maximum intensity corresponding to 002 plane which is found at 2θ between 22-23°. I_{am} is the intensity of the peak at amorphous region, which is found around 2θ ≈ 18° [39]. The X-ray diffraction patterns of holocellulose, α-cellulose and MCC isolated from Screw Pine leaves are shown in **Figure 5.2 (a-c).** All the diffractograms show predominant peaks at approximately 2θ values of around 22° and 16°, which are characteristic of cellulose Iβ [42]. **Figure 5.2 (a)** represents diffractogram of holocellulose which exhibits a prominent crystalline peak at 21.9° corresponding to (002) plane of the crystal. Additionally, a shoulder peak is observed near 15.6° and weak peak at 34.1° due to (110) and (004) planes respectively [43]. The small peaks found at 29.7°, 38.8° and 43.9° can be attributed to the contribution from lignin or other inorganic impurities [44]. The crystallinity index of holocellulose was calculated using the Segal method and is found to be 52%. **Figure 5.2(b)** shows the diffractogram of α-cellulose which exhibits more pronounced and sharper diffraction pattern due to the removal of non-cellulosic components like hemicellulose and lignin. The peak width of α-cellulose is lesser than that of holocellulose, indicating larger crystallite size and a more ordered structure. The XRD spectrum exhibited a sharp peak at 2θ≈22.2°, which indicates the crystalline nature of α- cellulose meanwhile, a blunt and widened peak around 2θ= 15-17°is attributed to its amorphous nature [45]. The characteristic peaks of cellulose I at 2θ values 15.2°, 22.2°and 34.2° corresponding to (110), (002) and (004) planes are clearly visible. The calculated crystallinity index is 65% which is higher than that of holocellulose. This enhanced crystallinity imparts several advantages to α-cellulose, particularly in applications requiring structural integrity and resistance to degradation.

MCC is a refined form of cellulose characterised by high crystallinity and structural integrity. The XRD spectrum of MCC (**Figure 5.2(c)**) reveals distinct peaks, confirming its crystalline nature. Consistent with holocellulose and α-cellulose, the diffractogram exhibited prominent peaks at 2θ values 16.3°, 22.4°and 34.6°, confirming the presence of cellulose I. A faint diffraction at 20.5° and a bulge at 12°, which are characteristic of cellulose II were also observed, which shows a slight mercerisation. Notably, the peak at 22.4° became sharper and narrower compared to the prominent peaks of holocellulose and α-cellulose. This enhancement is attributed to the removal of amorphous region of cellulose and non-cellulosic components during delignification, bleaching and acid hydrolysis processes. These treatments disrupt the β-1,4-glycopyranose linkages, leading to the elimination of amorphous regions and thereby increasing the crystallinity [46]. The crystallinity index of MCC is 78% which is much higher than that of α-cellulose, which imparts several advantageous properties to MCC, making it highly a valuable candidate across various fields.

5.4.4 Thermogravimetric Analysis

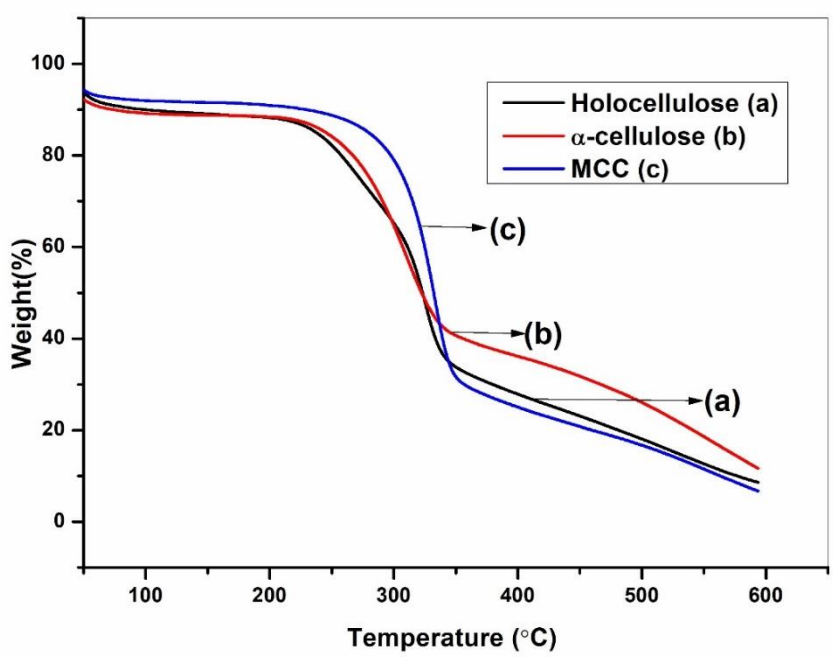

Figure 5.3 Thermogravimetric curves of (a) Holocellulose (b) α-cellulose and (c) MCC

Thermal studies of holocellulose, α-cellulose and MCC were conducted using Perkin Elmer's STA8000 instrument within the temperature range of 30 °C to 600 °C in an inert atmosphere of nitrogen at heating rate of 5 °C/minute. **Figures 5.3** depicts the thermogravimetric (TG) analysis of holocellulose, α- cellulose and MCC. In the case of holocellulose (**Figure 5.3 (a))**, a minor initial weight loss (4%) is observed below 130 °C due to the removal of adsorbed water molecules. There is no significant weight loss up to 230 °C. A subsequent sharp weight loss of about 51% occurs between 230 °C and 340 °C, primarily attributed to the decomposition of holocellulose component such as xylan, xyloglucan, etc. [47]. Analysis indicates that the onset temperature for holocellulose degradation occurs at approximately 260 °C. Analysis reveals that α-cellulose exhibit superior thermal stability compared to holocellulose. This is attributed to the higher crystallinity and purity of α-cellulose due to the removal of amorphous hemicellulose and lignin. The second stage degradation begins at approximately 235 °C, with the onset temperature estimated around 267°C. The second stage degradation concludes at 340 °C and the residual mass is 41% which is higher than that of holocellulose.

The minimal initial weight loss observed in MCC compared to α-cellulose during TGA can be attributed to several factors such as higher crystallinity, reduced moisture component and structural compactness due to the removal of amorphous region. The major weight loss was observed around 260-365 °C due to cellulose degradation caused by decarboxylation, depolymerisation and decomposition of glycosyl units [48]. MCC exhibit higher onset temperature compared to α-cellulose, which begins degradation at 308 °C. Thus, the material can withstand higher processing conditions without degradation, thereby enhancing product performance and shelf life.

5.4.5 Morphological Analysis

5.4.5.1 Field Emission- Scanning Electron Microscopy Analysis

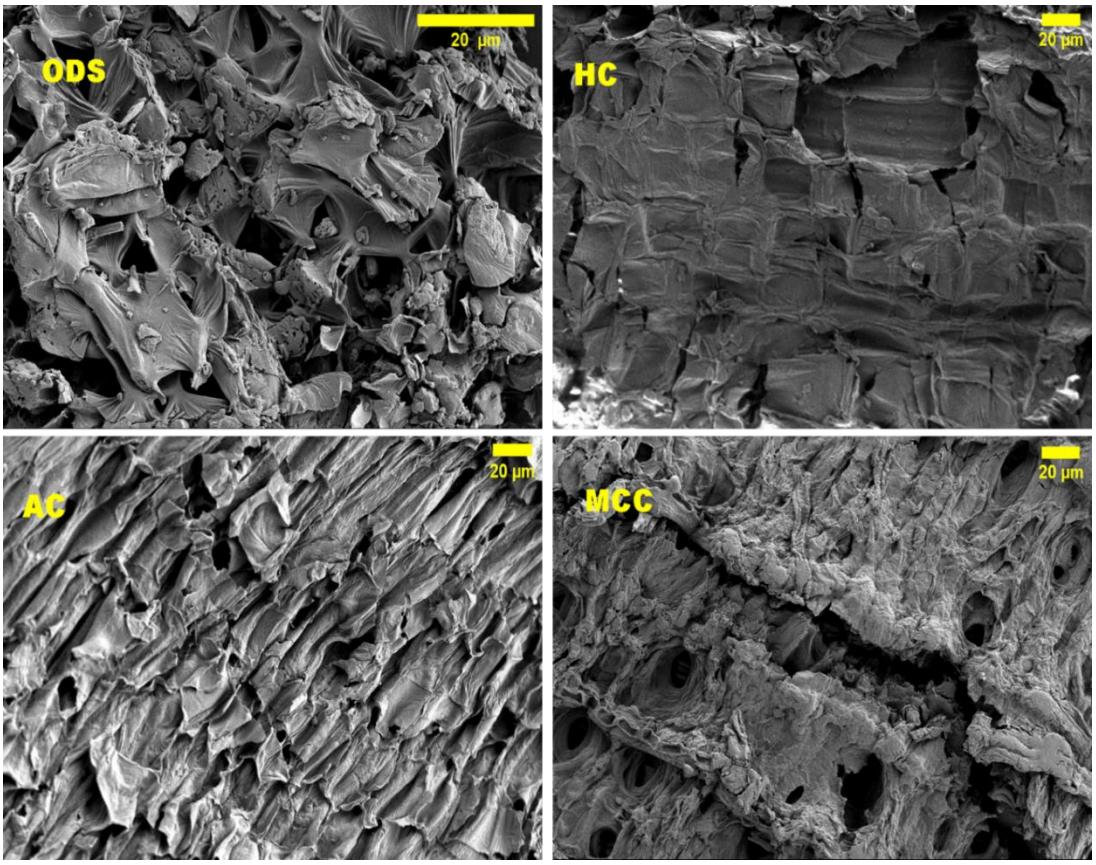

Figure 5.4 FE-SEM Images of (a) Oven Dried Sample (ODS) (b) Holocellulose (HC) (c) α-cellulose (AC) and (d) MCC

Figure 5.4 shows the FE-SEM images of ODS, holocellulose, α-cellulose, and MCC respectively. It is evident from the figures that different samples display remarkable differences in morphology. The image of ODS appeared as irregular, flaky microstructures at micrometre scale. Solvent extraction using ethylene-toluene mixture effectively removes pigments and other soluble components. Moreover, heating the residue in air oven dehydrate the material, causing the shrinkage and disruption of cellulose structure. FE-SEM image of holocellulose displays a rough and irregular surface with layered morphology. The material appears as thin and stalked sheets or lamellae. Numerous fractures and separations create spaces and potential pathways between the material which gives porous texture. This can be attributed to the effective delignification during sodium chlorite treatment. Highly textured and

wrinkled structures are observed in the image of α-cellulose. It is composed of numerous ridges, folds and depressions giving it a crumpled appearance. The structures are elongated and appeared to be aligned in a particular direction. The image also suggests layered, fibrous substructures within the elongated features. Small pores or voids are visible within the folds and between the layer structures. The mercerisation process of holocellulose using 17.5% NaOH significantly alters the crystalline structure and morphology [49]. The FE-SEM image shows that MCC is composed of irregular short fibres that are aggregated together to form small clusters. Numerous pores and voids are visible throughout the material. These pores vary in size and shape and appears as irregular opening within the aggregated mass. Some pores are oval while others are elongated or interconnected, suggesting a significant degree of internal porosity. The porous structure provides high surface area for MCC. When α-cellulose is treated with mineral acid, hydronium ion penetrates to the material and hydrolyse the glycosidic bond in amorphous region, leaving behind the crystalline region. Due to the removal of cementous amorphous cellulose, individual microfibril will be liberated and MCC is appeares as fibrous [50].

5.4.5.2 Atomic Force Microscopy Analysis

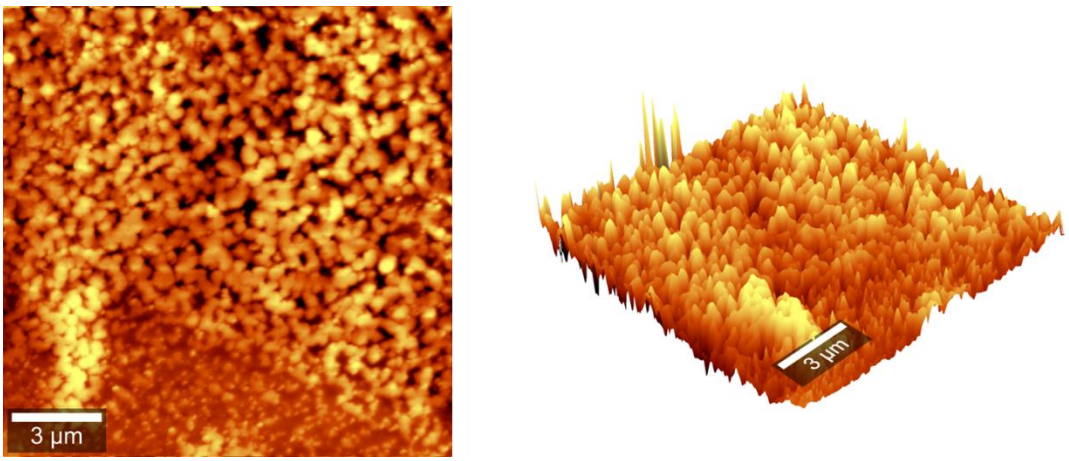

Figure 5.5 AFM Images of MCC a) 2D (3µm) b) 3D (3µm)

Further morphological studies were conducted by using an atomic force microscope. Images (**Figure 5.5)** indicate that MCC exhibit complex surface morphology with a collection of irregular fibrous structure. The presence of numerous

peaks and depressions suggests relatively rough surfaces at nanometre level. The collection of individual microcrystals forms a complex and textured landscape. This high degree of nanoscale roughness provides highly effective surface area. This large surface area is crucial in various applications as it provides number of sites for adsorption, enhances interface adhesion within the polymer matrix and offers vast surface for drug delivery.

5.4.5.3 High Resolution-Transmission Electron Microscopy (HR-TEM) Analysis

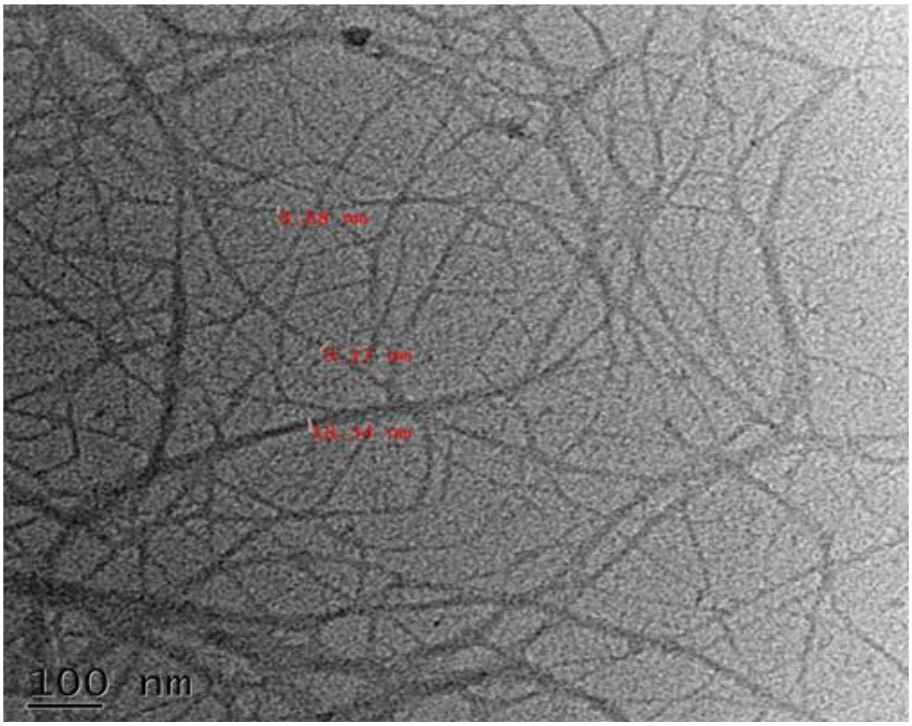

Figure 5.6 HR-TEM Image of MCC

Figure 5.6 shows the High Resolution-Transmission Electron Microscope image of MCC. HR-TEM image shows the fibrous nature of MCC with average diameter of 12.13 nm which is consistent with MCC extracted from other sources. The length of the fibre is in micron-scale and was found to be many folds higher than diameter. The fibrous nature of MCC was already identified from SEM image (**Figure 5.4 (d**)). High length to width ratio has a lot of advantages especially when it is used as filler in composites.

Conclusion

Microcrystalline cellulose and other derivatives of cellulose were effectively extracted from an underreported source, Screw Pine leaves through a series of feasible chemical process. Non-cellulosic constituents were removed by solvent extraction, followed by bleaching which yielded holocellulose. Alkali treatment of holocellulose yielded α-cellulose and this on acid hydrolysis MCC were obtained. The composition of SP leaves was determined by standard method and shown to contain substantial amount of cellulose. The isolated components were characterized using FT-IR, XRD, TG, DTG, FE-SEM, AFM and HR-TEM. All the studies revealed that MCC obtained from Screw Pine leaves possess crystalline nature, high thermal stability and decomposition temperature compared to holocellulose and α-cellulose. Morphological studies also confirmed the effective removal of amorphous parts during the conversion of α-cellulose to MCC. The studies revealed that compared to raw fibre, crystallinity and thermal stability increased after acid hydrolysis. Owing to its fibrous nature and high length to width ratio, Screw Pine MCC can be effectively utilized as good filler in the synthesis of bio-composites as a substituent to synthetic fibres. Finally, high cellulose content and widespread availability make SP leaves as an excellent renewable feedstock for the production of MCC using simple and scalable method.

References

1. Szabó L, Milotskyi R, Sharma G, Takahashi K. Cellulose processing in ionic liquids from a materials science perspective: turning a versatile biopolymer into the cornerstone of our sustainable future. Green Chem. 2023;25(14):5338–5389. https://doi.org/10.1039/D2GC04730F

2. Wyman CE, Decker SR, Himmel ME, Brady JW, Skopec CE, Viikari L. Hydrolysis of cellulose and hemicellulose. In: Dumitriu S, editor. Polysaccharides: Structural Diversity and Functional Versatility. 2nd ed. Boca Raton: CRC Press; 2005. 995–1033.

3. Abdul Khalil HPS, Bhat AH, Ireana Yusra AF. Green composites from sustainable cellulose nanofibrils: a review. Carbohydr Polym. 2012;87(2):963–979. https://doi.org/10.1016/j.carbpol.2011.08.078

4. Chen H. Chemical composition and structure of natural lignocellulose. In*:* Biotechnology of Lignocellulose: Theory and Practice. Springer; 2014. p. 25–71. https://doi.org/10.1007/978-94-007-6898-7_2.

5. Lu Y, He Q, Fan G, Cheng Q, Song G. Extraction and modification of hemicellulose from lignocellulosic biomass: a review. Green Process Synth. 2021;10:779–804. . https://doi.org/10.1515/gps-2021-0065

6. Siqueira G, Várnai A, Ferraz A, Milagres AMF. Enhancement of cellulose hydrolysis in sugarcane bagasse by the selective removal of lignin with sodium chlorite. Appl Energy. 2013;102:399–402. . https://doi.org/10.1016/j.apenergy.2012.07.029.

7. Aridi AS, Chin NL, Ishak NA, Mohamad Yusof NN, Kadota K, Manaf YN, Yusof YA. Effect of sodium hypochlorite concentration during pre-treatment on isolation of nanocrystalline cellulose from Leucaena leucocephala (Lam.) mature pods. BioResources. 2021;16(2):3137–3158.

8. Li K, Kollberg L, Almqvist H, Xu B, Hulteberg C. Maximizing yield of liquid-lignin from membrane filtration retentate of kraft black liquor. Ind Crops Prod. 2021;169:113657. . https://doi.org/10.1016/j.indcrop.2021.113657.

9. Chin DWK, Lim S, Pang YL, Lim CH, Shuit SH, Lee KM, Chong CT. Effects of organic solvents on the organosolv pretreatment of degraded empty fruit bunch for fractionation and lignin removal. Sustainability (Basel). 2021;13(12):6757. https://doi.org/10.3390/su13126757

10. Madadi M, Abbas A. Lignin degradation by fungal pretreatment: a review. J Plant Pathol Microbiol. 2017;8(2):398. https://doi.org/10.4172/2157-7471.1000398.

11. Li J, Henriksson G, Gellerstedt G Lignin depolymerization/repolymerization and its critical role for delignification of aspen wood by steam explosion. Bioresour Technol.2007; 98:3061–3068. https://doi.org/10.1016/j.biortech.2006.10.018

12. Victor A, Pulidindi IN, Gedanken A Assessment of holocellulose for the production of bioethanol by conserving Pinus radiata cones as renewable feedstock. J Environ Manage.2015; 162:215–220. https://doi.org/10.1016/j.jenvman.2015.07.038

13. Pitiphatharaworachot S, Chitbanyong K, Sungkaew S, Pisutpiched S, Khantayanuwong S, Puangsin B. Starch nanocomposites reinforced with TEMPO-oxidized cellulose nanofibrils derived from bamboo holocellulose. BioResources. 2019;14(2):2784–2797. https://doi.org/10.15376/biores.14.2.2784-2797.

14. Lu Y, He Q, Peng Q, Chen W, Cheng Q, Song G, Fan G. Directional synthesis of furfural compounds from holocellulose catalyzed by sulfamic acid. Cellulose. 2021;28(13):8343–8354. . https://doi.org/10.1007/s10570-021-04070-8.

15. Ya'aini N, Saidina Amin NAS. Catalytic conversion of lignocellulosic biomass to levulinic acid in ionic liquid. BioResources. 2013;8(4):5761–5772. . https://doi.org/10.15376/biores.8.4.5761-5772.

16. Carvalho SLBV, de Moraes Medeiros EB, de Souza Wanderley A, de Moura Ribeiro L, da Silva JG, de Almeida Simões IT, et al. Production of xylitol from acidic hydrolysates of lignocellulosic biomass by catalytic hydrogenation over a Ni–Ru/C catalyst. Chem Eng Res Des. 2021;174:11–18. . https://doi.org/10.1016/j.cherd.2021.07.025

17. Farzi A, Soltani M, Ostadrahimi A, et al Synthesis of a nanocomposite with holocellulose extracted from barley straw and montmorillonite, and optimization of the removal of methylene blue dye using the synthesized adsorbent. Appl Water Sci.2023;13:243. https://doi.org/10.1007/s13201-023-02046-6

18. Santawee N, Treesubsuntorn C, Thiravetyan P Lignin and holocellulose from coir pith involved in trimethylamine (fishy odor) adsorption. J Environ Sci (China).2019; 79:43–53. https://doi.org/10.1016/j.jes.2018.10.009

19. Joshi G, Rana V, Malik S, Bachheti RK. Assessment of different reaction media for the facile synthesis of cellulose-derived biorenewable polymer cationic cellulose: synthesis, characterization, and perspectives. ACS Omega. 2025;10(12):12476–12486. . https://doi.org/10.1021/acsomega.5c00044.

20. Lawal SA, Ugheoke BI. Investigation of alpha-cellulose content of agro-waste products as alternatives for paper production. AU J Technol. 2010;13(4):258–260

21. Wei L, Stark NM, McDonald AG. Interfacial improvements in biocomposites based on poly(3-hydroxybutyrate) and poly(3-hydroxybutyrate-co-3-hydroxyvalerate) bioplastics reinforced and grafted with α-cellulose fibers. Green Chem. 2015;17(10):4800–4814. . https://doi.org/10.1039/C5GC01568E.

22. Praveena SM, Han LS, Than LTL, Aris AZ. Preparation and characterisation of silver nanoparticle coated on cellulose paper: evaluation of their potential as antibacterial water filter. J Exp Nanosci. 2016;11(17):1307–1319. https://doi.org/10.1080/17458080.2016.1209790.

23. Rasheed M, Jawaid M, Karim Z, Abdullah LC Morphological, Physiochemical and Thermal Properties of Microcrystalline Cellulose (MCC) Extracted from Bamboo Fiber. Molecules.2020; 25:2824. https://doi.org/10.3390/molecules25122824

24. Li J, Wang Z, Xiu H, Zhao X, Ma F, Liu L, Yi C, Zhang M, Kozliak E, Ji Y. Correlation between the powder characteristics and particle morphology of microcrystalline cellulose (MCC) and its tablet application performance. Powder Technol. 2022;399:117194. https://doi.org/10.1016/j.powtec.2022.117194.

25. Singh GP, Madiwale PV, Adivarekar RV. Preparation and characterization of microcrystalline cellulose (MCC) from renewable source. Curr Appl Polym Sci. 2017;1(2):152–158. . https://doi.org/10.2174/2452271601666170721120343

26. Pervin S, Abdur Razzaque SM, Arifuzzaman Khan GM, et al Synthesis and characterization of microcrystalline and nanocrystalline cellulose from cotton linter for composite applications. Vietnam J Sci Technol.2025;63:311–326. https://doi.org/10.15625/2525-2518/18536

27. Pratama AW, Mahardika M, Widiastuti N, Piluharto B, Ilyas RA, Sapuan SM, Amelia D, Firmanda A. Isolation and characterization of highly thermal stable microcrystalline cellulose derived from belulang grass (Eleusine indica*)*. Case Stud Chem Environ Eng. 2024;9:100743. https://doi.org/10.1016/j.cscee.2024.100743

28. Bhandari K, Roy Maulik S, Bhattacharyya AR. Synthesis and characterization of microcrystalline cellulose from rice husk. J Inst Eng (India): Ser E. 2020;101(2):99–108. . https://doi.org/10.1007/s40034-020-00160-7.

29. Merci A, Marim RG, Urbano A, Mali S. Films based on cassava starch reinforced with soybean hulls or microcrystalline cellulose from soybean hulls. Food Packag Shelf Life. 2019;20:100321. . https://doi.org/10.1016/j.fpsl.2019.100321.

30. Tarchoun AF, Trache D, Klapötke TM Microcrystalline cellulose from Posidonia oceanica brown algae: Extraction and characterization. Int J Biol Macromol.2019; 138:837–845. https://doi.org/10.1016/j.ijbiomac.2019.07.176

31 Afolabi LO, Megat-Yusoff PSM, Ariff ZM, Hamizol MS. Fabrication of Pandanus tectorius (screw-pine) natural fiber using vacuum resin infusion for polymer composite application. J Mater Res Technol. 2019;8(3):3102–3113. https://doi.org/10.1016/j.jmrt.2017.05.021.

32. Ohwoavworhua FO, Adelakun TA. Some physical characteristics of microcrystalline cellulose obtained from raw cotton of Cochlospermum planchonii. Trop J Pharm Res. 2005;4(2):501–507. . https://doi.org/10.4314/tjpr.v4i2.14626.

33. Cichosz S, Masek A IR study on cellulose with the varied moisture contents: Insight into the supramolecular structure. Materials.2020 13:1–22. https://doi.org/10.3390/ma13204573

34. Javier-Astete R, Jimenez-Davalos J, Zolla G Determination of hemicellulose, cellulose, holocellulose and lignin content using FTIR in Calycophyllum spruceanum (Benth.) K. Schum. And Guazuma crinita Lam. PLoS One.2021;16:. https://doi.org/10.1371/journal.pone.0256559

35. Sun P, Heng M, Sun SH, Chen J Analysis of liquid and solid products from liquefaction of paulownia in hot-compressed water. Energy Convers Manag.2011; 52:924–933. https://doi.org/10.1016/j.enconman.2010.08.020

36. Adebawo F, Sadeghifar H, Tilotta D, Jameel H, Liu Y, Lucia L. Spectroscopic interrogation of the acetylation selectivity of hardwood biopolymers. *Starch/Staerke*. 2019;71(11–12):1900086. . https://doi.org/10.1002/star.201900086.

37. Thombare N, Mahto A, Singh D, et al Comparative FTIR Characterization of Various Natural Gums: A Criterion for Their Identification. J Polym Environ.2023; 31:3372–3380. https://doi.org/10.1007/s10924-023-02821-1

38. Ganesan M, Nallathambi G. Alkali-treated coir fibre-pith composite for waste water treatment. J Ind Textiles. 2022;51(Suppl):749S–768S. https://doi.org/10.1177/15280837211014247.

39. Salem KS, Kasera NK, Rahman MA, Jameel H, Habibi Y, Eichhorn SJ, French AD, Pal L, Lucia LA. Comparison and assessment of methods for cellulose crystallinity determination. Chem Soc Rev. 2023;52(18):6417–6446. https://doi.org/10.1039/D2CS00569G.

40. Guo X, Liu L, Wu J, et al Qualitatively and quantitatively characterizing water adsorption of a cellulose nanofiber film using micro-FTIR spectroscopy. RSC Adv.2018; 8:4214–4220. https://doi.org/10.1039/c7ra09894d

41. Chen W, He H, Zhu H, et al Thermo-responsive cellulose-based material with switchable wettability for controllable oil/water separation. Polymers (Basel).2018; 10:. https://doi.org/10.3390/polym10060592

42. Li X, Li J, Gong J, et al Cellulose nanocrystals (CNCs) with different crystalline allomorph for oil in water Pickering emulsions. Carbohydr Polym.2018;183:303–310. https://doi.org/10.1016/j.carbpol.2017.12.085

43. Yue F, Lan W, Zhang A, Liu C, Sun R, Ye J. Dissolution of holocellulose in ionic liquid assisted with ball-milling pretreatment and ultrasound irradiation. BioResources. 2012;7(2):2199–2208. https://doi.org/10.15376/biores.7.2.2199-2208.

44. Gomide RAC, de Oliveira ACS, Rodrigues DAC, et al Development and Characterization of Lignin Microparticles for Physical and Antioxidant Enhancement of Biodegradable Polymers. J Polym Environ.2020; 28:1326–1334. https://doi.org/10.1007/s10924-020-01685-z

45. Rivai H, Hamdani AS, Ramdani R, Lalfari RS, Andayani R, Armin F, Djamaan A. Production and characterization of alpha cellulose derived from rice straw (*Oryza sativa* L.). Int J Pharm Sci Rev Res. 2018;52(1):45–48.

46. Debnath B, Duarah P, Purkait MK Microwave-assisted quick synthesis of microcrystalline cellulose from black tea waste (Camellia sinensis) and characterization. Int J Biol Macromol.2023; 244:125354. https://doi.org/10.1016/j.ijbiomac.2023.125354

47. Liu Y, Wu S, Zhang H, Xiao R Fast pyrolysis of holocellulose for the preparation of long-chain ether fuel precursors: Effect of holocellulose types. Bioresour Technol.2021; 338:. https://doi.org/10.1016/j.biortech.2021.125519

48. Wang J, Zhang R, Quan C, et al. Green preparation of porous corncob microcrystalline cellulose, and its properties and applications. Cellulose.2022;29:7125–7138. https://doi.org/10.1007/s10570-022-04724-1

49. Kunusa WR, Isa I, Laliyo LAR, Iyabu H. FTIR, XRD and SEM analysis of microcrystalline cellulose (MCC) fibers from corncorbs in alkaline treatment. J Phys Conf Ser. 2018;1028(1):012199. https://doi.org/10.1088/1742-6596/1028/1/012199

50. Nasution H, Yurnaliza, Veronicha, Irmadani, Sitompul S. Preparation and characterization of cellulose microcrystalline (MCC) from fiber of empty fruit bunch palm oil. IOP Conf Ser: Mater Sci Eng. 2017;180(1):012007. https://doi.org/10.1088/1757-899X/180/1/012007.

Chapter 6

Biomass-Derived Silicified Microcrystalline Cellulose (SMCC): A Novel Method Based on Screw Pine leaves and Mission Grass

6.1. Introduction

6.1.1 Overview and Importance of Microcrystalline Cellulose

Microcrystalline Cellulose (MCC), commonly known as Avicel is a white, crystalline and partially depolymerised form of cellulose typically derived from α-cellulose. MCC is chemically stable, compressible and hydrophilic but does not dissolve in water [1]. MCC finds wide range of applications in various fields. In food industry it serves as a stabilizer, anticaking agent, texture modifier, etc. [2]. In cosmetics, MCC perform multiple roles such as thickener and viscosity controlling agent in cream, lotion and gels [3]. MCC is a versatile excipient in pharmaceuticals. It acts as a binder, filler, disintegrants and flow enhancer in tablets and capsules [4]. In polymer composite engineering, MCC serves as a sustainable reinforcement owing to its low density, high specific modulus and renewability. When MCC is paired with biodegradable polymers like Polylactic Acid [5], Polyvinyl Alcohol [6] etc., the overall performance of composites such as tensile strength, impact resistance, biodegradability, etc., will be significantly improved. MCC is primarily derived from wood pulp [7] and cotton linters [8]. However, increasing interest has shifted to more sustainable and cost-effective resources such as agricultural residues including wheat straw [9], sugarcane [10], soy hulls [11], olive stone [12], bamboos [13],etc. Recently, a number of works has been reported regarding the extraction of MCC from algae [14] and bacteria [15].

6.1.2 Limitations and Challenges of MCC

Despite its widespread application across the pharmaceutical and related industries, MCC is afflicted with several performance challenges. One of the significant drawbacks is its inherent insolubility in water and most commonly used

solvents, hence it cannot support fast release formulation. It has low bulk density and relatively poor flowability. Its low bulk density results in inefficient packing of particles. Additionally, MCC is hygroscopic in nature and readily absorb moisture which will further reduce the flow properties. As a consequence, the material may be sticky or clumpy, thus processing will be challenging. The hydrophilic nature of MCC adversely affect its compatibility with hydrophobic polymer matrices. The dispersibility of MCC in polymer is very low, usually agglomerates and forms heterogeneous composites. This will weaken interfacial adhesion, reduce the tensile strength and increase the brittleness of the polymer. Since MCC degrades at around 300 °C, it reduces the thermal stability of polymer composites.

6.1.3 Recent Advancements in the modification of MCC

The above-mentioned limitations can be effectively mitigated by surface modification and by adopting compatibilization strategies. The solubility of MCC can be enhanced by disrupting its highly crystalline hydrogen-bonded structure, introducing functional groups and altering electrostatic interactions [16]. Ionic liquid pretreatment disrupts intermolecular H- bonding, reduces crystallinity and converts MCC into more amorphous form. Thus, there will be significant improvement in solubility and chemical accessibility. Similarly, salt hydrate treatment decreases the crystallinity of MCC, thus enhances the porosity and accessibility [17]. The cationization of MCC through grafting quaternary ammonium groups impart positive charge on the surface that will induce repulsion between the chain, significantly increases the water dispersibility and solubility [18]. The bulk density of MCC can be enhanced by treating with alkali at low temperature followed by precipitation and drying [19]. The flow properties of MCC can be increased by coating it with magnesium stearate [20].In order to enhance the dispersibility of MCC in polymer matrix several approaches were adopted. MCC was modified using toluene 2,4 - diisocyanate (TDI) in tetrahydrofuran (THF) in order to make it hydrophobic and improve its dispersion in Polylactic Acid matrix [21]. MCC was also modified with urea and used as a better reinforcing filler in chitosan [22]. Acetylation of MCC enhances its dispersibility and compatibility with Polylactic Acid, leading to improved

mechanical and thermal properties [23]. Hydroxypropylmethyl Cellulose can be prepared from α-cellulose through alkalization, esterification and purification [24]. A controlled phosphorylation of micro fibrillated cellulose was achieved upon mild mechanical treatment followed by mixing with reduced amount of ammonium hydrogen phosphate and urea, as a result fire retardant composites were formed [25]. MCC can also be modified through physical processes like grinding, milling, spray drying, etc.

6.1.4 Silicified MCC (SMCC): A Promising Solution to Enhance MCC Performance

Silicified Microcrystalline Cellulose (SMCC) is a modified form of MCC prepared by incorporating nanosilica with MCC [26]. SMCC exhibits several superior properties such as high bulk density, better flowability, improved mechanical strength, higher thermal and chemical stability, less hygroscopic properties and hence more stability even in humid conditions [27]. SMCC can be synthesised by sol-gel, mechanical and impregnation methods. SMCC is widely used in pharmaceuticals as fillers and binders in tablets, wound care products, surgical implants and drug delivery systems due to their biocompatibility, biodegradability, non-toxicity, targeted delivery, etc [28]. In food industry it is used as a stabilizer and anticaking agent, since it prevents moisture absorption [29]. It is also used to make hair care and skin care products. Incorporating SMCC into the polymer will enhance the mechanical strength, improve thermal stability and decrease the tendency to shrink [30]. It is a cost-effective filler and is expected to improve the biodegradability of the polymer.

6.1.5 Aim and Objectives of the Study in the Present Chapter

The aim of the present chapter is to develop and characterize Silicified Microcrystalline Cellulose (SMCC) synthesised via a novel in situ approach using Screw Pine leaves as the cellulose source and Mission Grass as the silica precursor and evaluate its physicochemical properties compared to pure MCC and Silica. The objectives of the study include

- To perform in situ synthesis of Silicified MCC (SMCC), through dispersing MCC in sodium silicate followed by acid hydrolysis at optimum conditions.
- To prepare and compare SMCC blends with 10 wt% and 20 wt% silica.
- To carry out comprehensive characterisation including bulk density, true density, porosity, X-ray Diffraction (XRD), Fourier Transform Infra-Red (FT-IR) Spectroscopy, Field Emission- Scanning Electron Microscope (FE-SEM) and Thermogravimetry (TG) Analysis on extracted MCC, Mission Grass Silica and the blended SMCC (SMCC10 and SMCC20)
- To compare and analyse the influence of silica content on the structure, morphology, thermal stability and density of SMCC sample.
- To assess the sustainability and feasibility of Screw Pine and Mission Grass as cost- effective renewable raw material for the production of SMCC

6.2 Materials

Screw Pine (SP) leaves and Mission Grass (MG) were collected from the river side of Kerala, India. Ethanol, toluene, sodium chlorite ($NaClO_2$), hydrochloric acid and sodium hydroxide procured from Merck India. All the chemicals were of analytical grade and were used without further purification.

6.3 Methods

6.3.1 Preparation of Silicified Microcrystalline Cellulose

6.3.1.1 Isolation of Microcrystalline Cellulose

SP leaves were cut into small pieces, washed, dried in sunlight and powdered. It is sieved through a mesh and dried again in a hot air oven at 100-110 °C for 4 h. Oven-dried samples were extracted with a 2:1 ethanol-toluene mixture, using a Soxhlet apparatus for 5 h to remove pigments. After drying, 1 g of the sample was bleached with 20 ml of 0.7% sodium chlorite ($NaClO_2$) solution in a water bath at 80 °C for 5 h. It was filtered and washed till the washings became neutral. During this

process, lignin was removed, and holocellulose was obtained. The α- cellulose was extracted from holocellulose by treating 1 g of the sample with 15 ml of 17% NaOH solution (by adding 5 ml of the solution at three intervals in 45 minutes) under continuous stirring. The solution was then allowed to stand for 1 h and was diluted with distilled water to make the concentration of NaOH to 8.5%. The solution was filtered, washed with water and then with 10% acetic acid. Dried α-cellulose (1 g) was subjected to acid hydrolysis using 17 ml of 2.5N HCl at boiling temperature for 15 minutes. The hot solution was poured into 50 ml of cold water with vigorous stirring. It was kept to stand overnight and the resulting MCC was washed and dried in a hot air oven at 60 °C for 30 minutes.

6.3.1.2 Preparation of Sodium Silicate

The collected MG was washed to remove impurities, dried in sunlight and powdered. The sample was heated in a muffle furnace at 600 °C for 8 h to obtain MG ash, which contains silica. MG ash is heated with 2N HCl at 200 °C for 5 h using a magnetic stirrer in order to remove the metal ions like Na, K, Al, etc. They will be converted to the corresponding chlorides and removed by filtration. The residue (1 g) was digested with 3M NaOH using a magnetic stirrer at 80 °C for 5 h and kept overnight. It is filtered through Whatman No. 1 filter paper, and the filtrate is sodium silicate solution.

6.3.1.3 Synthesis of Silicified Microcrystalline Cellulose (SMCC)

MCC (0.9 g) was dispersed in 20 ml of sodium silicate solution (20 ml of filtrate on hydrolysis give 0.1 g amorphous silica) [31]. It was diluted to 80 ml and stirred well for 5 h and kept overnight. 2N HCl was added dropwise with constant stirring, till the solution became turbid. Silicified MCC containing 10% w/w silica in MCC (SMCC10) thus formed was filtered, the residue is washed, and dried in hot air oven. The procedure is repeated with 0.8 g MCC and 40 ml sodium silicate solution, thus SMCC20 (20% w/w silica) was obtained. A schematic overview of all steps was provided in **Scheme 6.1.**

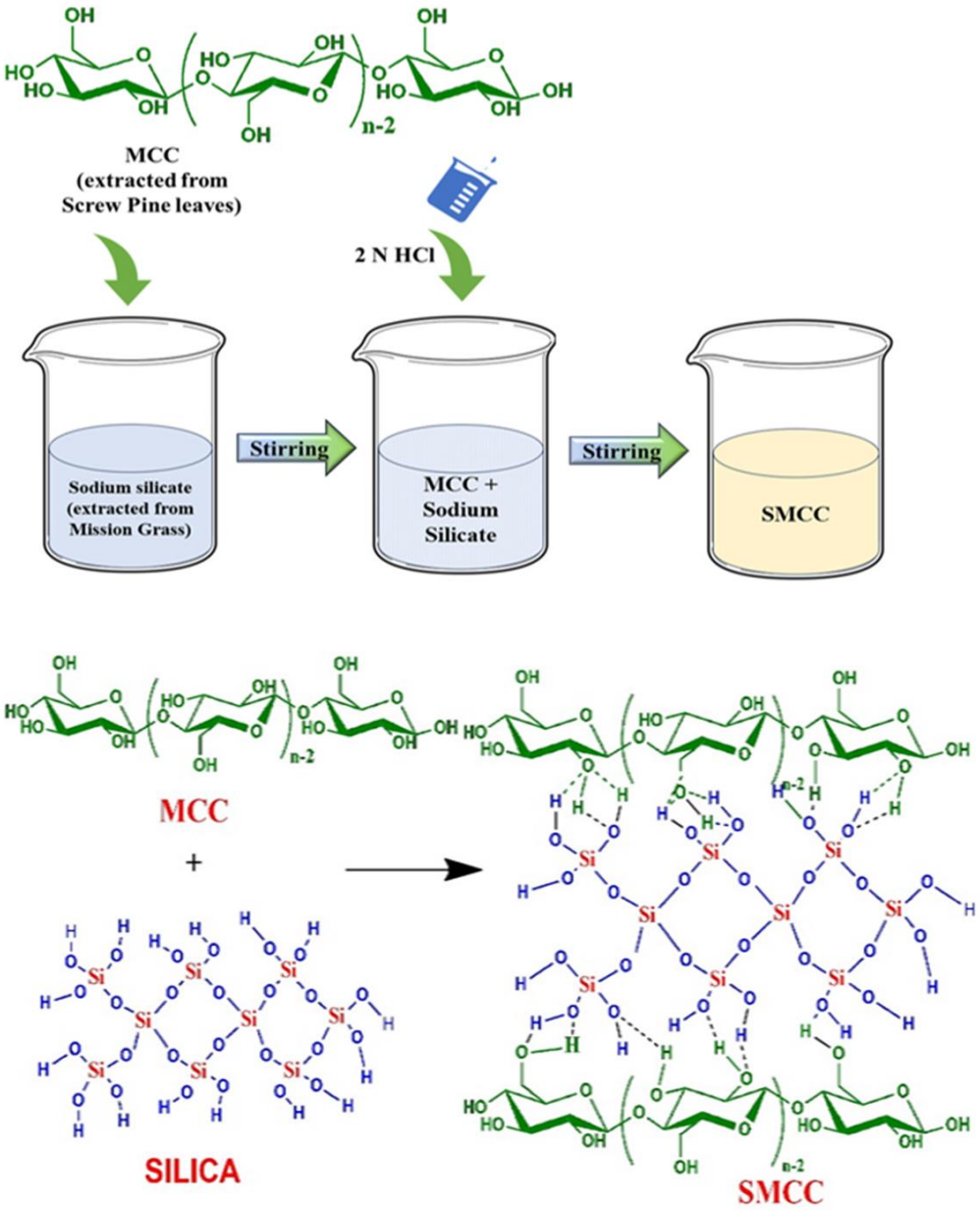

Scheme 6.1. Schematic Representation of Formation of Silicified Microcrystalline Cellulose

6.4. Results and Discussion

6.4.1True Density, Bulk Density and Porosity measurements

True Density (T.D), Bulk Density (B.D) and Porosity(P) of the samples were determined by solvent displacement method (as discussed in Chapter 3) and are given in the **Figure 6.1.** T.D and B.D of MCC is 1.12 and 0.64 respectively and became

1.42 and 0.878 for SMCC10 and 1.65 and 1.12 for SMCC20 respectively [32]. This value shows that the amount of silica has a significant effect on the densities [33]. Increasing the density of MCC by adding silica offer several key advantages. The silica deposit significantly improves the flowability and reduces cohesiveness. As a filler in polymer composites, enhancing the value of density is highly beneficial in the following aspects. The higher density helps the SMCC to disperse more uniformly in polymer, enhancing load transfer at the filler- matrix interface. The fillers with high density will improve the strength and stiffness of the composites [34], will provide high thermal stability hence making it suitable for high temperature applications, better dispersibility of filler in the polymer matrix, abrasive resistance, etc [35]. The studies showed that silicified MCC exhibits better mechanical properties when it is used as filler in thermoplastic matrices like polystyrene [36]. The lower porosity and denser structure of SMCC improve the thermal stability of composites, reduce void formation and moisture uptake.

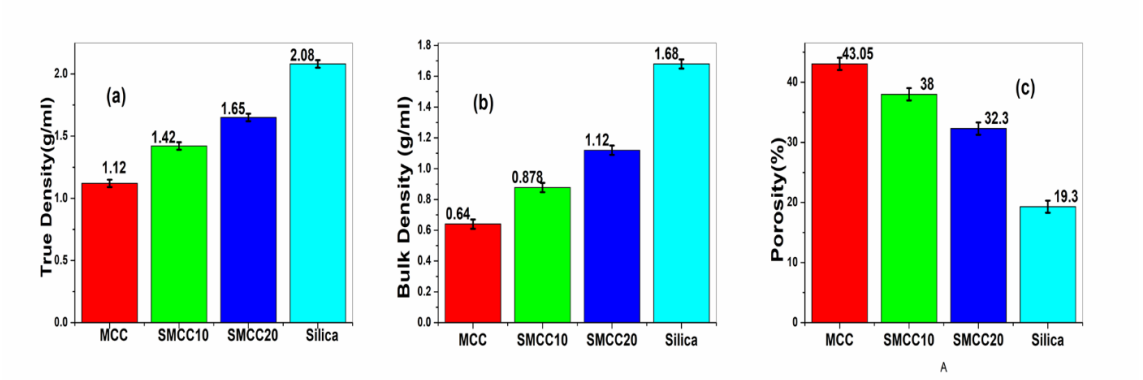

Figure 6.1 (a) True Density(g/ml) (b) Bulk Density(g/ml) and (c) Porosity (%) of MCC, SMCC10, SMCC20 and Silica

Superiority of these properties can be proved by XRD, TG, and FE-SEM analysis. As density is inversely proportional to porosity, MCC have the highest porosity and its value diminishes during silicification. It is due to the fibrous and porous nature of MCC which was proved by FE-SEM analysis. During silicification, nanoparticles of silica will infiltrate and fill the voids of MCC. Moreover, silica forms stronger interparticle bonds with MCC.

6.4.2 Fourier Transform- Infrared Spectroscopy Analysis

Figure 6.2 (a) shows the FT-IR spectrum of MCC obtained from SP leaves. The strong and broad absorption peak near 3450 cm^{-1} is due to H- bonded O-H stretching vibration [37]. The absorption peak near 2900 cm^{-1} corresponds to the stretching vibration of C-H bond [38]. The peak at 1749 cm^{-1} is attributed to C=O stretching vibrations, due to the presence of acetyl or ester linkage of carboxylic acid group, indicating trace amounts of hemicellulose and lignin present in the sample [39]. The peak at 1640cm^{-1} is associated with the O-H bending vibration of the absorbed water molecule on the surface of MCC [38].

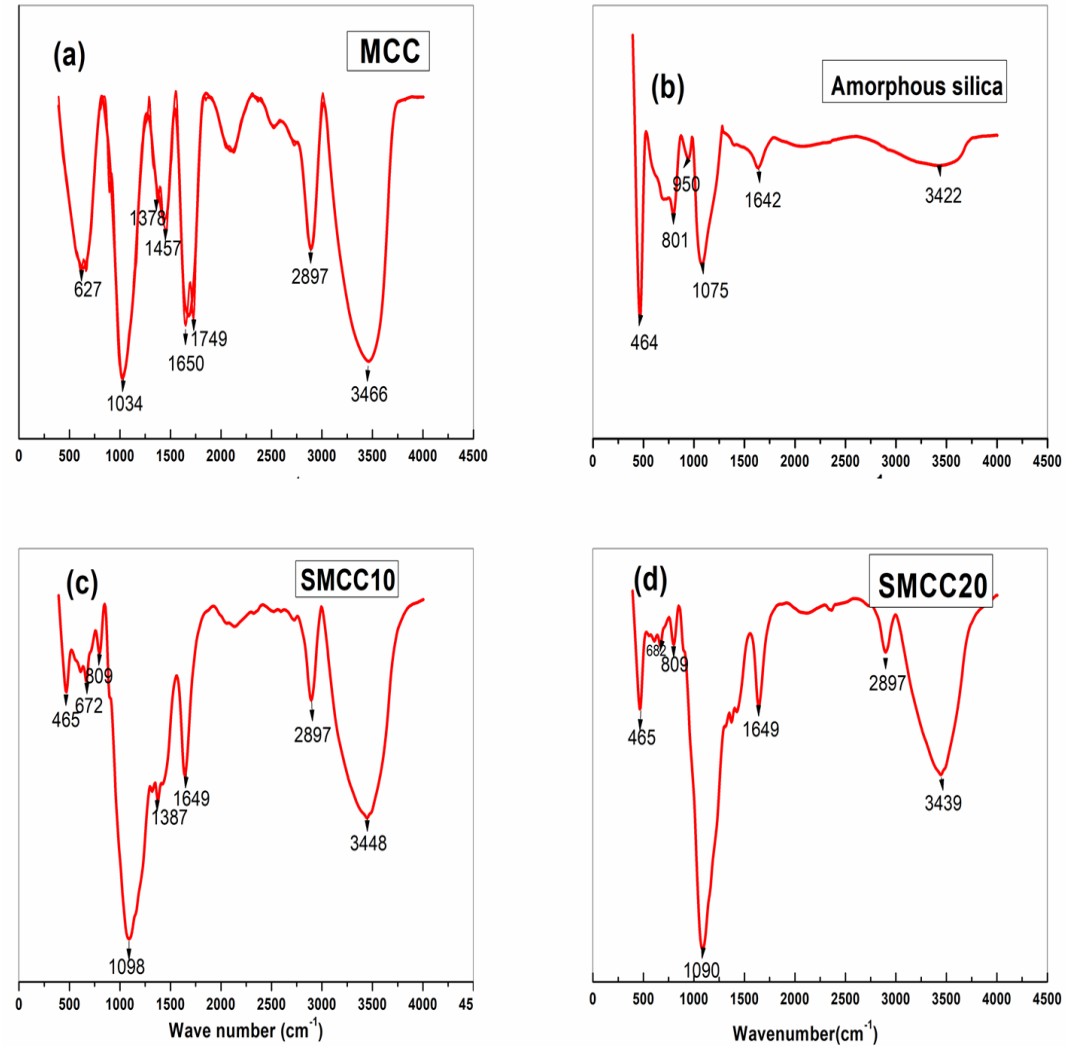

Figure 6.2 FT-IR spectra of (a) MCC (b) Amorphous silica (c) SMCC10 and (d) SMCC20

The peaks at 1457 cm^{-1} and 1378 cm^{-1} are due to symmetric and asymmetric deformation of the CH_2 group. The peaks at 1034 cm^{-1} and 627 cm^{-1} are due to C-O-C glycosidic stretching and bending vibration respectively. **Figure 6.2(b)** illustrates the FT-IR spectra of amorphous nanosilica extracted from MG. The peak around 3000-3500 cm^{-1},which is due to the O-H bond of the silanol group is appeared as very broad, which shows extensive hydrogen bonding and highly amorphous nature [40]. The small peak at 1642 cm^{-1} is due to the bending vibration of water molecule [41]. The peaks that appear at 450-1300 $cm^{-1}$is unique for silica. The peak at 464 cm^{-1} is due to symmetric rocking pulsation of O-Si-O bond in the silanol group. The absorption band at 801 cm^{-1} is due to the symmetric Si-O-Si bond [42]. The strong peak at 1075 cm^{-1} is due to Si-O-Si stretching vibration and is a characteristic absorption band of mesomorphous silica nanoparticle. A very small peak at 950 cm^{-1} is attributed to Si-O stretching vibration.

Figure 6.2(c) shows the FT-IR spectra of SMCC10. It is clearly visible that the spectra show the characteristic peak of both MCC and silica. The peak at 3448 cm^{-1} which is due to the H-bonded O-H group is less intense than that of MCC, which shows the interaction between MCC and silica [43]. The characteristic peak at 2897 cm^{-1}, which is due to the stretching vibration of C-H is also present in the spectra. The peak at 1750 cm^{-1} found in MCC due to C=O group is absent in SMCC10. The peak at 1649 cm^{-1} which is attributed to the O-H bending vibration of water is less intense than MCC, which shows that SMCC10 is less hygroscopic. The peak at 1387cm^{-1} is due to the asymmetric vibration of CH_2 group. The sharp peak at 1098 cm^{-1} corresponds to Si-O-Si stretching vibration. The peaks at 465 cm^{-1} and 809 cm^{-1} which are due to symmetric bending of O-Si-O bond and Si-O-Si bond are also present. In total, the appearance of FT-IR spectra of SMCC10 is entirely different from that of pure MCC and Silica. SMCC have a broader and diffuse peak compared to MCC and the resolution is less. But SMCC have sharper and well-defined peaks compared to amorphous silica. This shows that SMCC10 is less crystalline than MCC but more than that of Silica as seen in XRD studies. **Figure 6.2(d)**, which is that of SMCC20 shows almost similar spectra to that of SMCC10. The intensity of the peak due to O-

H stretching further diminishes. The low intensity peak at 2897 cm^{-1} which is due to the stretching vibration of C-H bond shows the reduced organic content in the sample. The peak at 1090 cm^{-1} due to Si-O-Si stretching vibration is more intense than that of SMCC10. The band due to silica is clearly visible at 465 cm^{-1} and 809 cm^{-1}.

6.4.3 X-ray Diffraction Analysis

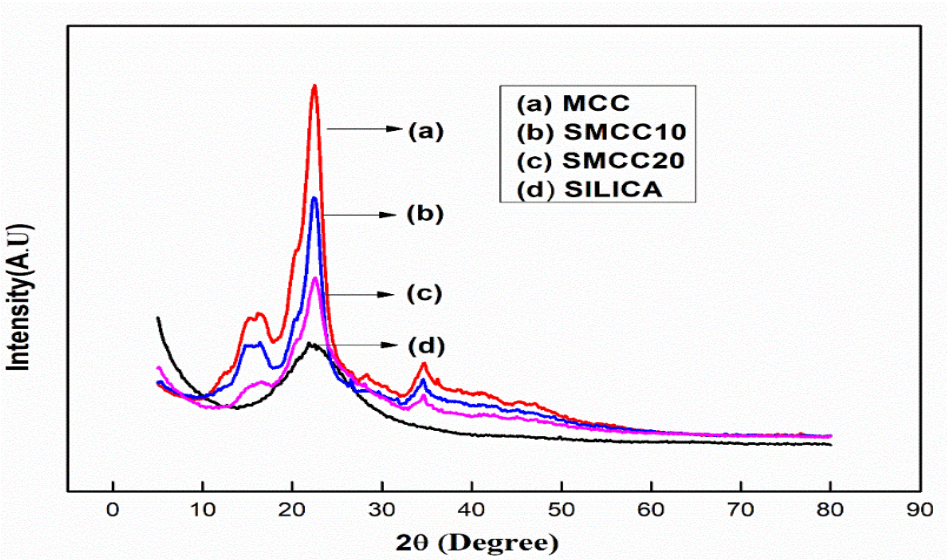

Figure 6.3 X-ray Diffraction Pattern of (a)MCC (b)SMCC10 (c)SMCC20 and (d) Silica

The XRD patterns of MCC, SMCC10, SMCC20 and amorphous silica are given in **Figure 6.3.** Typical cellulose I β exhibits characteristic diffraction peaks at 2θ values around 14.6°, 16.5° and sharp reflection at 22.7° corresponding to the $(1\bar{1}0)$, (110) and (200) planes respectively. In contrast, cellulose II is characterized by diffraction peaks located at approximately 12°, 20° and 22° corresponding to the $(1\bar{1}0)$, (110) and (020) planes respectively [44]. But the XRD pattern of MCC extracted from SP leaves exhibited merged peaks at 2θ value of 14.9° and 16.5° along with a sharp peak at 22.5°, which are characteristic of cellulose I (Iβ). A faint diffraction at 20.5° and a bulge at 12°, which are characteristic of cellulose II were also observed. There is a small peak at 35°,that corresponds to (004) crystallographic planes [45]. A narrow peak is also seen at 2θ=28.5° which is attributed to mineral impurities [46]. These peaks indicate that MCC sample contains mixed phase

dominated with Cellulose Iβ with partial conversion to Cellulose II. The incomplete conversion, despite treatment in 17% NaOH is due to the moderate temperature and limited exposure time during the extraction process. To obtain quantitative assessment of two phases, Rietveld refinement of MCC was carried out using MAUD software with crystallographic models of cellulose Iβ(Tunicate) and cellulose II. The CIFs of these phases were obtained from the work reported by French [44], Nishiyama et al. [47]and Langan et al. [48] . The details of refinement are given below.

6.4.3.1 Rietveld Refinement of MCC

The raw data of MCC (XRDM file) was loaded into the MAUD software along with the CIF file of cellulose 1β (Tunicate) and cellulose II. In the MAUD, data setting parameters such as wavelength and 2θ are defined. In the first stage background parameters and overall scale factors were allowed to refine to get initial fit between the observed and calculated pattern. Sample related specific parameters like crystallite size and micro strain were allowed to refine. After each cycle the fit quality was assessed by visual comparison and monitoring statistical indices. The Rietveld refined XRD pattern and corresponding refinement statistics are given in the **Figure 6.4**

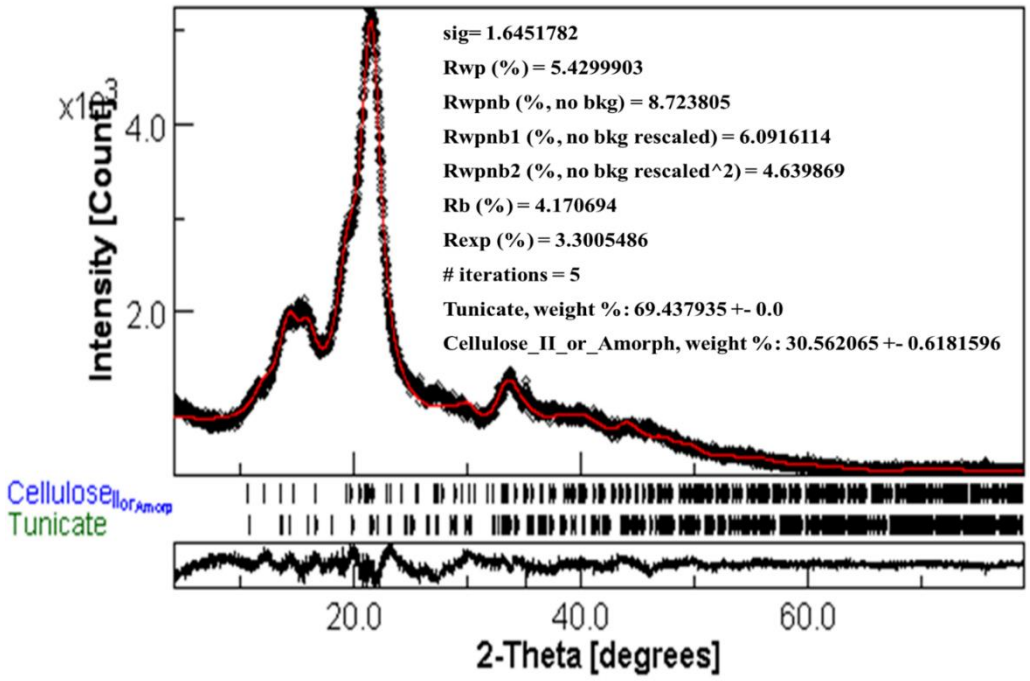

Figure 6.4 Rietveld Refined XRD of MCC with Refinement Statistics

The refinement statistics reveals that Rwp and Rb values are quite low, suggesting that the calculated diffraction pattern matches the observed pattern. The expected R factor and χ^2 is within the accepted range. The phase fraction is 69.4 wt% of cellulose Iβ and 30.6% cellulose II, appears stable and well defined. The full pattern XRD showing phase composition is given in **Figure 6.5**

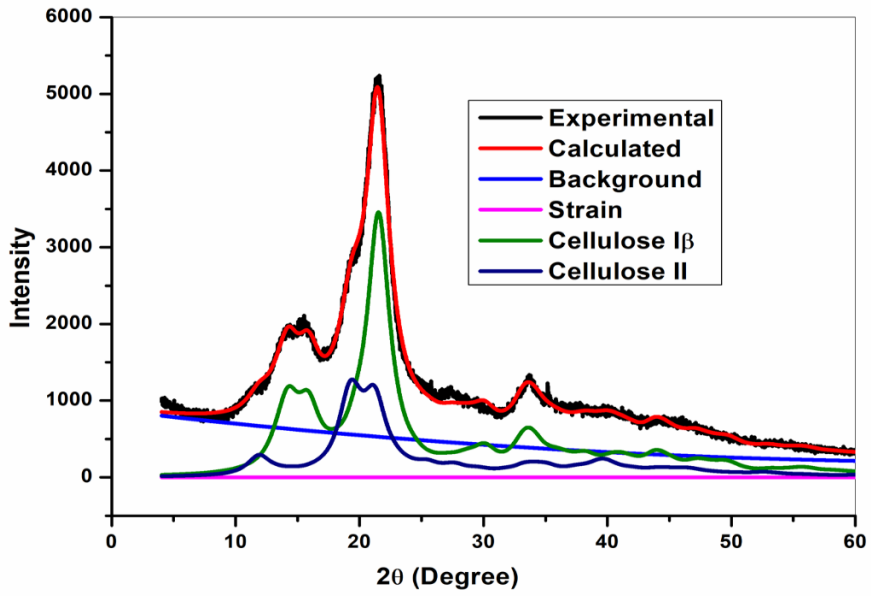

Figure 6.5 Full Pattern XRD of MCC showing Phase Composition.

6.4.3.2 Rietveld Refinement of SMCC10

A three-phase refinement was performed in the case of SMCC10. The CIF file of tunicate (cellulose Iβ) was loaded as the first phase and cellulose II as the third phase. The CIF file of silica obtained after refining XRD of silica from MG with cristobalite (1010954) was loaded as the second phase. All the relevant parameters were adjusted until a perfect fit was achieved. The refined XRD pattern and corresponding refinement statistics are provided in the **Figure 6.6**

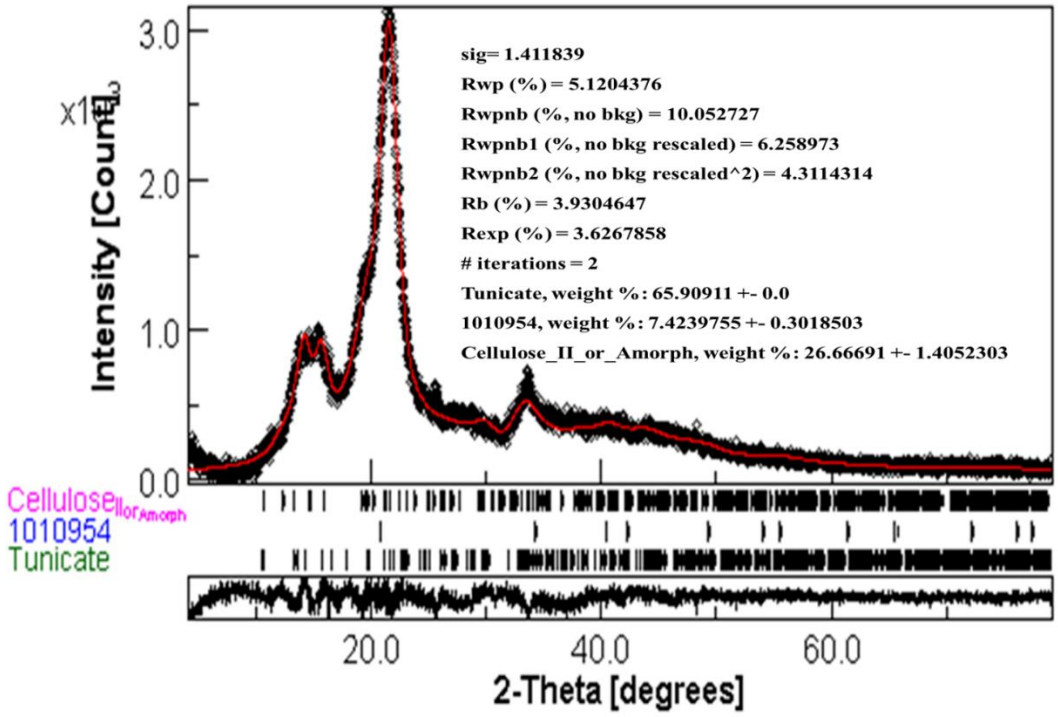

Figure 6.6 Rietveld Refined XRD of SMCC10 with Refinement Statistics

The multiphase refinement on two iteration yielded excellent agreement between the observed pattern and the calculated pattern. The weighted profile factor (Rwp) and the Bragg R-factor (Rb) are quite low which reveals high quality fit for the XRD pattern. The quantitative analysis shows that the sample contain 65.9 wt% cellulose Iβ, 7.4 wt% silica and 26.7 wt% cellulose II with reasonable uncertainties. **Figure 6.7** represents the phase composition of XRD which reveals that the peak of silica is very broad which indicates its amorphous nature.

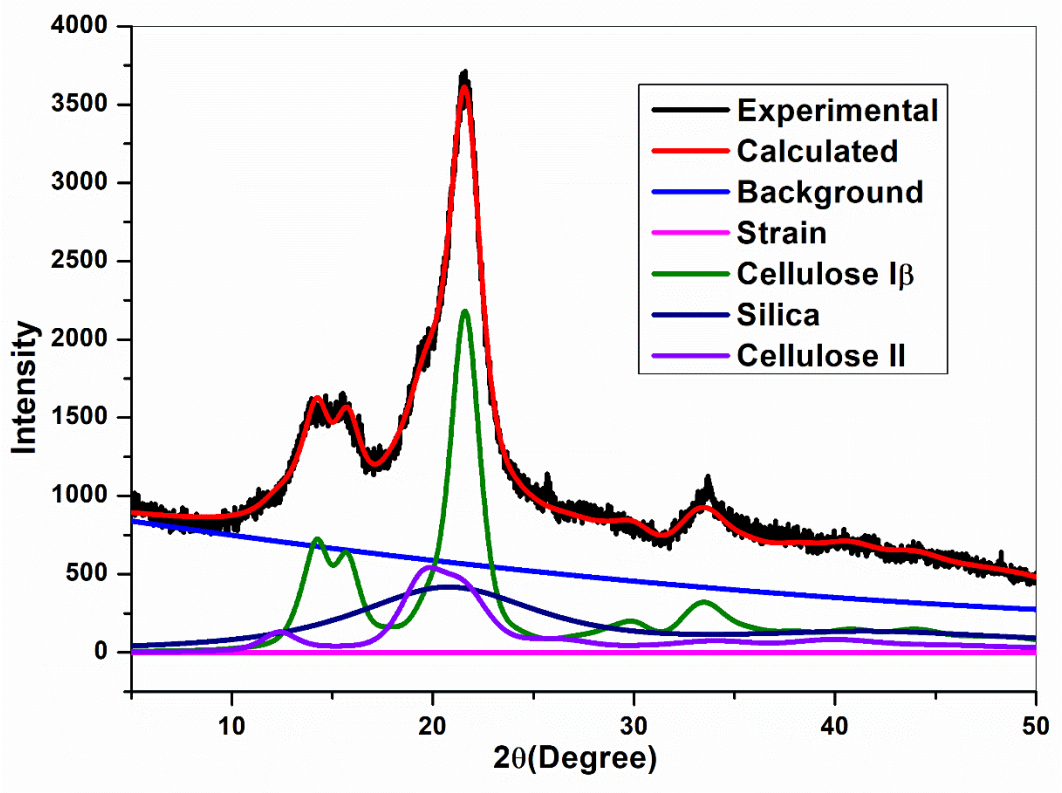

Figure 6.7 Full Pattern XRD of SMCC10 showing Phase Composition.

6.4.3.3 Rietveld Refinement of SMCC20

The above-mentioned procedure was also adopted for the Rietveld refinement of SMCC20. But, here the order of phase uploading has been changed. The re-refined CIF file of silica was assigned as the first phase and cellulose Iβ as the third phase. Since SMCC20 contains nominal percentage of amorphous silica, the refinement became more complex possibly due to greater peak overlap and increased amorphous contribution. The data provided in the refinement statistics (**Figure 6.8**) reveals that SMCC20 shows lesser agreement between observed pattern and calculated pattern than that of SMCC10 or MCC.

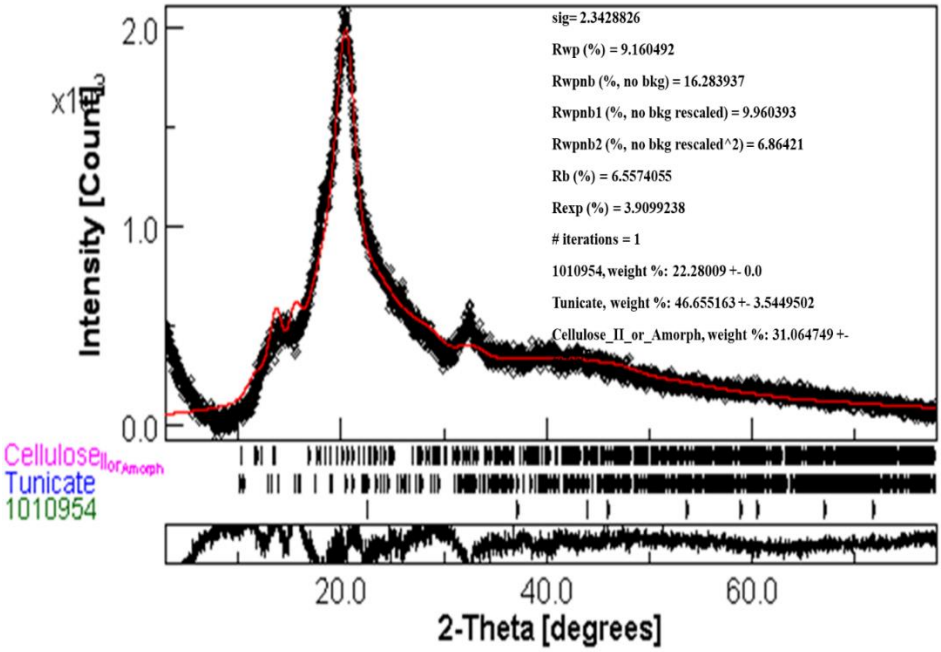

Figure 6.8 Rietveld Refined XRD of SMCC20 with Refinement Statistics

The fit quality of SMCC20 is inferior to that of SMCC10, however the result remains within the acceptable range for complex multiphase system [49]. The phase composition plot **(Figure 6.8)** indicates the broadness and higher composition of silica within SMCC20.

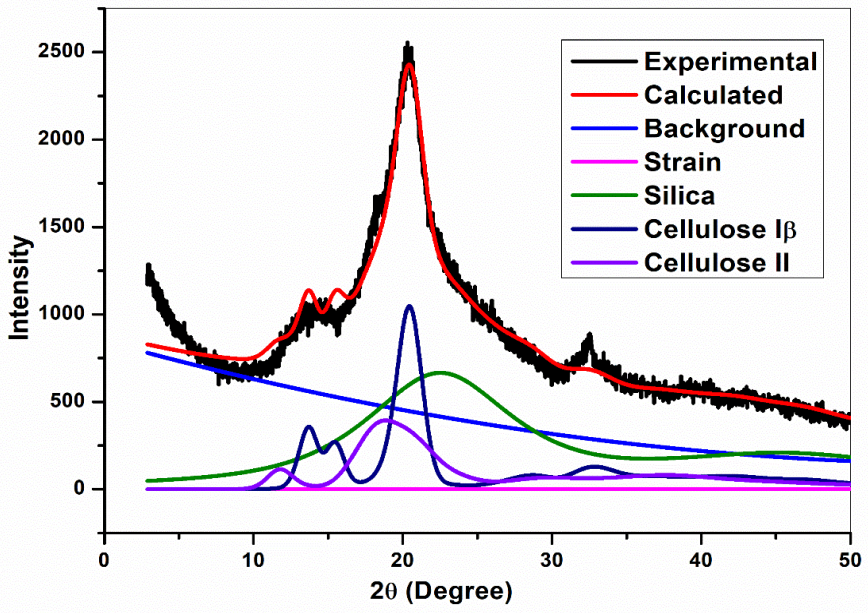

Figure 6.9 Full Pattern XRD of SMCC20 showing Phase Composition.

The phase composition obtained from the refinement are summarised in **Table 6.1**, which clearly indicates the expected increase in silica content from SMCC10 to SMCC20 and the corresponding adjustment in cellulose I and cellulose II. Diffractogram **6.3(d)** shows the XRD pattern of amorphous silica obtained from MG which was calcinated at 600 °C followed by sol gel synthesis. As reported in our previous chapter there is a broad hump from 15°-30° with central peak at 21.9° [31], which indicates its amorphous nature

Table 6.1. Phase Composition of MCC, SMCC10 and SMCC20 Obtained from Rietveld Refinement

Sample	Cellulose I (wt%)	Cellulose II (wt%)	Silica (wt%)
MCC	69.4	30.5	
SMCC10	65.9	26.6	7.42
SMCC20	46.7	31	22.3

The density and XRD studies show that silicifying MCC with amorphous silica will lead to two key material changes. Since amorphous silica has high intrinsic density, the overall density of MCC will be improved during silicification. Meanwhile, the incorporation of amorphous silica disrupts the ordered crystalline domain of MCC, leading to measurable drop in crystallinity. These modifications in physical properties is advantageous in the following aspects. This provide better flowability, high compatibility and improved manufacturability, making SMCC as a better excipient in material science where optimized powder behaviour and mechanical performance is necessary. The dual effect of high density and low crystallinity provides some superior properties for SMCC as a filler in polymer composites. It supports uniform microstructure, reduced brittleness, and allows more efficient reinforcement for SMCC than MCC [50]. The reduced crystallinity is due to amorphous region that facilitate better interfacial adhesion, plastic deformation under stress and ductility.

6.4.4 Thermogravimetric Analysis

Thermal stability and degradation characteristics of MCC, SMCC10, SMCC20 and silica were investigated by thermogravimetric analysis under an inert atmosphere. The TG and DTG curves of the samples are shown in **Figures 6.10 (a) and (b)**, respectively. In the case of MCC, only 5% initial weight loss is observed at a temperature range of 30-70 °C which shows that moisture content in the sample is very less. Since there is no significant weight loss in the temperature range 70-220 °C, MCC is thermally stable at this temperature. Considerable weight loss (80%) is observed from 220 °C to 380 °C due to cellulose degradation caused by decarboxylation, depolymerisation and decomposition of glycosyl units [51]. A weight loss of merely 1% is observed as the temperature rises from 400 °C to 700 °C, resulting in a residual weight of 7%.

A gradual decrease in weight is observed during the heating of silica. 16% weight loss is observed in the temperature range of 30 °- 90 °C due to the removal of physically absorbed water molecules. In the temperature range 90 - 330 °C the weight loss is 4.2% due to the removal of the internal water molecule from the silanol group [52]. The H- bonded hydroxy groups will be removed at a temperature of 200 - 400 °C, while the isolated hydroxy groups will be removed at higher temperature. At elevated temperatures, no substantial weight loss is observed, with 81% of the original sample retained even at 600 °C [41].

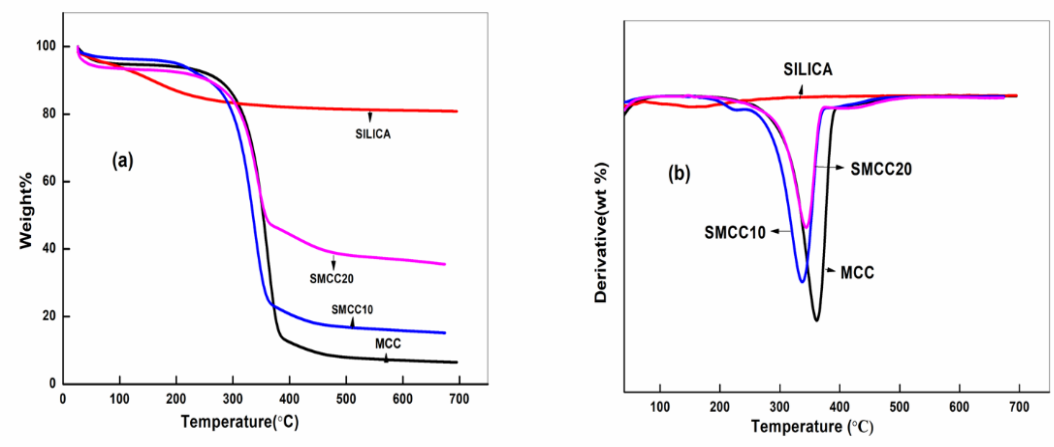

Figure 6.10 (a) TG and (b) DTG of MCC, SMCC10, SMCC20 and Silica

The thermal behaviour of SMCC10 is comparable to MCC, but it shows significant thermal stability than MCC. Only 3% weight loss in 30 -70 °C, and 1% in 70-190 °C. Within the range of 220 - 370 °C weight loss is 71% which is less than that of MCC. The TG of SMCC20 shows that thermal stability is higher than MCC and SMCC10. Within the range of 25 °C to 370 °C the weight loss is only 42% and even at 600 °C it retains 37% of the total weight. Thus, with increasing silica content in the MCC thermal stability can be upgraded. The onset temperature, determined by the tangent method, was found to be 308 °C for native MCC. In contrast, SMCC10 and SMCC20 exhibited higher onset temperatures of 313 °C and 326 °C, respectively, which can be attributed to the enhanced covalent interactions developed during the modification process. Overall, SMCC is advantageous over MCC in the following aspects. The material containing SMCC can withstand high processing temperature without degrading, making them suitable for engineering thermoplastics and thermosetting plastics that require elevated curing or moulding temperature. The silica has inherent flame-retardant properties therefore when it is integrated to MCC, it can delay ignition, reduce heat release and form a protective char layer, thereby improving fire safety in packaging, building material and textiles [53]. In biomedical devices and drug delivery system, maintaining structural and chemical integrity during sterilization process is critical, thus SMCC can endure this process better than raw MCC. Moreover, hybrid cellulose-silica material maintains ultra-low thermal conductivity while gaining mechanical strength and moisture resistance [54].

6.4.5 Morphological Analysis

Figure 6.11 shows the FE-SEM images of MCC, nanosilica and SMCC20 respectively. Morphology of MCC depends on several factors such as source of cellulose, processing methods, conditions of synthesis, etc. [55]. SEM analysis of MCC revealed spongy, porous appearance with irregular shaped aggregates composed of entangled fibres. The individual fibres have the length 60- 90 μm with the diameter in the range of 2-10 μm. Small and big sized lacunas (10-600 μm) with irregular shapes are visible within the structure. This shows the effective removal of the amorphous region during hydrolysis [56]. This void plays important role in

determining the physical properties such as porosity, bulk density, moisture retention capacity etc. This void offers room for nanoparticles such as nanosilica. Nano particles can easily intrude into the MCC and significantly change their property.

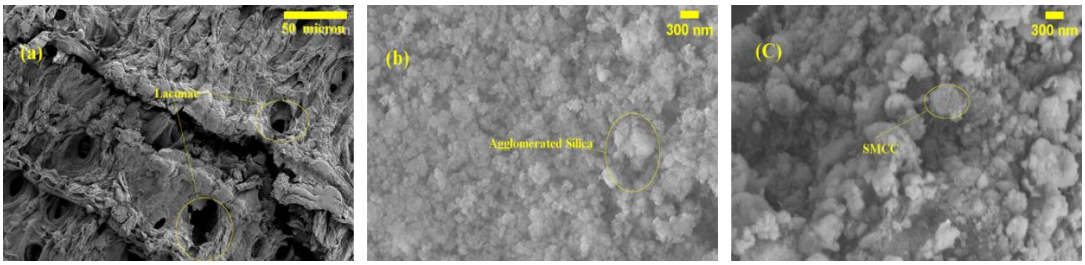

Figure 6.11 FE-SEM Images of (a) MCC (b) Nanosilica (c) SMCC 20

Figure 6.11(b) shows the high-resolution FE-SEM image of amorphous nanosilica obtained from MG. The image shows that particle size and shape are not uniform. Particles are in the nanometre range (10-100 nm) and shapes are spherical, irregular and appear as agglomerated [57]. The surface appears as rough and porous and this will give a high surface area for nanosilica. The reason for agglomeration is the presence of hydroxyl groups on the silica molecule which are bounded to each other through H- bonding. Van der Waal's attraction also contributes for agglomeration. The image shows the particle size of silica is less than the voids of MCC hence silica can easily accommodate the vacant site of MCC.

Figure 6.11(c) shows the image of Silicified MCC which is distinguishable from pure MCC and nanosilica. The coarse MCC particles are broken down to small fragments of SMCC with average particle size within the range100 nm to 1µm [43]. SMCC exhibit rough surfaces and the deposition of silica result coarser and granular texture. Since MCC have a lot of vacant space, sodium silicate solution can easily be infiltrated in to this site and this on treatment with HCl, silica gel will be formed and will be well trapped inside the lacunae. The adhered sodium silicate on the surface of MCC will be deposited silica coating during acid treatment. Silica is a rigid, inorganic material and when it infiltrates the MCC network, it fills the interstitial voids within MCC. Therefore, silica particles not only reinforce the cellulose network but also

decreases the porosity of MCC. Thus, bulk density, thermal stability and stiffness of SMCC will be higher than that of MCC

Conclusion

The present study successfully demonstrated a novel in situ method for the production of Silicified Microcrystalline Cellulose (SMCC) using Screw Pine (SP) leaves as the source of Microcrystalline Cellulose (MCC) and Mission Grass (MG), a highly invasive weed as a sustainable precursor for silica. This innovative approach not only addresses the need for sustainable and value-added utilisation of agro-waste and invasive biomass but also introduces a low cost and ecofriendly alternative for the functionalisation of cellulose. This method offers a unique environmental benefit by converting biomass waste into high performance composite material.

The synthesised SMCC were subjected to physicochemical characterization and revealed several notable improvements over pure MCC. Density analysis revealed that true density and bulk density of SMCC is higher than that of MCC and the rise is 47% and 75% respectively for SMCC20. This is attributed to the successful incorporation of silica within the cellulose matrix and this will provide better compressibility and flowability for SMCC. Fourier Transform-Infrared (FT-IR) spectroscopy provided clear evidence of successful integration of silica within the cellulose structure. The X-ray Diffraction (XRD) analysis revealed a notable reduction in the crystallinity of MCC after silicification. This is indicative of structural disruption of the crystalline region of cellulose due to the incorporation of silica. The reduction in crystallinity is advantageous in the following aspects, as it may reduce the inherent stiffness of cellulose, it can simultaneously enhance the material flexibility, surface area and reactivity which are beneficial in drug delivery system and polymer reinforcement. Thermogravimetric (TGA) analysis further revealed that SMCC exhibit superior thermal stability compared to MCC. This is due to the presence of silica phase which act as a thermally stable, insulating matrix that delays the onset of thermal degradation. This property makes SMCC an excellent candidate for high temperature processing applications. Field Emission- Scanning Electron

Microscopy (FE-SEM) revealed a distinct morphological change in SMCC relative to MCC. While native MCC displayed fibrous structure SMCC exhibit rough surfaces and the deposition of silica results in a coarser and granular texture.

Collectively, these findings underscore the success of the in-situ synthesis strategy and highlights the functional advantages of SMCC over MCC. The improved density, enhanced thermal stability, altered crystallinity, etc., offers new avenues in the development of bio-based composites, functional filler and advanced packaging materials. Future research can explore the optimisation of silicification process, scale up feasibility, biocompatibility assessments and broader applications in different fields.

References

[1] Arun L, Sujatha ER, Baldovino JA, Nuñez de la Rosa YE. Microcrystalline Cellulose—A Green Alternative to Conventional Soil Stabilizers. Polymers (Basel) 2024;16. https://doi.org/10.3390/polym16142043.

[2] Schvartz T, Shoseyov O. Defibrillated microcrystalline cellulose as an efficient emulsion stabilizer – Study of food-grade Pickering emulsions resistant to extreme conditions. LWT 2022;155. https://doi.org/10.1016/j.lwt.2021.113006.

[3] Meftahi A, Samyn P, Abbasi Geravand S, Khajavi R, Alibkhshi S, Bechelany M, et al. Nanocelluloses as skin biocompatible materials for skincare, cosmetics, and healthcare: Formulations, regulations, and emerging applications Nanocelluloses as Skin Biocompatible Materials for Skincare, Cosmetics, 1 and Healthcare: Formulations, Regulations, and Emerging Applications. Carbohydr Polym 2022;278:118956. https://doi.org/10.1016/j.carbpol.2021.118956ï.

[4] Janvalkar M, Shettigar R. Review. Int J of Pharm Sci 2025;3:3098–112. https://doi.org/10.5281/zenodo.15283152.

[5] Zhang Q, Lei H, Cai H, Han X, Lin X, Qian M, Zhao Y, Huo E, Villota EM, Mateo W. Improvement on the properties of microcrystalline cellulose/polylactic acid composites by using activated biochar. J Clean Prod. 2019;252:119898. https://doi.org/10.1016/j.jclepro.2019.119898

[6] Tang R, Liu L, Li M, Yao X, Yang Y, Zhang S, et al. Transparent Microcrystalline Cellulose/Polyvinyl Alcohol Paper as a New Platform for Three-Dimensional Cell Culture. Anal Chem 2020;92:14219–27. https://doi.org/10.1021/acs.analchem.0c03458.

[7] Abitbol T, Kubat M, Brännvall E, Kotov N, Johnson CM, Nizamov R, et al. Isolation of Mixed Compositions of Cellulose Nanocrystals, Microcrystalline Cellulose, and Lignin Nanoparticles from Wood Pulps. ACS Omega 2023;8:21474–84. https://doi.org/10.1021/acsomega.3c00295.

[8] González Martínez M, Marlin N, Da Silva Perez D, Dupont C, del Mar Saavedra Rios C, Meyer X-M, Gourdon C, Mortha G. Impact of cellulose properties on its behavior in torrefaction: commercial microcrystalline cellulose versus cotton linters and celluloses extracted from woody and agricultural biomass. Cellulose. 2021;28(8):4761–4779. https://doi.org/10.1007/s10570-021-03812-y.

[9] Krivokapić J, Ivanović J, Djuriš J, Medarević D, Potpara Z, Maksimović Z, et al. Tableting properties of microcrystalline cellulose obtained from wheat straw measured with a single punch bench top tablet press**.** Saudi Pharm. J. 2020;28:710–8. https://doi.org/10.1016/j.jsps.2020.04.013.

[10] Ugoeze KC, Nwachukwu N. Comparative physico-chemical evaluation of microcrystalline cellulose from sugarcane peel and bagasse. J. Pharm. Bioresour**.** 2018;15:37. https://doi.org/10.4314/jpb.v15i1.5.

[11] Schirmer MC, Bertoni FA, Giordano EDV. One-pot synthesis of quaternized microcrystalline cellulose obtained from soybean hulls. Next Materials 2023;1. https://doi.org/10.1016/j.nxmate.2023.100029.

[12] Hasanin MS, Kassem N, Hassan ML. Preparation and characterization of microcrystalline cellulose from olive stones. Biomass Convers Biorefin 2023;13:5015–22. https://doi.org/10.1007/s13399-021-01423-y.

[13] Rasheed M, Jawaid M, Karim Z, Abdullah LC. Morphological, Physiochemical and Thermal Properties of Microcrystalline Cellulose (MCC) Extracted from Bamboo Fiber. Molecules 2020;25. https://doi.org/10.3390/molecules25122824.

[14] Tarchoun AF, Trache D, Klapötke TM. Microcrystalline cellulose from Posidonia oceanica brown algae: Extraction and characterization. Int J Biol Macromol 2019;138:837–45. https://doi.org/10.1016/j.ijbiomac.2019.07.176.

[15] De Oliveira RL, Da Silva Barud H, De Assunção RMN, Da Silva Meireles C, Carvalho GO, Filho GR, et al. Synthesis and characterization of microcrystalline cellulose produced from bacterial cellulose. J Therm Anal Calorim 2011;106:703–9. https://doi.org/10.1007/s10973-011-1449-1.

[16] Acharya S, Liyanage S, Abidi N, Parajuli P, Rumi SS, Shamshina JL. Utilization of cellulose to its full potential: A review on cellulose dissolution, regeneration, and applications. Polymers (Basel) 2021;13. https://doi.org/10.3390/polym13244344.

[17] Lupidi G, Pastore G, Marcantoni E, Gabrielli S. Recent Developments in Chemical Derivatization of Microcrystalline Cellulose (MCC): Pre-Treatments, Functionalization, and Applications. Molecules 2023;28. https://doi.org/10.3390/molecules28052009.

[18] Guo Y, Feng S, Li Z, Jiang M, Xiao Z, Chen L, et al. Effect of Cationic Modified Microcrystalline Cellulose on the Emulsifying Properties and Water/Oil Interface Behavior of Soybean Protein Isolate. Foods 2022;11. https://doi.org/10.3390/foods11193100.

[19] Tasnim S, Tipu MFK, Rana MS, Rahim MA, Haque M, Amran MS, et al. Modification of Bulk Density, Flow Property and Crystallinity of Microcrystalline Cellulose Prepared from Waste Cotton. Materials 2023;16. https://doi.org/10.3390/ma16165664.

[20] Koskela J, Morton DAV, Stewart PJ, Juppo AM, Lakio S. The effect of mechanical dry coating with magnesium stearate on flowability and compactibility of plastically deforming microcrystalline cellulose powders. Int J Pharm 2018;537:64–72. https://doi.org/10.1016/j.ijpharm.2017.11.068.

[21] Olonisakin K, Li R, Zhang XX, Xiao F, Gao J, Yang W. Effect of TDI-Assisted Hydrophobic Surface Modification of Microcrystalline Cellulose on the Tensile Fracture of MCC/PLA Composite, and Estimation of the Degree of Substitution by Linear Regression. Langmuir 2021;37:793–801. https://doi.org/10.1021/acs.langmuir.0c03130.

[22] Huang X, Xie F, Xiong X. Surface-modified microcrystalline cellulose for reinforcement of chitosan film. Carbohydr Polym 2018;201:367–73. https://doi.org/10.1016/j.carbpol.2018.08.085.

[23] Yetiş F, Liu X, Sampson WW, Gong RH. Acetylation of lignin containing microfibrillated cellulose and its reinforcing effect for polylactic acid. Eur Polym J 2020;134. https://doi.org/10.1016/j.eurpolymj.2020.109803.

[24] Lismeri L, Karina AP, Taharuddin T, Darni Y, Azhar A, Arfiana A, Sudibyo S. Production of hydroxypropyl methylcellulose (HPMC) from α-cellulose derived from cassava stems. In: Proceedings of the 1st International Conference on Industry Science Technology and Sustainability (IConISTS 2023)**.** Adv Eng Res. Atlantis Press; 2024. p. 68–80**.** https://doi.org/10.2991/978-94-6463-475-4_8

[25] Khakalo A, Jaiswal AK, Kumar V, Gestranius M, Kangas H, Tammelin T. Production of High-Solid-Content Fire-Retardant Phosphorylated Cellulose Microfibrils. ACS Sustain Chem Eng 2021;9:12365–75. https://doi.org/10.1021/acssuschemeng.1c04403.

[26] Aljaberi A, Chatterji A, Shah NH, Sandhu HK. Functional performance of silicified microcrystalline cellulose versus microcrystalline cellulose: a case study SMCC versus MCC. Drug Dev Ind Pharm 2009;35:1066–71. https://doi.org/10.1080/03639040902774131.

[27] Sun J, Liang Y, Liu X, Liu Y. Effects of Replacement of Part of the Silica Reinforcement with Hybrid Modified Microcrystalline Cellulose on the Properties of their Rubber Composites. J. Macromol. Sci. Phys. 2018;57:243–54. https://doi.org/10.1080/00222348.2018.1452490.

[28] Steele DF, Tobyn M, Edge S, Chen A, Staniforth JN. Physicochemical and Mechanical Evaluation of a Novel High Density Grade of Silicified Microcrystalline Cellulose. Drug Dev Ind Pharm 2004;30:103–9. https://doi.org/10.1081/DDC-120027517.

[29] Kachrimanis K, Noisternig MF, Griesser UJ, Malamataris S. Dynamic moisture sorption and desorption of standard and silicified microcrystalline cellulose. Eur. J. Pharm. Biopharm. 2006;64:307–15. https://doi.org/10.1016/j.ejpb.2006.05.019.

[30] Kalita P, Roy PK, Das N, Pachuau L. Silicified microcrystalline cellulose from renewable banana pseudostem: Physicochemical and functional analysis. Int J Biol Macromol 2024;283. https://doi.org/10.1016/j.ijbiomac.2024.137620.

[31] Thayyullathil A, Naseera CM, Liyakhath FM, Vydhehi EK, Sheeja SR, Naduparambath S, et al. Effect of Temperature and Method of Synthesis on Morphology and Phase Transition of Amorphous and Crystalline Nano Silica Extracted from Mission Grass (Pennisetum Polystachion). Silicon 2024;16:3491–501. https://doi.org/10.1007/s12633-024-02932-x.

[32] Rojas J, Kumar V. Coprocessing of cellulose II with amorphous silicon dioxide: Effect of silicification on the powder and tableting properties. Drug Dev Ind Pharm 2012;38:209–26. https://doi.org/10.3109/03639045.2011.597400.

[33] Kiran MD, Govindaraju HK, Jayaraju T, Kumar N. Review – effect of fillers on mechanical properties of polymer matrix composites. Mater Today Proc**.** 2018;5(10):22421–22424**.** https://doi.org/10.1016/j.matpr.2018.06.611

[34] Praveenkumara J, Madhu P, Yashas Gowda TG, Sanjay MR, Siengchin S. A comprehensive review on the effect of synthetic filler materials on fiber-reinforced hybrid polymer composites. J. Text. Inst. 2022;113:1231–9. https://doi.org/10.1080/00405000.2021.1920151.

[35] Kiziltas A, Han Y, Gardner DJ, Nader JW. The effect of filler type on the mechanical, thermal and rheological properties of cellulose-filled thermoplastic composites. In**:** Proceedings of the International Convention of the Society of Wood Science and Technology and United Nations Economic Commission for Europe – Timber Committee*;* 2010 Oct 11–14; Geneva, Switzerland. p. 1–10.

[36] He C, Li H, Huan O, Wei H, Xiong H, Ni H, et al. Physicochemical properties and structure characterization of microcrystalline cellulose from pomelo fruitlets. J Food Process Preserv 2022;46. https://doi.org/10.1111/jfpp.17071.

[37] Kian LK, Saba N, Jawaid M, Fouad H. Characterization of microcrystalline cellulose extracted from olive fiber. Int J Biol Macromol 2020;156:347–53. https://doi.org/10.1016/j.ijbiomac.2020.04.015.

[38] Kian LK, Jawaid M, Ariffin H, Alothman OY. Isolation and characterization of microcrystalline cellulose from roselle fibers. Int J Biol Macromol 2017;103:931–40. https://doi.org/10.1016/j.ijbiomac.2017.05.135.

[39] Capeletti LB, Zimnoch JH. Fourier Transform Infrared and Raman Characterization of Silica-Based Materials. Applications of Molecular Spectroscopy to Current Research in the Chemical and Biological Sciences, InTech; 2016. https://doi.org/10.5772/64477.

[40] Ellerbrock R, Stein M, Schaller J. Comparing amorphous silica, short-range-ordered silicates and silicic acid species by FTIR. Sci Rep 2022;12. https://doi.org/10.1038/s41598-022-15882-4.

[41] Banoth S, Babu VS, Raghavendra G, Rakesh K, Ojha S. Sustainable Thermochemical Extraction of Amorphous Silica from Biowaste. Silicon 2022;14:5289–96. https://doi.org/10.1007/s12633-021-01293-z.

[42] Tobyn MJ, McCarthy GP, Staniforth JN, Edge S. Physicochemical comparison between microcrystalline cellulose and silicified microcrystalline cellulose. Int J Pharm 1998;169:183–94. https://doi.org/10.1016/S0378-5173(98)00127-6.

[43] French AD. Idealized powder diffraction patterns for cellulose polymorphs. Cellulose 2014;21:885–96. https://doi.org/10.1007/s10570-013-0030-4.

[44] Gómora-Hernández JC, Tecante A, del Carmen Carreño-de-León M, Flores-Álamo N, Ventura-Cruz S. Preparation of porous microcrystalline cellulose from mezcal industry agave bagasse by low reagent loading sequential chemical treatment. Cellulose 2023;30:2067–84. https://doi.org/10.1007/s10570-022-05022-6.

[45] Tarchoun AF, Trache D, Klapötke TM. Microcrystalline cellulose from Posidonia oceanica brown algae: Extraction and characterization. Int J Biol Macromol 2019;138:837–45. https://doi.org/10.1016/j.ijbiomac.2019.07.176.

[46] Nishiyama Y, Langan P, Chanzy H. Crystal structure and hydrogen-bonding system in cellulose Iβ from synchrotron X-ray and neutron fiber diffraction. J Am Chem Soc 2002;124:9074–82. https://doi.org/10.1021/ja0257319.

[47] Langan P, Nishiyama Y, Chanzy H. X-ray structure of mercerized cellulose II at 1 Å resolution. Biomacromolecules 2001;2:410–6. https://doi.org/10.1021/bm005612q.

[48] Toby BH. R factors in Rietveld analysis: How good is good enough? . Powder Diffr 2006;21:67–70. https://doi.org/10.1154/1.2179804.

[49] Iskakov RM, Bukanova AS, Kalauova AS, Kairliyeva FB, Nauashev AN, Shambilova GK, et al. Eco-Friendly Polypropylene Composites Reinforced with Cellulose Fibers and Silica Nanoparticles. Polymers (Basel) 2025;17. https://doi.org/10.3390/polym17101290.

[50] Singh GP, Madiwale P V., Adivarekar R V. Preparation and Characterization of Microcrystalline Cellulose (MCC) from Renewable Source**.** Curr. Appl. Polym. Sci. 2017;1. https://doi.org/10.2174/2452271601666170721120343.

[51] Huang M, Cao J, Meng X, Liu Y, Ke W, Wang J, et al. Preparation of SiO_2 nanowires from rice husks by hydrothermal method and the RNA purification performance. Chem Phys Lett 2016;662:42–6. https://doi.org/10.1016/j.cplett.2016.09.012.

[52] Brannum DJ, Price EJ, Villamil D, Kozawa S, Brannum M, Berry C, et al. Flame-Retardant Polyurethane Foams: One-Pot, Bioinspired Silica Nanoparticle Coating. ACS Appl Polym Mater 2019;1:2015–22. https://doi.org/10.1021/acsapm.9b00283.

[53] Munier P, Apostolopoulou-Kalkavoura V, Persson M, Bergström L. Strong silica-nanocellulose anisotropic composite foams combine low thermal conductivity and low moisture uptake. Cellulose 2020;27:10825–36. https://doi.org/10.1007/s10570-019-02912-0.

[54] Nsor-Atindana J, Chen M, Goff HD, Zhong F, Sharif HR, Li Y. Functionality and nutritional aspects of microcrystalline cellulose in food. Carbohydr Polym 2017;172:159–74. https://doi.org/10.1016/j.carbpol.2017.04.021.

[55] Abu-Thabit NY, Judeh AA, Hakeem AS, Ul-Hamid A, Umar Y, Ahmad A. Isolation and characterization of microcrystalline cellulose from date seeds (Phoenix dactylifera L.). Int J Biol Macromol 2020;155:730–9. https://doi.org/10.1016/j.ijbiomac.2020.03.255.

[56] Yadav VK, Suriyaprabha R, Khan SH, Singh B, Gnanamoorthy G, Choudhary N, et al. A novel and efficient method for the synthesis of amorphous nanosilica from fly ash tiles. Mater. Today Proc., vol. 26, Elsevier Ltd; 2019, p. 701–5. https://doi.org/10.1016/j.matpr.2020.01.013.

Chapter 7

Comparative Study of Polyvinyl Alcohol Composites Reinforced with MCC, Silica and Silicified MCC

7.1. Introduction

7.1.1. Background on Polyvinyl Alcohol

Bio-based polymers are increasingly important due to their environmental and functional advantages. A large number of composites are prepared using natural biodegradable polymers like Polylactic Acid [1] and synthetic biodegradable polymers like Polyvinyl Alcohol (PVA). PVA, $(C_2H_4O)_n$, is a water-soluble synthetic polymer prepared by the hydrolysis of Polyvinyl Acetate. Since vinyl alcohol is unstable, it cannot be polymerised directly. Instead, PVA is prepared by hydrolysis of Polyvinyl Acetate, where acetate groups are replaced by hydroxyl groups (-OH). The degree of hydrolysis significantly influences the solubility and crystallinity. Due to the presence of a large number of hydroxyl groups along its backbone, PVA exhibits strong hydrogen bonding, which provides good mechanical properties and compatibility with various fillers and polymers [2]. PVA forms transparent, flexible, and strong films, therefore, it is widely used in coating, packaging and pharmaceutical applications [3]. PVA is biodegradable, particularly under microbial action or in composting condition [4]. It is resistant to oils, greases and most organic solvents, but is sensitive to strong acids and bases [5]. PVA has excellent oxygen barrier properties but poor water barrier due to its hydrophilic nature [6]. Biodegradability, non-toxicity, film-forming ability, biocompatibility and adhesive properties make it a favourable candidate in the field of polymer science [7]. Nevertheless, PVA has several limitations that restrict its use in some applications. PVA absorbs water from the environment, which will adversely affect its mechanical properties and dimensional stability [8]. PVA films or hydrogels lose tensile strength and become fragile when hydrated, which limits their durability in real-world conditions [9]. Sometimes, PVA undergoes thermal decomposition before complete melting, thus, the processing

method, such as melt extrusion, becomes difficult [10]. The pure and dry PVA is brittle and lacks flexibility unless it is plasticized. While PVA is biodegradable under specific conditions, like microbial action in compost or wastewater, it does not degrade easily in the natural environment [11].

Based on their solubility characteristics, PVA is available in Cold water-soluble (CPVA) and Hot water-soluble (HPVA) forms. CPVA is readily soluble in cold water, making it convenient for use in processes where high-temperature dissolution is undesirable. It exhibits strong adhesive properties and excellent film-forming ability, which make it suitable for coatings, packaging and binder applications. However, CPVA has some limitations also. It is highly hygroscopic, has low thermal stability, and shows sensitivity to pH, which compromises its performance in various environmental and chemical conditions. On the other hand, HPVA requires high temperature for dissolution, but offers different advantages. It has lower hygroscopicity and generally better thermal stability compared to CPVA. But it has reduced biodegradability, weaker adhesive properties and shows inferior film-forming capacity. At higher concentrations, it may exhibit toxicity to aquatic life and undergo discolouration upon exposure to UV or visible light over time [12]. On considering these properties, blending of HPVA and CPVA presents a strategic approach to combine the advantages of both types while compensating for individual shortcomings. The blend promises a better material for the development of composite films, coatings, and biodegradable packaging, especially in applications, which require customizable performance under different environmental conditions.

7.1.2. Use of Fillers to Improve PVA film

The performance of PVA film can be significantly improved by various natural fillers, such as cellulose nanocrystals, starch, lignin, chitosan, etc. Among these, the most promising fillers are nanocellulose-based materials, such as cellulose nanocrystals and cellulose nanofibers. They will enhance the tensile strength, crystallinity, and flexibility due to strong hydrogen bonding and good dispersion in PVA [13]. The filler, chitosan forms hydrogen bond with PVA using amino group,

thus tensile strength and Young's modulus, etc., can be improved [14]. The biodegradability of PVA can be significantly improved by blending with starch [15]. Hybrid fillers like nanocellulose-nanosilica improve the stiffness and modulus, especially at optimized loading. Graphene oxide-nanoclay hybrid fillers provide excellent dispersibility and give substantial mechanical properties even at low concentration [16]. Metal oxide nanofillers play a crucial role in enhancing the properties of PVA components. Fillers such as TiO_2 and NiO increase the thermal degradation temperature and glass transition temperature of PVA [17]. The TiO_2 and ZnO are well-known UV blockers, that prevent the photodegradation of PVA under sunlight or UV exposure [18]. This makes composites durable for packaging applications. The AgO, CuO and ZnO exhibit broad-spectrum antibacterial properties to make the PVA composite suitable for food packaging, medical devices, and wound dressing [19]. The Fe_3O_4 and NiO impart magnetic responses to the film, therefore, it is useful in sensors, wastewater treatment and magnetically triggered drug delivery system [20]. However, excessive filler content causes agglomeration and reduces transparency and ductility. Overall, judicious selection is vital, especially at optimum concentration, which transforms PVA into a multifunctional material for advanced packaging, biomedical and electronic applications.

7.1.3. Use of Microcrystalline Cellulose as Filler in PVA film

Microcrystalline cellulose emerges as an effective filler for PVA, offering enhanced mechanical reinforcement, biodegradability, and thermal properties. Numerous studies have been reported regarding the PVA/MCC composite. For instance, the PVA incorporated with MCC derived from sago seed shell at 1-3% exhibited enhanced tensile strength, thermal resistance, uniform dispersion and higher glass transition temperature without losing the transparency of the film [21]. Similarly, when MCC derived from olive pits is added to PVA/starch film, there is a significant increase in Young's modulus and thermal stability [22]. Thermogravimetric analysis revealed that the PVA composite reinforced with carboxylated MCC from jute fibres exhibited a delayed onset of decomposition and enhanced overall thermal stability [23]. A transparent MCC/PVA paper with irregular

pores was developed through dissolution and regeneration of MCC, addition of porogen reagent (NaCl) and subsequently dipping in PVA solution [24]. The MCC was extracted from organosolv oil palm fronds pulp via acid hydrolysis method and then incorporated with PVA-$LiClO_4$ at different loading to produce a biodegradable polymer film [25]. However, the studies show that PVA/MCC composites have some shortcomings also. MCC often imposes significant drawbacks due to its rigid and highly crystalline nature, which restricts the mobility of the PVA chain, leading to reduced deformability and increased brittleness in the composite. MCC exhibits poorer interfacial adhesion, since the hydroxyl group of MCC tends to form hydrogen bonding among themselves rather than with the PVA, resulting in weak filler matrix interaction. Furthermore, MCC's natural agglomeration tendency, during drying and at higher loading, reduces the dispersibility, which leads to defects that hinder stress transfer, particularly when exceeding optimal filler concentration. Moreover, the nature of the source and method of extraction significantly affect the properties of MCC, thus there will be inconsistent results in composite processing and quality.

7.1.4. Nanosilica as Filler in PVA Composites

Polyvinyl Alcohol-silica composites were produced via sol-gel or in situ synthetic routes using precursors like TEOS. The fine silica nanoparticles will be dispersed within the PVA matrix, where strong H- bonding between silica's hydroxyl group and PVA's functional group ensures homogeneous dispersion and robust interfacial adhesion. Thus, the mechanical strength, modulus, thermal stability and other properties will be improved, compared to pure PVA [26]. For instance, a novel green silica-PVA hybrid membrane was created using the silica derived from rice husk for improving desalination performance by pervaporation [27]. PVA/nanosilica composites were fabricated and their antibacterial studies revealed that the composite remarkably prevents the growth of bacteria [28]. By dispersing silica and glass fibres in PVA aqueous solution, followed by freeze drying and thermal cross-linking at 180 °C, a green composite was developed, and this has enhanced mechanical properties, low thermal conductivity, excellent thermal insulation and strong hydrophobicity [29]. The hydrophilic silica nanostructures were synthesised by tuning templates and

trimethyl benzene content, then sprayed on a cost-effectively produced PVA-co-PE nanofiber membrane and the composite exhibits super hydrophilicity in air and, under water, oil-hating behaviour [30]. The researcher created a novel superhydrophobic underwater superoleophobic PVA/silica membrane by first creating a highly porous PVA via electrospinning method and then conducting in situ silica nanoparticle growth via modified Stober reaction [31]. Even though silica can enhance the mechanical and thermal properties, its effectiveness is constrained by processing and dispersion challenges. The important issue is the tendency of aggregation. It has poor dispersion at high concentration and creates a stress concentration zone that will weaken the mechanical properties, especially when silica content exceeds 1.5% in PVA-based hydrogels [32]. Moreover, while the moderate amount of silica improves the toughness, excess filler makes the material more brittle, reduces fracture strain and potentially causes premature fracture [33].

7.1.5 Silicified MCC- A Hybrid Filler in PVA Composites

The study of SMCC in Polyvinyl Alcohol matrices is still scarce. However, SMCC will be a superior filler compared to MCC or silica alone due to its synergistic combination of functional properties. While MCC offers good compressibility, its flowability is poor. On the other hand, silica provides excellent flowability but poor compressibility [34]. Thus, SMCC integrates both advantages, resulting in filler with enhanced flowability, compatibility and reduced sensitivity to moisture. The presence of silica within SMCC reduces interparticle friction, leading to better powder handling and low dust generation [35]. Moreover, SMCC minimizes the risk of blend segregation compared to a physically mixed MCC-silica system. This makes SMCC particularly valuable in formulations like PVA composites where uniform mixing, mechanical strength and moisture control are important. Recent studies highlighted that the SMCC contributes to improved thermal stability, which will further enhance the performance of polymers.

7.1.6. Aim and Objectives of the Study in the Present Chapter

The aim of the study is to systematically compare the performance of PVA films by leveraging a blend of Hot water-soluble PVA and Cold water-soluble PVA

as the matrix and reinforced with Microcrystalline Cellulose (MCC), silica and Silicified Microcrystalline Cellulose (SMCC). The study focuses on demonstrating the advantages of SMCC over both MCC and silica in terms of thermal stability, structural features, morphology and mechanical properties. The main objectives of the study include

- Prepare and optimize a matrix blended with Cold water-soluble PVA and Hot water-soluble PVA.
- Cast films using optimized PVA blend with different filler variations viz, PVA+MCC, PVA +silica, PVA+SMCC (with 10% Silica (SMCC10) and 20% Silica (SMCC20)) and further variants of SMCC20 with different percentage composition.
- Use FTIR to assess the molecular interaction within the blended PVA matrix and with each filler.
- Employ XRD to evaluate the changes in crystallinity during the introduction of different fillers.
- Use FE-SEM to analyse the microstructures and the dispersibility of MCC, silica and SMCC within the blended PVA matrix.
- Compare thermal degradation behaviour of the composites.
- Evaluate the tensile strength, stiffness and brittleness to reflect whether the blend with SMCC enhances the mechanical properties.
- Demonstrate how the combination of PVA blend with SMCC outperforms both MCC and silica films, particularly in achieving structural integrity and thermal/mechanical performance.

7.2 Materials

MCC extracted from Screw Pine leaves, Silica extracted from Mission Grass, Silicified Microcrystalline Cellulose, Polyvinyl Alcohol (Hot water-soluble PVA M. W~ 60,000-1,25,000 and Cold-water soluble PVA M.W ~ 1,60,000) procured from Hi Media were used for analysis. All the chemicals are analytical reagents (AR) and were used without purification.

7.3. Methods

7.3.1. Preparation of Bare PVA film

A homogeneous PVA solution was prepared by dissolving 2.5 g of Hot water-soluble PVA and 2.5 g of Cold water-soluble PVA in 100 ml of distilled water. The mixture was stirred continuously at 80 °C for 5 h, using a magnetic stirrer until a clear and uniform solution was obtained. The resulting solution was then poured onto a clean porcelain tile and dried at room temperature. After complete drying, the film was carefully peeled off to obtain the neat PVA film.

7.3.2. Fabrication of PVA/MCC Composite Film

The PVA/MCC composite film was prepared by dispersing 0.1g (2%) MCC in a blend of HPVA and CPVA solutions. The mixture was stirred at 80 °C until a uniform dispersion was achieved. The casting and drying procedures were same as described for the neat PVA film.

7.3.3. Fabrication of PVA/Silica and PVA/SMCC Composite Films

The PVA/SiO_2 and PVA/SMCC films were prepared by dispersing 0.1 g (2% w/w with respect to total polymer weight) of silica, SMCC10, and SMCC20 separately in the PVA solution. Each mixture was stirred thoroughly using a magnetic stirrer to ensure uniform dispersion of the filler. The films were then cast and dried as described previously.

7.3.4. Fabrication of PVA/SMCC20 Composite Films with Higher Composition

In order to study the effect of higher filler content, PVA/SMCC20 films were prepared with increasing concentrations of SMCC20 i.e., 4%, 6%, and 8% (w/w relative to total polymer weight). The SMCC20 was added directly to the PVA solution in the required amounts, stirred thoroughly, and cast on the porcelain tile and the same procedure as described above is followed. A schematic overview was provided in **Scheme 7.1.**

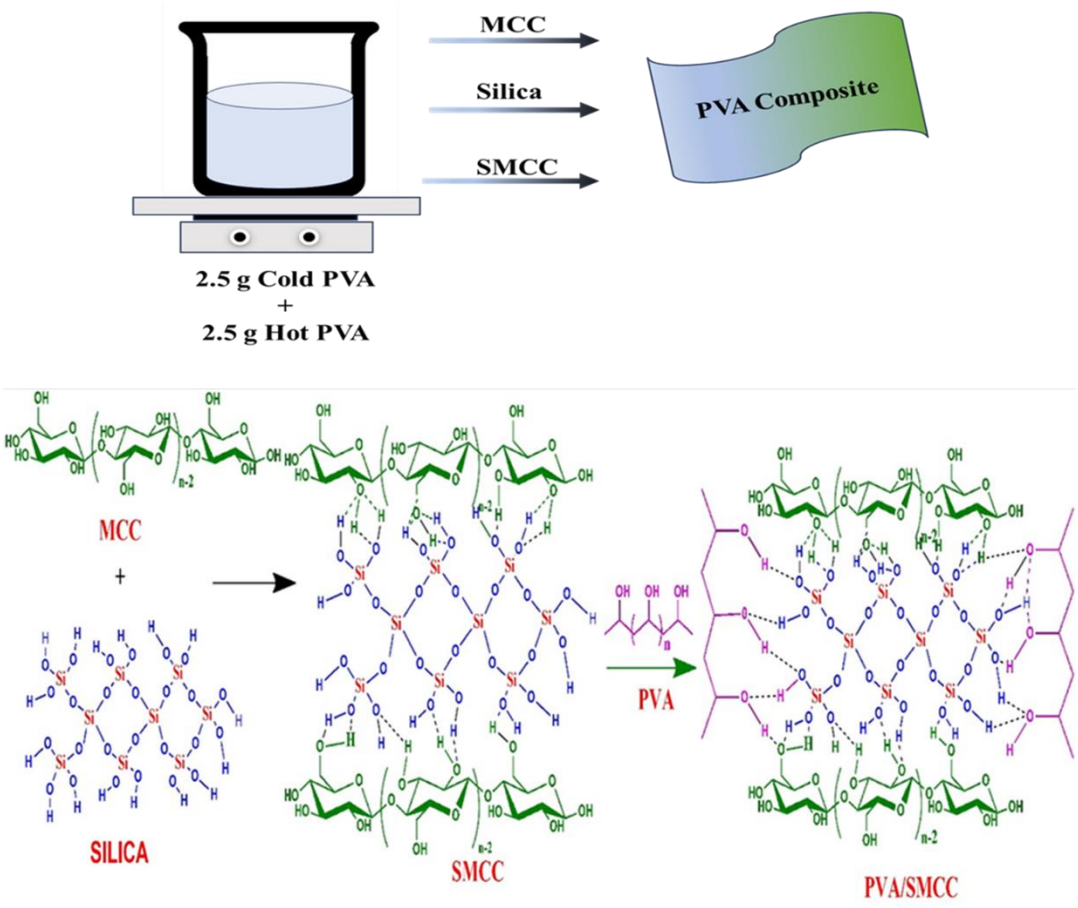

Scheme 7.1 Schematic Representation of Synthesis of PVA/MCC, PVA/SiO_2 and PVA/SMCC

7.4. Results and Discussion

7.4.1. Fourier Transform-Infrared Spectroscopy Analysis

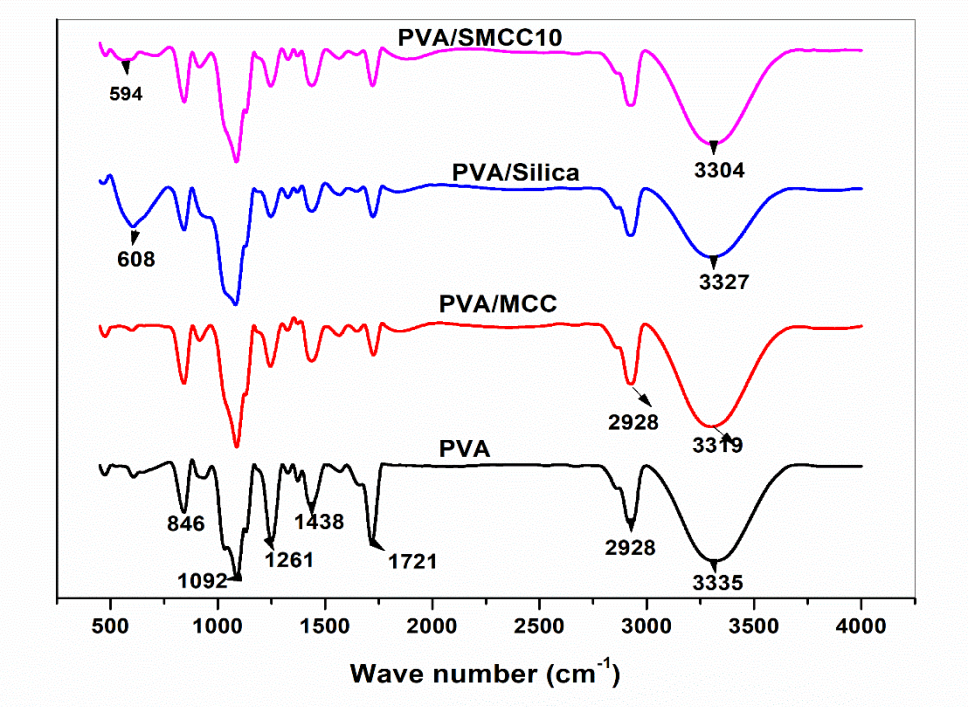

Figure 7.1. FT-IR Spectra of PVA, PVA/MCC, PVA/Silica and PVA/SMCC

The functional group analysis of the films was carried out by FT-IR analysis. **Figure 7.1** shows the FT-IR spectra of PVA, PVA/MCC, PVA/Silica and PVA/SMCC10. In the case of PVA, the broad band centred at 3335 cm^{-1} corresponds to an extremely H- bonded -OH group of the polymer chain [36]. The small peak at 2928 cm^{-1} corresponds to the stretching vibration of C-H bonds. The peak at 1721 cm^{-1} is attributed to the C=O bond of acetate group, since the precursor of PVA preparation is Polyvinyl Acetate [36]. The peak at 1438 cm^{-1} is due to the bending vibration of the CH_2 group in the polymer chain. A medium intense band is also present at wave number 1261cm^{-1} due to C-O-C asymmetric stretching vibration of the ester group present in the unhydrolyzed Polyvinyl Acetate group [37]. A very intense band at 1092 cm^{-1} is due to the C-O stretching vibration of CH_2-OH. A very small peak at 846 cm^{-1} is attributed to the out-of-plane bending vibration of C-H bond in the CH_2 group of the polymer backbone. The FT-IR spectrum of PVA/MCC appeared to be almost similar to that of PVA. The intensity of all peaks gets diminished. Frequency due to O-H stretching is shifted to 3319 cm^{-1}, which indicates

the disruption of H-bonding in PVA and the formation of a new H-bonding between PVA and MCC [38]. The intensity of the peak at 1721 cm^{-1} is very low, which shows the interaction between PVA and MCC is not only through the H-bonding from the O-H group, but also from the C=O group of PVA [39]. The only distinguishable peak found for PVA/silica compared to PVA is the signal at 608 cm^{-1}, which is attributed to the Si-O-Si bending vibration of the silanol group. During the addition of SMCC10 to PVA, no remarkable change is observed in the FT-IR spectrum. The spectrum of PVA/SMCC shows a broad O-H stretching band at 3304 cm^{-1}, and the redshift is higher than that of the other PVA composites. This indicates the formation of hydrogen bonds between hydroxyl groups of PVA and hydroxyl groups of both cellulose and silanol groups in SMCC. Moreover, the peak at 1720 cm^{-1} diminishes, and the signal at 594 cm^{-1}, due to Si-O-Si bonding, is visible with reduced intensity. FT-IR spectra show that there are no significant changes in the chemical structure of PVA during composite formation.

7.4.2. X-ray Diffraction Analysis

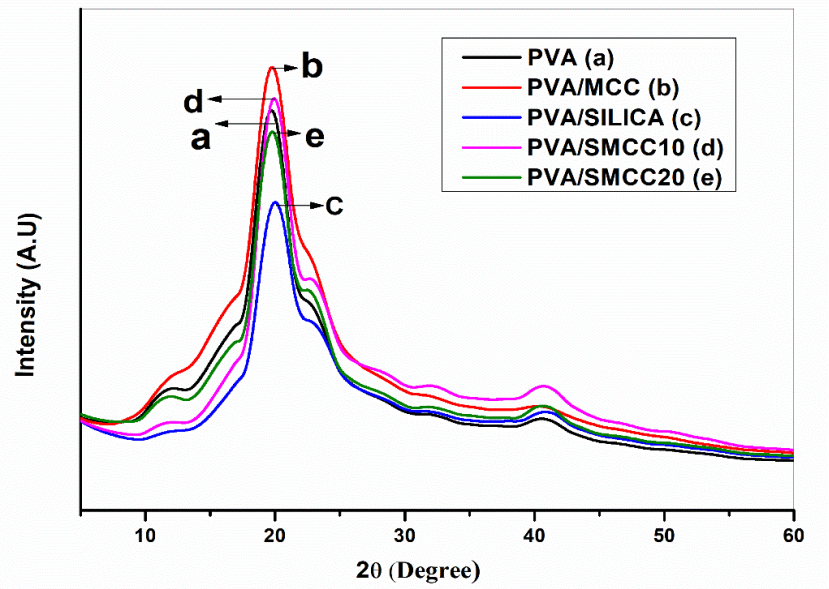

Figure 7.2 XRD of (a)PVA, (b)PVA/MCC, (c)PVA/Silica, (d)PVA/SMCC10 and (e) PVA/SMCC20.

The crystalline properties of PVA, PVA/MCC, PVA/silica, PVA/SMCC10 and PVA/SMCC20 composite films were studied using XRD analysis. **Figure 7.2** shows the XRD patterns of films. Pure PVA is a semicrystalline polymer with a monoclinic lattice. PVA shows mainly three characteristic peaks [40]. The prominent

peak is observed at 2θ= 19.55°, corresponding to the (110) planes. There are small shoulders at 23° and 40.6° that correspond to (200) and (220) planes, respectively [41]. Rietveld refinement of all PVA composites was carried out using the CIF file [42]. The refined output profile, fitted powder XRD pattern, fit quality parameters, unit cell parameters and deconvoluted XRD patterns with crystallinity (%) of all PVA based samples were determined using the relation 7.1.

$$\textbf{Crystallinity Index (\%)} = \frac{\textit{Area of Crystalline Peak} \times 100}{\textit{Area of Crystalline peak} + \textit{Area of Amorphous peak}} \qquad \textbf{(7.1)}$$

The Crystallinity Index of neat PVA is determined from Rietveld refinement and deconvolution and the value is 20.2% (**Figure 7.3**) and this value indicates its semi crystalline nature. The crystallinity of PVA depends on the extent of H- bonding between the PVA chains, which is due to the presence of -O-H group in PVA.

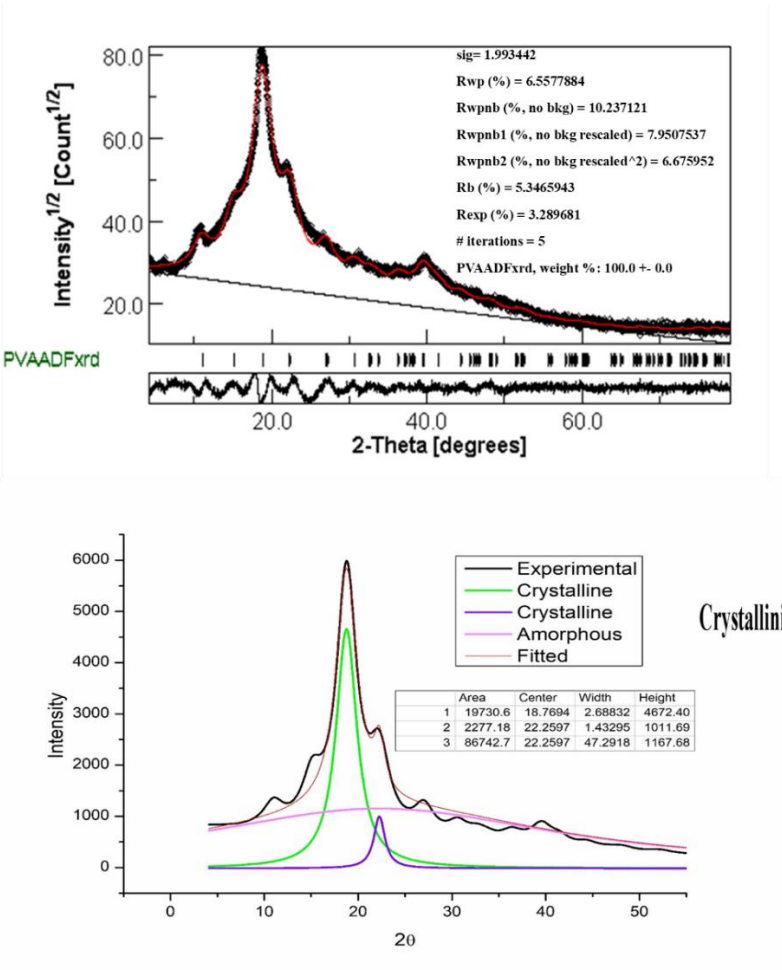

Figure 7.3. Rietveld fit, Refinement Statistics and Deconvoluted XRD of PVA

The diffraction pattern of PVA/MCC film is more intense, and the calculated crystallinity index (24.2%) is higher than that of bare PVA film (**Figure 7.4**). The peak at 2θ = 19.9° is sharper, and this indicates high crystallinity of composites and the persistence of I_β structure of cellulose [43]. The shoulder peaks corresponding to PVA at 23° and 40.6° are almost diminished. The low-intensity shoulder peak, observed at 16°, shows the presence of MCC. The characteristic peak of MCC at 22.5° is not seen, because it is overlapped by the prominent peak of PVA.

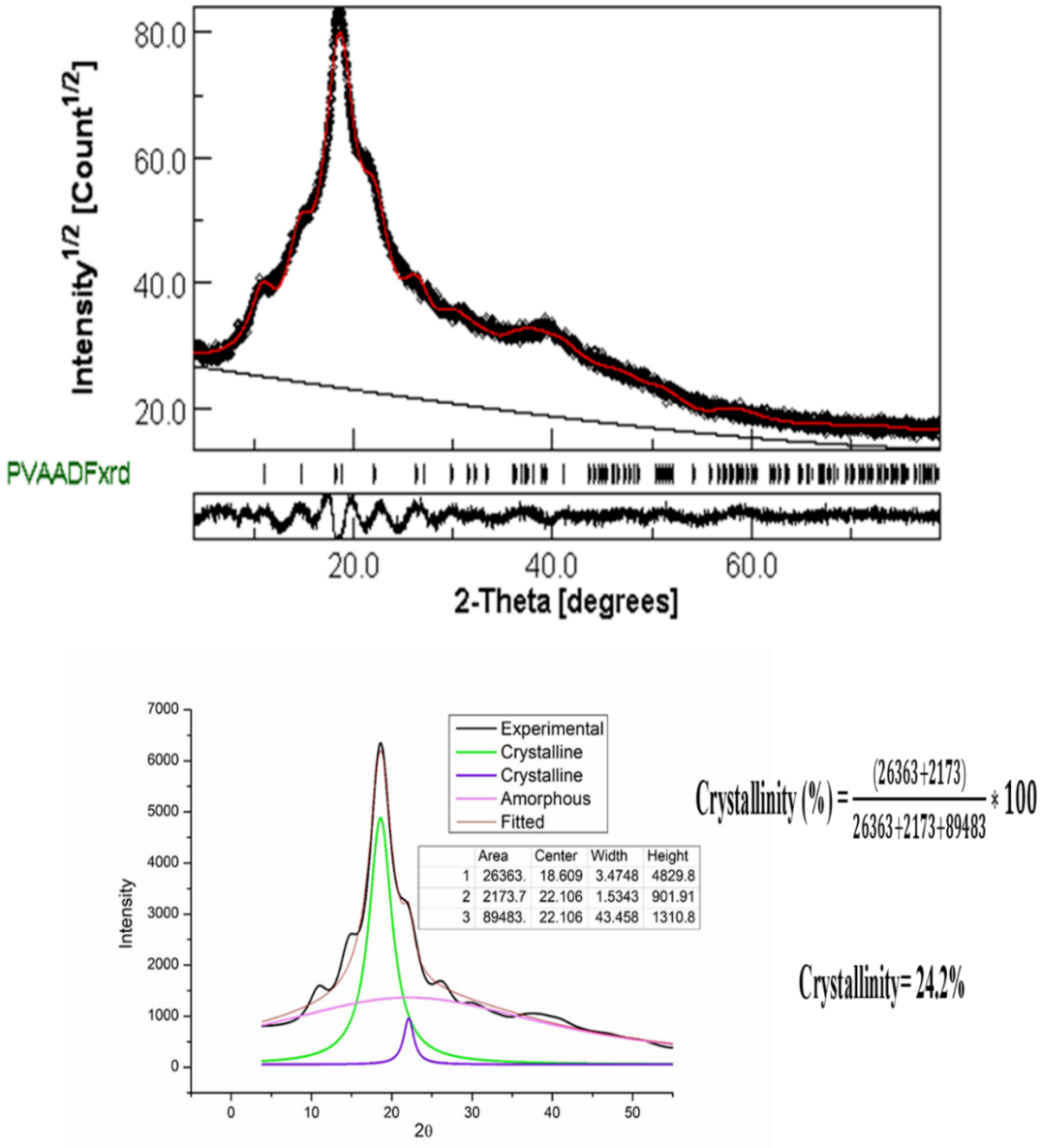

Figure 7.4. Rietveld fit, Refinement Statistics and Deconvoluted XRD of PVA/MCC

As shown in diffractogram **7.2 (c)** and **Figure 7.5,** the crystallinity of PVA decreases on the incorporation of amorphous silica, which can be attributed to the disruption of the regular packing of the PVA chain by uniformly dispersed silica nanoparticles. The prominent peak at 19.9° still exists, which shows the phase separation [44]. The characteristic peaks of PVA are clearly visible, but the intensities of all other peaks are found to be diminished.

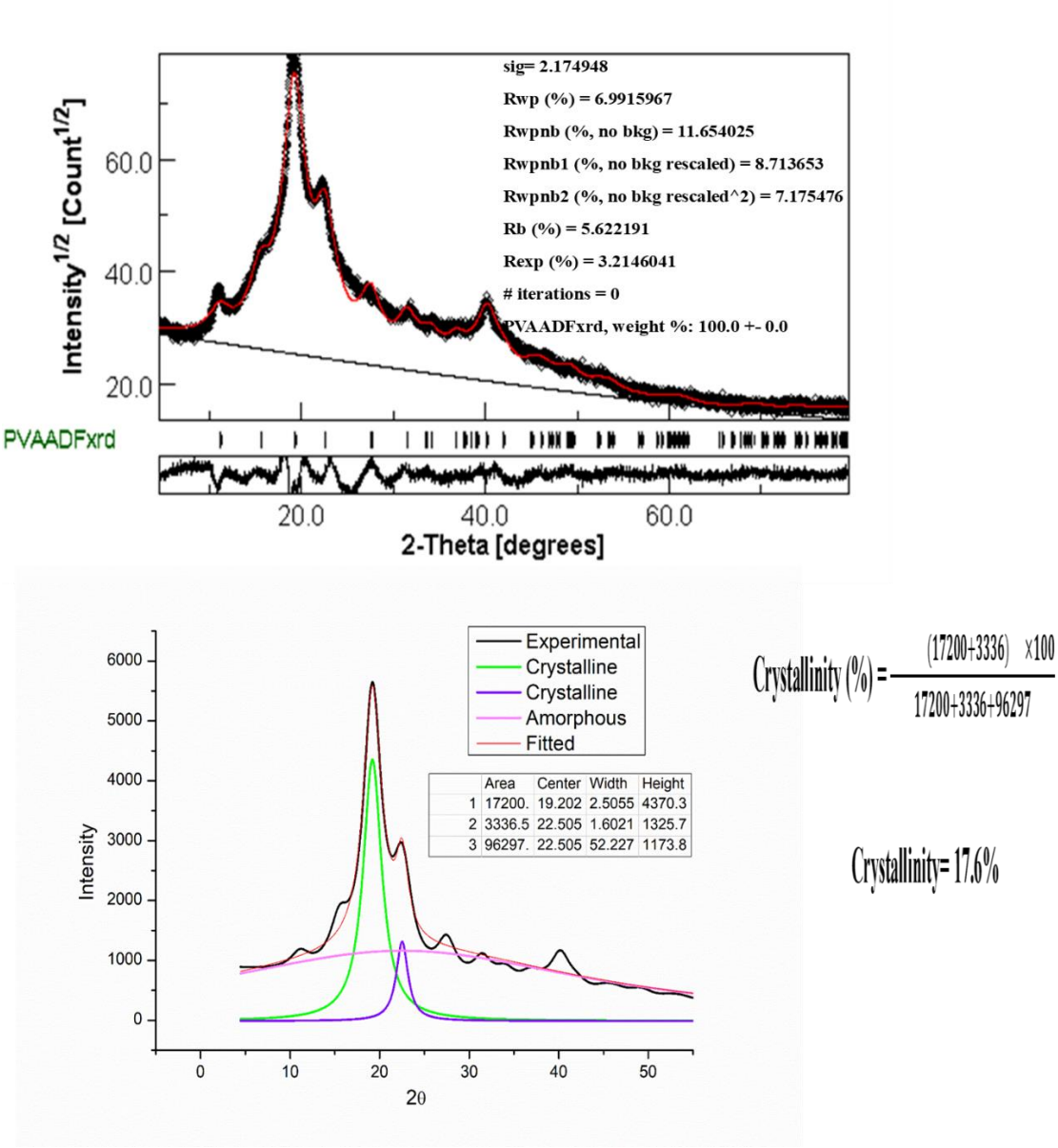

Figure 7.5. Rietveld fit, Refinement Statistics and Deconvoluted XRD of PVA/Silica

The Crystallinity Indices of other films (PVA/SMCC10 and PVA/SMCC20) were calculated using the peak deconvolution method and corresponding Rietveld fit, and the deconvoluted XRD patterns are presented in **Figures 7.6** and **7.7**, respectively.

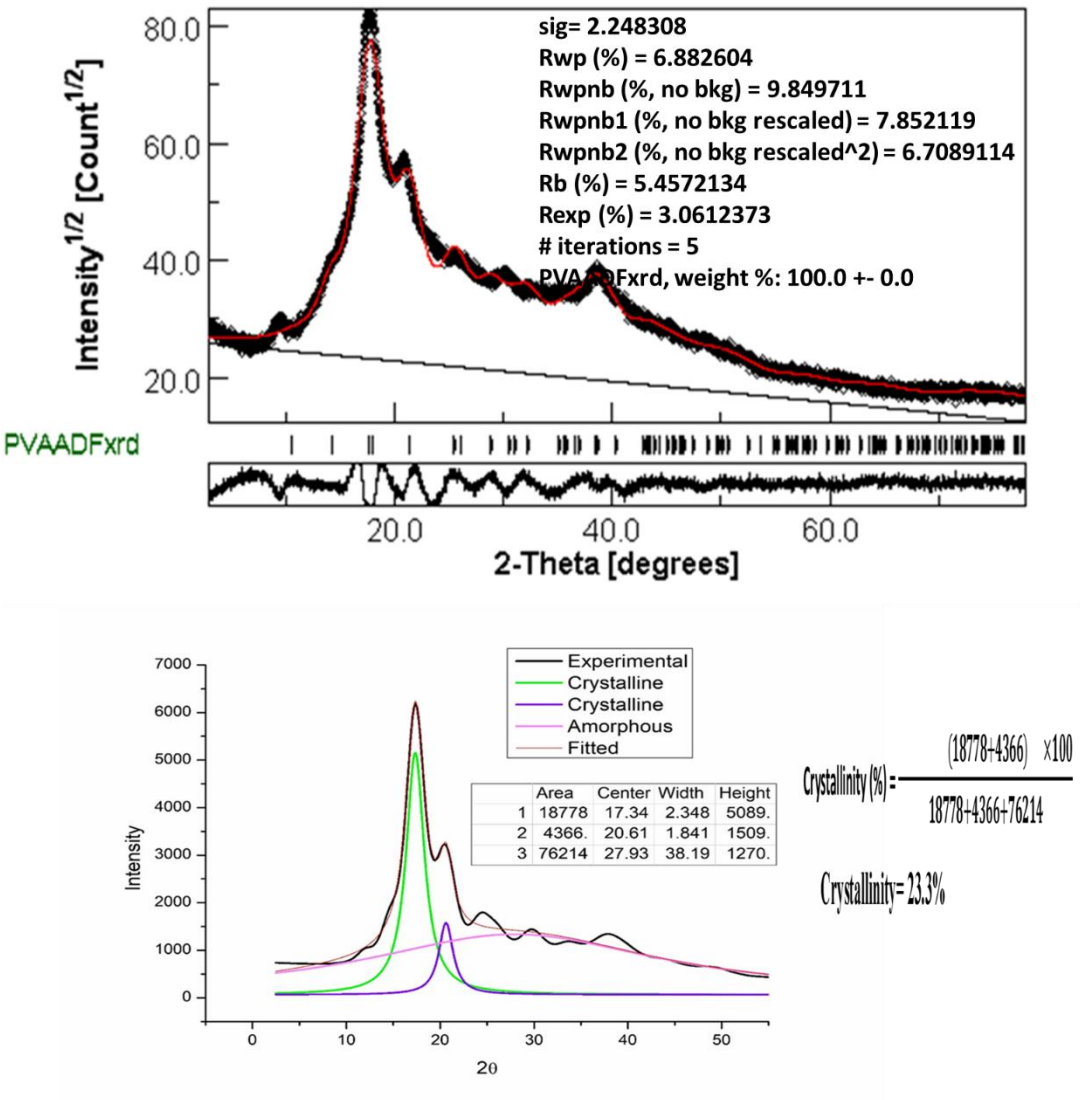

Figure 7.6. Rietveld fit, Refinement Statistics and Deconvoluted XRD of PVA/SMCC10

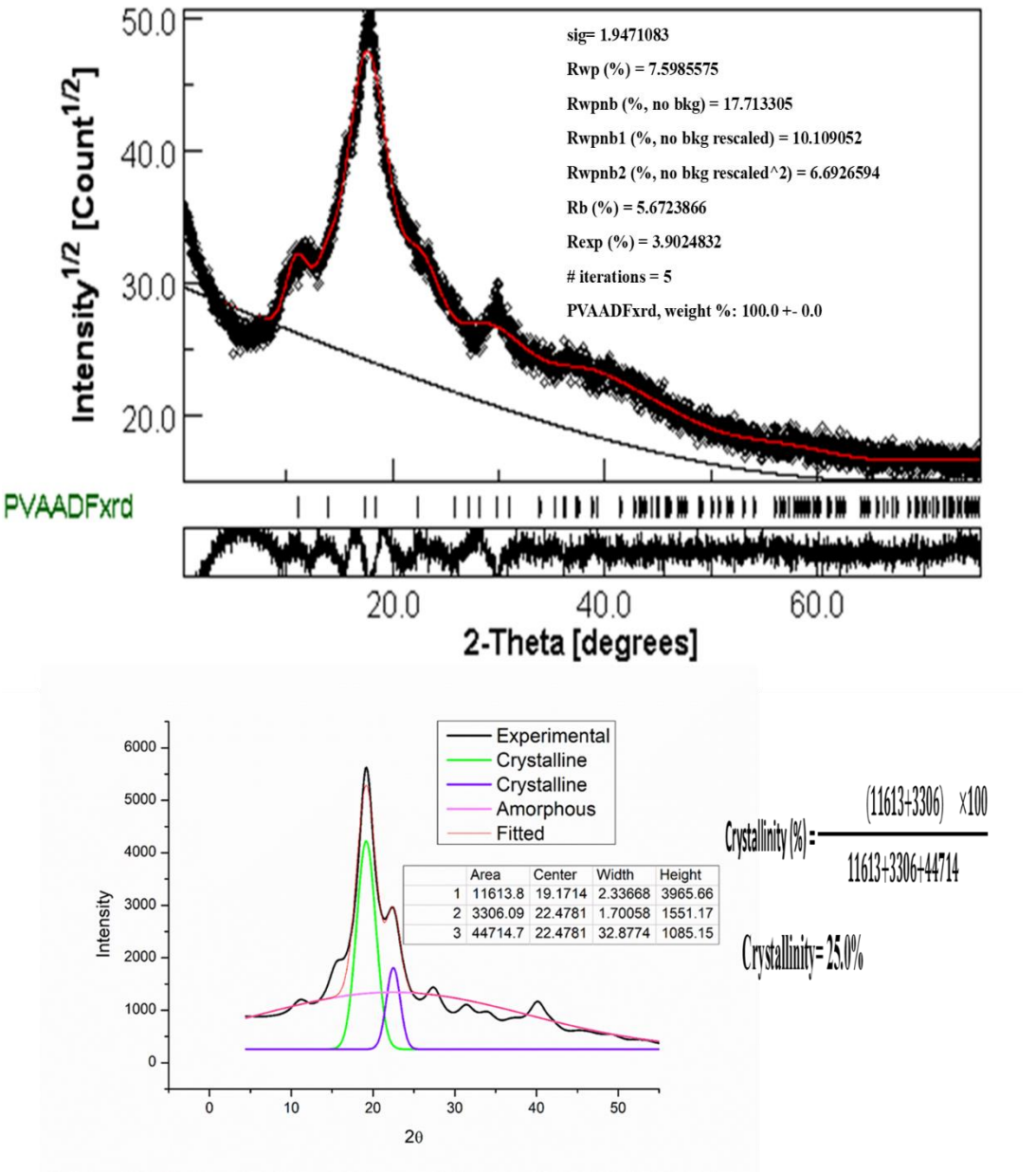

Figure 7.7 Rietveld fit, Refinement Statistics and Deconvoluted XRD of PVA/SMCC20

The overall study shows that upon incorporation of 2% MCC, the crystallinity increased slightly to 24.2%, suggesting that MCC act as a nucleating agent and promotes a more ordered arrangement. In contrast, the addition of silica results in the depreciation of crystallinity to 17%, which can be attributed to the amorphous nature

of silica and its disruptive effect on the regular packing. The SMCC also gives a high value of crystallinity and is summarized in **Table 7.1**

Table 7.1 Crystallinity Indices of PVA, PVA/MCC, PVA/Silica, PVA/SMCC10 and PVA/SMCC20

Sample	Crystallinity Index (%)
PVA	20.2
PVA/MCC	24.2
PVA/silica	17.6
PVA/SMCC10	23.3
PVA/SMCC20	25.0

7.4.3. Thermogravimetric Analysis

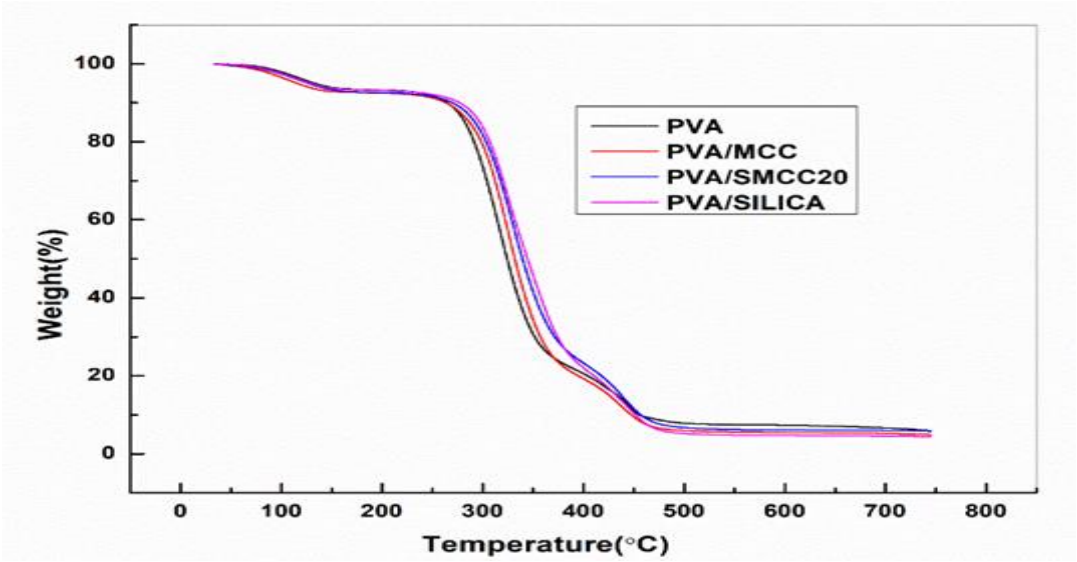

Figure 7.8. TG of PVA, PVA/MCC, PVA/SMCC20, and PVA/Silica

Thermal analysis was conducted in an inert atmosphere from room temperature to 750 °C. **Figure 7.8** represents the TG curves of PVA, PVA/MCC, PVA/Silica and PVA/SMCC20 films. All the samples show a nearly identical pattern of weight loss profile. In the case of PVA, no considerable weight loss is observed, up to 80 °C. The first stage degradation over the temperature range of 80 °C to 160 °C is due to the evaporation of adsorbed water molecules [45]. PVA is thermally stable

from 170 to 240 °C, and there is a rapid weight loss within the temperature range from 240 to 480 °C, due to the dehydration and degradation of the PVA main chain as well as the side chain [46]. The film retains 48% of the total weight even at 340 °C. The low extent of weight loss, over the temperature range of 480 °C to 750 °C, indicates the decomposition of PVA to ash residue. In the case of PVA/MCC film, there is no weight loss up to 80 °C and 7% weight loss is observed from 80 to 155 °C, due to the evaporation of physically and chemically bound water molecules [38]. The film is thermally stable from 155 to 248 °C and the onset temperature is higher than that of pure PVA [47]. This is due to the formation of additional hydrogen bonding between MCC and PVA. Thermogravimetric analysis revealed that all samples retained 5–7% residual weight at 700 °C, attributed to the presence of carbonaceous residues. The onset temperature, determined using the tangent method, was 282 °C for pure PVA. The incorporation of MCC led to a slight increase in the onset temperature to 287 °C. A more pronounced enhancement was observed in the PVA/SMCC20 composite (297 °C), while the PVA/silica composite exhibited the highest thermal stability among all samples. These trends underscore the efficiency of inorganic fillers, especially silica, which acts as a thermal barrier, improving heat resistance. The studies show that incorporating silica nanoparticles shifts PVA's thermal degradation to a higher temperature [48]. The SMCC composite synergises the structural reinforcement of MCC with the thermal resistance of silica, resulting in superior performance. Thus, it is an excellent candidate for the advanced applications, like heat-resistant coating, flame-retardant packaging and sustainable composite material, that require both durability and eco-friendliness.

7.4.4. Morphological Analysis

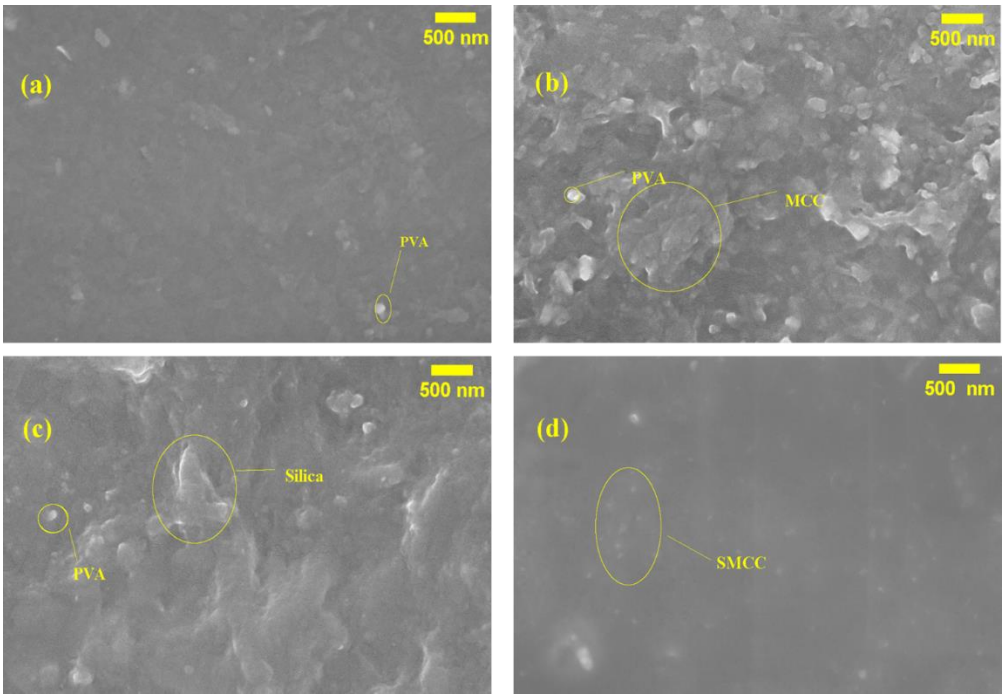

Figure 7.9. FE-SEM Images of (a) PVA (b) PVA/MCC (c) PVA/Silica and (d) PVA/SMCC20

Morphology, at high magnification, is studied using FE-SEM analysis. **Figure 7.9 (a)** represents the image of pure PVA, which has sponge-like texture with little agglomeration. The film has no cracks or pin holes. The FE-SEM image of PVA/MCC film (**Figure 7.9 (b)**) appeared to be rough with non-uniform topography [49]. MCC is visible as discrete, crystalline particles embedded within the PVA matrix, which shows that MCC is less miscible with the polymer matrix. As observed in XRD studies, PVA/MCC film is more crystalline than pure PVA, and it will decrease the biodegradability of the polymer. Silica, within the PVA film, (**Figure 7.9(c)**), appeared as round and irregularly shaped clusters [50]. The size of silica particles varies from nanometres to micrometres. Nevertheless, some parts of the film appeared homogeneous, due to the miscibility of silica, which is due to the extensive H-bonding between the -O-H group of silanol and PVA. The FE-SEM image of PVA/SMCC film (**Figure 7.9(d)**) is entirely different from the other three. The PVA/SMCC film appears to be homogeneous with fewer immiscible particles at all. Uniform mixing shows that SMCC is more compatible with PVA than with MCC or silica. The surface

appears to be smooth without any cracks, pin holes or defects. A homogeneous surface also suggests that there is a strong interfacial interaction between PVA and SMCC. The absence of any pores also suggests that the film would be denser than PVA, PVA/MCC and PVA/Silica films, and this will later be proved by mechanical property studies. The lack of proper miscibility of MCC and agglomeration behaviour of silica can be effectively minimised by the use of SMCC, as filler in PVA composites. This indicates that SMCC acts as a more effective filler by integrating the reinforcing characteristic of MCC with the surface-modifying benefit of silica leading to improved compatibility with the PVA matrix. Consequently, SMCC outperforms MCC and silica by promoting better structural integrity and potentially enhancing the overall performance of the composite film.

All the fabricated films are found to be transparent. The photographs of the same are provided in **Figure 7.10**. The photographs reveal that there are notable differences in the transparency of films, and it depends on the nature of the filler. The pure PVA film is almost transparent, while the addition of MCC slightly diminishes its clarity, resulting in a mildly opaque appearance, probably due to light scattering by poorly dispersed cellulose particles. However, when silica or silicified MCC are incorporated, there is no significant loss of transparency compared to pure PVA, indicating that these fillers maintain the film's optical clarity. This suggests that while SMCC provides reinforcement similar to MCC, the silica modification enhances its compatibility and dispersion within the polymer matrix, preventing agglomeration and preserving transparency. These findings underscore that SMCC can be used as an effective, aesthetically favourable filler in PVA composite films, especially in food packaging, for making agricultural film and in biomedical applications.



Figure 7.10. Photographs of PVA Composite films

7.4.5. Mechanical Properties

The mechanical properties of PVA, PVA/MCC, PVA/Silica, PVA/SMCC10 and PVA/SMCC20 are studied using UTM. All the composite were prepared with an initial filler content of 2%. Subsequently, PVA/SMCC20 containing 2%, 4%,6% and 8% of SMCC20 were also studied. **Figure 7.11** shows the tensile strength of blended films containing CPVA and HPVA and their composites. As shown in the bar diagram, the average tensile strength (T.S) of PVA can be enhanced by adding different fillers. There is a 6.8% increase in T.S during the addition of MCC to PVA. It is attributed to the interfacial adhesion between PVA and MCC and the high crystallinity of MCC particles. Amorphous silica also contributes to the uplift in the T.S of PVA. Since silica exhibits nanoscale dimensions, it can distribute uniformly within the polymer matrix. Moreover, it can form a stronger H-bond due to the presence of the -O-H group of the silanol group. The T.S of PVA is increased by 19.6% upon adding 2% silica [51]. The most remarkable findings from this study are that SMCC is a better reinforcing agent than pure MCC and silica. The T.S is increased by 37.2% and 38% for SMCC10 and SMCC20, respectively. This is attributed to the high surface area, better mechanical strength and high compatibility with PVA. Since SMCC is more renewable and biodegradable than silica, it is a better choice as a filler in polymer composites.

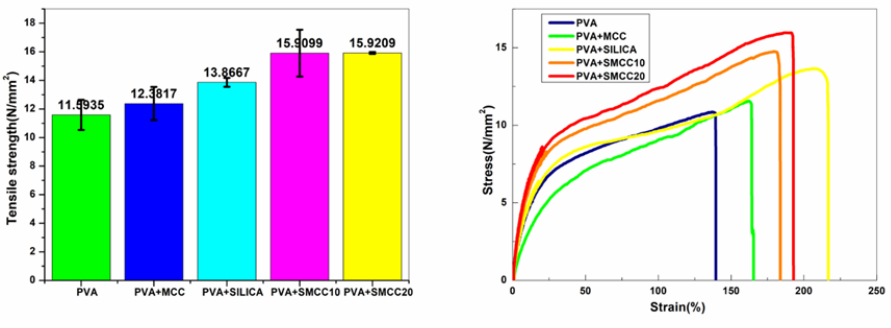

Figure 7.11. Tensile Strength and Stress- Strain Curves of PVA, PVA/MCC, PVA/Silica, PVA/SMCC10 and PVA/SMCC20

The stress-strain curves of different composites show that there is a gradual increase in T.S upon adding fillers. The slope of the stress -strain curve in the elastic

region corresponds to the stiffness or hardness of the film. Among the sample PVA/ SMCC20 exhibits highest slope, confirming its superior hardness. Brittleness, which is measured by finding the elongation at break, is the highest for PVA/ Silica and the lowest for pure PVA blend. Toughness is measured by finding the area under the stress-strain curve. This shows that PVA/SMCC20 is the toughest one. The decreasing order of T.S, stiffness, brittleness and toughness of different films is given **Table. 7.2.**

Table.7.2. Qualitative Comparison of the Mechanical Properties of Different films Based on the Stress-Strain curve

Mechanical Properties	**Comparison**
Tensile strength	PVA/SMCC20>PVA/SMCC10>PVA/Silica>PVA/MCC>PVA
Stiffness	PVA/SMCC20>PVA/SMCC10>PVA/Silica>PVA>PVA/MCC
Brittleness	PVA/Silica>PVA/SMCC20>PVA/SMCC10>PVA/MCC>PVA
Toughness	PVA/SMCC20>PVA/Silica>PVA/SMCC10>PVA>PVA/MCC

Since PVA/SMCC20 composites outperform PVA/SMCC10 in mechanical properties such as T.S, toughness and stiffness, further studies were conducted using SMCC20. The mechanical properties of PVA/SMCC20 film with different percentage compositions are given in **Figure 7.12.** The bar diagram and Stress- Strain curve show that the tensile strength and stiffness of the film increase up to 6% of SMCC20 and then decrease, whereas brittleness is the highest for PVA/SMCC (2%).

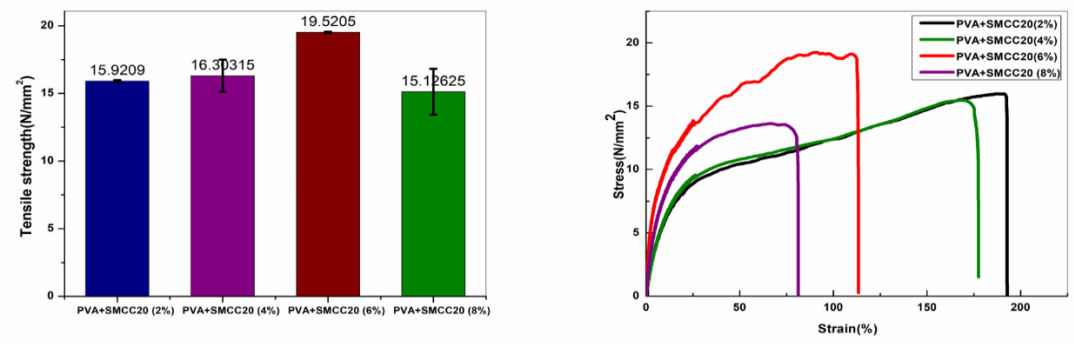

Figure 7.12. Tensile Strength and Stress- Strain Curves of PVA/SMCC20 films Containing (2%), (4%), (6%) and (8%) SMCC20

Conclusion

This chapter presented a comprehensive comparative study on the fabrication and characterization of Polyvinyl Alcohol (PVA) composite films reinforced with the filler, microcrystalline cellulose (extracted from Screw Pine leaves), silica (extracted from Mission Grass), and Silicified Microcrystalline Cellulose (SMCC). The base PVA film was synthesised by blending Hot water-soluble (2.5 g) and Cold water-soluble (2.5 g) PVA by solution casting, and composites were prepared by incorporating 2% MCC, silica, and SMCC individually. To understand the influence of filler content, additional films were prepared with varying filler loadings (2%, 4%, 6%, and 8%) of SMCC20. Various analytical techniques, including FT-IR, XRD, TGA, FE-SEM, mechanical testing, and transparency evaluation, were employed to assess the structure-property relationships of these composite films.

FT-IR spectroscopy revealed that the incorporation of fillers into the PVA matrix did not lead to any major structural modifications in the polymer backbone, indicating the physical nature of the interaction. However, the presence of silica in the composite was confirmed by the characteristic Si–O–Si peak near 600 cm^{-1}, particularly evident in silica and SMCC-reinforced films. XRD analysis revealed the effect of filler type on the crystallinity of the composites. The crystallinity index of bare PVA is 20.2% and the addition of 2% MCC increased crystallinity to 24.2%, confirming its role as a nucleating agent that enhances molecular ordering in the PVA matrix. In contrast, the incorporation of silica reduced the crystallinity to 17.6%, due to its inherently amorphous nature and its interference with the regular polymer chain alignment. SMCC exhibits an intermediate crystallinity, highlighting a balance effect, while the MCC component in SMCC promotes an ordered structure, and the presence of the silica content causes partial disruption. Thermogravimetric analysis shows that silica and SMCC enhance the thermal stability of the PVA composites. Silica nanoparticles, due to their heat resistance, were found to shift the degradation onset of PVA to higher temperatures. SMCC showed synergistic performance, combining MCC's reinforcement with silica’s thermal barrier effects. FE-SEM analysis revealed the distinct morphological features among the composites. MCC particles displayed

poor dispersion and partial agglomeration, whereas silica exhibited more uniform, but still limited, distribution. SMCC-reinforced films showed superior dispersion with minimal agglomeration, owing to the surface-modified silica components that enhanced compatibility with the PVA matrix.

Visual inspection and transparency measurements further supported the morphological findings. Neat PVA films were highly transparent. Films reinforced with MCC showed diminished transparency due to the light scattering by undispersed cellulose particles, resulting in a faintly opaque appearance. In contrast, films containing silica or SMCC retained optical clarity similar to that of pure PVA. Mechanical testing revealed a clear hierarchy in tensile strength performance: PVA/SMCC20 > PVA/SMCC10 > PVA/Silica > PVA/MCC > Pure PVA. Among all variations, the composite containing 6% SMCC (designated as SMCC20) exhibited the highest tensile strength and optimized mechanical performance, with improved flexibility, toughness, and stiffness. The stress-strain behaviour indicated that SMCC not only reinforces the matrix but also reduces brittleness, due to the better load transfer and energy dissipation through a well-dispersed filler network.

In conclusion, this study highlights the importance of filler type and composition in tuning the structure and properties of PVA-based composites. MCC enhances the crystallinity and reinforcement but suffers from dispersion issues. Silica improves thermal resistance and clarity, but can reduce mechanical integrity at higher concentrations due to poor matrix interaction. However, SMCC offers a multifunctional approach, combining the structural benefits of MCC with the thermal and dispersion advantages of silica. This hybrid filler provides a balanced improvement across crystallinity, mechanical strength, thermal resistance, morphology, and transparency. These studies validate SMCC as a superior reinforcing agent in the fabrication of high-performance, biodegradable PVA composites. The dual-phase functionality of SMCC opens pathways for its application in sustainable packaging, heat-resistant materials, biomedical products, and other environmentally friendly polymer-based technologies. Future work may focus on scaling up production, evaluating barrier properties, and exploring the biodegradation behaviour of these advanced films in real-world conditions.

References

[1] Baniasadi H, Äkräs L, Madani Z, Silvenius F, Fazeli M, Lipponen S, et al. Development and characterization of polylactic acid/starch biocomposites – From melt blending to preliminary life cycle assessment. Int J Biol Macromol 2024;279. https://doi.org/10.1016/j.ijbiomac.2024.135173.

[2] Soliman TS. Effects of SiO_2 nanoparticles on polyvinyl alcohol/carboxymethyl cellulose polymer blend films' structural, wettability, surface roughness, and optical characteristics. Adv Polym Technol. 2024;2024:3623198. https://doi.org/10.1155/2024/3623198

[3] Rahman Khan MM, Rumon MMH, Islam M. Synthesis, Rheology, Morphology, and Mechanical Properties of Biodegradable PVA-Based Composite Films: A Review on Recent Progress. Processes 2024;12:2880. https://doi.org/10.3390/pr12122880.

[4] Hasan MZ, Arafat Y, Bashar MM, Niloy MNN, Islam MI, Khandaker S, et al. Poly-(vinyl alcohol) composite films reinforced with carboxylated functional microcrystalline cellulose from jute fiber. Compos. Adv. Mater. 2022;31. https://doi.org/10.1177/26349833221103888.

[5] Chousidis N. Polyvinyl alcohol (PVA)-based films: insights from crosslinking and plasticizer incorporation. Engineering Research Express 2024;6:025010. https://doi.org/10.1088/2631-8695/ad4cb4.

[6] Liu B, Zhang J, Guo H. Research Progress of Polyvinyl Alcohol Water-Resistant Film Materials. Membranes (Basel) 2022;12;347. https://doi.org/10.3390/membranes12030347.

[7] Nagarkar R, Patel J. Polyvinyl alcohol: a comprehensive study. Acta Sci Pharm Sci. 2019;3(4):34–44.

[8] Elgharbawy AS, El Demerdash AGM, Sadik WA, Kasaby MA, Lotfy AH, Osman AI. Enhancing the Biodegradability, Water Solubility, and Thermal Properties of Polyvinyl Alcohol through Natural Polymer Blending: An Approach toward Sustainable Polymer Applications. Polymers (Basel) 2024;16. https://doi.org/10.3390/polym16152141.

[9] Wang M, Bai J, Shao K, Tang W, Zhao X, Lin D, et al. Poly(vinyl alcohol) Hydrogels: The Old and New Functional Materials. Int J Polym Sci 2021;2021. https://doi.org/10.1155/2021/2225426.

[10] Grymonpré W, De Jaeghere W, Peeters E, Adriaensens P, Remon JP, Vervaet C. The impact of hot-melt extrusion on the tableting behaviour of polyvinyl alcohol. Int J Pharm 2016;498:254–62. https://doi.org/10.1016/j.ijpharm.2015.12.020.

[11] Ben Halima N. Poly(vinyl alcohol): Review of its promising applications and insights into biodegradation. RSC Adv 2016;6:39823–32. https://doi.org/10.1039/c6ra05742j.

[12] Zicarelli G, Faggio C, Blahova J, Riesova B, Hesova R, Doubkova V, et al. Toxicity of water-soluble polymers polyethylene glycol and polyvinyl alcohol for fish and frog embryos. Sci. Total Environ. 2024;933. https://doi.org/10.1016/j.scitotenv.2024.173154.

[13] Alvarado MC. Recent progress in polyvinyl alcohol (PVA)/nanocellulose composite films for packaging applications: A comprehensive review of the impact on physico-mechanical properties. Food bioeng. 2024;3:189–209. https://doi.org/10.1002/fbe2.12086.

[14] Mata GC da, Morais MS, Oliveira WP de, Aguiar ML. Composition Effects on the Morphology of PVA/Chitosan Electrospun Nanofibers. Polymers (Basel) 2022;14:4856. https://doi.org/10.3390/polym14224856.

[15] Musa BH, Hameed NJ. Study of the mechanical properties of polyvinyl alcohol/starch blends. Mater. Today Proc., vol. 20, Elsevier Ltd; 2020, p. 439–42. https://doi.org/10.1016/j.matpr.2019.09.161.

[16] Simón-Herrero C, Peco N, Romero A, Valverde JL, Sánchez-Silva L. PVA/nanoclay/graphene oxide aerogels with enhanced sound absorption properties. Applied Acoustics 2019;156:40–45. https://doi.org/10.1016/j.apacoust.2019.06.023.

[17] Ningaraju S, Gnana Prakash AP, Ravikumar HB. Studies on free volume controlled electrical properties of PVA/NiO and PVA/TiO2 polymer nanocomposites. Solid State Ion 2018;320:132–47. https://doi.org/10.1016/j.ssi.2018.03.006.

[18] Channa IA, Ashfaq J, Gilani SJ, Shah AA, Chandio AD, Jumah MN Bin. UV Blocking and Oxygen Barrier Coatings Based on Polyvinyl Alcohol and Zinc Oxide Nanoparticles for Packaging Applications. Coatings 2022;12:897. https://doi.org/10.3390/coatings12070897.

[19] Wang Z, Zhao S, Hong L, Huang J. Preparation and Properties of Silver-Based Cellulose/Polyvinyl Alcohol Antibacterial Materials. J Inorg Organomet Polym Mater 2020;30:4382–93. https://doi.org/10.1007/s10904-020-01669-5.

[20] Bavel E, Afkhami A, Madrakian T. Removal and Preconcentration of Pb(II) Heavy Metal Ion from Water and Waste-Water Samples onto Poly (vinyl alcohol)/polyethyleneimine/Fe3O4 Microfibers Nanocomposite. J Polym Environ 2020;28:614–23. https://doi.org/10.1007/s10924-019-01632-7.

[21] Naduparambath S, Sreejith MP, Jinitha T V., Shaniba V, Aparna KB, Purushothaman E. Development of green composites of poly (vinyl alcohol) reinforced with microcrystalline cellulose derived from sago seed shells. Polym Compos 2018;39:3033–39. https://doi.org/10.1002/pc.24307.

[22] Sreekumar PA, Manirul Haque SK, Afzal HM, Sadique Z, Al-Harthi MA. Preparation and characterization of microcellulose reinforced polyvinyl alcohol/starch biocomposites. J Compos Mater 2019;53:1933–39. https://doi.org/10.1177/0021998318816437.

[23] Hasan MZ, Arafat Y, Bashar MM, Niloy MNN, Islam MI, Khandaker S, et al. Poly-(vinyl alcohol) composite films reinforced with carboxylated functional

microcrystalline cellulose from jute fiber. Composites and Advanced Materials 2022;31. https://doi.org/10.1177/26349833221103888.

[24] Tang R, Liu L, Li M, Yao X, Yang Y, Zhang S, et al. Transparent Microcrystalline Cellulose/Polyvinyl Alcohol Paper as a New Platform for Three-Dimensional Cell Culture. Anal Chem 2020; 92:14219–27. https://doi.org/10.1021/acs.analchem.0c03458.

[25] Hussin MH, Husin NA, Bello I, Othman N, Bakar MA, Mohamad Haafiz MK. Isolation of microcrystalline cellulose (MCC) from oil palm frond as potential natural filler for PVA-LiClO4 polymer electrolyte. Int J Electrochem Sci 2018; 13:3356–71. https://doi.org/10.20964/2018.04.06.

[26] Wei Q, Wang Y, Rao Y, Jiang A, Zhang K, Lu T, et al. Evaluating the effects of nanosilica on mechanical and tribological properties of polyvinyl alcohol/polyacrylamide polymer composites for artificial cartilage from an atomic level. Polymers (Basel) 2019; 11:76. https://doi.org/10.3390/polym11010076.

[27] Reino Olegário da Silva DA, Bosmuler Zuge LC, de Paula Scheer A. Preparation and characterization of a novel green silica/PVA membrane for water desalination by pervaporation. Sep Purif Technol 2020;247. https://doi.org/10.1016/j.seppur.2020.116852.

[28] Al-Kadhemy MFH, Ibrahim SA, Salman JAS. Studying the physical properties polyvinyl alcohol polymer mixture with silica nanoparticles and its application as pathogenic bacteria inhibitor. AIP Conf. Proc., vol. 2290, American Institute of Physics Inc.; 2020 p 050013. https://doi.org/10.1063/5.0028817.

[29] Duan D, Gao X, Dong Y, Qi X, Zhang X, Islam MZ, et al. Green Preparation of Thermal-Insulative, Flame Retardant, and Hydrophobic Silica Aerogel Reinforced Poly(vinyl alcohol) Composites. ACS Appl Polym Mater 2022;4:7352–62. https://doi.org/10.1021/acsapm.2c01136.

[30] Chen Y, Fan H, Zha X, Wang W, Wu Y, Xiong Y, et al. Fabrication of silica/PVA-co-PE nanofiber membrane for oil/water separation. Fash and Text 2021;8:14. https://doi.org/10.1186/s40691-021-00252-x.

[31] Qing W, Li X, Wu Y, Shao S, Guo H, Yao Z, et al. In situ silica growth for superhydrophilic-underwater superoleophobic Silica/PVA nanofibrous membrane for gravity-driven oil-in-water emulsion separation. J Memb Sci 2020;612. https://doi.org/10.1016/j.memsci.2020.118476.

[32] Wei Q, Wang Y, Zhang Y, Chen X. Aggregation behavior of nano-silica in polyvinyl alcohol/polyacrylamide hydrogels based on dissipative particle dynamics. Polymers (Basel) 2017;9:611. https://doi.org/10.3390/polym9110611.

[33] de Castro JG, Zargar R, Habibi M, Varol SH, Parekh SH, Hosseinkhani B, Adda-Bedia M, Bonn D. Nonmonotonic fracture behavior of polymer nanocomposites. Appl Phys Lett. 2015;106(22):221904. https://doi.org/10.1063/1.4922287.

[34] Aljaberi A, Chatterji A, Shah NH, Sandhu HK. Functional performance of silicified microcrystalline cellulose versus microcrystalline cellulose: a case study SMCC

versus MCC. Drug Dev Ind Pharm 2009;35:1066–71. https://doi.org/10.1080/03639040902774131.

[35] Kalita P, Roy PK, Das N, Pachuau L. Silicified microcrystalline cellulose from renewable banana pseudostem: Physicochemical and functional analysis. Int J Biol Macromol 2024; 283:137620. https://doi.org/10.1016/j.ijbiomac.2024.137620.

[36] Seera SDK, Kundu D, Banerjee T. Physical and chemical crosslinked microcrystalline cellulose-polyvinyl alcohol hydrogel: freeze–thaw mediated synthesis, characterization and in vitro delivery of 5-fluorouracil. Cellulose 2020;27:6521–35. https://doi.org/10.1007/s10570-020-03249-9.

[37] Ghazali NM, Mazuki NF, Samsudin AS. Characterization of Biopolymer Blend-based on Alginate and Poly (vinyl Alcohol) as an Application for Polymer Host in Polymer Electrolyte. IOP Conf Ser Mater Sci Eng 2021;1092:012047. https://doi.org/10.1088/1757-899x/1092/1/012047.

[38] Naduparambath S, Purushothaman E. Sago seed shell: determination of the composition and isolation of microcrystalline cellulose (MCC). Cellulose 2016;23:1803–12. https://doi.org/10.1007/s10570-016-0904-3.

[39] Hema M, Selvasekerapandian S, Sakunthala A, Arunkumar D, Nithya H. Structural, vibrational and electrical characterization of PVA-NH4Br polymer electrolyte system. Physica B Condens Matter 2008;403:2740–47. https://doi.org/10.1016/j.physb.2008.02.001.

[40] Sau S, Pandit S, Kundu S. Crosslinked poly (vinyl alcohol): structural, optical and mechanical properties. Surf Interfaces. 2021;25:101198. https://doi.org/10.1016/j.surfin.2021.101198.

[41] Menazea AA, Mostafa AM, Al-Ashkar EA. Effect of nanostructured metal oxides (CdO, Al2O3, Cu2O) embedded in PVA via Nd:YAG pulsed laser ablation on their optical and structural properties. J Mol Struct 2020;1203. https://doi.org/10.1016/j.molstruc.2019.127374.

[42] Takahashi Y. Neutron structure analysis of poly(vinyl alcohol). J Polym Sci B Polym Phys. 1997;35(2):193–198. https://doi.org/10.1016/0921-4526(95)00264-A

[43] Rahman IA, Padavettan V. Synthesis of Silica nanoparticles by Sol-Gel: Size-dependent properties, surface modification, and applications in silica-polymer nanocompositesa review. J Nanomater 2012;2012. https://doi.org/10.1155/2012/132424.

[44] Dodda JM, Bělský P, Chmelař J, Remiš T, Smolná K, Tomáš M, et al. Comparative study of PVA/SiO2 and PVA/SiO_2/glutaraldehyde (GA) nanocomposite membranes prepared by single-step solution casting method. J Mater Sci 2015;50:6477–90. https://doi.org/10.1007/s10853-015-9206-7.

[45] Abral H, Andriyanto H, Samera R, Sapuan SM, Ishak MR. Mechanical properties of screw pine (*Pandanus odoratissimus*) fibers–unsaturated polyester composites. Polym Plast Technol Eng. 2012;51(5):500–506. https://doi.org/10.1080/03602559.2011.651246.

[46] Lee DH, Song YH, Ahn HJ, Lee J, Woo HC. Fabrication and Characterization of Biopolymers Using Polyvinyl Alcohol and Cardanol-Based Polyols. Molecules 2024;29:4807. https://doi.org/10.3390/molecules29204807.

[47] Sun X, Lu C, Liu Y, Zhang W, Zhang X. Melt-processed poly(vinyl alcohol) composites filled with microcrystalline cellulose from waste cotton fabrics. Carbohydr Polym 2014;101:642–49. https://doi.org/10.1016/j.carbpol.2013.09.088.

[48] Peng Z, Kong LX. A thermal degradation mechanism of polyvinyl alcohol/silica nanocomposites. Polym Degrad Stab 2007;92:1061–71. https://doi.org/10.1016/j.polymdegradstab.2007.02.012.

[49] Wen Yi VN, Choo Huey N, Peng TY, Ooi ZX, Siew Hoong S. Isolation of cellulose derived from orange peel and its application in biodegradable films. Cellulose Chem Technol.2021;55:311–324. https://doi.org/10.35812/CelluloseChemTechnol.2021.55.31.

[50] Hanh PTH, Suwunwong T, Chantrapromma S, Choto P, Thanomsilp C, Phoungthong K. Preparation and characterization of polyvinyl alcohol (PVA)-glycerol composite films incorporating nanosilica from municipal solid waste incinerator bottom ash. Heliyon 2024;10(4). https://doi.org/10.1016/j.heliyon.2024.e25963.

[51] Sabr OH, Hussein AA, Obaid MN. Improving Mechanical and Morphological Characteristics Pva/Sio_2 Nanocomposites for Food Packing Applications . IOP Conf Ser Mater Sci Eng 2021;1094:012146. https://doi.org/10.1088/1757-899x/1094/1/012146.

Chapter 8

Application Studies and Functional Evaluation of Biodegradable PVA Composite films Reinforced with MCC, SMCC and ZnO

8.1 Introduction

8.1.1 Relevance and Applications of Biodegradable PVA-Based Composite films

Biodegradable films became an attractive alternative to conventional plastics because they can reduce persistent plastic pollution and support sustainable, closed loop material strategies in packaging, agricultural, and biomedical applications. Among biodegradable polymers Poly vinyl Alcohol (PVA) occupies a distinct position, since it is cost effective, water soluble and easily film forming material with excellent mechanical strength, chemical resistance and biocompatibility. Its biodegradability and other properties can be enhanced or tailored through sustainable eco-friendly methods or by incorporating fillers and additives. Accordingly, PVA based films have been extensively studied as biodegradable functional material for use in food packaging [1], wound dressing [2], agricultural mulch films [3] and various other single use or semi durable applications.

A novel composite film was developed using chestnut starch and PVA, where the effect of sorbitol and glycerol plasticizers on functional properties revealed that plasticization reduces the swelling capacity, improves the solubility and biodegradability [4]. An oxalic acid modified Ca^{2+}cross linked PVA coating was developed to enhance the water resistance and barrier performance of paper-based food packaging [5]. Biodegradable chitosan/Polyvinyl Alcohol nanocomposite films reinforced with quercetin-functionalised layered double hydroxy nanosheets was developed and it exhibited strong interfacial interaction, enhanced thermal stability, excellent UV barrier and antibacterial activity [6]. Microcrystalline cellulose- PVA hydrogel synthesised via combined physical (freeze-thaw) and chemical (ethylene glycol glycosidil ether) cross linking and it exhibited porous morphology, good

swelling behaviour and sustained 5-fluorouracil release, hence can be used in controlled drug delivery system [7]. A PVA/PAA based alkaline solid poly electrolyte membrane incorporating 5 wt% microcrystalline cellulose exhibited increase in ionic conductivity, enhanced alkali resistance, reduced crystallinity and improved mechanical properties which demonstrates that MCC is an effective functional filler for high performance membrane [8]. Hydrogel prepared from various blend of PVA, MCC, gelatin and chitosan were characterised for physicochemical and mechanical properties, revealing that PVA/MCC and chitosan hydrogel exhibited minimal mass loss, low permeability and mechanical behaviour reassembling corneal stroma, indicating their potential as corneal substitutes for early-stage drug permeation studies [9]. A biodegradable mulch film composed of PVA and lignin extracted from empty fruit bunches was developed showing that increasing lignin content enhanced water solubility, biodegradability, reduced light transmittance and weed growth, demonstrating its potential as a sustainable alternative [10].

An eco-friendly fluorine free superhydrophobic coating was developed by spray-coating hydrophilic silica nanoparticles bound with PVA modified with polydimethylsiloxane, achieving 160° water contact angle, good stability and easy removability [11]. A ternary PVA/CMC/aloe vera (60/20/20) biofilm was prepared via solvent casting, good mechanical and viscoelastic properties, UV absorption at 280 nm with defined optical parameters, and promising potential for future device and packaging applications [12]. Biodegradable PVA/CS films incorporated with 5% D-limonene was prepared and showed optimal antibacterial, mechanical, and barrier properties, effectively preserving mangoes for 10 days, demonstrating strong potential as eco-friendly food packaging materials [13]. Highly stretchable PVA films and tuneable PVA–cellulose composites were developed using trifluoroacetic acid as a common solvent and plasticizer, yielding hydrophobic films with adjustable mechanical and morphological properties [14]. Chitosan/PVA/nano-hydroxyapatite hybrid nanofibers loaded in situ with Cu/Ag nanoparticles were developed as biocompatible, non-toxic wound dressings exhibiting strong antibacterial activity against both Gram-positive and Gram-negative bacteria [15]

8.1.2 Role of MCC, Silica, Silicified MCC, and ZnO as Functional Fillers in PVA-Based Films

Microcrystalline cellulose (MCC) is a biodegradable, renewable, and cost-effective natural polymer derived from cellulose and it is an ideal reinforcing filler for PVA films [16]. Its incorporation enhances the mechanical strength, thermal stability, and crystallinity of PVA through strong hydrogen bonding between hydroxyl groups [17]. MCC also acts as a nucleating agent, promoting a more ordered crystalline structure that improves barrier properties against gases and moisture [18]. Moreover, it reduces film solubility and swelling, improving dimensional stability. Owing to its biocompatibility and biodegradability, MCC-filled PVA composites are well-suited for eco-friendly packaging [19], biomedical [20], and controlled-release applications**.** While MCC improves strength, stiffness, and biodegradability of PVA films, its poor dispersion, moisture sensitivity, and limited multifunctionality restrict its performance. Surface modification or combination with other fillers can effectively overcome these drawbacks.

Silica (SiO_2) is an effective inorganic filler in PVA films owing to its high surface area, stability, and strong hydrogen bonding with PVA's hydroxyl groups. Its incorporation enhances mechanical strength [21], thermal stability [22], and barrier performance by restricting polymer chain mobility and forming a tortuous path for gas and moisture diffusion [23]. Silica also improves dimensional stability, UV resistance [24], and water resistance, making the composite suitable for packaging and coating applications [25]. However**,** excessive silica loading can cause agglomeration**,** reducing film transparency and flexibility. Therefore, maintaining optimal silica content and ensuring uniform dispersion are essential for achieving balanced film performance.

Silicified Microcrystalline Cellulose (SMCC) is a hybrid filler composed of microcrystalline cellulose embedded with silica, combining the reinforcing ability of cellulose with the stability and surface functionality of silica. When incorporated into PVA, SMCC improves mechanical strength, thermal stability, and interfacial compatibility more effectively than pure MCC due to enhanced hydrogen bonding

and silica–hydroxyl interactions. The presence of silica on the cellulose surface reduces agglomeration, promotes uniform filler dispersion, and enhances moisture resistance and dimensional stability of the composite. SMCC also provides a synergistic effect**,** improving both the rigidity and flexibility balance of PVA films. Thus, SMCC serves as a superior filler that enhances the structural integrity and durability of biodegradable PVA-based composites compared to unmodified cellulose.

Zinc Oxide (ZnO) is an important functional filler in PVA matrix due to its unique optical [26], antimicrobial [27], and reinforcing properties. The incorporation of ZnO nanoparticles enhances the mechanical strength, thermal stability, and UV-shielding ability of PVA films through strong interfacial interactions and uniform nanoparticle dispersion [28]. ZnO also imparts excellent antibacterial activity by generating reactive oxygen species and releasing Zn^{2+} ions, making the composite suitable for food packaging and biomedical applications [29]. Additionally, ZnO improves the optical transparency and barrier properties of the film by reducing oxygen and moisture permeability.

In the previous chapter, PVA composite films were developed using different fillers such as MCC, silica, and Silicified Microcrystalline Cellulose (SMCC) containing 10% and 20% silica (designated as SMCC10 and SMCC20 respectively). These composites were systematically characterized for their thermal stability, miscibility, structural behaviour, and mechanical strength, revealing that SMCC20 exhibited superior performance among all formulations. Further optimization with varying concentrations of SMCC20 indicated that a 6% loading provided the most balanced enhancement in thermal and mechanical properties. Building upon these findings, the present chapter introduces a new composite system, PVA/SMCC–ZnO, designed to impart additional multifunctionality such as UV-blocking capability, antibacterial activity, improved hydrophobicity, and controlled biodegradability, while retaining the favourable structural and mechanical characteristics observed in the optimized SMCC-filled films.

8.1.3 Aim and Objectives of the Study in the Present Chapter

The aim of the study is to develop and characterize Polyvinyl Alcohol/Silicified Microcrystalline Cellulose–Zinc Oxide (PVA/SMCC–ZnO) composite films with enhanced multifunctional properties such as mechanical strength, UV-blocking, antibacterial activity, hydrophobicity, and biodegradability and to compare their performance with previously developed PVA, PVA/MCC, and PVA/SMCC20 films for potential use in sustainable packaging applications. The main objectives of the study include

- To prepare PVA/SMCC–ZnO composite films with varying ZnO nanoparticle loadings based on the optimized SMCC20 formulation.
- To analyse the crystalline structure and surface morphology of the developed films using X-ray Diffraction (XRD) and Field Emission-Scanning Electron Microscopy (FE-SEM)**.**
- To determine the tensile strength**,** elongation at break**,** and Young's modulus of the films, and compare these mechanical properties with those of PVA, PVA/MCC, and PVA/SMCC20 films.
- To evaluate biodegradation behaviour through soil-burial weight-loss studies at different time intervals, supported by FE-SEM observation of the degraded surfaces, and compare the results with earlier films.
- To measure the contact angle and UV–Visible absorption spectra of the PVA/SMCC–ZnO films to determine their hydrophobic and UV-blocking properties relative to the previous composites.
- To assess the antibacterial efficacy of the PVA/SMCC–ZnO films against *Escherichia coli* and *Staphylococcus aureus* using the zone of inhibition method, and compare with the antibacterial performance of other PVA-based films.
- To establish correlations between the composition, structure, and morphology of the films and their mechanical, optical, and biodegradation behaviours,

highlighting the improvements of PVA/SMCC–ZnO over PVA, PVA/MCC, and PVA/SMCC20 systems.

8.2 Materials

MCC derived from Screw Pine leaves (Laboratory prepared), sodium silicate derived from Mission Grass used as silica precursor for the preparation of Silicified Microcrystalline Cellulose, Zinc Oxide nanoparticle (<100 nm, Merck India) Poly Vinyl Alcohol (Hot water-soluble M. W~ 60,000-1,25,000 and Cold-water soluble M.W ~ 1,60,000) procured from Hi Media were used for analysis. All the chemicals are Analytical Reagents (AR) grade and were used without purification.

8.3 Methods

As detailed in the previous chapters MCC was prepared from Screw Pine leaves by sequential alkaline delignification with 17 % NaOH followed by acid hydrolysis using 2.5N HCl. SMCC was prepared by an in situ silicification process using sodium silicate derived from Mission Grass as the silica source. A measured amount of MCC was dispersed in aqueous sodium silicate solution and kept overnight. Hydrochloric acid (2N) is added drop by drop with vigorous stirring to initiate the hydrolysis and deposition of silica onto the MCC surface. The reaction was maintained at 70 °C for 2 h to ensure complete silicification within the voids and surface of MCC fibres. The precipitated product was filtered, washed several times with distilled water and ethanol to remove residual ions and dried at 60 °C**.** The method of fabrication of bare PVA, PVA/MCC and PVA/SMCC film were already discussed in chapter 7.

8.3.1 Fabrication of PVA/SMCC–ZnO Composite Films

A series of PVA/SMCC–ZnO composite films were prepared by the solution casting method. Each formulation contained a total of 5 g of mixture with 6 wt.% SMCC and concentration of ZnO nanoparticle varies from 0.5, 1.0, 1.5 to 2.0 wt.%. The remaining portion was PVA. For the 0.5% ZnO composition, the PVA content was 4.675 g, consisting of 2.34 g Hot water soluble PVA and 2.34 g Cold water soluble PVA. A homogeneous PVA solution was prepared by dissolving requisite

amount of PVA in 100 mL of distilled water. The fillers, SMCC and ZnO were added to this with vigorous stirring and the mixture was continuously stirred at 80 °C for 5 h using a magnetic stirrer until a clear and uniform solution was obtained. The resulting solution was then poured on to a clean porcelain tile and dried at room temperature. The dried films were carefully peeled off and stored in a desiccator until further testing. For comparison, films of pure PVA**,** PVA/MCC, and PVA/SMCC20 were also prepared under identical conditions using the solution casting technique.

8.4 Results and Discussion

8.4.1 Water Absorption (Swelling) Analysis.

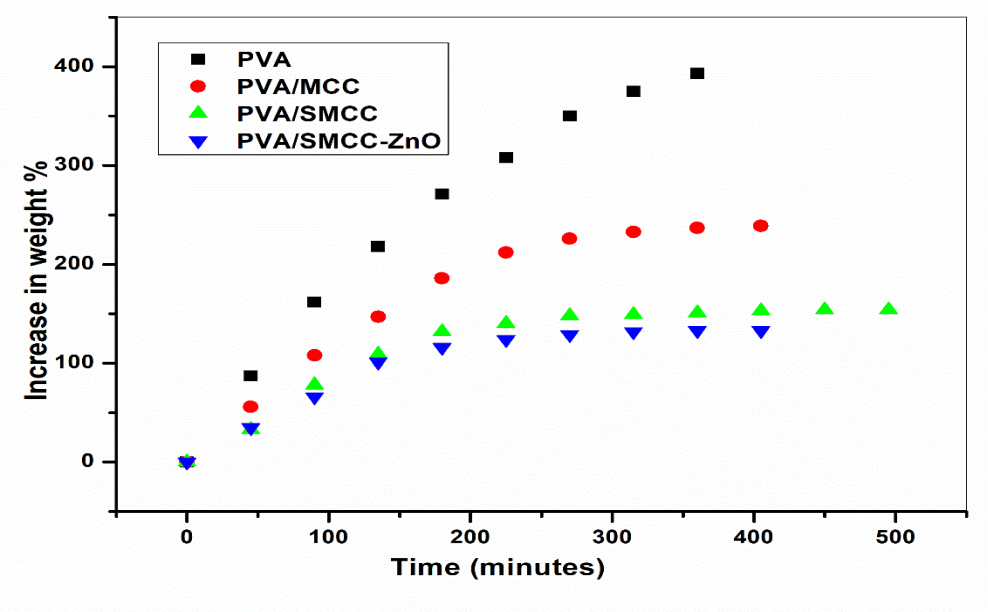

Figure 8.1 Comparative Swelling Behaviour of PVA, PVA/MCC, PVA/SMCC and PVA/SMCC-ZnO over time

The percentage weight increase over time during immersion in water for PVA, PVA/MCC, PVA/SMCC and PVA/SMCC-ZnO are given in **Figure 8.1.** The detailed procedure is discussed in Chapter 3. The curves clearly demonstrate the decrease in water absorption when fillers were incorporated. The bare PVA (HPVA+CPVA) exhibits highest water absorption due to its hydrophilic nature and due to the presence of free hydroxyl groups, which readily forms H-bond with water [30]. Within 6 h PVA film swelled so much and began to dissolve. Thus, weight determination became very difficult. This clearly reflects the limitation of bare PVA in the application of humid

condition. When MCC is incorporated to PVA, the swelling decreases significantly. This is attributed to the strong interaction between the cellulose and PVA matrix. The hydroxyl groups of MCC form H-bond with polymer chain, restricting their mobility and reduces their free volume available for occupancy of water molecule [31]. Moreover, MCC is more rigid and less swellable which also hinders the water penetration and diffusion. The effect is more pronounced when SMCC is used as filler. The PVA/SMCC shows further decrease in water uptake relative to PVA/MCC. It is because surface modification of MCC reduces the density of hydrophilic sites and modify the interface between the filler and polymer. Thus, SMCC reduces water affinity or slow down water diffusion and increase barrier properties against water uptake. When inorganic nanoparticle ZnO is added together with SMCC, water uptake drops further and it gives lowest weight increase among all samples. This suggest that ZnO act as additional obstacle to water diffusion since the size of ZnO nanoparticle is very small, they will easily penetrate to the free volume and restrict the chain mobility [32]. The overall trend shows that addition of fillers progressively reduces water absorption and swelling of PVA. This enhanced property is valuable for applications where dimensional stability, mechanical integrity in humid or wet environment are important (eg: packaging, barrier film, coating). But decrease in water uptake will slow down the rate of biodegradability of PVA.

8.4.2 Water Vapour Transmission Rate (WVTR) Analysis

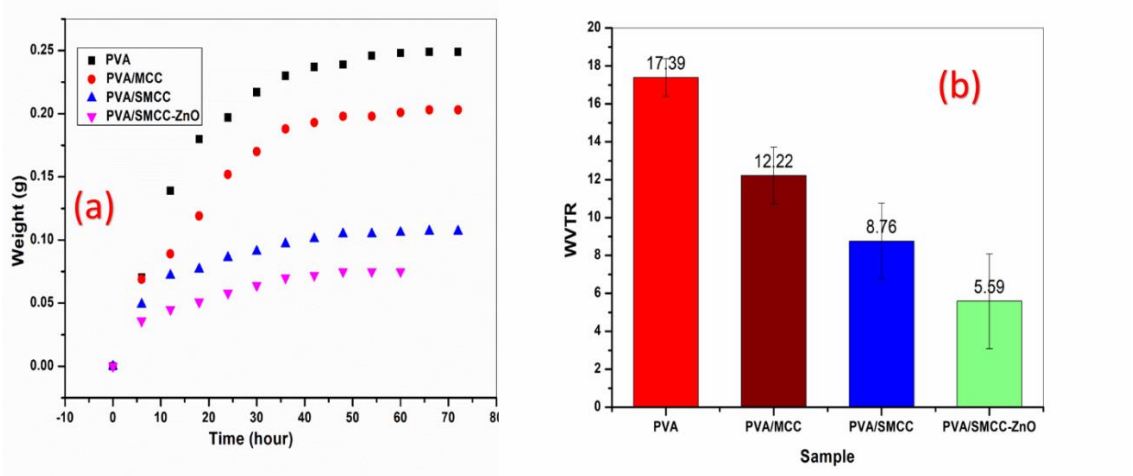

Figure 8.2 (a) Water Vapour Transmission through PVA, PVA/MCC, PVA/SMCC and PVA/SMCC-ZnO as a function of time (b) Water Vapour Transmission Rate

Figure 8.2 (a) and (b) shows the water vapour uptake and Water Vapour Transmission Rate (WVTR) of PVA and its composites over 72 h of exposure (The detailed procedure is discussed in chapter 3). All the samples show the characteristic increase in weight; however, the extent and rate of weight gain depend on the nature of the filler. Bare PVA film shows the highest water uptake at the initial stage followed by gradual approach to the equilibrium, reflecting its high hydrophilicity and permeability. The incorporation of MCC to PVA results significant reduction in weight gain but the overall uptake remains lower than neat PVA which indicates that cellulose imposes a modest barrier to vapour transport [33]. A more pronounced resistance for transmission is observed for the PVA/SMCC film. Since the particle is small, SMCC will occupy the free volume within the polymer matrix and hence molecular diffusion pathways will be restricted. Thus, the rate of water vapour absorption and the equilibrium value is remarkably lower than PVA and PVA/MCC. Among all the samples PVA/SMCC-ZnO displays the lowest water vapour transmission. The combined effect of SMCC and ZnO gives more impact and impermeable structure. Thus PVA/SMCC-ZnO exhibit minimum weight gain and the lowest uptake at equilibrium confirming its highest resistance to water permeation [34].

8.4.3 Anti-Bacterial Performance of PVA Composites

The antibacterial efficacy of PVA composite films was evaluated against two representative bacteria, *Escherichia coli* and *Staphylococcus aureus*, using the zone inhibition method (**Figure 8.3**). Streptomycin (100 µg) was used as the reference standard. The experimental results are given in **Table 8.1.**

Table 8.1. Antibacterial Activity of PVA Composite Films Against *E. coli* and *S. aureus*

Sample	Zone of Inhibition (mm)-*E. coli*	Zone of Inhibition(mm)-*S. aureus*
Streptomycin (100 µg)	24–30	22–27
PVA	Nil	Nil
PVA/MCC	Nil	Nil
PVA/SMCC	Nil	Nil
PVA/SMCC-ZnO	11	11

Antibacterial study demonstrated that pure PVA, PVA/MCC and PVA/SMCC films exhibited no measurable inhibition zone against *E. coli* or *S. aureus*, which reveals that these materials lack inherent antibacterial activity under the condition tested, this aligns with previous studies [35]. In contrast, the PVA/SMCC-ZnO composite film showed a distinct inhibition zone of approximately 11 mm for both Gram positive and Gram-negative bacteria which indicates the inclusion of ZnO nanoparticle imparts significant antibacterial properties. ZnO nanoparticles are widely known to exhibit broad spectrum antimicrobial activity through the mechanism such as generation of reactive oxygen species [36,37], release of Zn^{2+} which can disrupt cellular process and direct physical interaction with bacterial cell envelope [38].

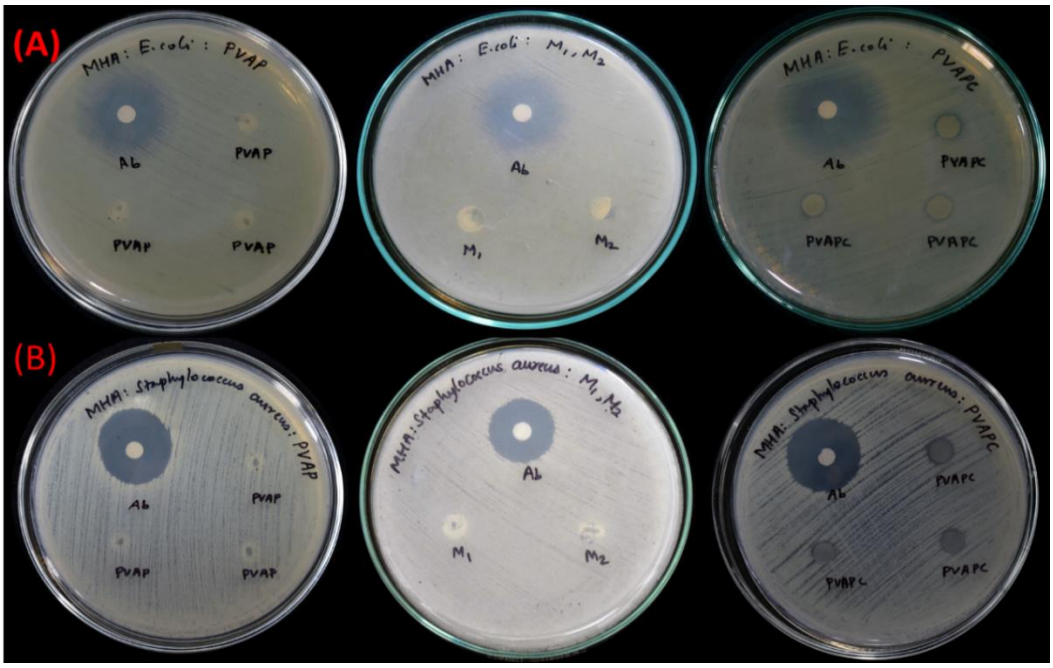

Figure 8.3 Antibacterial Activity against (A) *Escherichia coli (*B) *Staphylococcus aureus*

PVAP= PVA, M_1=PVA/MCC, M_2=PVA/SMCC and PVAPC=PVA/SMCC-ZnO

8.4.4 Evaluation of Soil Burial Degradability of PVA Composites

After soil burial, weight-loss measurements and FE-SEM images taken before and after the test were used to assess the film's biodegradation behaviour

8.4.4.1 Weight Loss Analysis

The weight loss of different films after 30 days of soil burial is given in the following **Table 8.2**

Table 8.2 Percentage Weight Loss of PVA-Based films After Soil-Burial Test.

Sample	Weight Loss (%)
PVA	26.8
PVA/MCC	30.4
PVA/SMCC	21.5
PVA/SMCC-ZnO	15.8

The weight loss results from soil burial test clearly indicates that the incorporation of different fillers significantly influences the biodegradability of films. The results demonstrated that the pure PVA films undergo moderate biodegradation with a weight loss of 26.8% over 30 days, aligning with the trends seen in other biodegradability studies of PVA. When MCC was incorporated to the PVA the weight loss raised to 30.4% confirming that MCC promoted biodegradation. This is likely due to the natural cellulose structure of MCC, which improves water absorption and provides additional sites for microbial colonisation and enzymatic activity [39].

In contrast, the inclusion of silicified MCC reduces the biodegradability of the film, evidenced by the lower weight loss of 21.5%. This suggests that presence of silica limits the enzymatic access and reduces the microbial attack on the cellulose component [40]. The addition of ZnO nanoparticle further drops the weight loss to 15.8%, it is attributed to its antimicrobial effect, which restricts the microbial colonization and enzymatic effects [41]. Overall results imply that while MCC

enhances the biodegradability, the functional additives like silica and ZnO inhibit the biodegradation by limiting microbial interaction with the film surface.

8.4.4.2 Field Emission- Scanning Electron Microscopy (FE-SEM) Analysis

The FE-SEM images of all samples before and after the soil burial were captured and is given in **Figure 8.4. Figure 8.4.1(a)** corresponds to the FE-SEM image of bare PVA before degradation. The micrograph reveals a uniform, smooth polymer surface with only faint irregularities. The overall morphology suggests amorphous, homogeneous matrix without features like pores, cracks or phase separated domain. After 30 days of soil burial, the FE-SEM image of bare PVA (**Figure 8.4.1(b)**) shows clear signs of degradation. The surface exhibits numerous pin holes with area in the order of 0.002μm^2 and a marked increase in roughness, suggesting erosions likely facilitated by microbial activity and physical degradation through soil interactions. The scattered bright patches and irregular structures may be due to the PVA fragmentation, soil deposition, or degraded material clusters [42]. The FE-SEM image of PVA/MCC composite film (**Figure 8.4.2(a)**) prior to biodegradation revealed discrete, irregular MCC clusters dispersed within the polymer matrix, while surrounding PVA surface appeared smooth and the presence of filler agglomeration indicates incomplete dispersion. The **Figure 8.4.2(b)** shows the FE-SEM micrograph of PVA/MCC film after the burial period, which reveals substantial surface deterioration with deep voids, cavity and irregular fissures with approximate area of 25-60 μm^2. Around these cavities there are flaky textured residues that suggests surface fragmentation possibly due to microbial attack. As seen in the weight loss analysis MCC is a good facilitator for the degradation of PVA.

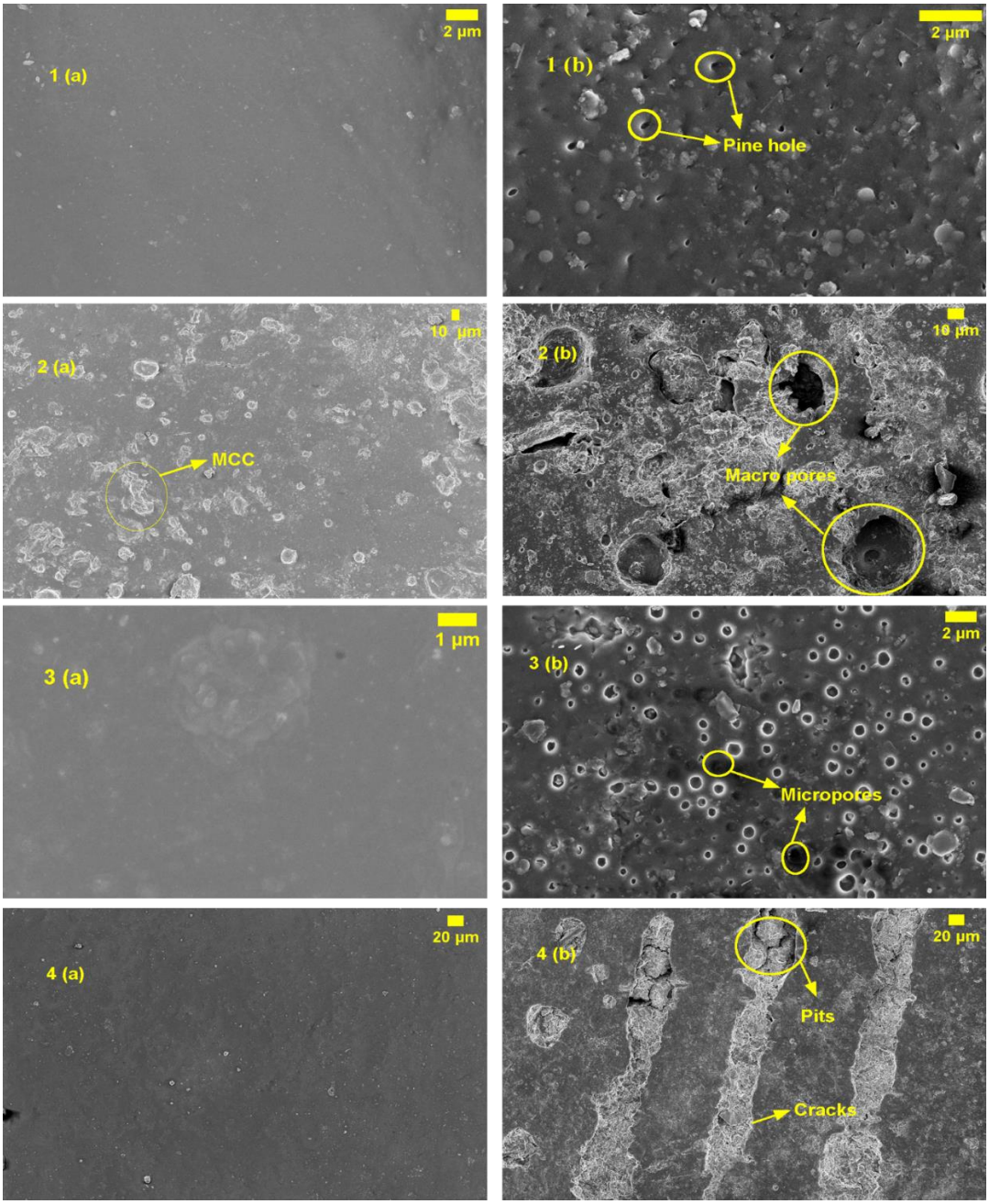

Figure 8.4. FE-SEM Images of PVA, PVA/MCC, PVA/SMCC and PVA/SMCC-ZnO before (1(a)- 4(a)) and after (1(b)-4(b)) Soil Burial.

The FE-SEM image of PVA/SMCC (**Figure 8.4.3(a)**) before burial appears predominantly smooth uniform surfaces with only faint and diffused patches suggesting relatively fine integration of SMCC within the polymer matrix. The image confirms that silicification aided in blending of MCC into the PVA matrix, since silica improves the flowability and reduces the cohesiveness. After 30 days of soil burial,

the FE-SEM image of PVA/MCC (**Figure 8.4.3(b)**) also shows pronounced degradation. The morphology shows numerous microscale cavities, increased roughness, and flaky debris indicating erosion and structural fragmentation. The once continuous film matrix is now discontinuous with significant disruption. On comparing with PVA/MCC film, PVA/SMCC film retains better surface with fewer fractures. The silica fillers strengthen the film's resistance to soil erosion presumably through the improved polymer-filler adhesion and reduced permeability [43].

The FE-SEM image of PVA/SMCC-ZnO (**Figure 8.4.4(a)**) film appears largely even with only a few subtle and faint textures across the surface. This is indicative of well dispersibility SMCC and ZnO particle within the PVA matrix. The surface lacks pores, voids, and no macroscopic clusters suggesting uniform filler incorporation. The image **Figure 8.4.4(b)** revealed that PVA/SMCC-ZnO film maintains surface continuity with some superficial cracks even after 30 days of soil burial. No significant voids or extensive damage were detected indicating minimum morphological changes. The preserved surface reflects exceptional resistance to biodegradation probably due to reinforced interaction from SMCC and structural support from ZnO. Moreover, the antimicrobial character of ZnO also prevents the biodegradation and PVA/SMCC-ZnO is least biodegraded among the other films.

8.4.5 Fourier Transform-Infrared Spectroscopy Analysis

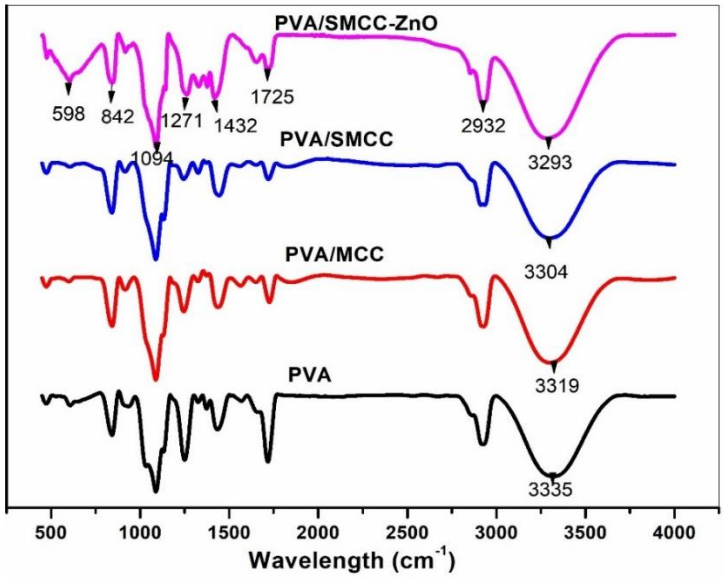

Figure 8.5 FT-IR Spectra of PVA, PVA/MCC, PVA/SMCC and PVA/SMCC-ZnO

Figure 8.5 shows the FT-IR of PVA, PVA/MCC, PVA/SMCC and PVA/SMCC-ZnO respectively. The broad band in the region of 3200-3600 cm^{-1} is the characteristic feature of PVA and cellulose material due to the presence of abundant hydrogen bonded O-H groups in their structure [44]. Incorporation of MCC into PVA leads to enhanced H-bonding, resulting in broadening of the peak and shift towards lower wave number. When SMCC is added, additional hydroxyl groups and silanol groups from the silica surface participate in hydrogen bonding, further modifying this region. The incorporation of ZnO also influences the O-H bond leading to additional changes. All the samples show a doublet peak in the region of 2850-2950 cm^{-1} due to the symmetric and asymmetric vibration of CH_2 group in the polymer backbone of PVA [45]. The slight shift in these peaks indicates the structural changes during the incorporation of MCC, SMCC and ZnO nanoparticles. The small band in the region of 1710-1740 cm^{-1} is attributed to the stretching vibration of C=O groups, which originates from the residual acetate group of incompletely hydrolysed PVA [46]. The intensity of this band decreases during blending since the vibrational freedom of C=O groups reduce due to the hydrogen bonding with hydroxyl groups.

The band in the region1000-1200 cm^{-1} corresponds to C-O and C-O-C stretching vibration of PVA and glycosidic linkage of cellulose [47]. The intensity of C-O bond will be increased during the addition of MCC due to the contribution of cellulose hydroxy and glycosidic bond. The SMCC exhibits characteristic peak of Si-O-Si stretching vibration in the range of 1080-1120 cm^{-1}. This peak often appears as strong and broad band but, in this sample, they overlap with cellulose C-O region [48]. The region below 700 cm^{-1} particularly between 400 and 600 cm^{-1} confirms the presence of ZnO nanoparticles [49]. This band is due to ZnO lattice vibration and is absent in other samples. Moreover, interaction of hydroxyl or silanol group on SMCC causes minor shift, reflecting coordination at the polymer- filler interface.

8.4.6 X-ray Diffraction Analysis

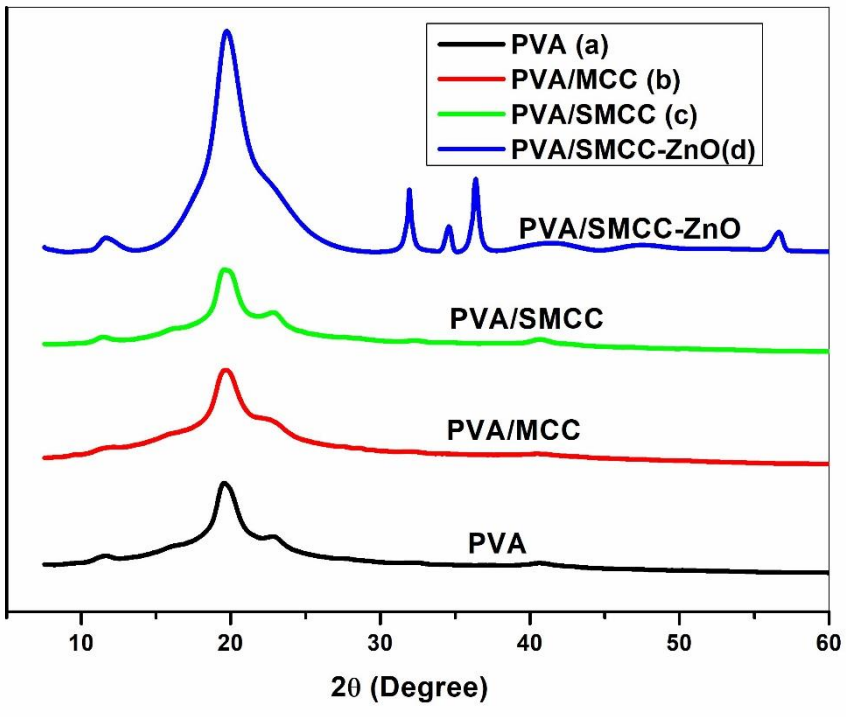

Figure 8.6 XRD Spectra of (a) PVA, (b) PVA/MCC, (c) PVA/SMCC and (d) PVA/SMCC-ZnO

X- Ray Diffraction analysis (XRD) was carried out to study the crystallinity and structural changes of PVA during the addition of fillers. Here the diffraction pattern of pure PVA (blend of HPVA and CPVA) is compared with other PVA films incorporated with MCC, SMCC and SMCC-ZnO composites. Difference in crystalline behaviour gives an insight on the interaction between PVA and fillers. **Figure 8.6 (a)** illustrates the XRD pattern of blended PVA film. It was noticed that the film exhibited a broad, diffused peak centred at 2θ≈20° which is related to its semi crystalline nature [50]. The broad peak suggests that PVA possess both crystalline and amorphous nature and blending two grades of PVA with different solubility and molecular weight disrupts the polymer chain [51]. The shoulder at 2θ≈23°can be attributed to higher order reflection from (200) plane [52]. A very small peak which is observed at 2θ≈40.6° is likely due to the second order diffraction from (220) plane. The incorporation of MCC into PVA matrix resulted a slight sharpening and increasing the intensity of prominent peak at 19.5°, which can be attributed to crystalline nature of MCC. This indicates the partial reinforcement of crystalline

region in the film. MCC displays a characteristic peak around 2θ = 22°, associated with the crystalline cellulose I structure. But in PVA/MCC film, this peak is not visible since, it is assumed to be superimposed on the broader PVA peak [53]. The shoulder peaks at 23°and 40.6° are very weak which shows that the MCC disrupts the regular pattern of PVA chain. The XRD pattern of PVA/SMCC composite reveals significant changes in crystallinity and structural features compared to PVA and PVA/MCC film. The shoulder peak at 2θ≈22.9° becomes pronounced, which may be attributed to the cellulose I. The overall features suggest that SMCC not only interfere the regular chain alignment of PVA but also contributes to new structural domain likely due to PVA-silica interaction [54].

The XRD pattern of PVA/SMCC-ZnO composite film shows a significant change compared to other samples, which confirms the successful incorporation of ZnO nanoparticle and their impact on the crystallinity of the film. A notable increase is observed at 2θ≈19.6° for the prominent peak of semi crystalline PVA and this increase suggests that ZnO acts as a crystallisation promoter. The appearance of sharp peaks at 2θ≈31.9°, 34.6° and 36.6° correspond to (100), (002) and (101) planes of hexagonal wurtzite structure of ZnO [55]. These strong, well-defined peaks confirm the crystalline nature of ZnO particle in the film. Moreover, broad but distinct peak at 41.3°, 47.6°, 56.7°,62.9°and 68.3°can be assigned to higher order reflection from ZnO [56]. Higher crystallinity makes the composite film more stable and this will provide long- term performance and consistent properties.

The crystallinity index of all composites was determined by deconvolution of XRD pattern and fitting parameters obtained from Reitveld refinement using standard CIF file of PVA and ZnO. The diffractograms were resolved to individual peaks, where sharp and well-defined peaks with low FWHM values were designated as crystalline while broad components as amorphous. The percentage of crystallinity was then calculated as the ratio of the cumulative integrated area of the crystalline peaks to the total area of all peaks. The same procedure was uniformly applied to all PVA composites and the corresponding results of PVA, PVA/MCC, and PVA/SMCC were already reported in Chapter 7. The Reitveld refinement results and deconvoluted diffractogram of PVA/SMCC-ZnO is represented in **Figure 8.7.** As discussed in chapter 7 the crystallinity indices of all samples are calculated from the area of

crystalline and amorphous peaks obtained from deconvoluted XRD diagram and is given in **Table 8.3**

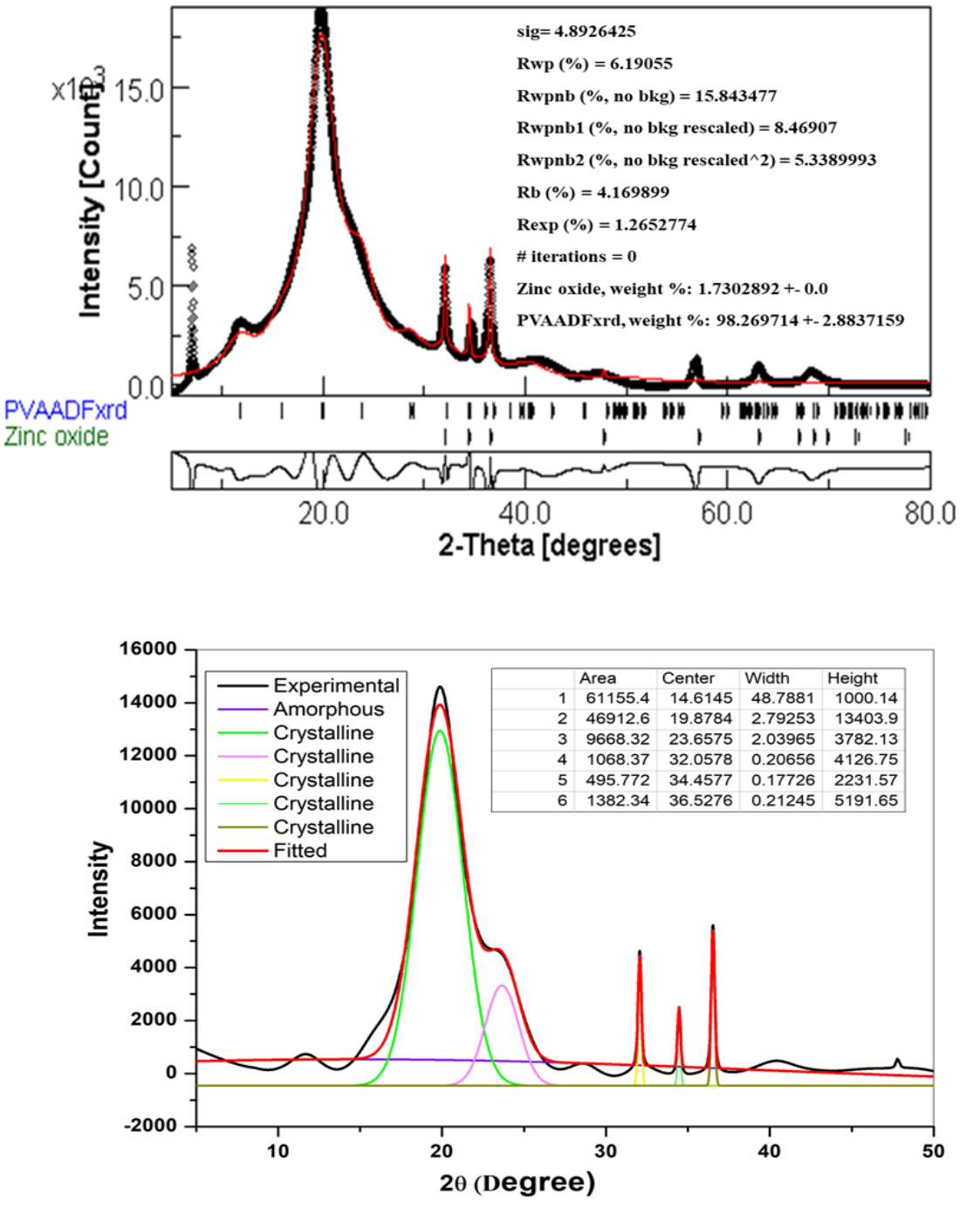

Figure 8.7 Reitveld Refined and Deconvoluted XRD of PVA/SMCC-ZnO

Table 8.3 Crystallinity Indices of PVA, PVA/MCC, PVA/SMCC and PVA/SMCC-ZnO

Sample	Crystallinity Index (%)
PVA	20.2
PVA/MCC	24.2
PVA/SMCC	25.0
PVA/SMCC-ZnO	49.3

Table 8.3 shows the systematic increase in crystallinity index value during the incorporation of fillers. The bare PVA exhibits lowest crystallinity, while the addition of MCC and SMCC produces slight enhancement due to nucleating effect. However, PVA/SMCC-ZnO displays significant rise in crystallinity, which proves that ZnO act as highly efficient nucleating agent which promotes chain order within the polymer matrix [57].

8.4.7 Optical Absorption Behaviour of Films in UV-Visible Region

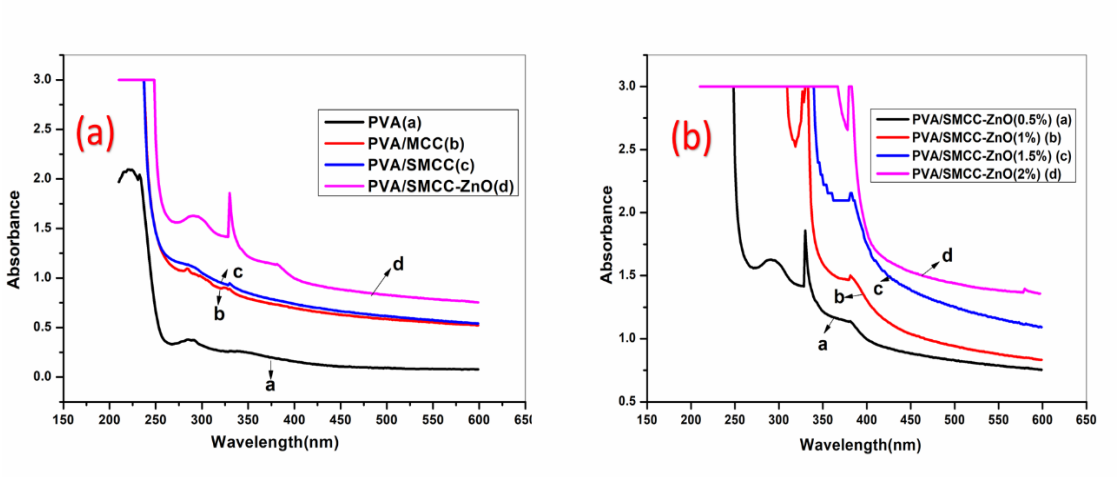

Figure 8.8 (a) UV-Visible Spectra of (a) PVA, PVA/MCC, PVA/SMCC and PVA/SMCC-ZnO (b) PVA/SMCC-ZnO , ZnO in different composition

The optical behaviour of polymer films towards UV-Visible light is shown in **Figure 8.8 (a) and (b). Figure 8.8 (a)** represents the UV-Visible absorption spectra of PVA, PVA/MCC, PVA/SMCC and PVA/SMCC- ZnO (0.5%). The analysis revealed that pure PVA exhibits only weak absorption in the deep UV region, with

negligible activity beyond 300 nm, which limits its application as a UV shielding material. The spectrum shows a weak shoulder at 286 nm corresponding to π-π^* transition, possibly from residual carbonyl group [58]. Beyond 400 nm, the absorbance remains nearly constant at a very low value, confirming the high optical transparency of pure PVA in the visible region. When MCC is incorporated to the PVA matrix, the UV absorption intensity increases slightly and 100% absorption is observed up to 240 nm. While in the visible region only 20% of the light is transmitted and this could be due to scattering effect caused by MCC particles dispersed in the polymer matrix [59].

A comparable spectral profile is observed in PVA/SMCC films, though the overall absorbance is slightly higher. The study shows that silica does not inherently enhances the absorption of UV light. However, the modified silica alters the electronic environment of PVA chain, leading to slight shift in the absorption features [60]. In the case of PVA/SMCC film containing 0.5% ZnO,a noticeable change in the UV absorption is observed. The film shows 100% absorption of light up to 250 nm. A distinct peak is observed at 330 nm due to ZnO and this particle is known to have strong absorption in the UV region due to its wide band gap (~3.37 e V) and their intermediation with PVA and SMCC can result in additional electronic transition and thus enhancing UV blocking capacity [61].

Figure 8.8 (b) shows how the concentration of ZnO effect UV blocking ability of PVA/MCC-ZnO composite films. As seen in the figure even very low concentration of ZnO (0.5%) significantly block the UV light. When ZnO loadings increased to 1% the absorption edge extends further in the UV region. A new absorption features emerges at 333 nm followed by rapid decline towards 380 nm. At 1.5% ZnO the spectrum broadens further. The absorbance of visible light gradually decreases from 1.8 and becomes 1.07. This change suggests that the film is becoming less transparent in the visible region while maintaining strong UV attenuation. At 2% ZnO loading the absorption edge extends up to 370 nm and a distinct shoulder appears at 385 nm confirming the dominance of ZnO band edge absorption [62]. The overall result confirms that ZnO plays a dominant role in tuning the optical properties of

PVA/SMCC films. Increasing ZnO content enhances UV absorption and shielding capacity, but at the cost of reduced transparency in the visible region due to scattering and defect related absorption. Thus, by carefully controlling the ZnO concentration, PVA based composites can be optimized for high UV protection (eg: - in packaging and protective coatings) or for applications requiring a balance between UV shielding and visible transparency (eg: - optical films and biomedical coatings)

8.4.8 Contact Angle/Surface Wettability study of PVA Composites

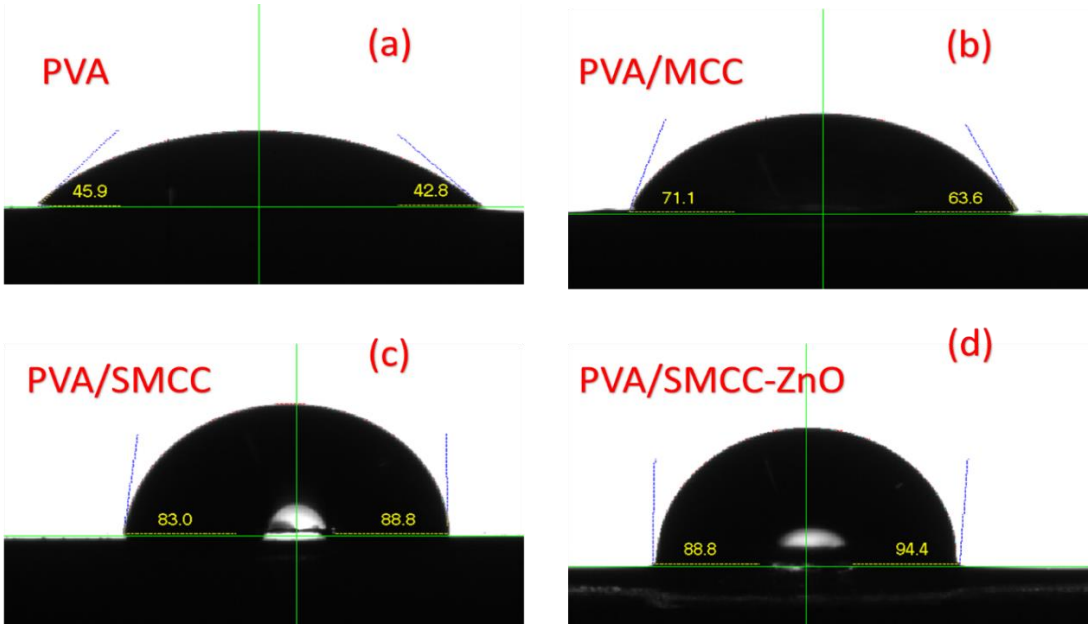

Figure 8.9. Contact Angle Images of (a) PVA (b) PVA/MCC (c) PVA/SMCC and (d) PVA/SMCC-ZnO

The contact angle (CA) measurement of water droplet is widely employed to gauge how well a film resist the liquid water, as it reveals the hydrophilic or hydrophobic nature of its surface. As shown in **Figure 8.9,** the mean CA of pure PVA film was measured to be 45.3°, confirming its inherent hydrophilic character due to abundant surface -OH groups and relatively smooth morphology. This value is comparable to that of 40.9° reported by Kim et al. [63] and 45.5°reported by Wu et al. [64]. The measured value suggests that PVA shows moderate affinity towards water and in real application such as coatings, packaging, barrier film etc, this much degree of wettability may promote relatively rapid water uptake, swelling or

permeation through the film. Therefore, to promote water resistance further surface modification is necessary. Upon incorporation of MCC into the PVA matrix, the mean CA is markedly increased to 67.3° and is in agreement with previously reported value [65]. This rise suggests that MCC particularly at or near the surface partially mask the accessible PVA hydroxy groups, alters the surface topography and reduce the effective solid-water interaction area, all of which contribute to decreased wettability [66].

Upon silicifying MCC to form SMCC, a significant enhancement in hydrophobicity is observed, as evidenced by a substantiable increase in the water contact angle from 67.3° to 86°. This is because silicification effectively masks the hydroxyl groups on the cellulose surface, the interaction between the water molecule and film surface will be reduced, which leads to decrease in surface energy and increase in hydrophobicity. Moreover, the silica coating also contributes to an increase in nanoscale roughness, which can trap air beneath a water droplet, promoting Cassie-Baxter wetting state [67]. These dual effects lead to a significant enhancement in the hydrophobicity of PVA/SMCC composite making them more suitable for applications requiring water resistance.

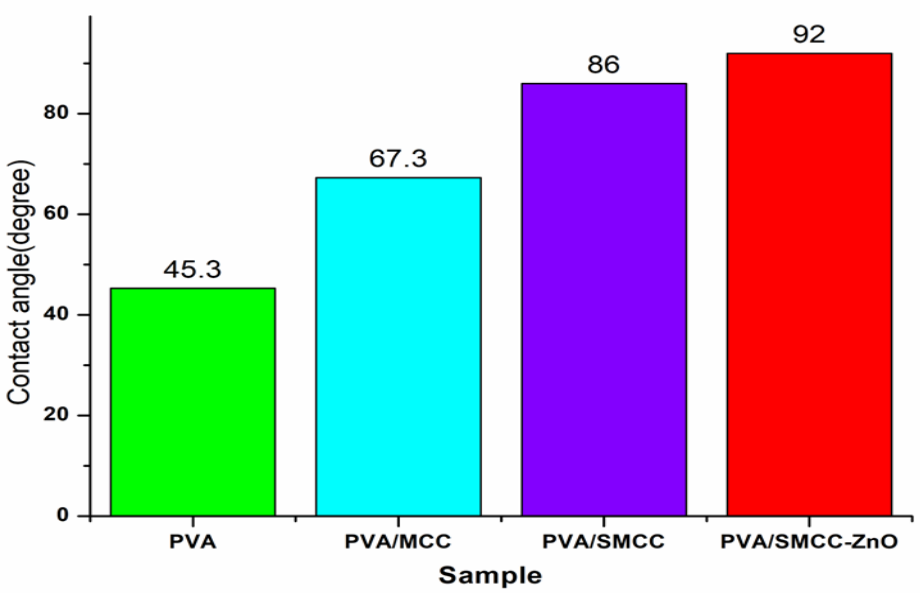

Figure 8.10 Comparison of Contact Angles for PVA, PVA/MCC, PVA/SMCC and PVA/SMCC-ZnO

The incorporation of ZnO nanoparticle into PVA/SMCC composite further enhances the hydrophobicity, elevating the contact angle to 92°. The presence of ZnO nanoparticle can obstruct residual hydrophilic sites on the composite surface [68]. Through modifying the surface energy, ZnO can reduce the interaction between the composite surface and water molecule. Moreover, ZnO nanoparticle introduces additional nanoscale roughness and this will also promote Cassier- Baxter wetting state [69].

8.4.9 Tensile Behaviour of PVA Composites

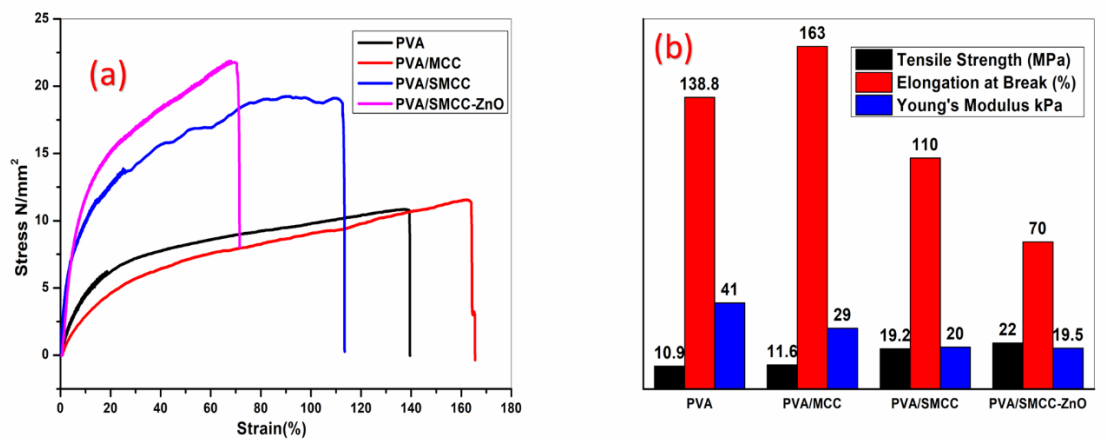

Figure 8.11 a) Stress-Strain Curves b) Tensile Strength, Elongation at Break and Young's Modulus of PVA Composites

To evaluate the reinforcing effect of the incorporated fillers, the tensile properties of PVA composite films were studied. The stress-strain curve and tensile strength (T.S), Elongation at break and Young's modulus of PVA composites are given in **Figure 8.11.** The graph shows that tensile behaviour of PVA changed significantly during the addition of MCC, SMCC and ZnO. The graph shows that neat PVA exhibited lowest T.S and stiffness but highest ductility. Incorporation of MCC resulted a slight improvement in strength and toughness whereas SMCC produced significant increase in stiffness and ultimate tensile strength accompanied by reduction in elongation at break. Among all samples, PVA/SMCC-ZnO composites exhibited the highest tensile strength but the lowest elongation at break, suggesting that incorporation of rigid ZnO particles promotes reinforcement while concurrently

increasing the brittleness [70]. The results clearly show a balance between strength and flexibility. The SMCC makes the material stiffer and ZnO increases the strength even further by reducing the movement of polymer chain.

Adjusting the tensile properties of PVA based films by incorporating MCC, SMCC and ZnO is highly beneficial from an application standpoint. By varying the filler type and composition, the balance between strength, stiffness and flexibility can be precisely controlled to meet the specific requirement. More flexible and ductile films such as PVA and PVA/MCC are suitable for applications, which requires high deformability, including flexible packaging, wound dressing and biomedical films, etc. In contrast, enhanced strength and stiffness achieved in PVA/SMCC and PVA/SMCC-ZnO make them promising for load bearing packages, protective coating and biomedical devices that require enhanced mechanical support. Additionally, the incorporation of ZnO not only increases the reinforcement but also provides benefits such as antimicrobial activity and UV shielding.

Conclusion

This chapter demonstrates the fabrication of biodegradable PVA composite films using MCC, Silicified MCC and ZnO as filler, and their physicochemical, optical, mechanical, antibacterial and biodegradation properties were systematically compared with neat PVA. The incorporated fillers significantly changed the hydrophobicity, crystallinity, mechanical and functional performance of PVA.

Water absorption and WVTR studies revealed a remarkable reduction in moisture sensitivity when MCC is replaced with SMCC and further with SMCC-ZnO. The decline in water uptake is attributed to the enhanced structural compactness and crystallinity imparted by SMCC and ZnO. The contact angle measurement further validated this behaviour since PVA/SMCC-ZnO exhibited highest contact angle (92°) due to synergic effect of silica and ZnO. The XRD analysis confirmed that the incorporation of SMCC-ZnO significantly improved the crystallinity of PVA matrix, up to 49% compared to other composites which is in the range of 20-25%. This

enhanced crystallinity provided better mechanical stability and analysis revealed that SMCC reinforced films showed improved tensile strength with acceptable flexibility.

Although high ZnO loading enhanced the UV absorption, 2% SMCC-ZnO exhibited low transparency. Thus 1.5% loading were taken as the optimum concentration for subsequent analysis. UV-Visible studies showed that UV shielding capacity increased steadily in the order PVA<PVA/MCC<PVA/SMCC<PVA/ SMCC-ZnO. Only the SMCC-ZnO film exhibited antibacterial activity against *E. coli* and *S. aureus* confirming the bioactive functionality imparted by ZnO nanoparticles. The soil burial test demonstrated that PVA/MCC degraded fastest due to its high hydrophilicity and porous morphology. PVA showed moderate degradation, while PVA/SMCC and PVA/SMCC-ZnO exhibited lower weight loss. FE-SEM analysis supported these results and it was found that PVA/MCC underwent extensive structural breakdown while PVA/SMCC exhibited moderate erosion. However, PVA/SMCC-ZnO film-maintained surface integrity with only minor superficial cracks.

Overall, the integration of SMCC and ZnO to PVA matrix improved the barrier properties, crystallinity, UV shielding mechanical strength and antibacterial activity while enabling controlled biodegradation. Among all formulations PVA/SMCC-ZnO (1.5%) emerged as a multifunctional composite, balancing mechanical performance, stability, UV protection, reduced moisture sensitivity and antibacterial activity making it as a promising candidate for environmentally friendly packaging and biomedical film applications.

References

[1] Li Y, Han W, Ding Q, Yang D, Li X, Liu Z, Wu Q. High-barrier bacterial cellulose/polyvinyl alcohol based active packaging material for food preservation. Carbohydr Polym. 2025;363:123603. https://doi.org/10.1016/j.carbpol.2025.123603.

[2] Deng S, Huang X, Kang Z, Xu D, Luo W, Li D. Adoption of polyvinyl alcohol electrospinning materials for skin wound dressing. J Mater Sci Mater Med 2025;36:84. https://doi.org/10.1007/s10856-025-06945-9.

[3] Shen T, Ma Y, Zhang X. Urea–Formaldehyde Strengthened by Polyvinyl Alcohol: Impact on Mulch Film Properties and Cucumber Cultivation. Polymers (Basel) 2025;17. https://doi.org/10.3390/polym17091277.

[4] Zehra K, Nawab A, Alam F, Hadi A, Raza M. Development of novel biodegradable water chestnut starch/PVA composite film. Evaluation of plasticizer effect over physical, barrier, and mechanical properties. J Food Process Preserv 2022;46. https://doi.org/10.1111/jfpp.16334.

[5] Kwon HJ, Hong SM, Park SM, Lee CW. Characterization of acid-modified polyvinyl alcohol and its application to barrier-coated paper for eco-friendly food packaging. Food Packag Shelf Life 2024;43. https://doi.org/10.1016/j.fpsl.2024.101271.

[6] Wang C, Mao L, Zheng B, Liu Y, Yao J, Zhu H. Development of Sustainable and Active Food Packaging Materials Composed by Chitosan, Polyvinyl Alcohol and Quercetin Functionalized Layered Clay. Polymers (Basel) 2024;16. https://doi.org/10.3390/polym16060727.

[7] Seera SDK, Kundu D, Banerjee T. Physical and chemical crosslinked microcrystalline cellulose-polyvinyl alcohol hydrogel: freeze–thaw mediated synthesis, characterization and in vitro delivery of 5-fluorouracil. Cellulose 2020;27:6521–35. https://doi.org/10.1007/s10570-020-03249-9.

[8] Cai X, You X, Wang F, Zhang Y, Li C, Wang Q, et al. Performance improvement of PVA-based alkaline polymer electrolyte membrane using micro-crystalline cellulose as functional filler. Appl Phys A Mater Sci Process 2021;127. https://doi.org/10.1007/s00339-021-04487-9.

[9] Burgalassi S, Zucchetti E, Ling L, Chetoni P, Tampucci S, Monti D. Hydrogels as Corneal Stroma Substitutes for In Vitro Evaluation of Drug Ocular Permeation. Pharmaceutics 2022;14. https://doi.org/10.3390/pharmaceutics14040850.

[10] Sirivechphongkul K, Chiarasumran N, Saisriyoot M, Thanapimmetha A, Srinophakun P, Iamsaard K, et al. Agri-Biodegradable Mulch Films Derived from Lignin in Empty Fruit Bunches. Catalysts 2022;12. https://doi.org/10.3390/catal12101150.

[11] Gong X, Zhang L, He S, Jiang S, Wang W, Wu Y. Rewritable superhydrophobic coatings fabricated using water-soluble polyvinyl alcohol. Mater Des 2020;196. https://doi.org/10.1016/j.matdes.2020.109112.

[12] Dhineshbabu NR, Vettumperumal R, Kokila R. A study of linear optical properties of ternary blends PVA/CMC/aloe vera biofilm for UV shielding. Appl Nanoscience. 2021;11(2):669–678. https://doi.org/10.1007/s13204-020-01629-y.

[13] Lan W, Wang S, Chen M, Sameen DE, Lee KJ, Liu Y. Developing poly(vinyl alcohol)/chitosan films incorporate with D-limonene: Study of structural, antibacterial, and fruit preservation properties. Int J Biol Macromol 2020;145:722–32. https://doi.org/10.1016/j.ijbiomac.2019.12.230.

[14] Guzman-Puyol S, Ceseracciu L, Heredia-Guerrero JA, Anyfantis GC, Cingolani R, Athanassiou A, et al. Effect of trifluoroacetic acid on the properties of polyvinyl alcohol and polyvinyl alcohol-cellulose composites. Chem. Eng. J 2015;277:242–51. https://doi.org/10.1016/j.cej.2015.04.092.

[15] Kharaghani D, Khan MQ, Tamada Y, Ogasawara H, Inoue Y, Saito Y, et al. Fabrication of electrospun antibacterial PVA/Cs nanofibers loaded with CuNPs and AgNPs by an in-situ method. Polym Test 2018;72:315–21. https://doi.org/10.1016/j.polymertesting.2018.10.029.

[16] Elgharbawy AS, El Demerdash AGM, Sadik WA, Kasaby MA, Lotfy AH, Osman AI. Synthetic Degradable Polyvinyl Alcohol Polymer and Its Blends with Starch and Cellulose—A Comprehensive Overview. Polymers (Basel) 2024;16. https://doi.org/10.3390/polym16101356.

[17] Naduparambath S, Sreejith MP, Jinitha T V., Shaniba V, Aparna KB, Purushothaman E. Development of green composites of poly (vinyl alcohol) reinforced with microcrystalline cellulose derived from sago seed shells. Polym Compos 2018;39:3033–9. https://doi.org/10.1002/pc.24307.

[18] Mahmud S, Wang J, Shao N, Xiong Z, Zhang R, Zhu J. Nucleation and crystallization of poly(propylene 2,5-furan dicarboxylate) by direct blending of microcrystalline cellulose: improved tensile and barrier properties. Cellulose 2020;27:9423–36. https://doi.org/10.1007/s10570-020-03448-4.

[19] Shukla SK, Rizwana, Bharadvaja A, Dubey GC. Micro-cellulose Sheet and Polyvinyl Alcohol Blended Film for Active Packaging. Chemistry Africa 2019;2:723–32. https://doi.org/10.1007/s42250-019-00088-5.

[20] Rahman MM, Afrin S, Haque P. Characterization of crystalline cellulose of jute reinforced poly (vinyl alcohol) (PVA) biocomposite film for potential biomedical applications. Prog Biomater 2014;3. https://doi.org/10.1007/s40204-014-0023-x.

[21] Pingan H, Mengjun J, Yanyan Z, Ling H. A silica/PVA adhesive hybrid material with high transparency, thermostability and mechanical strength. RSC Adv 2017;7:2450–9. https://doi.org/10.1039/C6RA25579E.

[22] Peng Z, Kong LX. A thermal degradation mechanism of polyvinyl alcohol/silica nanocomposites. Polym Degrad Stab 2007;92:1061–71. https://doi.org/10.1016/j.polymdegradstab.2007.02.012.

[23] Kim SW. Preparation and barrier property of poly(vinyl alcohol)/SiO_2 hybrid coating films. Korean J Chem Eng. 2008;25(5):1195–1200. https://doi.org/10.1007/s11814-008-0197-9..

[24] Hashim A, Hamad ZS. Lower cost and higher UV-Absorption of polyvinyl alcohol/ silica nanocomposites for potential applications. Egypt J Chem 2020;63:461–70. https://doi.org/10.21608/ejchem.2019.7264.1593.

[25] Chen C, Ding R, Yang S, Wang J, Chen W, Zong L, et al. Development of thermal insulation packaging film based on poly(vinyl alcohol) incorporated with silica aerogel for food packaging application. LWT 2020;129. https://doi.org/10.1016/j.lwt.2020.109568.

[26] Abd-Elnaiem AM, Rashad M, Hanafy TA, Shaalan NM. Improvement of Optical Properties of Functionalized Polyvinyl Alcohol-Zinc Oxide Hybrid Nanocomposites for Wide UV Optoelectronic Applications. J Inorg Organomet Polym Mater 2023;33:2429–44. https://doi.org/10.1007/s10904-023-02616-w.

[27] Pulit-Prociak J, Pszczółka K, Chwastowski J, Staroń P, Staroń A, Sikora E, et al. Preparation of PVA-Based Composites with the Addition of Zinc Oxide Nanoparticles. J Inorg Organomet Polym Mater 2019;29:390–401. https://doi.org/10.1007/s10904-018-1009-2.

[28] Channa IA, Ashfaq J, Gilani SJ, Shah AA, Chandio AD, Jumah MN Bin. UV Blocking and Oxygen Barrier Coatings Based on Polyvinyl Alcohol and Zinc Oxide Nanoparticles for Packaging Applications. Coatings 2022;12. https://doi.org/10.3390/coatings12070897.

[29] Kim I, Viswanathan K, Kasi G, Thanakkasaranee S, Sadeghi K, Seo J. ZnO Nanostructures in Active Antibacterial Food Packaging: Preparation Methods, Antimicrobial Mechanisms, Safety Issues, Future Prospects, and Challenges. Food Rev. Int. 2022;38:537–65. https://doi.org/10.1080/87559129.2020.1737709.

[30] Song Y, Zhang S, Kang J, Chen J, Cao Y. Water absorption dependence of the formation of poly(vinyl alcohol)-iodine complexes for poly(vinyl alcohol) films. RSC Adv 2021;11:28785–96. https://doi.org/10.1039/d1ra04867h.

[31] Qiu K, Netravali AN. Fabrication and characterization of biodegradable composites based on microfibrillated cellulose and polyvinyl alcohol. Compos Sci Technol 2012;72:1588–94. https://doi.org/10.1016/j.compscitech.2012.06.010.

[32] Phadkule SS, Navin K, Nigrawal A, Ball RJ, Kurchania R. Effects of ZnO and SiO_2 nanoparticle additions on the structural, water absorption and mechanical properties of polyvinyl alcohol (PVA) films. Nano Hybrids Compos. 2022;35:41–54. https://doi.org/10.4028/p-9y7z3x.

[33] Alvarado MC. Recent progress in polyvinyl alcohol (PVA)/nanocellulose composite films for packaging applications: A comprehensive review of the impact on physico-mechanical properties. Food bioeng 2024;3:189–209. https://doi.org/10.1002/fbe2.12086.

[34] Channa IA, Ashfaq J, Gilani SJ, Shah AA, Chandio AD, Jumah MN Bin. UV Blocking and Oxygen Barrier Coatings Based on Polyvinyl Alcohol and Zinc Oxide Nanoparticles for Packaging Applications. Coatings 2022;12. https://doi.org/10.3390/coatings12070897.

[35] Abd El-Mohdy HL, Ghanem S. Biodegradability, antimicrobial activity and properties of PVA/PVP hydrogels prepared by γ-irradiation. Journal of Polymer Research 2009;16:1–10. https://doi.org/10.1007/s10965-008-9196-0.

[36] Kairyte K, Kadys A, Luksiene Z. Antibacterial and antifungal activity of photoactivated ZnO nanoparticles in suspension. J Photochem Photobiol B 2013;128:78–84. https://doi.org/10.1016/j.jphotobiol.2013.07.017.

[37] Seil JT, Webster TJ. Antibacterial effect of zinc oxide nanoparticles combined with ultrasound. Nanotechnology 2012;23. https://doi.org/10.1088/0957-4484/23/49/495101.

[38] Zhang L, Jiang Y, Ding Y, Daskalakis N, Jeuken L, Povey M, et al. Mechanistic investigation into antibacterial behaviour of suspensions of ZnO nanoparticles against E. coli. J. Nanopart. Res. 2010;12:1625–36. https://doi.org/10.1007/s11051-009-9711-1.

[39] Wen Yi VN, Choo Huey N, Peng TY, Ooi ZX, Siew Hoong S. Isolation of cellulose derived from orange peel and its application in biodegradable films. Cellulose Chem Technol.2021;55:311–324. https://doi.org/10.35812/CelluloseChemTechnol.2021.55.31.

[40] Cacciari M. Nomes de lugar: confim. Revista de Letras. 2005;45(1):13–22. https://doi.org/10.2307/26459823..

[41] Chong WJ, Shen S, Li Y, Trinchi A, Pejak Simunec D, Kyratzis IL, Sola A, Wen C. Biodegradable PLA-ZnO nanocomposite biomaterials with antibacterial properties, tissue engineering viability, and enhanced biocompatibility. Smart Mater Manuf. 2023;1:100004. https://doi.org/10.1016/j.smmf.2022.100004.

[42] XU X, SUN Q, XU A, GUO X. Biodegradable and Biocompatible Polyvinyl alcohol/Silk Fibroin-Based Composite with Improved Strength. J. Polym. Mater.2022;39:167–81. https://doi.org/10.32381/JPM.2022.39.1-2.11.

[43] Moya SE, Hernández RR, Angelomé PC. Degradation of Mesoporous Silica Materials in Biological Milieu: The Gateway for Therapeutic Applications. Adv Nanobiomed Res 2024;4. https://doi.org/10.1002/anbr.202400005.

[44] Mahardika M, Masruchin N, Amelia D, Ilyas RA, Septevani AA, Syafri E, et al. Nanocellulose reinforced polyvinyl alcohol-based bio-nanocomposite films: improved mechanical, UV-light barrier, and thermal properties. RSC Adv 2024;14:23232–9. https://doi.org/10.1039/d4ra04205k.

[45] Seera SDK, Kundu D, Banerjee T. Physical and chemical crosslinked microcrystalline cellulose-polyvinyl alcohol hydrogel: freeze–thaw mediated synthesis, characterization and in vitro delivery of 5-fluorouracil. Cellulose 2020;27:6521–35. https://doi.org/10.1007/s10570-020-03249-9.

[46] Mansur HS, Sadahira CM, Souza AN, Mansur AAP. FTIR spectroscopy characterization of poly (vinyl alcohol) hydrogel with different hydrolysis degree and chemically crosslinked with glutaraldehyde. Mater. Sci. Eng., C Materials Science and Engineering C 2008;28:539–48. https://doi.org/10.1016/j.msec.2007.10.088.

[47] Nazir A, Abbas M, Iqbal DN, Ameen F, Al-Mijalli SH, Ahmad N, et al. Fabrication of CMC/PVA/Dextrin-Based Polymeric Membrane for Controlled Release of Cefixime With Enhanced Antibacterial Activity. Dose-Response 2024;22. https://doi.org/10.1177/15593258241264951.

[48] Jia N, Li S-M, Ma M-G, Zhu J-F, Sun R-C. Synthesis and characterization of cellulose-silica composite fiber in ethanol/water mixed solvents. BioResources. 2011;6(2):1186–1195.

[49] Gong X, Tang CY, Pan L, Hao Z, Tsui CP. Characterization of poly(vinyl alcohol) (PVA)/ZnO nanocomposites prepared by a one-pot method. Compos B Eng 2014;60:144–9. https://doi.org/10.1016/j.compositesb.2013.12.045.

[50] Sachchu MdMH, Anik FK, Ahmed S, Aman S, Podder U, Sayeem NR, et al. Crystallographic Investigation of PVA@PLA Nanocomposite Film by X-ray Diffraction: Insight from High Resolution TEM. J. Eng. Res. Rep. 2025;27:310–27. https://doi.org/10.9734/jerr/2025/v27i31436.

[51] Chousidis N. Polyvinyl alcohol (PVA)-based films: insights from crosslinking and plasticizer incorporation. Engineering Research Express 2024;6. https://doi.org/10.1088/2631-8695/ad4cb4.

[52] Menazea AA, Mostafa AM, Al-Ashkar EA. Effect of nanostructured metal oxides (CdO, Al2O3, Cu2O) embedded in PVA via Nd:YAG pulsed laser ablation on their optical and structural properties. J Mol Struct 2020;1203. https://doi.org/10.1016/j.molstruc.2019.127374.

[53] Lu J, Wang T, Drzal LT. Preparation and properties of microfibrillated cellulose polyvinyl alcohol composite materials. Compos Part A Appl Sci Manuf 2008;39:738–46. https://doi.org/10.1016/j.compositesa.2008.02.003.

[54] Khedr RF, Elhady MA. Development the Hydrophobic Property of Polyvinyl Alcohol/Silicon Dioxide/Titanium Dioxide Nanocomposites for Self-Cleaning and Soil Stabilization. Molecules 2025;30. https://doi.org/10.3390/molecules30081664.

[55] Abd-Elnaiem AM, Rashad M, Hanafy TA, Shaalan NM. Improvement of Optical Properties of Functionalized Polyvinyl Alcohol-Zinc Oxide Hybrid Nanocomposites for Wide UV Optoelectronic Applications. J Inorg Organomet Polym Mater 2023;33:2429–44. https://doi.org/10.1007/s10904-023-02616-w.

[56] Greeshma K P, Muthulingam S, R Thamizselvi, Dhanya B Sen. Antimicrobial studies and characterization of ZnO nanoparticles by chemical method. GSC Adv Res Rev.2021; 8:071–7. https://doi.org/10.30574/gscarr.2021.8.2.0150.

[57] Gopinath P, Suresh P, Jeevanantham V. Mechanical, structural and optical properties of pristine and PVA capped zinc oxide nanocomposites. J Ovonic Res. 2023;19(1):23–30. https://doi.org/10.15251/JOR.2023.191.23.

[58] Sau S, Pandit S, Kundu S. Crosslinked poly (vinyl alcohol): Structural, optical and mechanical properties. Surf. Interfaces 2021;25. https://doi.org/10.1016/j.surfin.2021.101198.

[59] Sachcha IH, Paddar K, Minar MM, Rahman L, Hasan SMK, Akhtaruzzaman M, et al. Development of eco-friendly biofilms by utilizing microcrystalline cellulose extract from banana pseudo-stem. Heliyon 2024;10. https://doi.org/10.1016/j.heliyon.2024.e29070.

[60] Mousa E, Hafez Y, Nasr GM. Optical Study on PVA/PEG Blend Doped with Nano-Silica. J Electron Mater 2021;50:2594–604. https://doi.org/10.1007/s11664-021-08785-z.

[61] Channa IA, Ashfaq J, Gilani SJ, Shah AA, Chandio AD, Jumah MN Bin. UV Blocking and Oxygen Barrier Coatings Based on Polyvinyl Alcohol and Zinc Oxide Nanoparticles for Packaging Applications. Coatings 2022;12. https://doi.org/10.3390/coatings12070897.

[62] Abd-Elnaiem AM, Rashad M, Hanafy TA, Shaalan NM. Improvement of Optical Properties of Functionalized Polyvinyl Alcohol-Zinc Oxide Hybrid Nanocomposites for Wide UV Optoelectronic Applications. J Inorg Organomet Polym Mater 2023; 33:2429–44. https://doi.org/10.1007/s10904-023-02616-w.

[63] Kim D, Lee S, Kwon H, Seo J. Water resistance and antimicrobial properties of poly (vinyl alcohol) composite films containing surface-modified tetrapod zinc oxide whiskers. Macromol Res 2015; 23:1134–43. https://doi.org/10.1007/s13233-015-3148-4.

[64] Wu H, Xiao D, Lu J, Li T, Jiao C, Li S, et al. Preparation and Properties of Biocomposite Films Based on Poly (vinyl alcohol) Incorporated with Eggshell Powder as a Biological Filler. J Polym Environ 2020; 28:2020–8. https://doi.org/10.1007/s10924-020-01747-2.

[65] Gadhave RV, Vineeth SK. Synthesis of microcrystalline cellulose–polyvinyl alcohol stabilized polyvinyl acetate emulsion. Green Sustain Chem. 2023; 13:23–33. https://doi.org/10.4236/gsc.2023.131003.

[66] Song M, Yu H, Gu J, Ye S, Zhou Y. Chemical cross-linked polyvinyl alcohol/cellulose nanocrystal composite films with high structural stability by spraying Fenton reagent as initiator. Int J Biol Macromol 2018; 113:171–8. https://doi.org/10.1016/j.ijbiomac.2018.02.117.

[67] Fourmentin A, Galy J, Charlot A, Gérard JF. Bioinspired silica-containing polyurethane-acrylate films: Towards superhydrophobicity with tunable water adhesion. Polymer (Guildf) 2018; 155:1–12. https://doi.org/10.1016/j.polymer.2018.09.016.

[68] Khan MQ, Kharaghani D, Nishat N, Shahzad A, Hussain T, Khatri Z, et al. Preparation and characterizations of multifunctional PVA/ZnO nanofibers composite membranes for surgical gown application.J.Mater.Res.Technol Journal of Materials Research and Technology 2019;8:1328–34. https://doi.org/10.1016/j.jmrt.2018.08.013.

[69] Ghannam H, Chahboun A, Turmine M. Wettability of zinc oxide nanorod surfaces. RSC Adv 2019;9:38289–97. https://doi.org/10.1039/c9ra05378f.

[70] Gharoy Ahangar E, Abbaspour-Fard MH, Shahtahmassebi N, Khojastehpour M, Maddahi P. Preparation and Characterization of PVA/ZnO Nanocomposite. J Food Process Preserv 2015;39:1442–51. https://doi.org/10.1111/jfpp.12363.

Chapter 9

Summary and Future Scope of the Work

In the present scenario, petroleum-based biodegradable polymers such as Polyvinyl Alcohol are highly significant, since they offer biodegradability while retaining processing and functional properties of conventional polymers. As global consumption of plastics and concerns about environmental pollution continue to rise, these polymers play an important role as a bridge between conventional plastics and bio-based materials. On comparing to conventional plastics, PVA have some drawbacks such as its high-water sensitivity, relatively poor moisture barrier properties, low thermal stability, lower mechanical strength and relatively higher cost. Therefore, some modifications or reinforcements are needed to enhance the performance of PVA for wide and real-world applications. Such improvements can be achieved by incorporating suitable fillers, blending PVA with other polymers or through chemical modifications. The reinforcing agents like cellulose, biosilica and hybrid fillers significantly enhance the overall performance of PVA composites without compromising its inherent property of biodegradability. The present study focuses on uplifting physicochemical and functional properties of PVA by incorporating fillers extracted from renewable resources.

The thesis entitled **Fabrication of Polyvinyl Alcohol Composites using Biomass-Derived Silicified Microcrystalline Cellulose and Zinc Oxide Nanoparticles** is organized in eight chapters. Each chapter systematically addresses the distinct facts of the research, collectively providing a comprehensive understanding of the research. A brief summary of each chapter is outlined below.

The introduction chapter (Chapter 1) describes how the polymers influence our daily lives, classification of polymers, importance of biodegradable polymers and need for their modification. Since PVA is used as the matrix in the current study, its characteristics, applications and limitations were discussed in detail. Microcrystalline cellulose, silica, Silicified Microcrystalline Cellulose and Zinc Oxide were used as

fillers in the study. Therefore, their sources, physicochemical properties and applications are briefly described in the chapter. Chapter 2 covers a review on isolation of silica and MCC from renewable sources. This review also discusses the different strategies adopted for modification of MCC, and how this modification alters the properties of polymer composites, when they are incorporated into different polymer matrices. The structure, composition, morphology, and functional properties of materials studied by various analytical methods and characterization techniques. Chapter 3 of the thesis describes the principles and methodology of different analytical techniques used for the characterization of newly isolated fillers and polymer composites.

Mission Grass (*Pennisetum polystachion*) is generally considered an aggressive weed, but it is an underreported source of biosilica. Chapter 4 discusses the extraction of amorphous and crystalline silica through acid leaching followed by the sol-gel process. The effect of temperature on the morphology and phase transition of silica was analyzed. The results showed that the calcination at 600 °C favored the formation of amorphous silica, while 850 °C favors crystalline silica. Analysis showed that silica obtained by heating MG at 600 °C, followed by acid leaching and sol-gel processing is highly pure and it contained 95.6 % SiO_2. Thermal analysis revealed that crystalline silica is more hygroscopic than amorphous silica. FE-SEM images showed the aggregated appearance for amorphous silica while crystalline silica exhibited densely packed structure. Microcrystalline cellulose is another bio-derived filler used in this research. Chapter 5 discusses the isolation of MCC from Screw Pine leaves through a series of chemical treatments. During bleaching of Oven Dry Sample, holocellulose is obtained. Holocellulose on alkali treatment α-cellulose is obtained and this on acid hydrolysis MCC is formed. All the derivatives of cellulose are characterized using FT-IR, XRD, TGA, DTG, FE-SEM, AFM and HR-TEM analysis. All the studies showed that MCC is most crystalline and thermally stable compared to others. The XRD studies revealed regular increase in crystallinity during the conversion of holocellulose to amorphous cellulose. Morphology studies confirmed the removal of amorphous region from the cellulose leaving various sized lacunas.

Chapter 6 demonstrates a novel method for the synthesis of Silicified Microcrystalline Cellulose using MCC and sodium silicate extracted from Mission Grass. The SMCC was subjected to physicochemical characterization and its properties were compared with MCC. The results show that the densities and thermal stability of SMCC is higher than MCC. However, there is notable reduction in the crystallinity of MCC during silicification. The morphology of SMCC is distinct from MCC-while native MCC displayed fibrous structure, SMCC exhibited rough surface. On Reitveld refinement of XRD, it is found that both MCC and SMCC contain Cellulose I β and Cellulose II but their relative proportion varied depending upon the extent of alkali treatment. The studies revealed that the lacunae present in the MCC provide enough room for the infiltration of sodium silicate solution and thereby facilitating the formation of silica during acid hydrolysis.

Chapter 7 discusses the fabrication of Polyvinyl Alcohol composites reinforced with MCC, silica, and SMCC. A blend of Hot water soluble PVA and Cold water soluble PVA was used as polymer matrix and the films were fabricated by solution casting. All composites were prepared by incorporating 2 wt% of the respective fillers. To understand the influence of filler content, PVA/SMCC20 films with 2 ,4 ,6 and 8% SMMC20 loadings were also fabricated. All the XRD spectra were subjected to Rietveld refinement and Deconvolution and it is found that the Crystallinity Index of PVA increased during the addition of MCC and SMCC, but decreased during the addition of silica. Thermogravimetric analysis shows that silica and SMCC enhances the thermal stability of PVA composites and there is significant shift in degradation and onset temperature. As per FE-SEM images, MCC displayed poor dispersion and significant agglomeration, while SMCC showed superior dispersion and minimal agglomeration. Mechanical testing revealed that SMCC20 with 6% loading exhibited the highest tensile strength with improved flexibility, toughness and stiffness.

The functional properties of PVA, PVA/MCC, PVA/SMCC and PVA/SMCC-ZnO composite film were discussed in Chapter 8. The study revealed that addition of filler significantly changed the hydrophobicity, crystallinity and mechanical

performances. Water absorption and Water Vapour Transmission Rate analysis revealed that there is significant reduction in moisture sensitivity when MCC is replaced by SMCC and ZnO. The contact angle measurements validated these findings and it is found that PVA/SMCC-ZnO exhibited highest contact angle (92°), while that of bare PVA is 45.3 °. The XRD analysis revealed that there is significant improvement in the crystallinity index when SMCC-ZnO is added as filler. Even though ZnO enhanced the UV absorption, the loading beyond 2% reduces the transparency of the film remarkably. Only PVA/SMCC-ZnO exhibited antibacterial activity against E. coli and S. aureus, confirming the inherent antibacterial potential of ZnO. The biodegradability test of all samples was conducted by Soil burial test and FE-SEM images showed that there is significant degradation in the case of PVA/MCC but PVA/SMCC-ZnO film-maintained surface integrity with minor superficial cracks.

Future Scope of the Work

The present study provides a foundation for further research on biomass-derived functional fillers and biodegradable polymer composites. Here, crystalline and amorphous silica are isolated from the weed, Mission Grass. Further studies should focus on optimizing the synthesis conditions to control particle size, phase purity, and surface properties. Moreover, the extracted silica may be functionalised to enhance the compatibility with polymer matrices and to achieve specific functional properties. The extraction of MCC from Screw Pine leaves may be extended to improve yield, purity and crystallinity. The concentration and contact time, especially mercerisation with NaOH may be varied to get MCC with different phase composition, viz. Cellulose 1β and Cellulose II.

In the current study, SMCC is prepared from biomasses, studies may be extended to synthesis of SMCC from petroleum-based precursors and compare their properties. The percentage of silica in SMCC can be varied to control interfacial interactions and to optimize mechanical, barrier and functional properties of the composites. Further modification of the SMCC may be explored to improve compatibility with polymer matrix. The developed fillers MCC, silica, SMCC can be incorporated with other biodegradable polymers such as Polylactic Acid, Poly

Caprolactam and starch-based system to expand their applications. Biodegradability and environmental stability studies can be extended to different conditions such as compost and marine environment. The studies should be focused on safety, biocompatibility and exploring additional functional properties, thereby widening the practical applications.

Publications

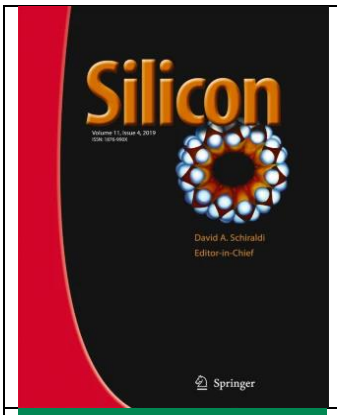	**Ajmal Thayyullathil**, C.M Naseera, F. M Liyakhath, E. K Vydhehi, S. R Sheeja, Subair Naduparambath & Swetha Sasidharan "Effect of Temperature and Method of Synthesis on Morphology and Phase Transition of Amorphous and Crystalline Nano Silica Extracted from Mission Grass (Pennisetum Polystachion)". Silicon **16**, 3491–3501 (2024). https://doi.org/10.1007/s12633-024-02932-x
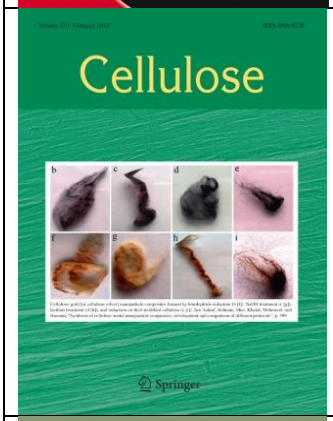	**Ajmal Thayyullathil,** C. M. Naseera, F. M. Liyakhath, E. K.Vydhehi, T.M.Anjana, Subair Naduparambath, Swetha Sasidharan & K. M. Muhammad Ismayil "Synthesis of silicified microcrystalline cellulose (SMCC) for the fabrication of SMCC-poly vinyl alcohol composites". Cellulose (2025). https://doi.org/10.1007/s10570-025-06872-6
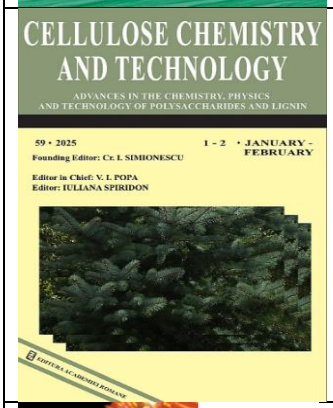	E.K.Vydhehi, **Ajmal Thayyullathil**, Subair Naduparambath and T. M. Anjana, Valorization of Kapok (Ceiba pentandra (l.) Gaertn.) pods for Microcrystalline Cellulose: Extraction and Characterization, Cellulose Chemistry and Technology, 59 (3-4), 271-282 (2025), DOI:) https:// doi. org/ 10.35812/ CelluloseChemTechnol. 2025. 59. 24
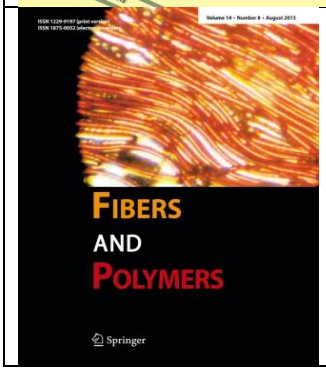	E K Vydhehi, V C Saheer, **A Thayyullathil**, S Naduparambath, TM Anjana, "A Comparative Assessment of Cationic and Anionic Dye Adsorption Capacity of Allomorphs of Microcrystalline Cellulose",Fibers and Polymers, 1-17 (Springer Nature). 2025, DOI: 10.1007/s12221-025-01248-w